DUCTILITY OF PRESTRESSED CONCRETE FRAMES UNDER SEISMIC LOADING

A thesis presented for
the degree of Doctor of Philosophy
in Civil Engineering
in the University of Canterbury,
Christchurch, New Zealand.

by

R.W.G. BLAKELEY

1971

ABSTRACT

This thesis is concerned with the behaviour of prestressed concrete framed structures under earthquake loading.

An experimental programme investigated the performance of four full-size, precast, prestressed concrete beam-column assemblies under high intensity cyclic load, and in particular studied the energy dissipation and ductility characteristics of the members.

Theoretical methods for predicting the moment-curvature characteristics of prestressed concrete members are developed and compared with experimental results. A monotonic loading analysis is utilised to show the effect of a number of practical section variables on ductility for seismic design. A further analysis to determine moment-curvature curves for cyclic loading of a general prestressed concrete section showed good correlation with experiment, including the behaviour subsequent to crushing of the cover concrete. An idealization of the moment-curvature characteristics is also presented for use in seismic response analyses.

A study is made of the relative earthquake responses of comparable prestressed concrete and reinforced concrete single-degree-of-freedom structures. On the basis of the greater response displacements indicated for prestressed concrete structures, a small increase in the seismic load factor for ultimate strength design of prestressed concrete structures over that for reinforced concrete structures is recommended.

ACKNOWLEDGEMENTS

I wish to make grateful acknowledgement for help received during the course of this project and extend my thanks to the following people:

Professor H.J. Hopkins, Head of the Civil Engineering Department, under whose overall guidance this study was made;

Professor R. Park, supervisor for this study, for his encouragement and constructive guidance throughout this project, and for his many helpful suggestions during the preparation of this thesis;

Mr R. Shepherd, Reader in Civil Engineering, and the late Mr I.L. Holmes, Consulting Engineer, Christchurch, for their interest and practical advice;

Messrs H.T. Watson and P.C. Dawson, Technical Officers, and the Technical Staff of the Civil Engineering Department for their assistance in the experimental programme. I wish to particularly thank Mr J.S. Sheard, Senior Technician, for his conscientious preparation of the test equipment and test specimens, and also Messrs J.N. Byers, A.G. Foot, K.L. Marrion, and N.W. Prebble, Senior Technicians, for their valuable help in testing;

Miss K.E. Evans for typing the manuscript;

Mr W. McClelland for draughting assistance;

Mr H. Patterson for photographic work;

Members of the University Computer Centre, for punching cards and for executing programs.

I wish also to gratefully acknowledge financial aid from the following: The University Grants Committee,

The New Zealand Portland Cement Association,

The Ministry of Works,

Certified Concrete Christchurch Ltd;

and the support of the New Zealand Prestressed Concrete Institute.

Finally I wish to thank my wife, Lyn, for her constant encouragement and help.

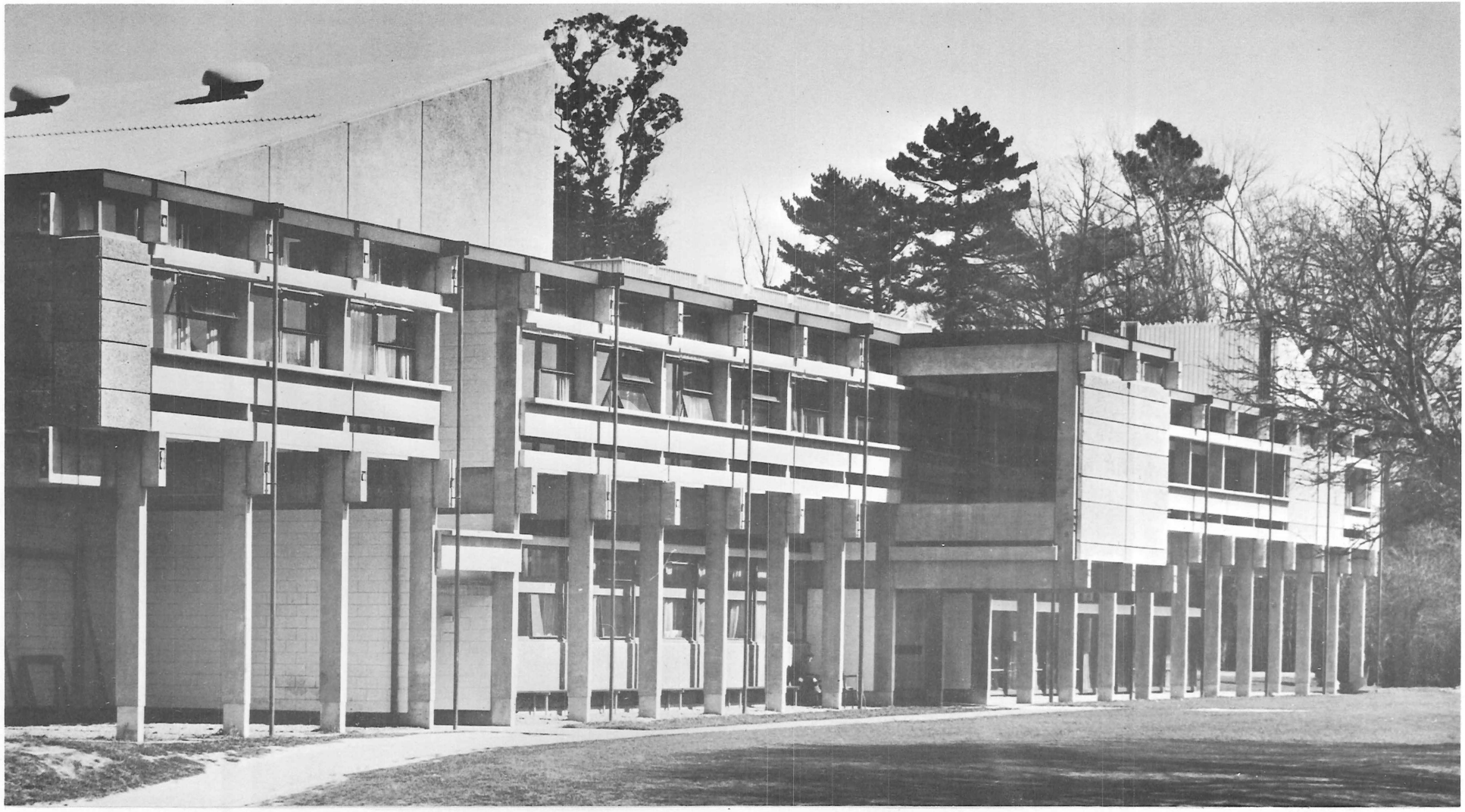

FRONTISPIECE : PRESTRESSED CONCRETE FRAMES OF STUDENTS' UNION BUILDING, UNIVERSITY OF CANTERBURY

CONTENTS

Page

Page

Page

Page

APPENDIX B: MATERIALS, EQUIPMENT AND TESTING PROCEDURE FOR BEAM-COLUMN TESTS

Page

LIST OF FIGURES

Figure | Page

Figure | Page

LIST OF TABLES

INDEX OF NOTATION

(Greek letters are at end)

A_g	=	gross area of cross section
A_s	=	total steel area
A_{s1}, A_{s2},...	=	area of steel at tendon positions 1,2,...
b	=	width of cross section
b"	=	width of confined core measured to outside of hoops
C	=	total compressive force in concrete
ΣC	=	sum of compressive forces within section
c	=	viscous damping coefficient
c_{cr}	=	critical viscous damping coefficient
D	=	overall depth of section or dead load
D_{ct}	=	depth from top of section to top of confined core
D_{cb}	=	depth from top of section to bottom of confined core
D_1, D_2	=	maximum deflection of systems 1 and 2
d	=	distance from extreme compression fibre to centroid of prestressing steel, or to centroid of tension reinforcing steel
EI	=	flexural stiffness of cross section
E_c	=	modulus of elasticity of concrete
E_s	=	modulus of elasticity of steel
E_{s1}, E_{s2},...	=	modulus of elastic recovery of steel in cycles 1,2,...
e	=	eccentricity of axial load
F	=	bond factor
F_c	=	modulus of elasticity factor for concrete
F_{c1}, F_{c2},...	=	modulus of elasticity factor for concrete during cycles 1,2,...
ΔF_D	=	incremental damping force
ΔF_I	=	incremental inertia force
F_s	=	modulus of elasticity factor for steel
F_{s1}, F_{s2},...	=	modulus of elasticity factor for steel during cycles 1,2,...

F_1, F_2 = maximum forces for systems 1 and 2

f_c = stress in concrete

f'_c = concrete cylinder compressive strength

f_{cm} = stress in concrete element at current maximum strain

f_s = stress in prestressing steel

f'_s = ultimate steel stress

f_{sa}, f_{sb} = see Fig. 4.2

f_{se} = steel stress due to effective prestress

f_{sm} = stress in prestressing steel tendon at current maximum strain

f_{su} = stress in prestressing steel at maximum moment as defined by ACI code[40,41]

f'_t = tensile strength of concrete

f_y = yield stress of reinforcing steel

f_{s1}, f_{s2}, ... = steel stress in tendons 1,2,...

G_l = Demec gauge length

H = height of single storey frame or reactive lateral load

h = storey height

hD = depth of cover concrete to top of hoop steel

jD = distance between centroids of compressive and tensile forces in section

K = initial stiffness of systems 1 and 2

k = distance to neutral axis from extreme compression fibre/D or stiffness

k_e = elastic stiffness

k_1, k_2 = post-cracking and post-crushing stiffnesses

L = span of beam

L_B = distance from centre of column to mid-span of beam

L_b = distance from plastic hinge in a beam to column junction

L_e = seismic live load

L_h = distance from point of contraflexure in column to top or bottom of shear block at joint

L_p = equivalent plastic hinge length

L_{pb}, L'_{pb} = equivalent plastic hinge lengths at negative (hogging) and positive (sagging) moment hinges in beam

L_{pc}, L'_{pc} = equivalent plastic hinge lengths at bottom and top of column

L_w = loop width value

l_1, l_2 = height and breadth of joint shear block

M = bending moment or mass

M_C = moment in section due to concrete compressive force

M_{cr} = moment at first cracking

M_e = moment due to design earthquake loading

M_{li}, M_{ld} = initial and degraded loop depth moment values

M_P = moment in section due to axial load

M_S = moment in section due to steel force

M_T = moment in section due to concrete tensile force

M_u = maximum moment capacity

N = number of tendon positions

N_e = number of discrete concrete elements

P = axial load on column

p = steel area ratio, A_s/bD

p'' = ratio of volume of steel hoops to volume of confined concrete

$r_{c1}, r_{c2}, r_y, r_\gamma$ = defined by equation (C.4)

s = spacing of transverse reinforcement

T = period of vibration

T_c = tensile force in concrete

T_s = forces due to steel

ΣT = sum of tensile forces in section

$t, \Delta t$ = time and time interval

U = ultimate strength design load

u = cube strength

$V, \Delta V$ = lateral force and incremental lateral force

V_{cr} = lateral force at first cracking in the frame

V_d = design lateral load from seismic coefficients[84]

V_{li}, V_{ld} = initial and degraded loop depth load values

V_u = maximum lateral load capacity

V_y = yield strength

W = weight of structure

X = load at end of beam

$x, \Delta x$ = displacement and incremental displacement

x_{cr} = displacement at first cracking

x_g = displacement of ground relative to reference axis

x_m = maximum displacement from initial zero

x_{mn}, x_{mp} = current maximum displacements from initial zero in negative and positive directions

x_T = displacement relative to reference axis

x_u = displacement at maximum moment capacity

x_y = initial yield displacement

x_o = maximum vibration amplitude

$\dot{x}, \Delta\dot{x}$ = velocity and incremental velocity relative to ground

$\ddot{x}, \Delta\ddot{x}$ = acceleration and incremental acceleration relative to ground

$\ddot{x}_g, \Delta\ddot{x}_g$ = acceleration and incremental acceleration of ground relative to reference axis

$\ddot{x}_T, \Delta\ddot{x}_T$ = acceleration and incremental acceleration of structure relative to reference axis

y = distance to a fibre from extreme compression fibre/D

Z = slope of "falling" branch of stress-strain curve for concrete as defined by equation (4.3)

Z_{core}, Z_{cover} = Z values for core and cover concrete

α = distance to fibre with strain of ϵ_o from extreme compression fibre/D

$\alpha_1, \alpha_2, \ldots$ = distance to tendon position 1,2,... from extreme compression fibre/D

β = distance to fibre with strain of ϵ_{20core} from extreme compression fibre/D or strength ratio as defined by equation (6.10)

β_1 = distance from bottom of column to point of contraflexure/H

γ = distance to top of crack from extreme compression fibre/D

γ_1, γ_2 = ratios of post-cracking and post-crushing stiffnesses to elastic stiffness

γ_{LF} = ratio of maximum strength to cracking strength

γ_s = total angle of shear distortion

$\gamma_{s1}, \gamma_{s2}, \gamma_{s3}$ = angles of shear distortion (see Fig. B.18)

Δ = imposed horizontal displacement

Δ_{cr} = displacement at top of frame at first cracking in frame

Δ_e = displacement at top of frame due to elastic area of column curvature distribution profile at maximum deflection

Δ_g = change in readings of Demec gauge

Δ_m = absolute change in length as measured by travelling microscope

Δ_{max} = maximum displacement at top of frame at ultimate

Δ_s = component of beam end deflection due to joint shear distortion

δ_1, δ_2 = measured compression and extension of diagonals of shear block

ϵ_c = concrete strain

$\epsilon_{cc}, \epsilon_{ct}$ = concrete strains at extreme compression and tension fibres

ϵ_{ce} = strain in concrete due to effective prestress

ϵ_{ci} = strain in concrete element i

ϵ_{cm} = current maximum concrete strain sustained in an element

ϵ_{cu} = limiting concrete strain

$\epsilon_{c1}, \epsilon_{c2}, \ldots$ = strain in concrete at level of tendons 1,2,...

$\epsilon_{ce1}, \epsilon_{ce2}, \ldots$ = strain in concrete due to effective prestress at level of tendons 1,2,...

ϵ_r = concrete strain at rupture in tension

ϵ_s = steel strain

$\epsilon_{sa}, \epsilon_{sb}$ = see Fig. 4.2

ϵ_{se} = steel strain due to effective prestress

$\epsilon_{se1}, \epsilon_{se2}, \ldots$ = steel strain due to effective prestress in tendons 1,2,...

ϵ_{sp} = strain in concrete at spalling

ϵ_{sm} = current maximum steel strain sustained in a tendon

ϵ_{su} = ultimate steel strain

$\epsilon_{s1}, \epsilon_{s2}, \ldots$ = steel strain in tendons 1,2,...

ϵ_{y} = strain at a fibre at a depth yD from extreme compression fibre

ϵ_{0} = concrete strain at maximum stress

ϵ_{20c} = strain at 0.2 of maximum stress on "falling" branch of stress-strain curve for concrete

$\epsilon_{20core}, \epsilon_{20cover}$ = ϵ_{20c} for core and cover concretes

ϵ_{50h} = defined by equation 4.5

ϵ_{50u} = strain at 0.5 of maximum stress on "falling" branch of stress-strain curve for concrete and defined by equation (4.4)

ζ = distance to fibre with strain of ϵ_{sp} from extreme compression fibre/D

η = depth to fibre with strain of $\epsilon_{20cover}$ from extreme compression fibre/D

θ = rotation

θ_{p} = plastic rotation at a plastic hinge

θ_{pc} = plastic rotation at a hinge in a column

θ_{pb} = plastic rotation at a hinge in a beam

λ = damping ratio

μ = displacement ductility factor as defined on Figs. 6.2 and 6.4

μ_1, μ_2 = displacement ductility factors defined by equation (2.1)

ν, ξ, χ, ψ = limits of integration as defined in equation (C.26)

φ = curvature or capacity reduction factor

φ' = dimensionless curvature expression defined by equation (C.4)

φ_{cr} = curvature at first cracking

$\varphi_{crb}, \varphi'_{crb}$ = curvature in beam at negative (hogging) and positive (sagging) moment sections at first cracking in the beam

$\varphi_{crc}, \varphi'_{crc}$ = curvature at bottom and top of the column at first cracking in the column

$\varphi_{c1}, \varphi'_{c1}$ = curvature at bottom and top of the column at first cracking in the frame

φ_e = maximum elastic curvature calculated assuming an uncracked section

$\varphi_{eb}, \varphi'_{eb}$ = maximum elastic curvature in the beam at negative and positive moment sections

$\varphi_{ec}, \varphi'_{ec}$ = maximum elastic curvature at bottom and top of the column

φ_{max} = maximum curvature that may be sustained in member

$\varphi_{maxc}, \varphi'_{maxc}$ = maximum available curvature at the bottom and top of the column

$\varphi_{maxb}, \varphi'_{maxb}$ = maximum available curvature in the beam at negative and positive moment sections

$\varphi_{mn}, \varphi_{mp}$ = current maximum curvature sustained in negative and positive directions

φ_y = curvature at first yield

φ_u = ultimate curvature

$\varphi_{.004}$ = curvature at a strain of 0.004 in the extreme compression fibre

CHAPTER 1

INTRODUCTION AND SCOPE OF RESEARCH

1.1 INTRODUCTION

The use of prestressed concrete components has been accepted for many years for structures under gravity loading. The applications of the material are increasing rapidly, encouraged by such advantages as the possibility of pleasing architectural forms and the suitability of prestressed concrete to modern precast construction. However, the use of prestressed concrete in primary seismic resistant elements, such as shear walls and frames, has not met with such ready acceptance. While some investigators[1,2,3,4,5] have expressed confidence in the ability of certain types of prestressed concrete structures, designed using a conventional code approach, to withstand strong earthquakes, design engineers have generally been cautious in their use of the material for seismic resistance. The principal reasons for caution have been; firstly, the absence of information on the practical performance of such structures in earthquakes, and secondly, the shortage of experimental evidence on the behaviour of prestressed concrete members under high intensity cyclic loading. Because of this lack of information most building codes do not offer detailed provisions for the seismic design of prestressed concrete members.

1.2 SCOPE OF RESEARCH

This study has been prompted by three broad areas of concern regarding the seismic resistance of prestressed concrete structures. They are as follows:

(i) Dynamic analyses of the elastic response of structures, using earthquake acceleration records, have shown that a structure is subjected to considerably greater loads than are provided for by the equivalent static load design coefficients recommended by codes. This means that structures must be capable of developing large post-elastic deformations if they are to survive severe earthquakes. Although research has shown that large ductility is available in properly designed reinforced concrete members, concern has been expressed that prestressed concrete may be a rather more brittle material. In particular, the likely behaviour at the joints of precast post-tensioned members under seismic load reversals has been questioned.

(ii) A second source of concern arises from the energy dissipation capacity of the members under cyclic load. The moment-rotation characteristics of prestressed concrete members under cyclic load are generally idealized by a bilinear elastic system as shown in Fig. 1.1. The principal feature of this loop is the large elastic recovery of prestressed concrete. For comparison, the traditional idealization for reinforced concrete under cyclic loading has been an elasto-plastic system as shown in Fig. 1.2. For loading in a particular direction the areas under the moment-rotation curves represent the energy absorption. On unloading the member this energy is largely released as kinetic energy for the bilinear elastic system, whereas in the elasto-plastic system it is largely dissipated by plasticity. The area within the hysteresis loop is a measure of the energy dissipation characteristics of the system, and clearly is lower for the elastic bilinear system. The energy dissipation capacity of the members has an important effect on the response of a structure to earthquake excitation, yet little study has been made of these characteristics for prestressed concrete.

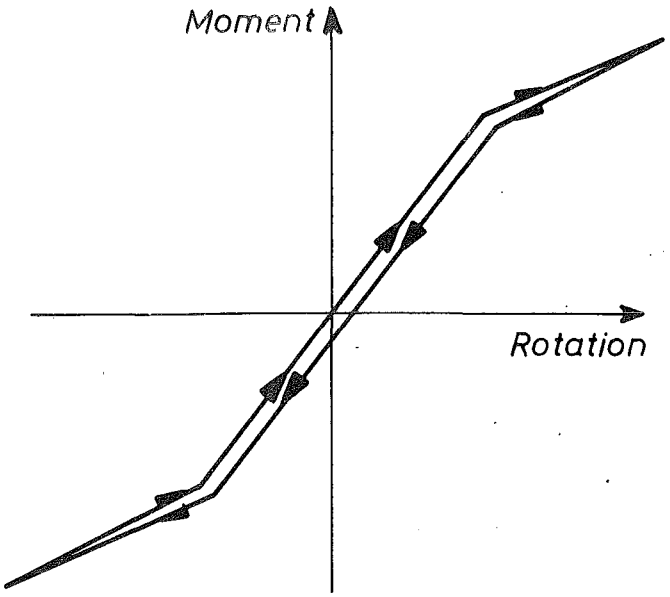

FIG.1.1 : IDEALIZED BILINEAR ELASTIC SYSTEM

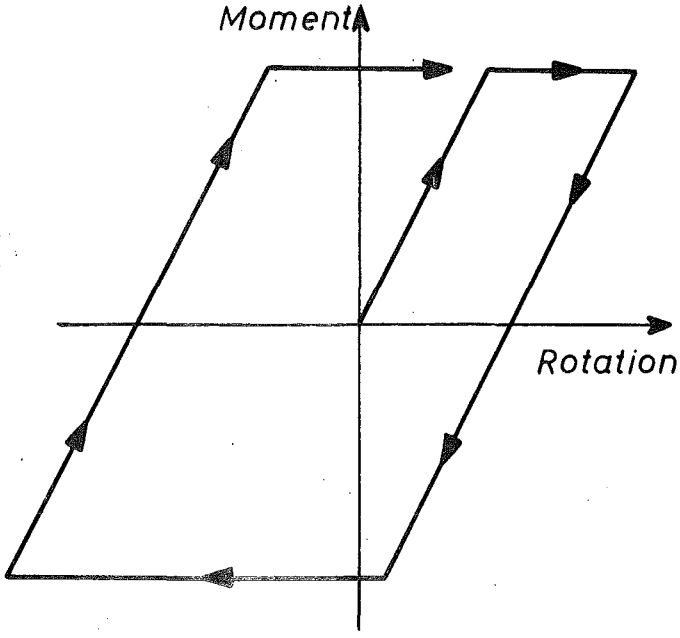

FIG.1.2 : IDEALIZED ELASTO-PLASTIC SYSTEM

(iii) It is generally assumed that the response of a prestressed concrete structure to a severe earthquake will be greater than that of a comparable reinforced concrete structure. The reasons behind this assumption are; firstly, the lower percentage critical viscous damping usually expected for prestressed concrete structures relative to reinforced concrete structures, and secondly the lower energy dissipation characteristics for prestressed concrete members. However, there is still little analytical evidence of the seismic response of prestressed concrete structures, although a significant beginning has been made by Spencer[6]. Consequently the ductility demands on individual members are not yet clear.

The scope of this investigation covered all of the above listed points of concern for the seismic resistance of prestressed concrete structures. It included an experimental and analytical study of the ductility and cyclic loading behaviour of prestressed concrete members, followed by application of the characteristics obtained to a seismic analysis of simple structures.

1.3 FORMAT

The chapters of this thesis have been arranged as follows:

In Chapter 2 a historical review is presented, which traces the approach of design and research engineers to the suitability or otherwise of prestressed concrete for seismic resistance. Evidence from research and observation after actual earthquakes are presented, and the current principles for prestressed concrete seismic design are discussed.

Chapter 3 presents the experimental results from four prestressed concrete beam-column assemblies, which were subjected to high intensity cyclic loading. The variables in the test sequence included the degree of lateral confinement and the position of the formation of the plastic hinges in either the beam or the column.

A theory is developed in Chapter 4 to predict the moment-curvature relationship of prestressed concrete members under monotonic load. The theory is compared with experimental results, and then used to study the influence on ductility of a number of practical section variables.

In Chapter 5 a theory is developed to derive the moment-curvature characteristics of cyclically loaded prestressed concrete members. An idealization of the moment-curvature relations is also postulated for use in seismic response analyses of multistorey framed structures. Both sets of curves are compared with experimentally obtained moment-curvature curves.

The previous results are focussed in Chapter 6 on analyses of the seismic response of simple structures. Load-displacement idealizations representing reinforced concrete and prestressed concrete structures are used and the resulting responses are compared. Conclusions are drawn on appropriate load factors for the seismic design of prestressed concrete structures.

The conclusions that have been reached are summarised in Chapter 7, and suggestions are made for future research. Generally the conclusions for each section of the work appear at the end of the appropriate chapter, and consequently the formal conclusions in this chapter are comparatively brief.

CHAPTER 2

HISTORICAL REVIEW OF THE SEISMIC RESISTANCE OF PRESTRESSED CONCRETE

SUMMARY

A historical review is presented, which traces the approach of design and research engineers to the use of prestressed concrete in primary seismic resistant structural elements. Observations of the behaviour of prestressed concrete structures during earthquakes are collated and the current principles for seismic resistant design are discussed.

2.1 THE BEGINNINGS: DYNAMIC LOADING OF MEMBERS

The first dynamic load tests to be carried out on prestressed concrete were reported by Freyssinet[7] in 1934. He applied a fatigue loading to two concrete telegraph posts, both being 40 feet in length. One post was prestressed concrete and the other reinforced concrete, but each had similar ultimate strengths. The maximum magnitude of load was 50% of the static ultimate load and the direction of loading was reversed during each cycle. It is reported that the reinforced concrete post had failed after "a few thousand cycles", whereas the prestressed concrete post was still in good condition after 500,000 cycles. This type of test involving a direct comparison of a prestressed concrete component with an equivalent reinforced concrete component was common in tests carried out in the early development stages of prestressed concrete. Since Freyssinet's initial test a large number of fatigue tests have been conducted. Research into the fatigue characteristics of prestressed concrete has been extensively reviewed by Hunt[8] (1966) and Jacobs[9] (1968). Consequently in this review only those fatigue-type tests which directly aid understanding

of the seismic behaviour of prestressed concrete structures will be discussed.

2.2 FIRST USES IN PRIMARY SEISMIC RESISTANT ELEMENTS

Ellison and Lin[10] (1955) reported the construction of a 9 storey car parking building in San Francisco, in which the key element in resisting seismic forces was a prestressed concrete shear wall. Preliminary calculations had indicated that most of the deflection of the shear wall under lateral forces would be caused by bending in the lower portion. Hence it was felt that the deflection could be reduced, at low cost, if the bottom 40 feet of the shear wall was prestressed. The amount of prestress required was determined by the condition that no tensile stress would be created in the shear wall under the equivalent lateral loading required by the San Francisco Code. This code specified a 6% seismic coefficient. It is interesting to note that the tendons were not bonded to the concrete because a factor of safety of 1.65 against cracking was deemed to justify this. At this stage in development the importance of the availability of post-elastic deformations was apparently not recognised. In a later paper Lin[11] (1962) made a convincing case for the advantages of prestressed concrete shear walls. However, this was based on elastic considerations alone.

In a paper presented to the World Conference on Prestressed Concrete (1957) Ban[12] commented that in Europe studies to obtain a building frame appropriate for prestressed concrete structures had been undertaken, and several multistorey office buildings had been completed there. The frames were composed of reinforced concrete columns and prestressed concrete beams. Ban went on to say that the prestressed concrete structures encountered were mainly built up with precast members, the joints of which were considered to be simply supported or hinged. However he advocated rigid connection between the beams and the columns

in order to resist lateral load. A current method of fabricating multistorey framed buildings was to assemble prestressed concrete beams and reinforced concrete columns with a reinforced concrete joint. Ban introduced his own proposals for extending the prestressing cable through to the column, thus placing the whole joint in compression. His scheme was the forerunner of modern precast, prestressed beam-column connection details.

2.3 THE DEVELOPMENT OF A PHILOSOPHY OF SEISMIC DESIGN

In the early 1960's a philosophy of seismic design of concrete structures came to be accepted. Design requirements were that under a moderate earthquake such as may be expected several times during a structure's life it should survive without damage, and that it should survive without major structural damage in the most severe probable earthquake expected during its life. A further condition is that the structure should not collapse even under earthquake loading of an abnormal intensity.

However authorities differed as to the ability of prestressed concrete structures to fulfil these requirements. While Lin[11] (1962) was enthusiastic about its suitability, Glogau[13] (1963) commented "In view of the ductility required to reduce the response, caution is advocated by such authorities as Prof. Tanabashi and Prof. Penzien, and Mr Steinbrugge."

The publication of a further paper by Lin[14] (1964) was a stimulus to the debate. In it he discussed several important aspects of the seismic design of prestressed concrete structures. He showed that for working stress design a reduction of 25% of all seismic moments, shears, and loads was equivalent to the normal 33⅓% allowable stress increase for seismic loading used for conventional materials. Also, some results were presented of flexural tests of prestressed concrete members under

monotonic load to failure. Large areas beneath the moment-rotation curves were evident.

Of particular interest in the paper was the result of a dynamic computer analysis of a 19 storey prestressed concrete apartment building. The building was first designed using the earthquake forces specified by the 1961 Uniform Building Code. The dynamic response of the structure to the North-South component of the 1940 El Centro earthquake was calculated assuming linear elastic behaviour. Comparison of the static and dynamic forces and displacements obtained by Lin are shown in Fig. 2.1. The fact that the El Centro earthquake produced forces and displacements about five times the code values emphasised the need for prestressed concrete structures to be capable of developing large post-elastic deformations, if they are to be able to survive major earthquakes.

In discussing Lin's paper Rosenbleuth[15] (1966) warned against establishing conclusions based only on the curve for first loading. He then postulated a relationship between the responses of prestressed and reinforced concrete systems based on idealizations of their complete cyclic load-deformation characteristics. It is worth noting at this point that Rosenbleuth has since made other such comparisons[16,17], the latest of which is shortly to be published in a book by Newmark and Rosenbleuth. The expression evolved in the latter case assumes that the force-deformation curves for prestressed and reinforced concrete single-degree-of-freedom systems may be idealized respectively as elastic bilinear and elasto-plastic systems, as shown in Fig. 2.2. The design acceleration spectrum is idealized as hyperbolic in the range of interest, and the two systems are assumed to have the same mass and same initial stiffness and a coefficient of damping not smaller than 2% for small oscillations. The relationship between the responses is as follows:

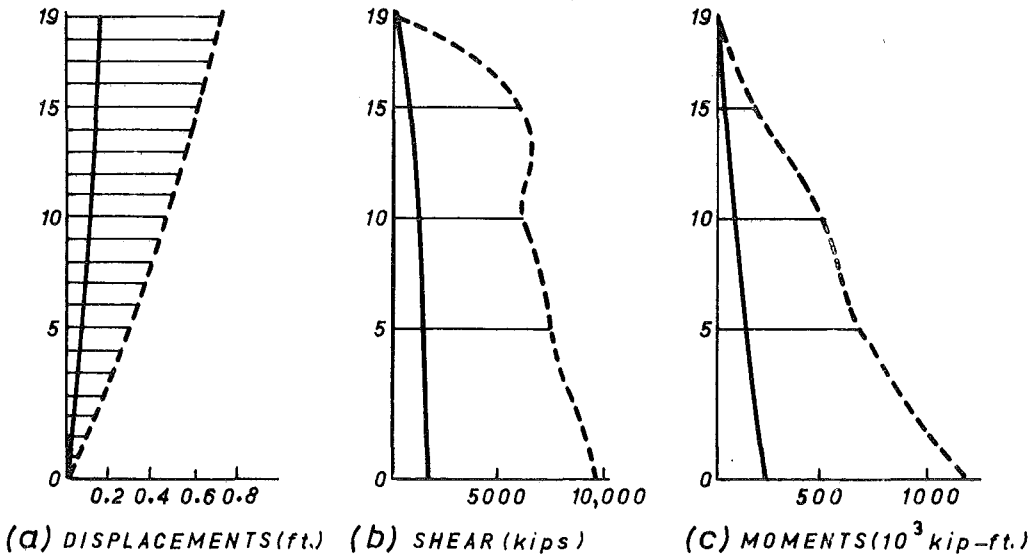

FIG. 2.1 : CODE VALUES vs. EL CENTRO EARTHQUAKE, AFTER LIN[14]

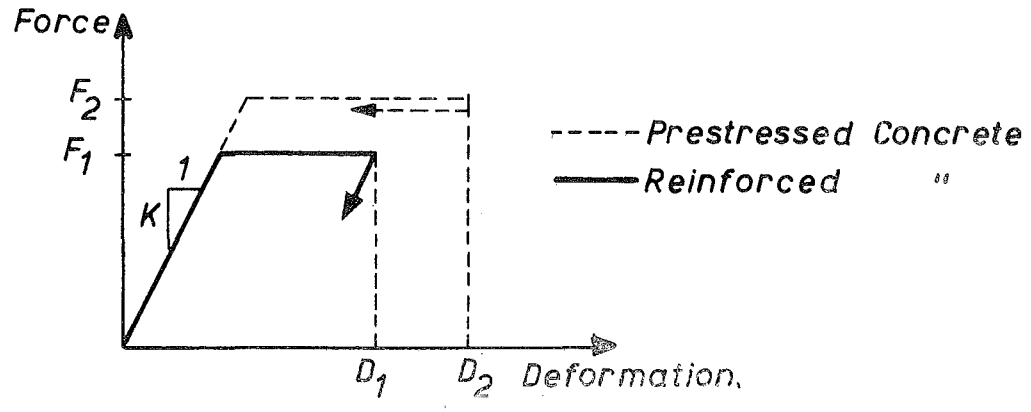

FIG. 2.2 : DETAILS FOR ROSENBLEUTH'S[17] EXPRESSION.

$$\frac{F_2}{F_1} = \frac{\mu_1}{\mu_2}\left[\frac{1 + 2\mu_2}{3\mu_2}\right]^{3/2\ 0.6} \qquad \ldots (2.1)$$

where the displacement ductility factors μ_1, μ_2 are given by:

$$\mu_1 = D_1 K/F_1 \ , \quad \text{for reinforced concrete}$$

$$\text{and} \quad \mu_2 = D_2 K/F_2 \ , \quad \text{for prestressed concrete.}$$

The solution of this expression shows that if the deformation of the two systems is to take them to the same displacement ductility factor of 6, the required force level in the elastic bilinear system will be 1.4 times that in the elasto-plastic system. Alternatively, if the two systems have the same maximum forces, the displacement requirements of the elastic bilinear system will be approximately 1.3 times those of the elasto-plastic system.

The above treatment can serve as a rough guide only as the actual load-deformation curves, particularly for prestressed concrete, are rather different from their idealizations. However, it does emphasise that because of the particular force-deformation characteristics and the lower damping applicable to prestressed concrete relative to reinforced concrete, a prestressed concrete structure is likely to suffer greater deformations or be called to resist higher forces under most strong earthquakes than a reinforced concrete structure of comparable mass and stiffness. A point noted by Rosenbleuth[15] in favour of prestressed concrete is that to resist a given set of forces a prestressed concrete structure is normally considerably more flexible than its reinforced counterpart. This is a desirable feature for seismic loading resistance and partly counteracts the effect of the smaller energy dissipation under cyclic loading.

With the particular response characteristics of prestressed concrete structures noted above in mind, designers paid close attention to detail in the use of prestressed concrete in primary seismic resistant elements.

Allardice[18] (1966) and Brisac[19] (1967) published details of the design of such structures in New Zealand and Greece respectively, and Korchinskii[20] (1965) reported on the use of prestressed concrete in seismic regions in the U.S.S.R.

2.4 OBSERVATION OF BEHAVIOUR UNDER ACTUAL EARTHQUAKES

A survey of the literature shows that structures incorporating significant amounts of prestressed concrete have been involved in few major earthquakes. However the following observations give useful information on the seismic resistance of such structures.

2.4.1 Skopje, 1963

Several buildings in Skopje incorporated prestressing in some elements. Berg[21] reported one case of structural damage amongst the prestressed buildings. One of the shop buildings at the new Skopje steel works was a precast prestressed concrete structure consisting of precast roof construction on continuous prestressed concrete girders, which in turn were supported by prestressed concrete columns. The columns were I-shaped and pretensioned. The earthquake caused the building to rock on the columns in the direction of the girders. This induced severe bending moments at the top and bottom of each flange in the weak direction of bending, resulting in crushed concrete at the toes of the flanges. The prestress in the flanges was thus destroyed and while the columns could be readily repaired to restore their vertical load carrying capacity, the prestress could not be restored. Consequently the stiffness under horizontal loadings would be reduced because the column would crack earlier. Therefore an auxiliary bracing system had to be provided if the structure was to have the ability to resist horizontal forces in the longitudinal direction.

2.4.2 Alaska, 1964

Kunze et al[22] reported that of some 28 structures in Anchorage employing precast prestressed concrete elements, five suffered partial or total collapse. Of these, two were still under construction and, as a consequence, had not yet been tied together to resist an earthquake force. A sixth structure involving post-tensioned lift-slab construction also collapsed. However, there appear to have been no failures of the prestressed concrete members themselves. In nearly every case the supporting structure, which was built of traditional materials, collapsed or connections were ineffective. Even the controversial failure of the Four Seasons Apartment Building appears to have been due to a bond failure at a splice in the mild steel reinforcement of the concrete shear walls, rather than a failure of the unbonded 8 inch thick prestressed concrete slab.

Sutherland[4] observed 13 structures incorporating prestressing which suffered no damage other than very minor cracking of the blockwork. Included in these were two buildings using prestressed concrete tees and columns as frames.

2.4.3 Niigata, 1964

Sutherland[4] reported on a study of the three structures in Niigata incorporating prestressing to any material degree. Two were bridges and in both cases the prestressed members were not damaged, despite considerable settlement and displacement of the foundations of the abutments.

The third structure, the railway station, had an entire canopy over the foyer of precast post-tensioned members on precast columns. Although the foundation material appeared to have subsided by two feet, the structure itself had withstood the movement exceedingly well.

Inomata[23] reported on the behaviour of 68 structures, which incorporated prestressing, during the Niigata earthquake. One of the

significant sources of damage was unequal settlement of foundations.

2.4.4 Caracas, 1968

Fintel[24] reported on the behaviour of structures in the earthquake. No prestressed concrete structures were in the area of high damage, and none of the 12 structures in Caracas with significant amounts of prestressing were affected.

2.5 DAMPING TESTS

Hisada and Nakagawa[25] (1956) dynamically tested a two storey prestressed concrete structure, 18 feet 5 inches high and 14 feet 10 inches by 18 feet in plan. Loading was applied by a shaking machine fixed to the roof slab. Damping was calculated from the resonance curves obtained experimentally. For vibrations of small amplitude, values from 3% to 5% of critical damping were measured, while for large non-linear vibrations the damping was from 6% to 10% of critical. Failure occurred by the formation of plastic hinges firstly at the ends of the beams and then at the column bases.

Penzien[26] (1962) carried out a series of tests on model prestressed concrete beams of dimensions 6 inches by 6 inches by 7 feet 6 inches. He set out to determine the damping characteristics of prestressed concrete using both steady state and transient vibrations. He measured values of damping of less than 1% critical viscous for beams in which no cracks were present. Upon the development of even microscopic tension cracks the value could be expected to rise to the order of 2% of critical. The previous history of loading was seen to be an important factor, especially when large dynamic loads had been applied and the beam had been loaded well into the cracking range. Damping from 3 to 6% of critical was present after cracking. It should be noted that the damping values obtained apply to members, but are not directly applicable

to structures because the whole mass of the structure must be considered.

Nakano[27] (1965) studied the lateral loading of a four storey model structure in prestressed concrete. The model consisted of a rectangular structural frame 13 feet 10 inches high and 8 feet 11 inches by 8 feet 6 inches in plan, supporting four slab floors. It was tested by applying alternating cycles of horizontal static load to each floor level. Load deflection diagrams were plotted at each storey. Recovery of deflection was good and consequently energy dissipation by plasticity had been relatively small. Values of percentage of critical damping were calculated for each storey. Typical results at the first storey were a variation of 3% to 7% over increasing loading stages in the test. Nakano pointed out that this is lower than the likely damping of reinforced concrete structures, and the consequent greater seismic response of prestressed concrete structures may necessitate the use of greater equivalent static lateral forces in their design. It was concluded from the tests that prestressed concrete frames can be capable of considerable ductility, provided care is taken in the design of the joints.

Although many full scale shaking tests have been carried out on prestressed concrete bridges to determine damping characteristics, there is little such information for actual prestressed concrete buildings. Allardice[18] (1966) reported the testing under small vibrations of a ten storey framed structure composed of reinforced concrete columns and relatively flexible prestressed concrete ribbed flat plate floors. A value of 2% critical viscous damping was measured. Also, recent tests in Japan by Nakano on a full scale four storey structure, comprising prestressed concrete columns and flexible reinforced concrete beams, showed 2% critical viscous damping for the structure under small amplitude vibrations.

2.6 TEST MEMBERS UNDER REVERSED CYCLES OF LOADING

The cyclic lateral loading of prestressed concrete portal frames was examined by Nakano[1] (1964). His test specimens consisted of three frames, 2 feet 11 inches in height and 8 feet 6 inches in span, with concentric prestressing in all the members. They were studied for their resistance against lateral force, their ductility, and their dynamic characteristics. The lateral loads that the frames sustained at failure were 1.52, 1.92, and 1.94 times the elastic design horizontal loads based on first cracking. The specimen which was ungrouted showed a decreased resistance to horizontal load of approximately 24 per cent, when compared with the grouted specimens.

The ratio of maximum horizontal deflection to the measured deflection corresponding to the design force was found to be 9 for frame No. 1, and for frames Nos. 2 and 3 was 12.5.

A limited number of cycles of alternating load were applied to the frames at a loading rate of one cycle per 52 seconds. Fig. 2.3 shows one set of load-deflection curves obtained. Significant area within the hysteresis loops was only present once load was taken close to the maximum resistance of the member.

The vibrating characteristics of the frame under horizontal impact loading were also studied. The percentage of critical viscous damping was found to be 4% after loading just beyond elastic design load, and 8% after the final loading.

Nakano concluded from these tests; "That the ultimate strength design method is applicable for prestressed concrete portal frames, that deviation of deflection characteristics under repeated loading is not considerable, that ample ductilities are guaranteed, and that increment of period of natural vibration and of fraction of critical damping with increment of load is small."

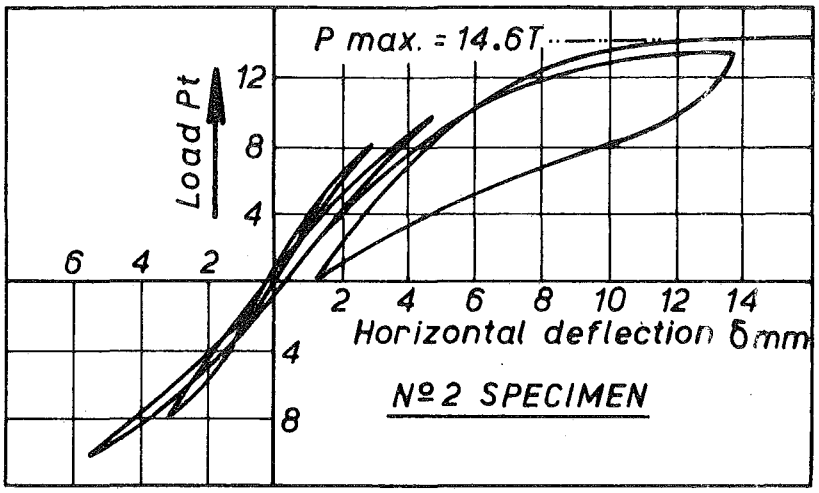

FIG. 2.3 : LOAD-DEFLECTION CURVES, AFTER NAKANO [1]

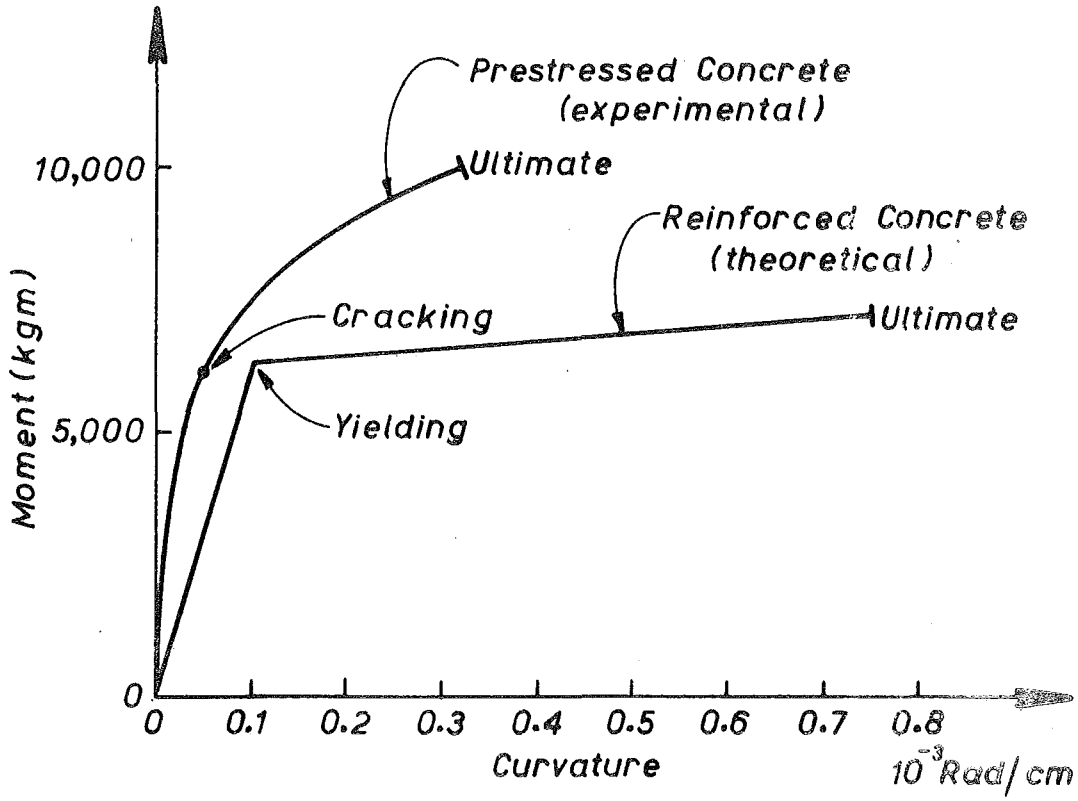

FIG. 2.4 : ENERGY ABSORPTION CONSIDERATIONS, AFTER DESPEYROUX [2]

The statement that "ample ductilities are guaranteed" would seem to apply to Nakano's tests rather than as a general conclusion. This should be so; firstly because careful detailing is required for ductility, and secondly because the ductility demands on prestressed concrete structures during earthquakes are not yet clear.

Inomata[28] (1969) made a comparative study of prestressed and reinforced concrete beams subjected to reversed loading. The beams had a span length of 8 feet 6 inches with a stub at midspan to give a simulated beam-column connection. Static cyclic loading was applied. A comparison was made of prestressed, partially prestressed, and reinforced concrete beams, with: (a) the same ultimate strength, and (b) the same working strength. For both design criteria the factors of safety against failure at working stress were higher for prestressed concrete than for reinforced concrete; for example, 3.5 for prestressed concrete and 2.4 for reinforced concrete beams conforming to case (a) above. Inomata recommended that, to provide adequate ductility and reduce excessive loss of stiffness, the ultimate limit load of a prestressed concrete member should be calculated in accordance with the F.I.P.-C.E.B. recommendations[29]. These require the calculation of the flexural ultimate limit strength on the basis of both reduced design strengths and limits of strain. The strain limits were; firstly, 1% maximum steel elongation, and secondly, a maximum concrete compressive strain of 0.0035. Inomata presented his deflection results in terms of ductility factors, which he defined as the ratio of the measured deflection under the maximum measured load to that under the limit load. The values obtained varied from 3.8 to 5.7 for prestressed concrete members, which he felt to be sufficient compared with the reinforced concrete members.

Entrican[30] (1969) tested the behaviour under cyclic load of a reinforced concrete beam containing a central unbonded prestressing

tendon. It was proposed that the addition of sufficient prestress in reinforced concrete frame members to create an initial concrete compression of about 250 psi would overcome the effects of shrinkage and microcracking. The cyclic load characteristics of the hybrid beam were compared with those of a conventional reinforced concrete beam. It was found that the prestressing tendon increased the moment resistance of the reinforced concrete section by 50%. Further, the load-deflection hysteresis loops plotted for the hybrid beam showed the best features for seismic resistance of both the component prestressing steel and mild steel. That is, there was less stiffness degradation than for the conventional reinforced concrete member due to the action of the prestressing tendon, but at the same time there was no loss of available energy dissipation due to yielding of the mild steel.

The work of Inomata[28] and Entrican[30] highlights the possible advantages of the use of non-prestressed steel at the joints of prestressed concrete frames. However there are associated difficulties in detailing for precast construction, and the extra problems involved are not warranted if a fully prestressed frame can be shown to be adequate for seismic resistance.

2.7 EFFECT OF RATE OF LOADING

Experiments have been carried out to determine the validity of using static cyclic loading, such as that used by Nakano[27] and Inomata[28], to represent the effect of relatively rapid vibrations such as would be experienced in an earthquake. Oladapo[31] (1964) described tests to investigate the effects of the rate of loading on the moment-rotation relationship of prestressed concrete beams. It was found that the moment-rotation relationship was displaced upwards as the rate of loading increased. This was due to the reduction of creep effects for increased loading rates. A typical set of tests by Oladapo compared loading to failure of identical prestressed concrete model beams over the time

periods of 1 second and of 40 minutes. For the dynamically loaded beam, moments were greater than in the statically loaded beam by 9% at the elastic limit and by 7% at rupture. There were also corresponding increases in flexural stiffness as the rotation at cracking was reduced in the dynamic case. The rotations at ultimate were similar. From these results static cyclic loading tests would appear to give slightly conservative results as the probable greater response of the structure due to apparent greater stiffness would be more than offset by the apparent greater strength.

Later tests by Spencer[32] (1966) involved cyclic loading tests to measure stiffness and damping properties of prestressed concrete members. End rotations were applied, which varied about a mean of zero, with frequencies of 0.5 to 2.0 c.p.s. They produced either uniform shear or uniform moment loading up to failure. Stiffness and damping values were found to be dependent on the type of loading, but were independent of frequency and the number of cycles applied.

2.8 WORLD EARTHQUAKE ENGINEERING CONFERENCES

The work of Hisada and Nakagawa[25], which was presented at the First World Earthquake Engineering Conference, California (1956), has already been discussed. Although no paper was presented on the seismic resistance of prestressed concrete at the Second World Conference (1960), a significant number of papers on this topic were presented at the Third World Conference, New Zealand (1965). Both Despeyroux[2] and Guyon[3] emphasised the energy absorbing capacity of prestressed concrete as represented by the area under the moment-curvature curve for monotonic loading. Despeyroux presented the comparative curves shown in Fig. 2.4 and concluded that there was no reason for the area under the curve for prestressed concrete to be systematically smaller than that for reinforced concrete, and could in fact be the contrary. However, in the subsequent discussion to this paper it was pointed out that the critical

factor affecting the response of a structure under the cyclic loading from most earthquakes is not the energy "absorption" characteristics of its members, but rather their energy "dissipation" capacity. Although the energy absorbed by a prestressed concrete member and a reinforced concrete member may be the same for loading in a single direction, the greater elastic recovery of the prestressed concrete member will result in a lower energy dissipation for cyclic loading. (This distinction is apparently still not recognised as being important in a recent publication by Lin[5] (1970).)

Further papers presented at the Third World Conference were by Sutherland[4] and Nakano[27] which have been discussed elsewhere in this review. Also, Zavriev[33] reported some large scale investigations of the seismic behaviour of prestressed concrete bridges in the Soviet Union. He felt that the use of prestressed concrete in seismic resistant structures was expedient. Under moderate earthquakes the resistance to plastic deformations would result in little damage to structures and he felt that under heavy earthquakes the behaviour of prestressed concrete sections would be similar to that of reinforced sections, thus eliminating the characteristics of prestressed concrete which increase dynamic loads.

At the Fourth World Earthquake Engineering Conference, Chile (1969), only one paper was presented specifically on prestressed concrete. This was by Spencer[6] and is discussed in a subsequent section.

2.9 F.I.P. CONGRESSES

At the Fifth Congress of La Fédération Internationale de la Précontrainte in Paris (1966) several papers relating to research on the seismic resistance of prestressed concrete were presented. Hognestad[34], reporting on research on prestressed concrete outside of Europe and U.S.S.R., listed the three principal subjects of research as being fire resistance, earthquake effects, and side effects of these two.

He commented on the importance of jointing of prestressed, precast elements under seismic conditions and felt that the study of this question had been relatively neglected. Ligtenberg[35] reported on research on prestressed concrete in Eastern Europe but made no mention of seismic investigations. Gvodzev[36] reported on research on prestressed concrete in U.S.S.R. and neighbouring countries. Considerable attention had been given to fatigue loading, but there was no mention of seismic research. The F.I.P. Commission on Seismic Structures presented a document "General Principles of Earthquake - Resistant Design of Prestressed Concrete Structures"[37]. This report indicated the need for consideration of regional and local conditions, permissible degrees of damage, safety of structures and foundations, and the formation of ductile joints and connections.

At the Sixth Congress in Prague (1970) one significant contribution to seismic design was made by a further report from the F.I.P. Commission on Seismic Structures[38]. This is discussed in a later section.

2.10 RESPONSE ANALYSES OF FRAMED STRUCTURES

Spencer[6] (1969) studied the non-linear dynamic responses to a strong earthquake of two reinforced, and six prestressed concrete versions of a twenty storey framed structure. An idealized bilinear moment-rotation hysteresis loop for the prestressed concrete members was used in the analysis. The effects on response and energy dissipation of different member properties, different amounts of hysteretic damping, and two different viscous damping mechanisms were compared. The excitation used in each analysis was the first 8 seconds of the accelerogram of the El Centro 1940 earthquake, N-S component. The prestressed concrete structures had higher lateral displacements and interstorey drifts than the comparable reinforced concrete structures. However the section ductility requirements of

the prestressed concrete structures were markedly lower. The maximum rotation at the girder plastic hinge of the prestressed concrete frames was 5.4 times the rotation there at first cracking of the concrete; for the reinforced concrete frames the maximum rotation at the girder plastic hinge was 16.8 times the rotation there at first yield of the steel. Spencer explained this apparently surprising result by saying that the difference was partly due to the greater hinge length assumed for the prestressed concrete members. He justified this assumption on the grounds that the prestressing steel delays the development of curvature concentration due to yielding.

This paper was a significant beginning to the non-linear response analysis of prestressed concrete structures. From this study it appears that a prestressed concrete structure similar to that analysed could be designed to withstand a strong earthquake. There would apparently be no structural damage to the prestressed concrete members, but non-structural damage arising from greater interstorey drifts may be greater than with a reinforced concrete frame.

The accuracy of the results obtained was very dependent upon such factors as;

(a) the correct representation of damping,

(b) whether the analysis technique of taking the same initial stiffness for the prestressed concrete as for the reinforced concrete members is reasonable;

(c) the correct assumption for the plastic hinge lengths.

The final answer will only become clearer as more such analyses are carried out.

2.11 PRINCIPLES AND RECOMMENDATIONS FOR SEISMIC DESIGN

Several recommendations for the seismic design of prestressed concrete structures have been published.

2.11.1 P.C.I. Principles

The American P.C.I.[39] (1966) have presented "Principles of the Design and Construction of Earthquake Resistant Prestressed Concrete Structures". The recommendations allow for design by elastic theory using Chapter 26 A.C.I. 318-63[40] with a 25% reduction of all moments, shears and loads in place of the normal $\frac{1}{3}$ stress increase. Alternatively, ultimate strength theory may be used provided the service load deformations are checked. Special attention is devoted to connections.

It should be noted that ultimate strength design by the A.C.I. 318-63 code[40] or A.C.I. 318-71 code[41] requires the use of the same load factors for prestressed concrete as for reinforced concrete.

2.11.2 N.Z.P.C.I. Recommendations

N.Z.P.C.I.[42] (1966) have published "Seismic Design Recommendations for Prestressed Concrete". The ultimate strength design method is recommended, and minimum load factors which are greater than those of the A.C.I. codes[40,41] are suggested. Other recommendations are that all prestressing tendons should be fully grouted throughout their length, and that where structures incorporate mortar joints suitable binding or enclosure of the joint itself should be provided to prevent loss of material.

2.11.3 F.I.P. Commission Report

The F.I.P. Commission on Seismic Structures[38] reported to the Congress of the F.I.P. in Prague, 1970. This report complemented the Commission's previous document[37].

The report acknowledges that to give complete protection against earthquakes is not economically feasible. Instead it suggests; firstly, that a structure should be designed in such a way that member deformations causing a significant loss of prestress, and hence reducing the serviceability for normal use, should be prevented in moderate earthquakes

which occur occasionally (for example, once in 10 years). Secondly, collapse or serious damage should be avoided in severe earthquakes which very seldom occur (for example, once in 100 years).

The requirement for a moderate earthquake is satisfied provided the elastic limit of the prestressing steel is not exceeded. In these circumstances there would be no permanent set in the steel and the prestress would resume its original value after the earthquake motions ceased. The maximum deformations for the severe earthquake conform to the ultimate limit state specified by the F.I.P.-C.E.B. Joint Committee[29]. Thus the maximum allowable concrete compressive strain in flexure is 0.0035. It is also suggested by the report that statically determined values of modulus of elasticity, steel stress-strain relationships, and member strengths may be used as approximations for the dynamic values in design calculations.

Attention is drawn to the need to supply adequate ultimate strength for both directions of loading in the joints of rigid framed structures. It is also noted that sufficient transverse web reinforcement must be provided in the members of a structure to ensure that their capacity is governed by flexure and not shear. The use of extra lateral reinforcement to ensure adequate ductility in beams and columns is recommended.

It may be commented that the member curvature limits for moderate and severe earthquakes are rather difficult criteria for the design engineer to implement with the current state of knowledge. A non-linear dynamic analysis would be necessary to determine the likely member curvatures in a frame under such earthquakes, in order to verify that the limits are not exceeded.

2.12 CONCLUSIONS

Most structures containing prestressed concrete elements which have been subjected to earthquakes have performed well. Failures which have occurred appear to have been due mainly to failure of the supporting structure or of joint connections. However, there is relatively little information on the behaviour of fully framed prestressed concrete structures under strong earthquakes.

From the results of testing of prestressed concrete members the following three points are apparent. Firstly, the percentage of critical viscous damping for members is less than 2% prior to cracking, but between 3 and 6% subsequently. A second conclusion arises from monotonic loading tests, which have shown that quite large ductilities are possible. Thirdly, most tests under cyclic loading have been for relatively low loading intensities and the ensuing small area within the hysteresis loops would be expected. However, little is known of the energy dissipation capacity of prestressed concrete members under high intensity cyclic loading. The energy dissipation would be greater for partially prestressed members once the mild steel yields, but the joints of such members present particular difficulties for precast construction.

One non-linear dynamic analysis of a prestressed concrete structure has supported the intuitive assumption that such structures will have a greater response than a comparable reinforced concrete structure. Nevertheless it was found that the rotational ductility factor requirements of the members were lower for the prestressed concrete structure. The results of more such analyses will clarify whether or not the use of higher load factors in the ultimate strength design of prestressed concrete structures for seismic loading is warranted.

It is apparent from the literature that research is needed in the

following areas: damping tests of prestressed concrete structures, high intensity cyclic loading tests of prestressed concrete members, tests of joint details under moment reversals, and non-linear seismic analyses of prestressed concrete structures.

CHAPTER 3

HIGH INTENSITY CYCLIC LOADING OF PRESTRESSED CONCRETE BEAM-COLUMN ASSEMBLIES

SUMMARY

A series of four tests were conducted on full size, precast, prestressed concrete beam-column assemblies under reversed cyclic loading of high intensity. The test variables included the amount of transverse confining steel for ductility, and the formation of the plastic hinge in either the beam or the column of the assembly. The results presented include the moment-rotation and load-displacement characteristics of the members, which indicate their respective ductilities and energy dissipation capacities. Curvature distribution plots, deflection profiles, and steel strains in the stirrups are also discussed.

3.1 INTRODUCTION

One of the critical factors affecting the seismic resistance of prestressed concrete structures is the behaviour of the members under cyclic load. Previous researchers have subjected prestressed concrete members either to fatigue-type loading, for example[7,8,9], or cyclic loading at levels rather lower than the maximum strength[1,27,28,32]. It would seem to be necessary, if one is to simulate the effect of a severe earthquake, to study the cyclic load characteristics of members under high intensity cyclic load including the behaviour subsequent to crushing of the cover concrete. The object of the tests reported here was to make such a study.

Three specific details sought from the tests were the likely values of ductility, energy dissipation, and stiffness degradation to be

expected from prestressed concrete beams and columns. Firstly, it was desired to assess the available ductility in members designed according to current prestressed concrete codes, and to find if confinement by special transverse reinforcement for ductility is necessary in seismic resistant prestressed concrete members. Secondly, the energy dissipation as shown by the area within the hysteresis loops has been small for previous low intensity cyclic loading tests, but has yet to be determined when large post-elastic deformations have occurred. Thirdly, the stiffness degradation of the members under cyclic load may have a significant influence on the response of the structure to an earthquake, and is a necessary parameter for seismic analyses.

Some definitions must be given for terms which will be referred to in this chapter. The three general regions of a moment-rotation curve for a prestressed concrete member under monotonic loading are illustrated in Fig. 3.1. These correspond to an initial stiffness for the uncracked concrete section, a reduced stiffness after cracking of the section, and a further reduced stiffness once the prestressing steel or the concrete begin to behave inelastically. These three regions will be referred to as the "elastic", "cracked elastic", and "inelastic" regions. Also, the ratio of the rotation over a small increment of length to the rotation over that length at first cracking will be referred to as the "rotational ductility factor", and the ratio of the perpendicular displacement at the end of the member to the displacement there at first cracking will be referred to as the "displacement ductility factor".

A detailed description of the material properties, equipment, and testing procedure used in these tests is given in Appendix B.

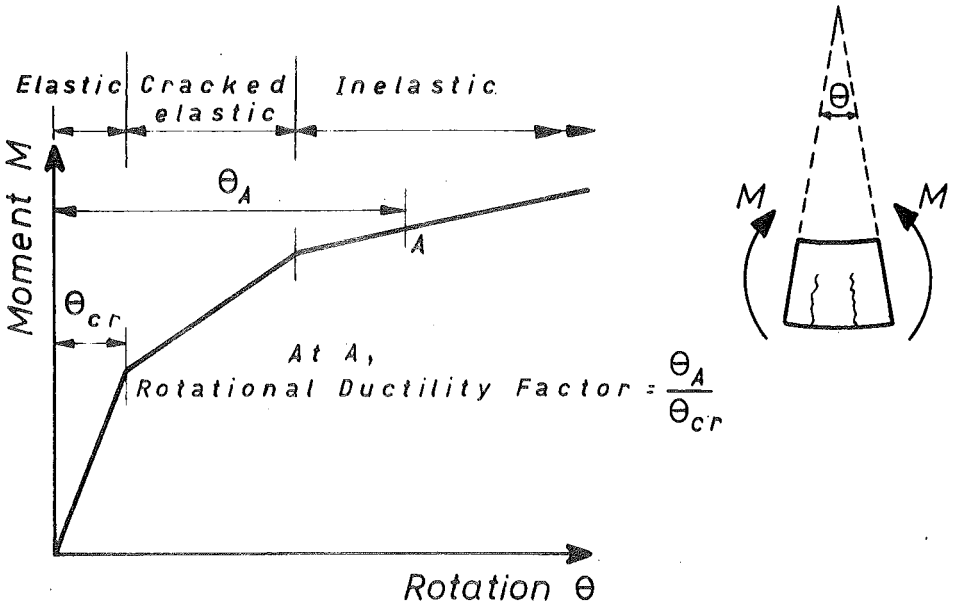

FIG. 3.1 : IDEALIZED MOMENT-ROTATION CURVE

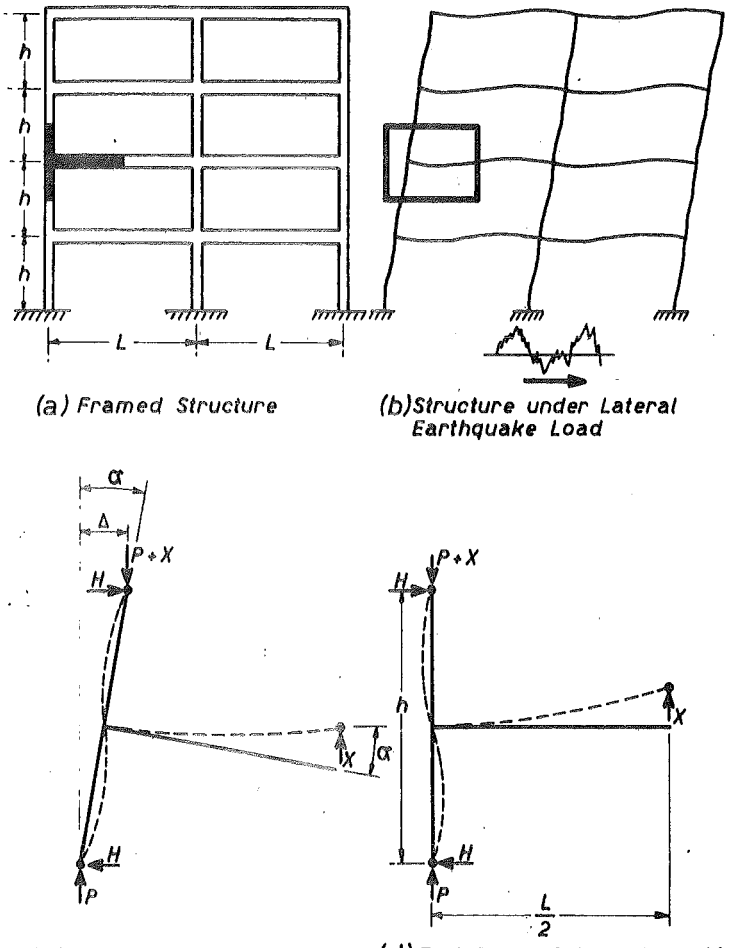

FIG. 3.2 : BEAM-COLUMN TEST SPECIMEN

3.2 EXPERIMENTAL PROGRAMME

The details of the experimental programme are as follows:

3.2.1 Selection of Test Specimen

The test specimen is the portion of a multistorey prestressed concrete frame shown shaded in Fig. 3.2(a). The structure under lateral inertia loading due to an earthquake is shown in Fig. 3.2(b). Fig. 3.2(c) is an isolated view of the external beam-column test assembly under consideration. Points of contraflexure are assumed to occur at the mid-points of the members. An imposed horizontal displacement , Δ , induces horizontal and vertical reactions, H and X. In Fig. 3.2(d) the entire beam-column assembly has been rotated until the two column inflection points are on the same vertical line, giving a more convenient orientation for testing purposes. The column axial load, P , represents the loading due to firstly, the weight of the building above the particular assembly, and secondly, the over-turning moment on the structure. The reversible load, X , applied at the end of the beam and the reactive lateral loads, H , induced at the ends of the column represent the shears applied by the earthquake.

The behaviour of joints such as the test specimen is a critical factor affecting the behaviour of building frames under seismic load reversals. Of particular interest is the behaviour of the joint assembly formed when precast members are post-tensioned together with mortar joints at the critical sections.

3.2.2 Earthquake Loading Representation

The test specimens were subjected to a series of high intensity static load reversals. The sequence of loading was similar to that followed by Hanson and Conner[43] for tests on reinforced concrete beam-column joints, except that greater deformations were enforced. This loading sequence is said to be representative of the effect of two

major earthquakes on the structure. The origin of this simulation is not clear, and it is apparent that for a particular earthquake the number and magnitude of the load reversals will depend on the properties of the earthquake itself and of the structural system. However, it was felt that the important requirement of the loading simulation used was to generate a post-elastic loading history covering the likely range of deformations from moderate to severe earthquakes. The extent of the imposed deformations was based on the rotational ductility factor at the plastic hinge. For the first test (Unit 1) in which the plastic hinge formed in the beam, the maximum value taken for this factor in the loading sequence was 5. The basis for this figure was that the only non-linear dynamic analysis of a prestressed concrete framed structure available, which was carried out by Spencer[6], showed this to be the order of maximum beam rotational ductility factor (same definition as in this thesis) required. In subsequent tests the maximum rotational ductility factors for the test sequence were increased to approximately 15. The pattern of the loading sequence used for Units 1 and 2 is illustrated in Fig. 3.3, with the magnitude of rotations as for Unit 2. The loading sequences for Units 3 and 4 were based on rotations of the plastic hinges in the columns and a range of likely column rotational ductility factors under seismic conditions was considered, as shown in Fig. 3.4. The rotational limits for each half-cycle were determined from the critical plastic hinge for the particular direction of loading in that half-cycle.

Apart from the magnitude of the applied deformations, the only deviation from Hanson and Conner's sequence was to precede and follow the earthquake simulation by three cycles to design load, to determine the likely behaviour of the members under gravity loading prior and subsequent to the earthquake. Each test was concluded by loading the unit in both directions until either reaching the limit of the available

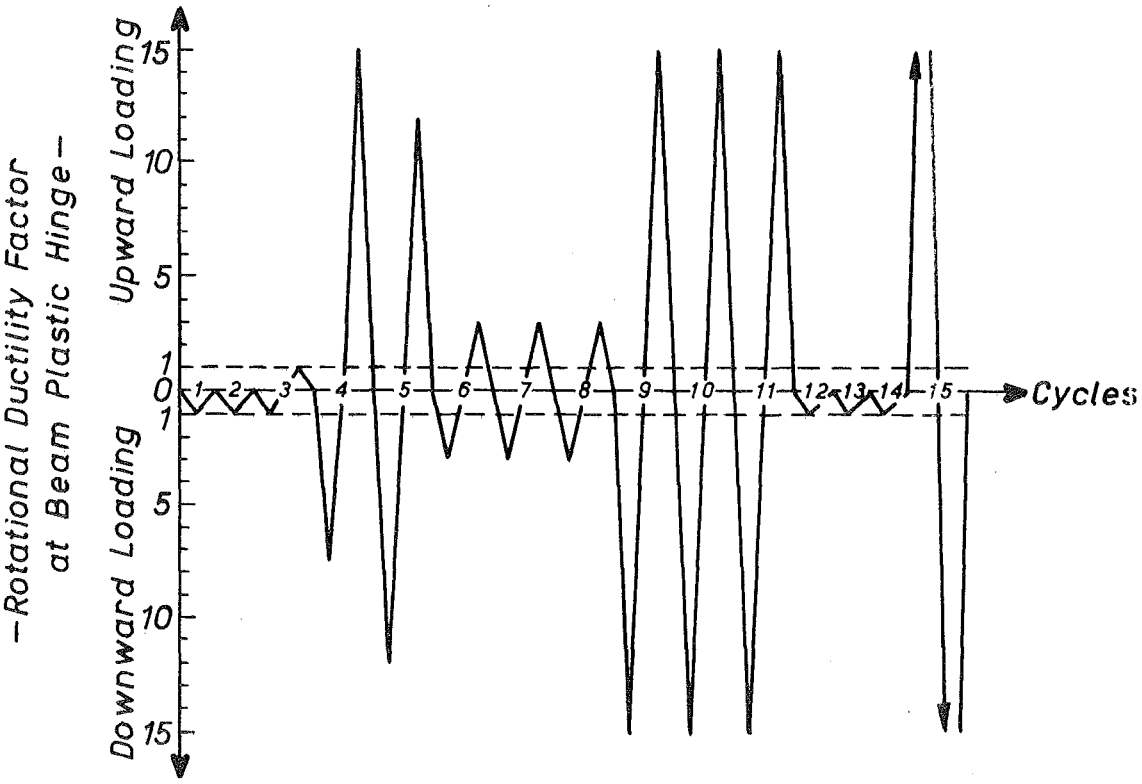

FIG.3.3 : EARTHQUAKE LOADING SEQUENCE FOR UNITS 1 & 2

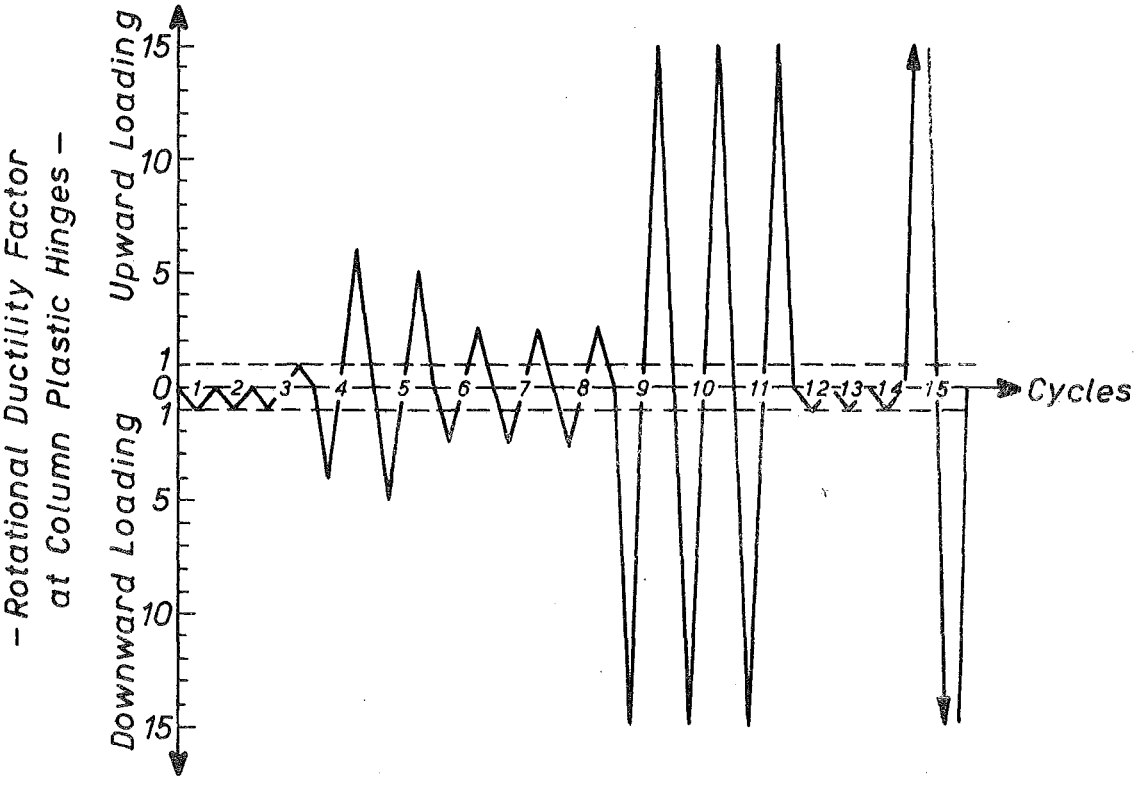

FIG.3.4 : EARTHQUAKE LOADING SEQUENCE FOR UNITS 3 & 4

deflection, or sustaining failure.

3.2.3 Effect of Rate of Loading

Static cyclic loading was used because of the associated ease of collection of test data. The work of several investigators appears to justify the use of this type of loading to represent the rapid load reversals of an earthquake. The research of Oladapo[31] and Spencer[32] was discussed in Section 2.7. Oladapo showed that static loading gives conservative strength values relative to dynamic loading for prestressed concrete beams, while making little difference to the ultimate curvature, and Spencer found the stiffness and damping of cyclically loaded prestressed concrete beams was independent of frequency over the range 0.5 to 2.0 c.p.s. Similarly it is claimed[43] that for reinforced concrete members the strength and energy absorption characteristics are increased with increased speed of loading. Various studies, for example [44,45], comparing the static and dynamic loading of the component concrete and steel materials have indicated an increase of strength for the dynamic case.

More recent research has been carried out on this question by Takeda, Sozen and Nielsen[46]. A vertical reinforced concrete member, with a mass on the top, was tested under static cyclic loading. A load-displacement model was then postulated to represent the hysteresis loops obtained. The expected response at the centroid of the mass for a base motion of the El Centro 1940 N-S earthquake record was then calculated, using the proposed load-displacement relationship and a step-by-step numerical integration method. This was compared with the actual dynamic response of the mass obtained by applying the displacement record of this earthquake to the base of the system. Good correlation was obtained between the measured and calculated response histories.

The consensus of research information available would seem to justify the use of static cyclic loading to represent seismic effects, and indicate that the ensuing results are likely to be conservative.

3.2.4 Design of Test Units

The four test units consisted of full-scale elements of dimensions as shown in Figs. 3.5 and 3.6. Details of the design stresses and material strengths are given in Appendix B. The columns were pre-tensioned. The beams were lightly pretensioned for handling stresses, and post-tensioned with cables passing through the column into an exterior anchor block. Freyssinet anchorages were used and the cables were grouted. One inch thick moist pack mortar joints were formed between the elements. The section sizes were similar to those of an existing prestressed concrete two storey framed structure (see frontispiece). In the prototype structure the prestressing force was concentric in the joint region to give maximum flexural strength under seismic reversals of load, and this configuration was reproduced in the test specimens. The post-tensioning cables in the beams of the test specimens were not draped, with the result that prior to applying the earthquake loading in the tests the members were in direct stress only. This represents the situation achieved in common design practice in New Zealand, when the gravity loads considered to be present with seismic loading (that is, dead load plus generally one third live load) are balanced by the prestressing uplift and thus the earthquake moments act on a frame with direct stresses only. In the prototype structure the mortar joints had a one half inch recess for architectural reasons. This detail was also reproduced in the test specimens.

In the test specimens there were three variables:

(a) Position of formation of the plastic hinges

Units 1 and 2 were designed to form plastic hinges in the beam at the joint, and Units 3 and 4 were designed to form plastic hinges in the

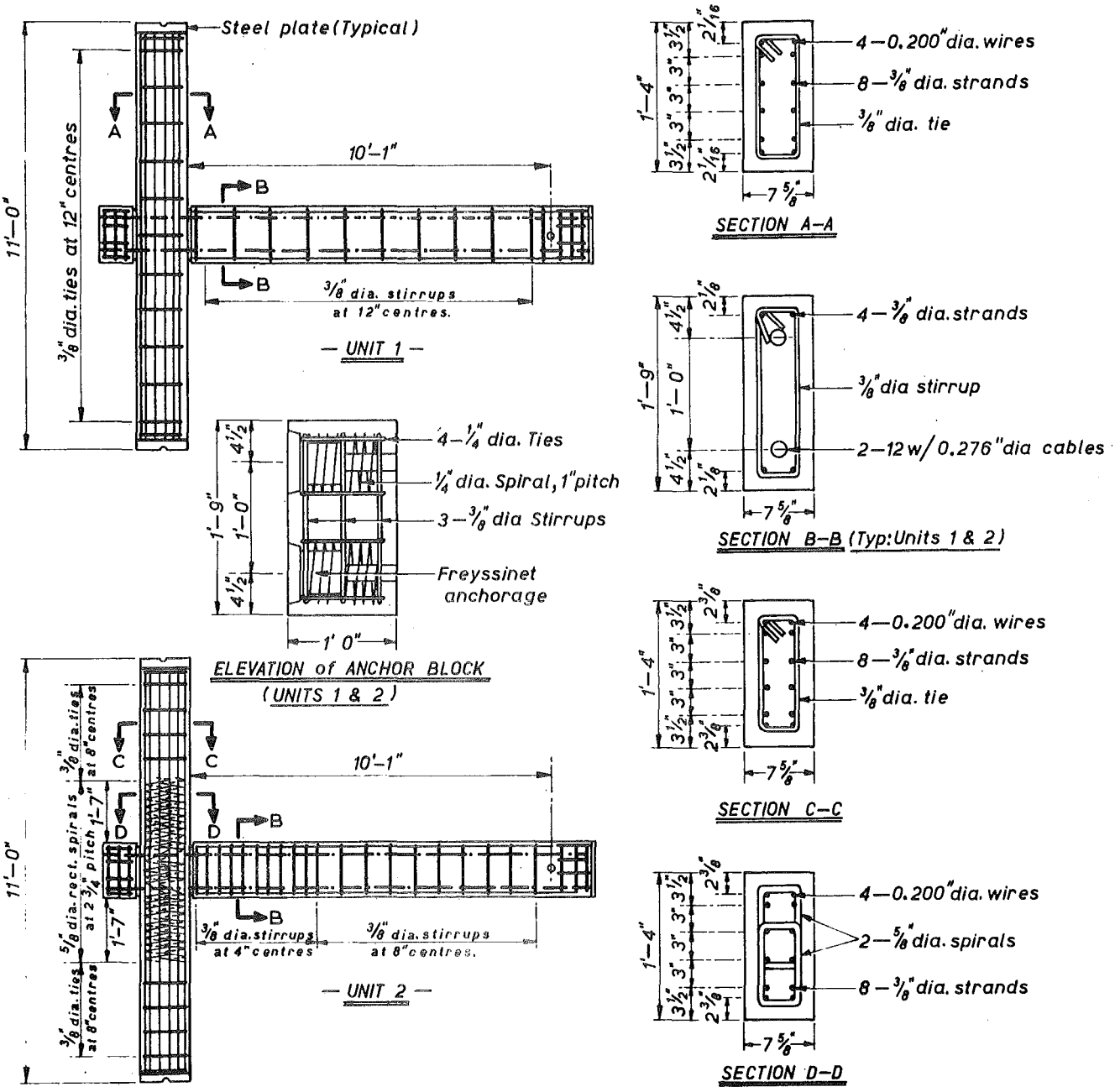

FIG. 3.5 : DETAILS OF UNITS 1 AND 2.

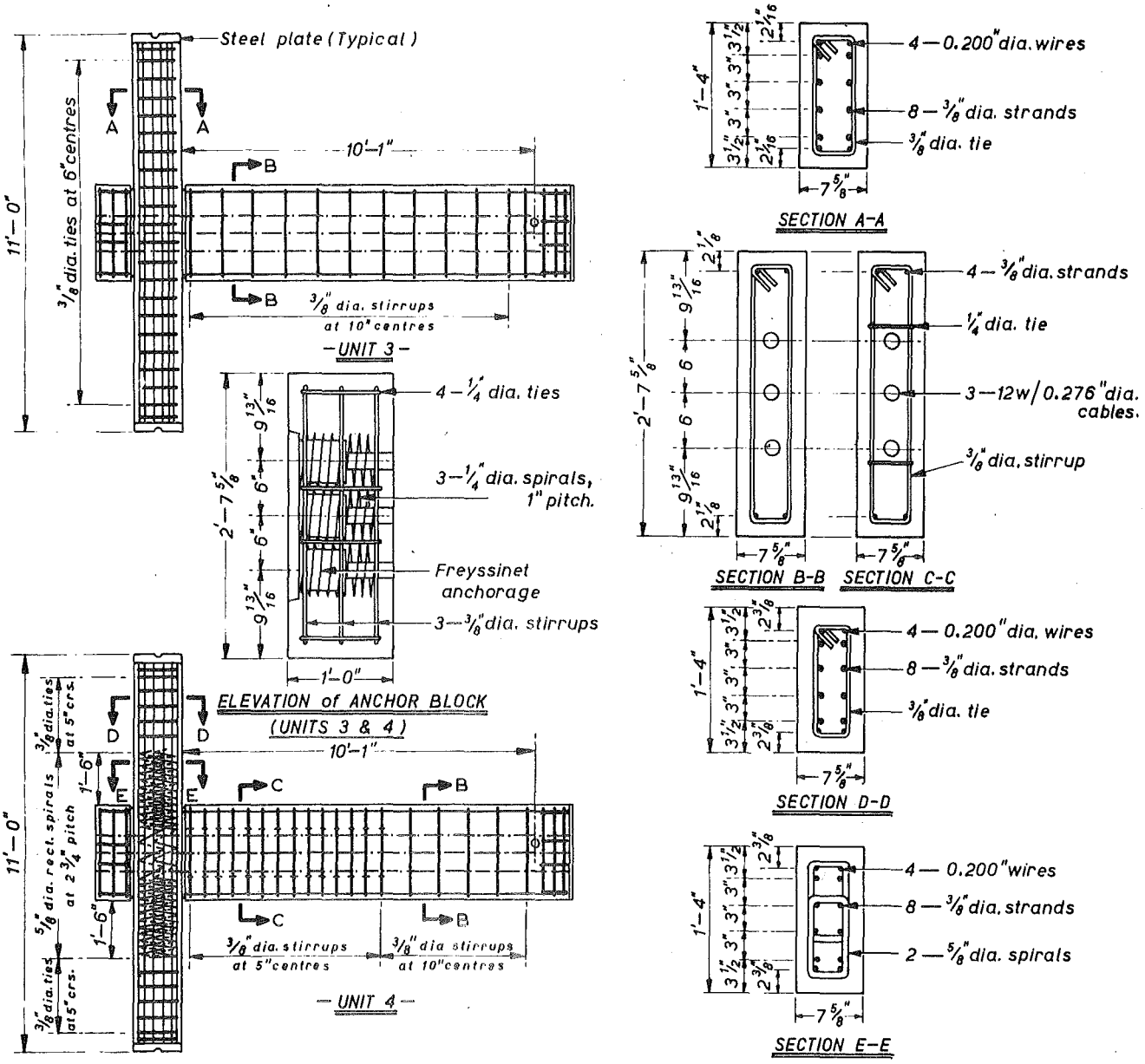

FIG. 3.6 : DETAILS OF UNITS 3 AND 4.

column immediately above or below the beam connection. The situation represented by Units 3 and 4 is typical of many prestressed concrete framed structures. This arises from the design of long spans requiring large cable eccentricity, and hence a large beam section size with a consequent high ultimate moment capacity. The columns of the frame, even when catering for the required seismic design moment, may have a very much lower ultimate moment capacity than the beams. Hence under earthquake loading the plastic hinges would form in the column rather than in the beam in many prestressed concrete frames. It is recognised that it is desirable to have plastic hinges forming in the beams rather than in the columns, because in this type of failure mechanism considerably greater energy absorption is possible[47]. However this condition is not too critical for structures of three storeys or less.

(b) Confinement of the Concrete

The effect of varying the degree of confinement on the ductility of the section was also studied. The mild steel stirrups and ties in Units 1 and 3 satisfied the shear requirements of the commonly used codes for prestressed concrete: A.C.I. 318-63[40], American P.C.I.[48], and British CP115[49]. These codes contain no requirements for special transverse reinforcement at beam-column joints for ductility. On the other hand Units 2 and 4 contained special transverse steel for confinement. For reinforced concrete, recommendations for the amount of special transverse steel required are given by Blume, Newmark, and Corning[50] and the SEAOC code[51]. However, since the column hooping recommended by those authorities[50,51] is to preserve the axial load carrying capacity of the concrete after spalling of the cover concrete, there is no reason why the same recommendations should not be taken as a guide for prestressed concrete. The column regions adjacent to the joint were provided with approximately one half of the rectangular spiral steel required by the SEAOC code for special transverse

reinforcement. Only one half of the recommended amount was placed, since it is considered that the recommendations are very conservative for columns with small cross-sections in which the ratio of gross concrete area to area of concrete core is high. Even so, very heavy hooping was required. The transverse reinforcement in both Units 3 and 4 columns satisfied the volume of hoop binding required by the F.I.P.- C.E.B. recommendations[52], but neither satisfied the minimum spacing requirements (a $2\frac{3}{4}$ inch pitch was used for Unit 4, whereas the recommended spacing was 0.2 of the smallest dimension of the bound core, that is less than 1 inch in this case). It appears that these recommendations are not realistic for small columns such as would be found in a frame of three storeys or less. In Units 2 and 4 the shear reinforcement in the beams satisfied the SEAOC code. The shear capacity of the columns in these units was also adequate, but no attempt was made to analyse the shear strength of the joint region, because of the complication of the arrangement of the prestressing tendons across and down the depth of the joint region and the confining effect of the anchor block.

(c) Binding of Mortar Joints

When considering the behaviour of packed mortar joints under reversed loading of high intensity, the N.Z.P.C.I.[42] recommends that "suitable binding or enclosure of the joint itself should be provided to prevent loss of material". To study the effect of binding, Units 2 and 4, which were detailed for ductility, had the mortar joint bound internally with a light wire stirrup, whereas Units 1 and 3 had the joint moist packed without binding. In all units the interfaces of the precast members at the joints had been roughened to a depth of approximately 1/16 inch to help hold the mortar.

3.2.5 Summary of Testing Procedure

The test rig with a unit under test is shown in Fig. 3.7. For Units 1 and 2 a constant axial load of 100 kips was applied to the column through a hydraulic jack. This column load was approximately 0.13 of the axial load capacity of the column and was chosen to represent the loads carried by a column in the lower storeys of a building frame. For Units 3 and 4, where the column loading was critical, axial loads were varied about this mean value to simulate the effect of varying axial load with lateral overturning moment. The beam end was loaded by two 35 kips mechanical screw jacks for upward and downward loading. The use of screw jacks enabled a controlled displacement to be applied to the beam end. The time taken to load each unit through the cycles of the loading sequence, and to collect the test data, was 10 to 15 working days.

3.3 TEST RESULTS

A detailed description of the performance of each unit will be included in the discussion of the moment-rotation and moment-displacement characteristics. The appearance of the units during testing is shown in a subsequent section.

3.3.1 Moment-Rotation and Moment-Displacement Characteristics

Throughout the tests the rotations were recorded at the plastic hinge positions by dial gauges attached to frameworks around the members. As expected, the plastic hinges formed in the beams of Units 1 and 2, and the columns of Units 3 and 4. Figs. 3.8 and 3.9 illustrate the moment-rotation curves for 12 inches plastic hinge lengths on the beams adjacent to the columns of Units 1 and 2. For comparison the plots of plastic hinge moment against beam end displacement for these units are shown in Figs. 3.10 and 3.11.

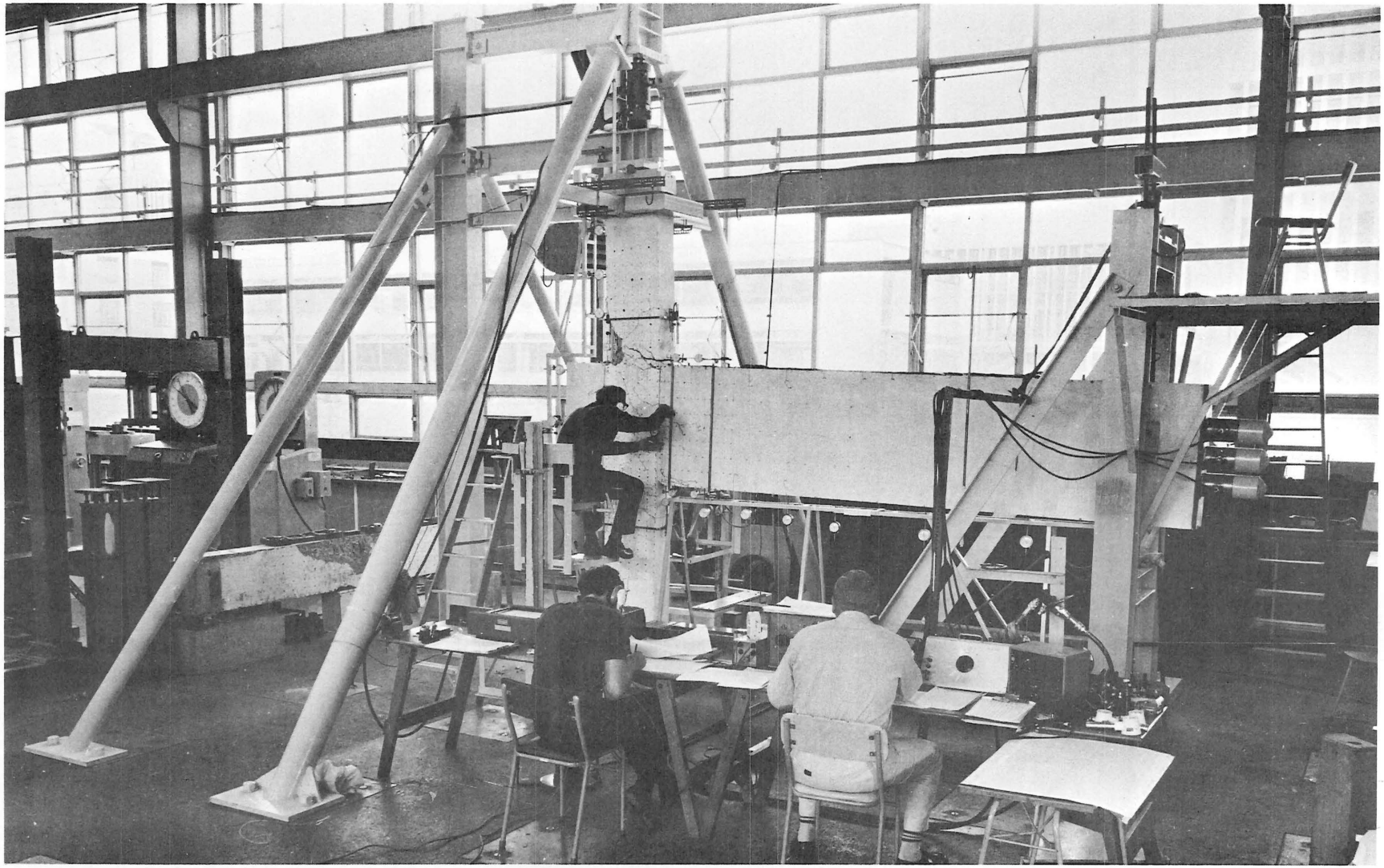

FIG. 3.7 : UNIT 4 UNDER TEST

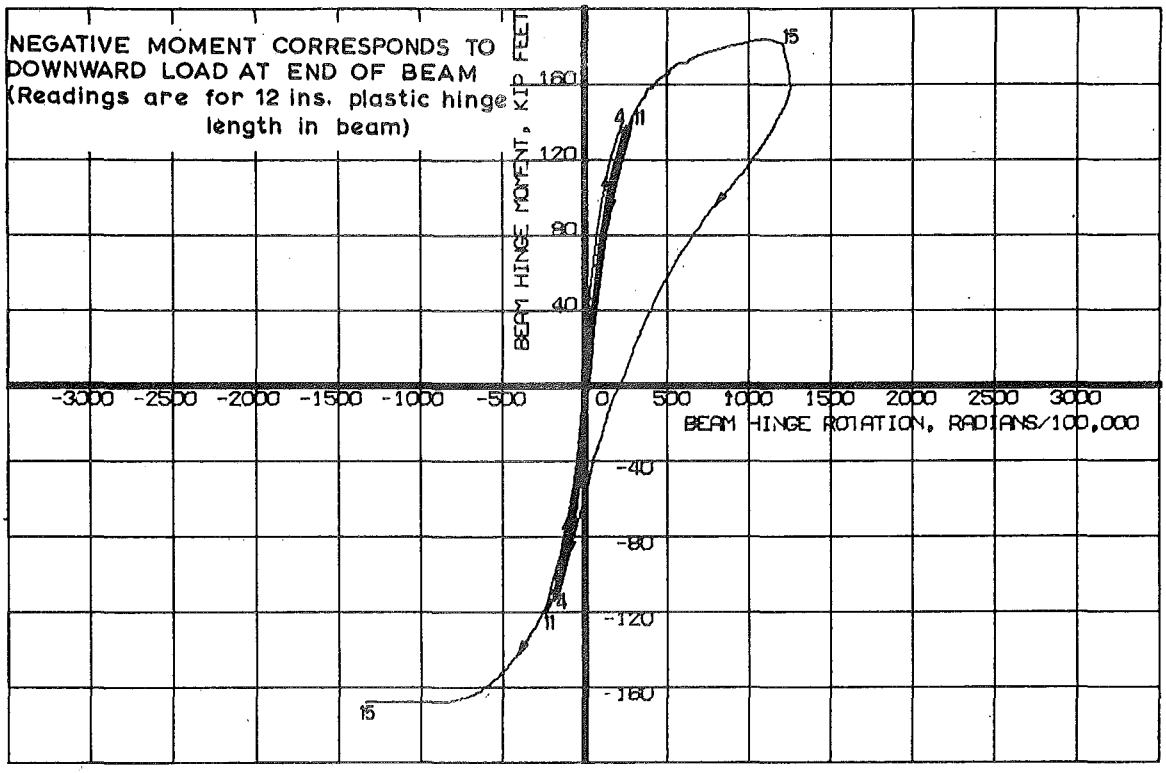

FIG. 3·8: MOMENT-ROTATION CURVES FOR UNIT 1.

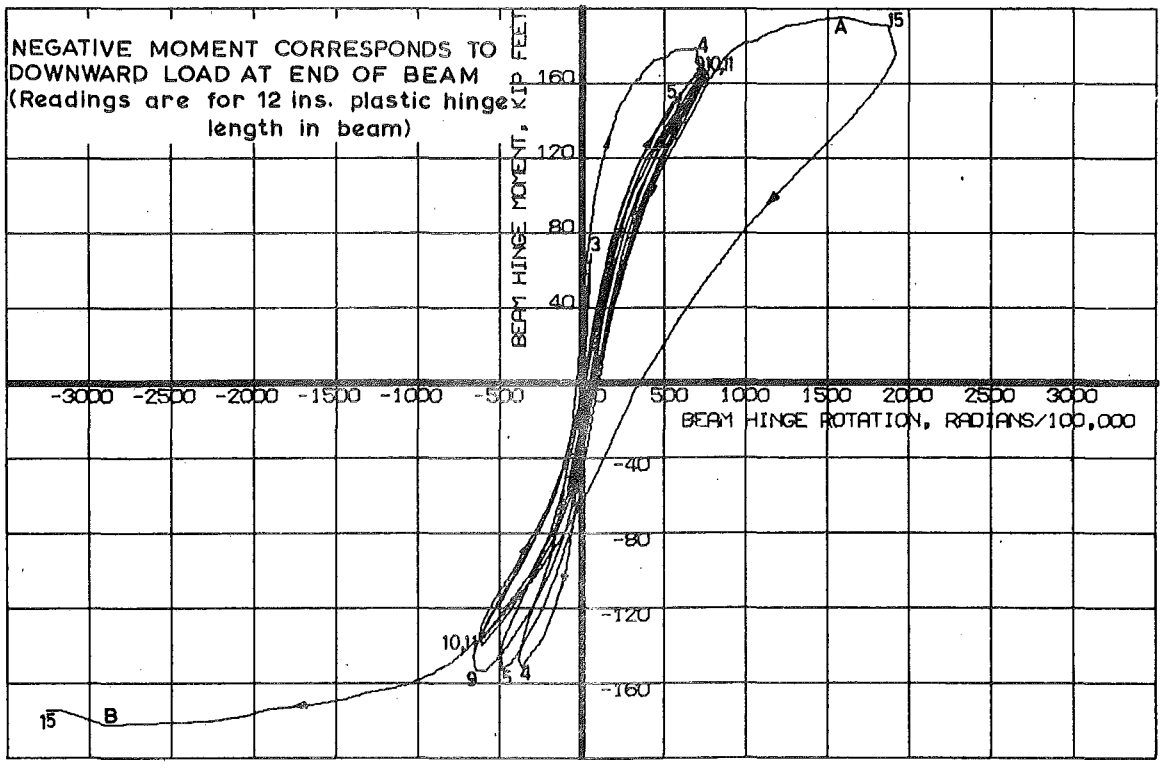

FIG. 3·9 : MOMENT-ROTATION CURVES FOR UNIT 2.

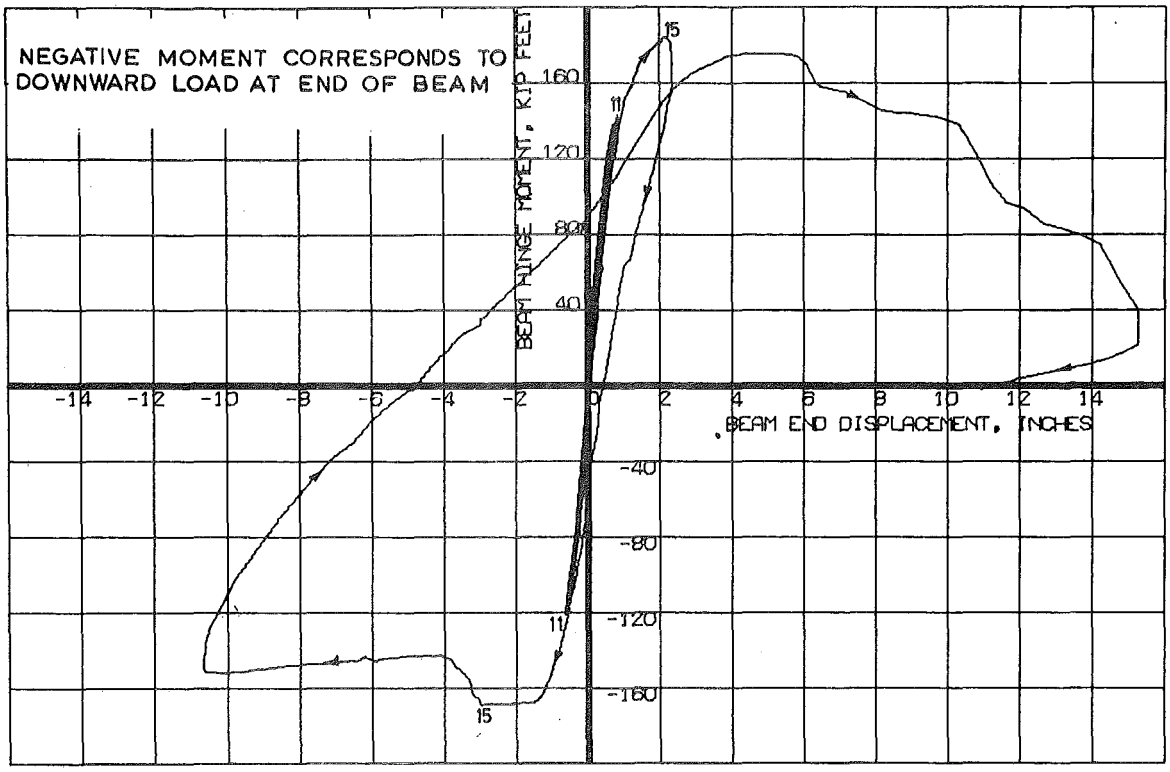

FIG. 3·10 : MOMENT-DISPLACEMENT CURVES FOR UNIT 1.

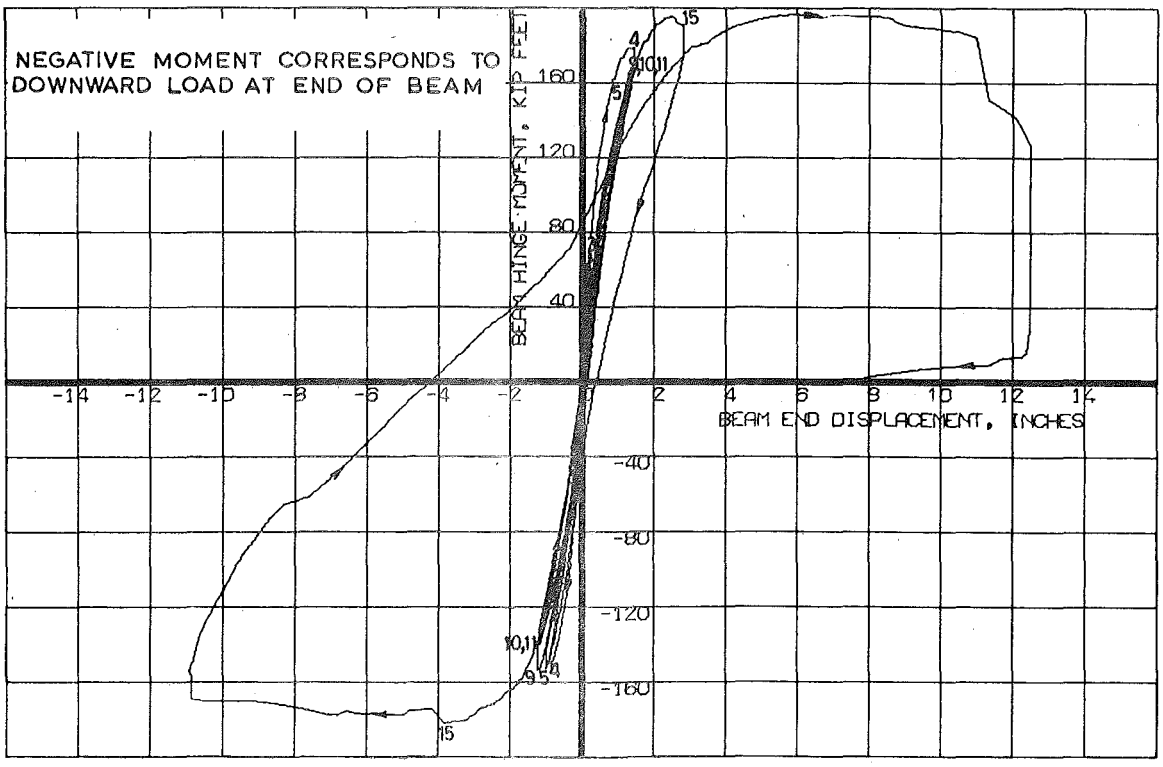

FIG. 3·11 : MOMENT-DISPLACEMENT CURVES FOR UNIT 2.

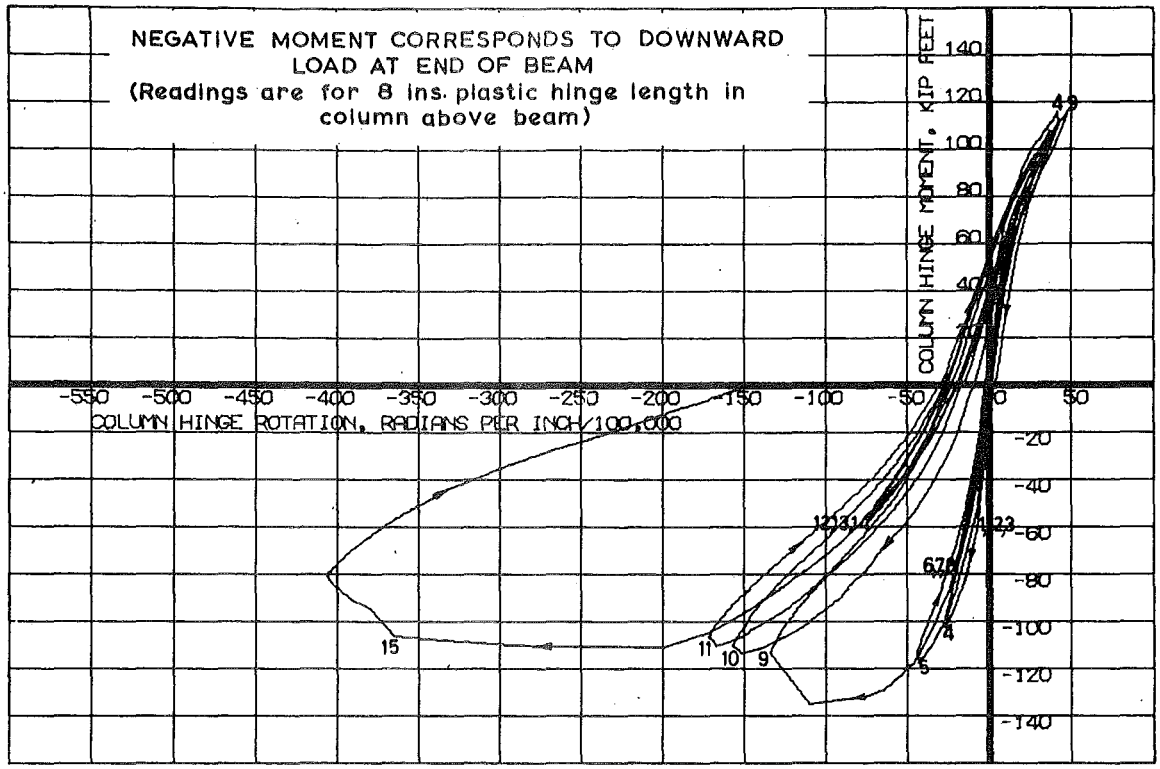

(a) Upper Column Plastic Hinge.

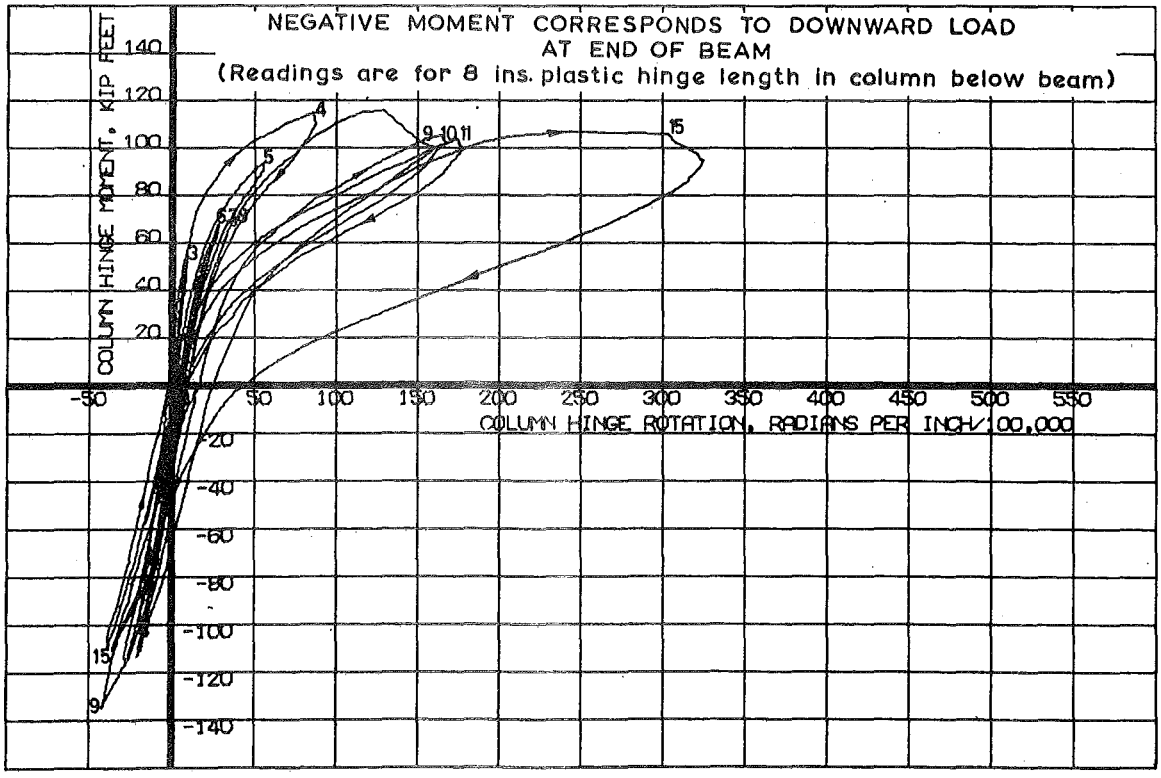

(b) Lower Column Plastic Hinge

FIG. 3·12 : MOMENT-ROTATION CURVES FOR UNIT 3.

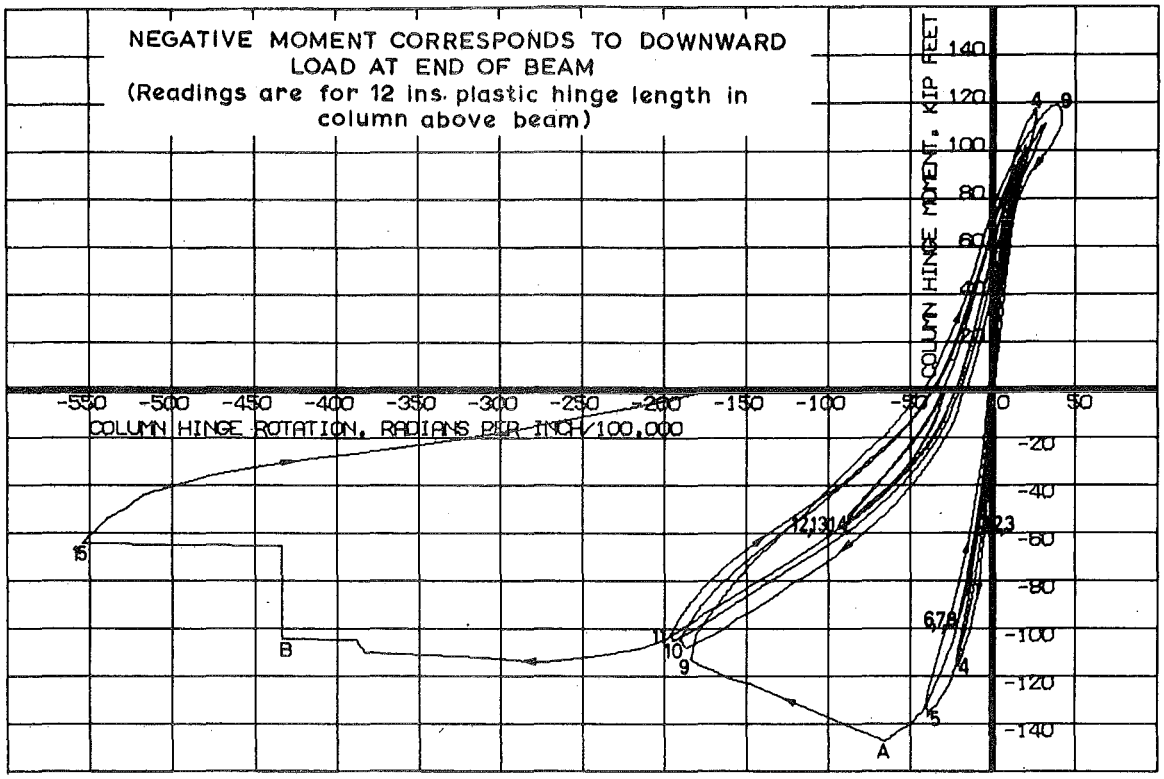

(a) Upper Column Plastic Hinge.

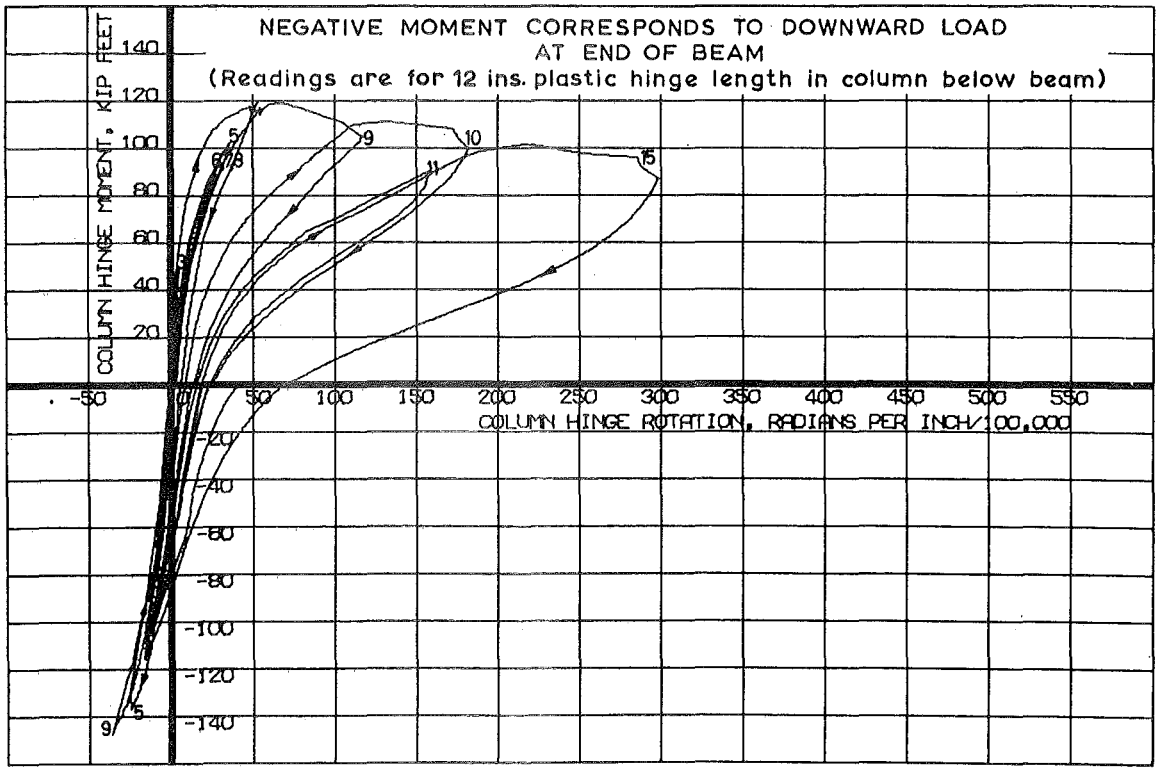

(b) Lower Column Plastic Hinge.

FIG. 3·13 : MOMENT-ROTATION CURVES FOR UNIT 4.

For each of the columns of Units 3 and 4 there were two zones of plastic hinging, and their moment-rotation characteristics are illustrated in Figs. 3.12 and 3.13. Rotations were again measured from dial gauges over the hinge length. A gauge length of half the member depth, 8 inches, was chosen for Unit 3. For a better coverage of the plastic curvature, this was increased to 12 inches for Unit 4. To facilitate a comparison, the abscissa used for the moment-rotation curves was rotation per unit length. Column moments were measured at the level of the top and bottom of the beam.

The numbers on all of the curves correspond to the peak of the cycle number given in Figs. 3.3 and 3.4. Significant values of moments and rotational ductility factors are presented in Tables 3.1 and 3.2.

The characteristics for each of the units were as follows:

(a) Comparison of Units 1 and 2

An indication of the available energy dissipation in the beam plastic hinges of Units 1 and 2 may be gained from the hysteresis loops of Figs. 3.8 and 3.9. The deformations during the first 11 cycles on Unit 1 were all within the elastic or cracked elastic ranges and the ensuing energy dissipations, as represented by areas within the hysteresis loops, were small. The first signs of crushing of the concrete in the compression zones of the beam appeared during the upward loading half-cycle 15 for Unit 1, and during the upward loading half-cycle 4 for Unit 2. It is apparent that there was substantial energy dissipation for these half-cycles. On unloading of the beams after they had sustained large rotations, there was a greater elastic recovery than would be expected of a comparable reinforced concrete beam.

It is clear from the moment-rotation curves that significant post-elastic rotations were available in the beams. Large values of maximum rotational ductility factor (based on first cracking at the joint) were

Table 3.1. MOMENT AND DUCTILITY CHARACTERISTICS OF UNITS 1 AND 2

Unit No.	Direction of beam loading	At maximum beam moment (e.g. at A and B on Fig.3.9)		Maximum beam moment kip ft.	Maximum beam end displacement inches	Beam moment at maximum displacement kip ft.
		Beam rotational ductility factor	Beam displacement ductility factor			
1	Upward	28.1	12.3	183.9	15.25	40.3
	Downward	33.3	11.8	169.0	10.71	149.5
2	Upward	30.8	9.9	195.2	12.50	126.7
	Downward	56.2	19.5	183.1	10.93	154.9

Table 3.2. MOMENT AND DUCTILITY CHARACTERISTICS OF UNITS 3 AND 4.

	Unit No.	Direction of beam loading	Upper column			Lower column			Beam displacement ductility factor
			Rotational ductility factor	Moment kip ft.	Axial load kips	Rotational ductility factor	Moment kip ft.	Axial load kips	
At maximum column moment (e.g. at A on Fig. 3.13(a)	3	Upward				12.9	115.7	48.3	5.7
		Downward	13.8	135.7	121.6				5.9
	4	Upward				8.2	119.2	49.0	6.3
		Downward	9.7	148.1	125.6				6.1
At maximum column rotation (e.g. at B on Fig. 3.13(a)	3	Upward				31.3	105.6	57.5	9.3
		Downward	45.6	106.8	114.7				8.8
	4	Upward				36.2	96.0	59.5	10.6
		Downward	63.2	104.5	114.2				10.6

Note: Details are given only for the critical plastic hinge in each case.

measured at the maximum loads, and are recorded in Table 3.1. This table also shows that the displacement ductility factors of the members were close to one third of the rotational ductility factors.

The moment-displacement curves in Figs. 3.10 and 3.11 include the fifteen cycles for which the moment-rotation curves are plotted. In addition they show the behaviour when the maximum allowable displacement was imposed at the end of the beams in each direction. The beams were first loaded downwards, and both units retained over 89% of their maximum moment capacity up to the maximum allowable downward deflection in the rig of nearly eleven inches. This corresponds to an interstorey displacement of approximately ten inches for the frame represented. On unloading the beam and imposing an upward deflection, both units attained almost their previous maximum moment capacities for upward loading. However, beyond this point Unit 1 showed a gradual reduction of moment capacity with increased deflection. The reason for this behaviour lay in a bond failure of the top prestressing cable duct in the column (between the duct tube and the column) which resulted in the top cable pushing through the column and causing a flexural failure of the anchor block. This phenomenon did not occur to such an extent in Unit 2, which was specially detailed for ductility, apparently because the heavy rectangular steel spirals in the column restricted the splitting bond failure of the top prestressing duct. In this case a moment close to maximum was maintained up to an upward deflection of 12.5 inches, when failure occurred suddenly due to buckling of the top prestressing cable in compression. The more gradual failure of Unit 1 at very large deflections is preferable from a seismic design viewpoint. However, the magnitude of the distortions sustained, even for the case of no special detailing for ductility, are much greater than would be expected under any earthquake.

(b) Comparison of Units 3 and 4

The elongated shape of the moment-rotation curves for the plastic hinges in the columns of Units 3 and 4, as shown in Figs. 3.12 and 3.13, arises because the plastic rotations occurred at different hinges for different directions of loading. For downward loading at the end of the beam the plastic rotations occurred in the column hinge above the beam, and for upward loading they occurred in the column below the beam.

It should be noted that the energy dissipation capacity of the column hinges depends on the previous loading history. For example, in Figs. 3.12(a) and 3.13(a) for the hinges above the beams, the maximum rotations during cycles 1 to 3 and cycles 4 to 8 were in the elastic and cracked elastic ranges respectively and the resultant energy dissipations were small. In each case the rotational ductility factor at the peak of downward load half-cycle 5 was slightly greater than the prescribed value of 5. It was only during downward load half-cycle 9, when crushing of the concrete commenced, that substantial energy dissipation became apparent. The subsequent cycles had larger hysteresis loops than those for the cracked elastic cycles. The sudden drop in moment capacity during downward load half-cycle 15 in Fig. 3.13(a) was due to a fracture of two prestressing strands in tension.

For the four column plastic hinges considered, there was a sudden spalling of the cover concrete only for the Unit 4 hinge above the beam (Fig. 3.13(a), peak of downward load half-cycle 9). In all other cases, initial crushing took the form of a gradual propagation of longitudinal cracking in the compression zones. It appears that the heavy rectangular spirals in the column of Unit 4 tended to precipitate the spalling of the cover concrete. Stiffness degradation became apparent only after significant signs of crushing had occurred during

cycle 9 for all of the hinges.

The similarity of the moment-rotation curves for the corresponding hinges of Units 3 and 4 was remarkable in view of the much heavier confinement of Unit 4. A comparison for the two units may be obtained from Table 3.2 by considering the rotational ductility factors of the critical sections, for the points of maximum moment and maximum rotation in each test. It may be seen that large rotational ductility factors can be sustained subsequent to crushing of the cover concrete, even if the column section is not specially detailed for ductility.

3.3.2 Strength of Sections

The maximum moments sustained at the critical sections, for all of the units, are presented in Tables 3.1 and 3.2. A comparison is made in Table B.3 (Appendix B) of the experimental moments and the theoretical values calculated for nominal concrete strengths and column loads. Tables 3.1 and 3.2 also show the effect of confinement of the concrete on the maximum moment capacity. Units 2 and 4, which were specially detailed for ductility, have greater moment capacities than their more lightly bound counterparts, Units 1 and 3.

3.3.3 Appearance of Units During Testing

UNIT 1

Fig. 3.14 shows two composite photographs of Unit 1 during testing. Fig. 3.14(a) shows the appearance after maximum moments have been sustained for both directions of loading. The lines of cracks have been marked for clarity. Points worthy of note at this stage of loading are as follows:

1. Horizontal cracks formed in the mortar joint and the beam nearby, because of flexure in the adjacent column section. In several

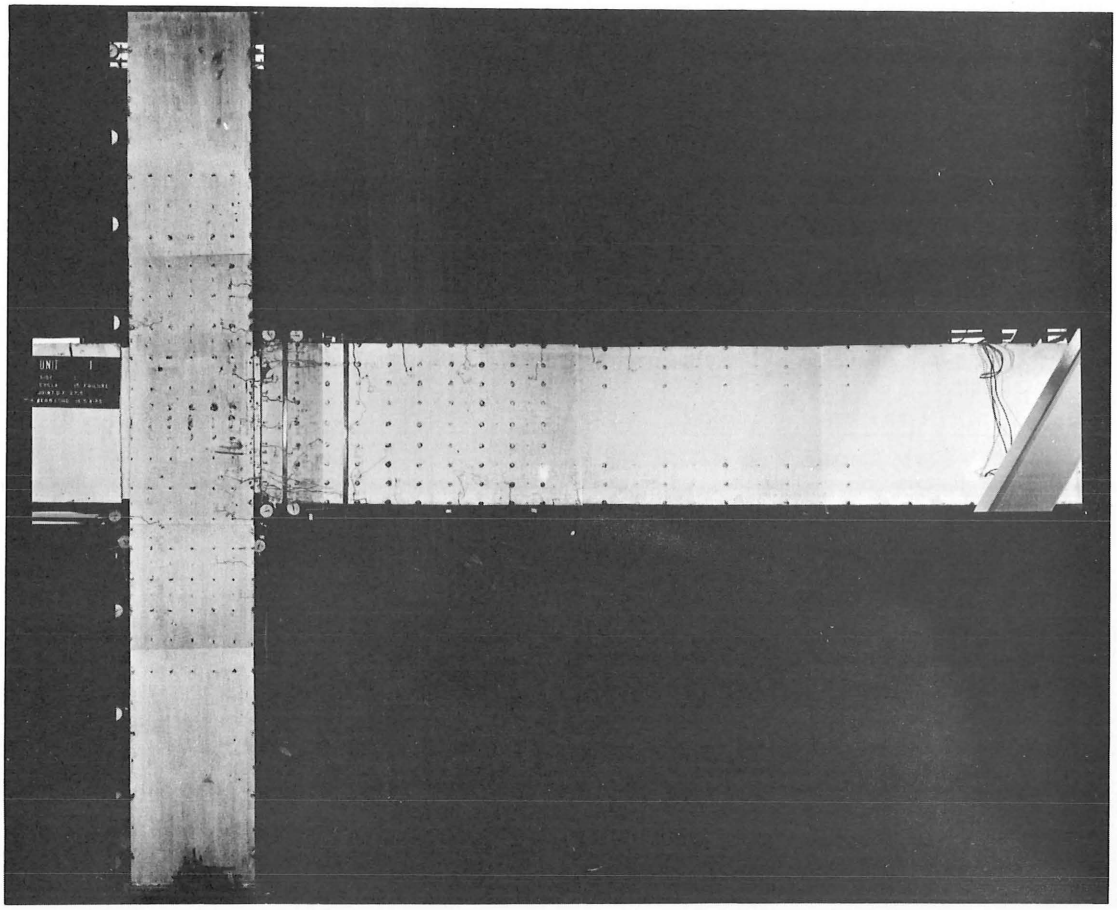

(a) At Maximum Moment Capacity

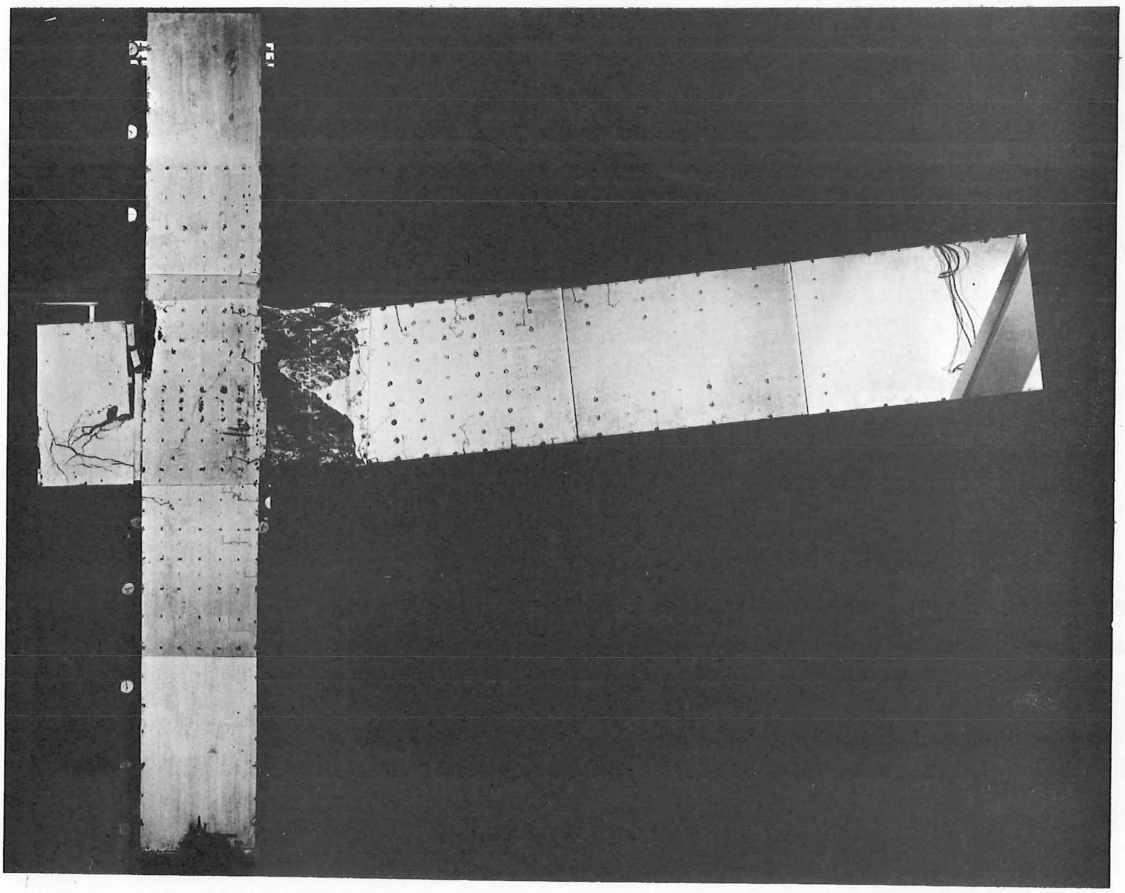

(b) At Maximum Upward Displacement

FIG.3.14 : APPEARANCE OF UNIT 1 DURING TESTING

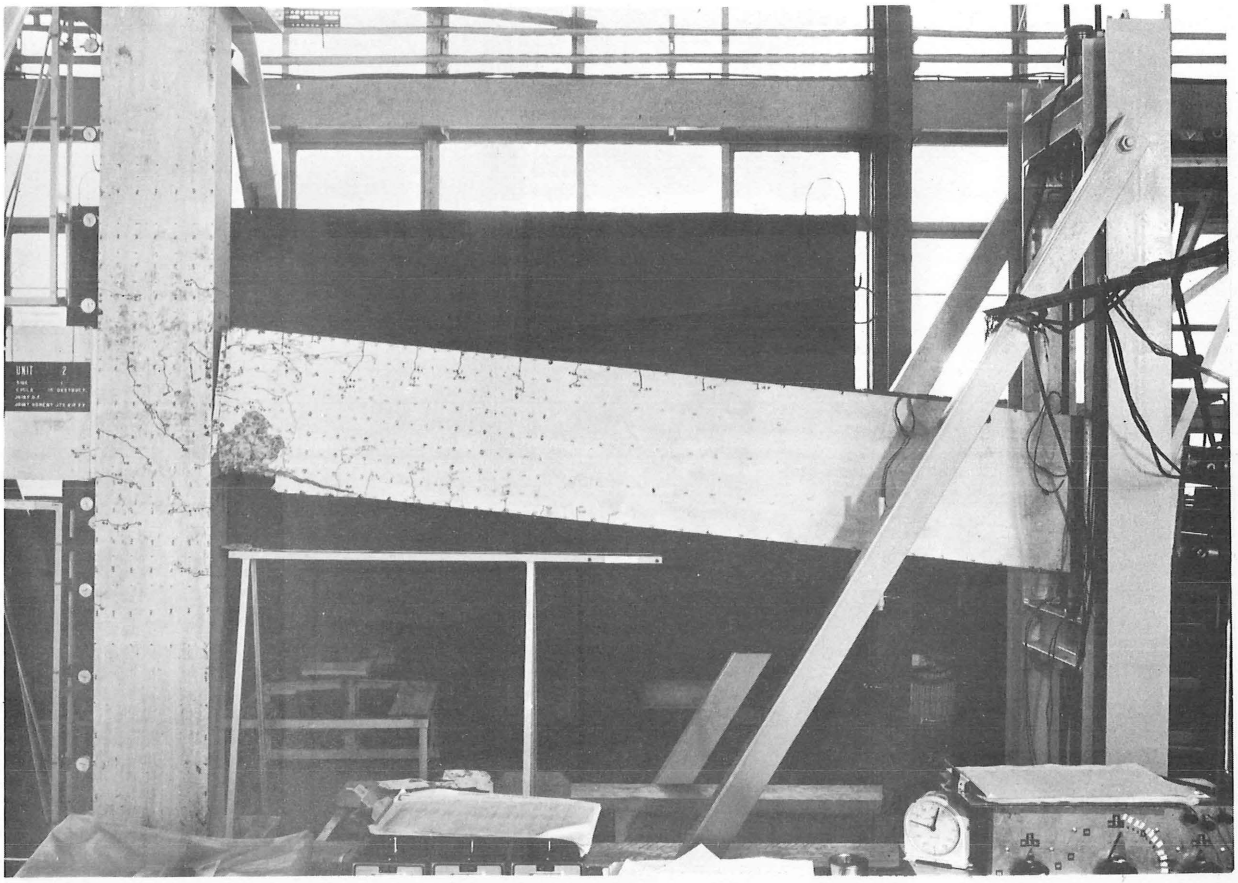

(a) At Maximum Downward Deflection

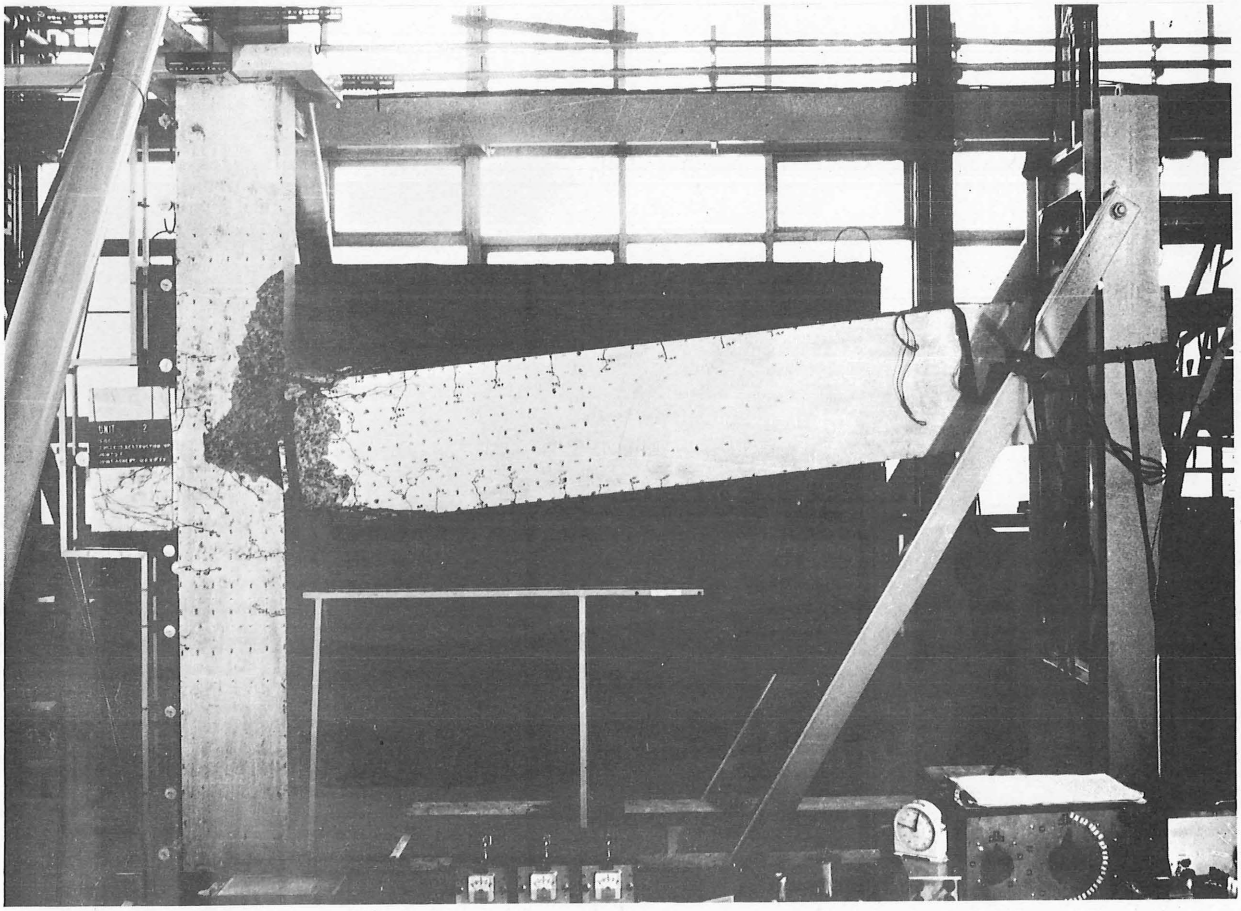

(b) At Maximum Upward Deflection

FIG.3.15 : APPEARANCE OF UNIT 2 DURING FINAL CYCLE

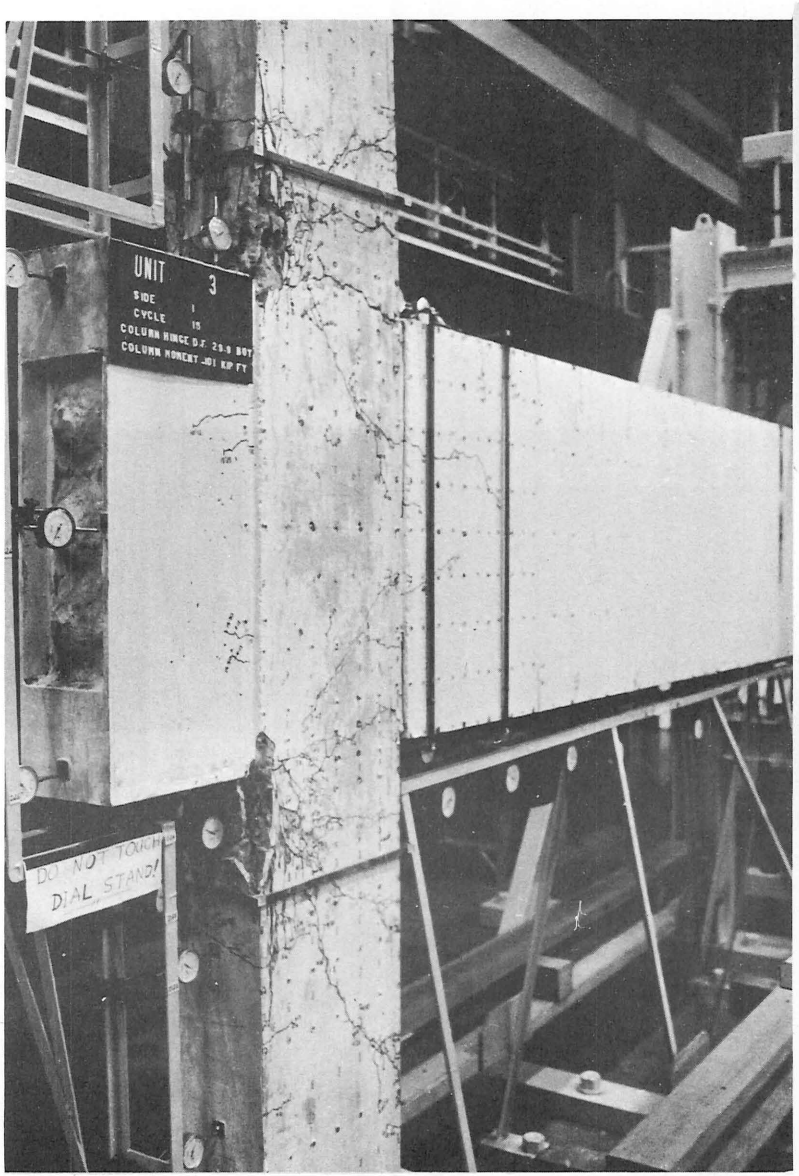

(a)

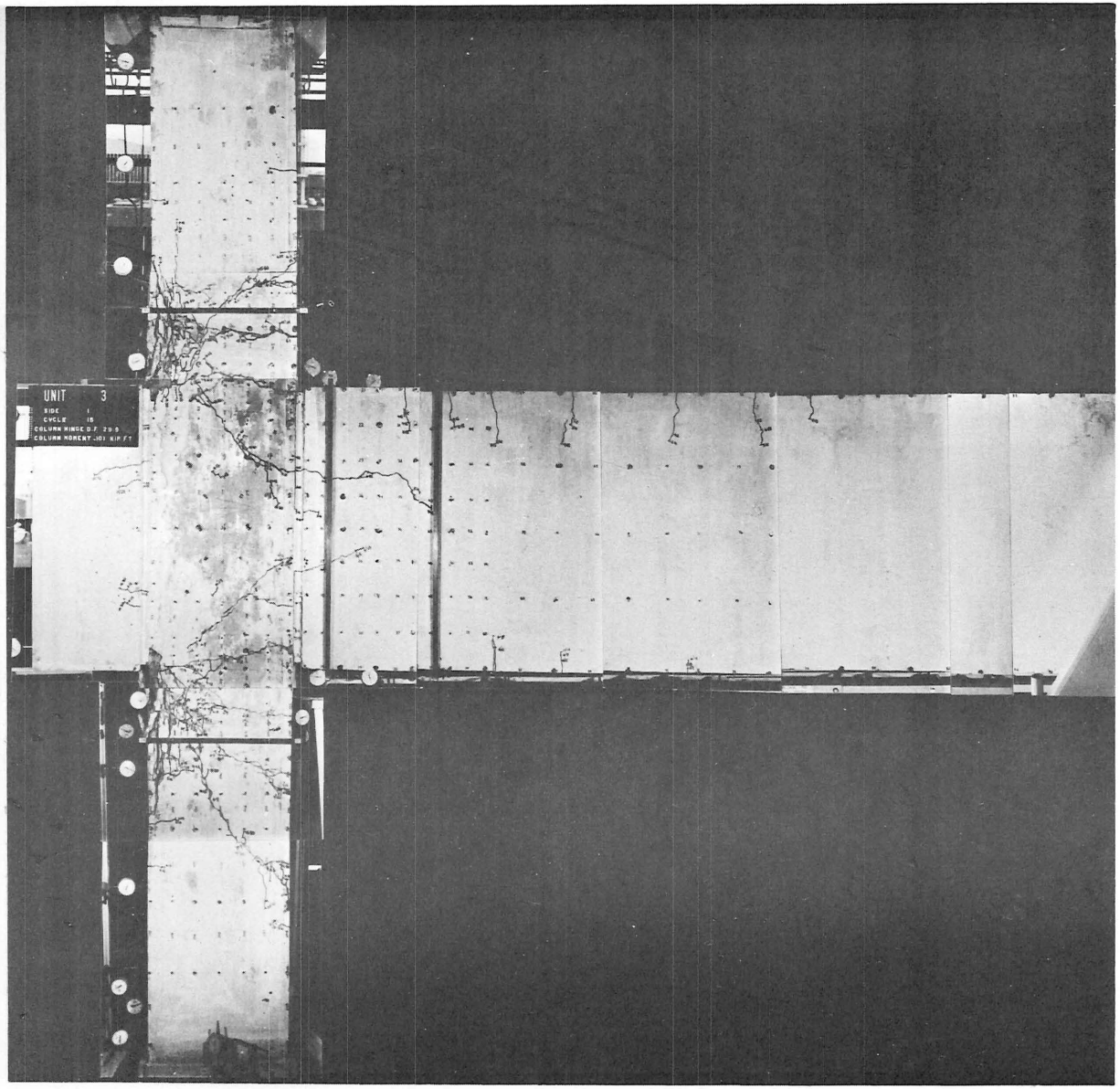

(b)

FIG. 3.16 : UNIT 3 AT MAXIMUM DOWNWARD DEFLECTION, CYCLE 15.

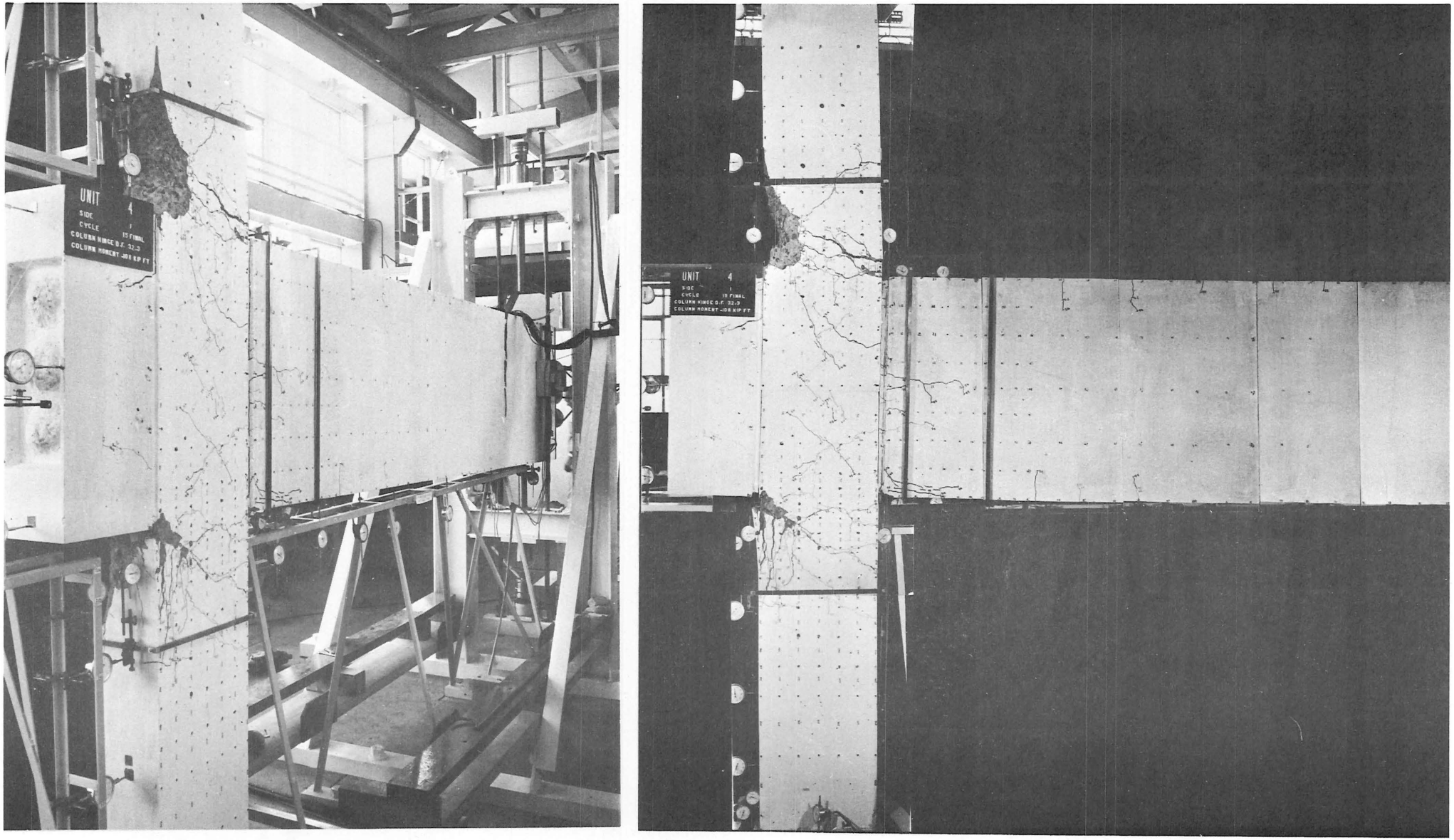

(a) (b)

FIG. 3.17 : UNIT 4 AT MAXIMUM DOWNWARD DEFLECTION, CYCLE 15.

cases a corresponding tension crack has not formed in the column because there it is delayed by compression due to the vertical prestressing and axial load.

2. Longitudinal cracks may be observed in the compression zones at the top and bottom of the beam near the joint. Spatial curvilinear stress paths exist in the beam, because of the recession of the mortar joint, and the resulting radial stresses cause tension cracks.

3. The mortar at the joint was practically undamaged. It is in the favourable position for compression of being confined by friction with the interfaces of the beam and the column.

The appearance of Unit 1 after sustaining maximum upward deflection is shown in Fig. 3.14(b). Points of interest are:

1. The top prestressing cable was pushed through the column after severe crushing of the concrete in the beam. The duct was found to have been displaced by $\frac{7}{8}$ inch, indicating a bond failure between the duct itself and the concrete of the column. The associated splitting effect caused a large vertical crack in the column, along the centreline of the top duct. The anchor block failed in flexure under the force of the top cable.

2. Over the course of testing, a crack at the mortar joint had been wide open for half the depth of the member during several cycles. Even though in this case the joint was not bound, little of the mortar was lost.

UNIT 2

The appearance of Unit 2 at the maximum downward and upward deflections is shown in Fig. 3.15(a) and (b) respectively. The following comments may be made on the behaviour of this unit:

1. Diagonal tension cracks are apparent in Fig. 3.15(a) at the joint region. These were caused by horizontal shear forces in the

joint due to tension in the top cable and compression at the bottom of the beam.

2. When the beam was loaded upwards to failure, the top cable again pushed through the column after severe concrete crushing in the beam. However, in this case the displacement was only 3/16 inch, and it is likely that the smaller movement relative to Unit 1 was due to the heavy column binding restricting the bond failure of the cable duct.

3. The extent of the crushing in the beam at failure is shown in Fig. 3.15(b). The compressive force at the top of the beam also caused the cover concrete on the column in this region to split off.

UNIT 3

Fig. 3.16(a) and (b) show the appearance of Unit 3 at maximum downward deflection in the final cycle. Points of interest are as follows:

1. The position of formation of the plastic hinge for a particular direction of loading depended on whether the moment capacity of the column section above or below the beam was critical in that case. As shown on the interaction curve in Fig. B.6 (Appendix B) the column section with the lower axial load had a lower moment capacity. In the test specimen the level of axial load in the column sections above and below the beam differed by the value of load applied at the end of the beam. For downward loading at the end of the beam there was a lower axial load in the upper column section than in the lower column section, and consequently the plastic hinge formed in the column above the beam. Similarly for upward loading at the end of the beam there was a lower axial load in the lower column section, and thus in this case the plastic hinge formed in the column below the beam.

2. The presence of inclined cracks in the column clearly shows the influence of the shear forces. The secondary cracking, noticeable particularly on the lowest diagonal crack in the column, is

characteristic of the effect of aggregate interlock under cyclic loading. The good performance of the joint region, even though it had no special transverse reinforcement, is attributable to the prestress in the column and the confining effect of the anchor block.

UNIT 4

Similar characteristics may be observed in Fig. 3.17, for Unit 4, as have been noted for Unit 3. The photographs were taken at the maximum downward deflection in the final cycle, and the discontinuity in the column at the upper plastic hinge is noticeable. At this hinge the cover concrete spalled suddenly. Even for the closely spaced spirals used, there was a loss of material below the line of the end of the spiral between successive hoops. Two strands in the upper column fractured at the section where a wide crack is visible in Fig. 3.17.

3.3.4 Curvature Distribution

The curvatures along the members of the units were calculated from the surface concrete strains. The pattern of demountable mechanical (Demec) gauge locations is shown in Figs. B.16 and B.17 (Appendix B). In each case an average strain reading was calculated from the corresponding gauge locations on the two sides of the member. For each set of gauges at a particular section, a line of best fit was drawn through the strains measured in the compression zone. From the strain profile so plotted the neutral axis depth, kd, and the strain in the extreme compression fibre, ϵ_{cc}, were obtained. The curvature, φ, at that section was then calculated from $\varphi = \epsilon_{cc}/kD$. The curvature distribution along the members of Units 1 to 4, calculated at selected half-cycle peaks for upward and downward beam end loading, are shown in Figs. 3.18 to 3.25. The curvatures have been plotted at the midpoints of the appropriate gauge length. The peaks of curvature in these figures

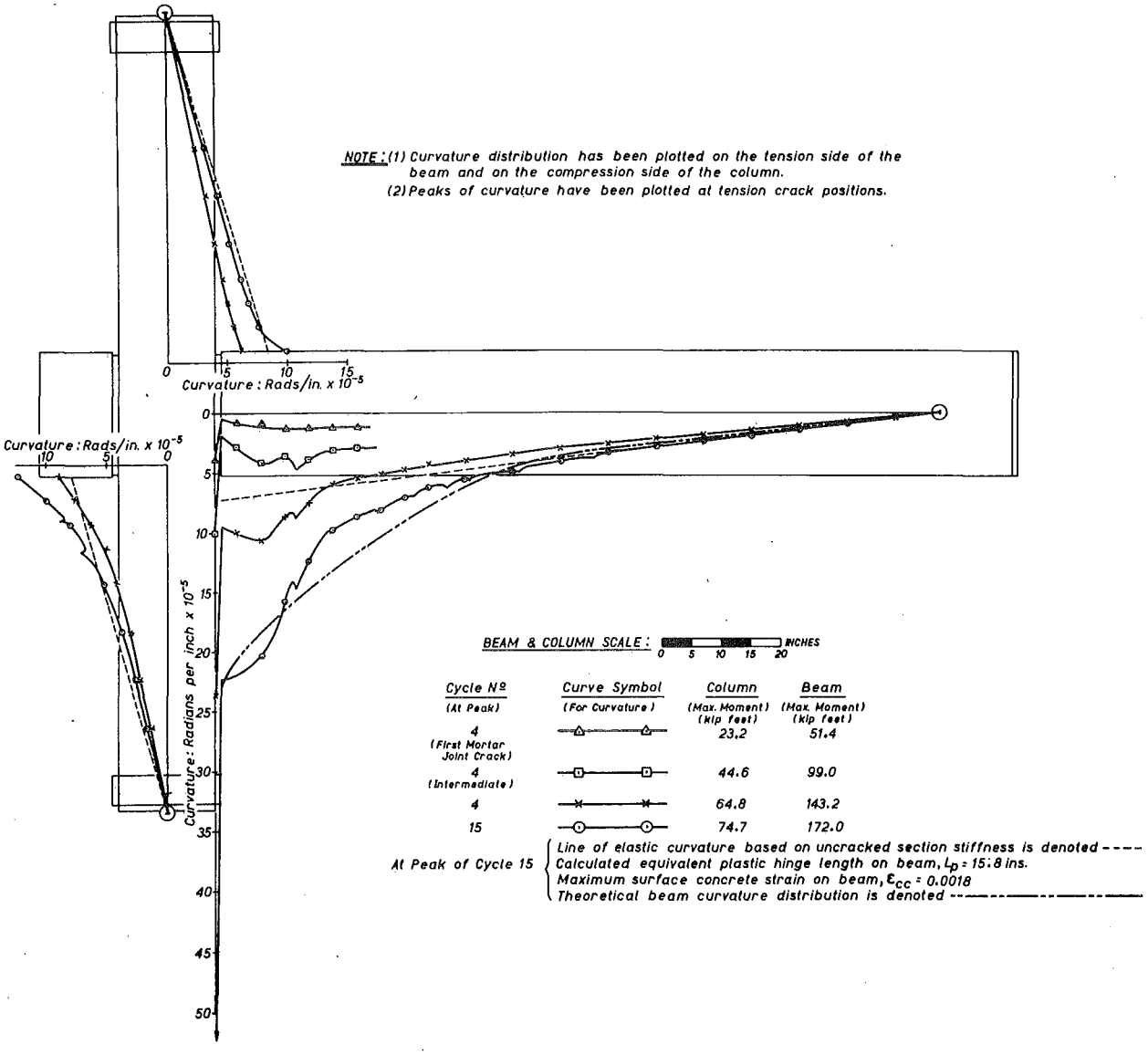

FIG. 3.18 : UNIT 1 CURVATURE DISTRIBUTION FOR UPWARD LOAD AT END OF BEAM

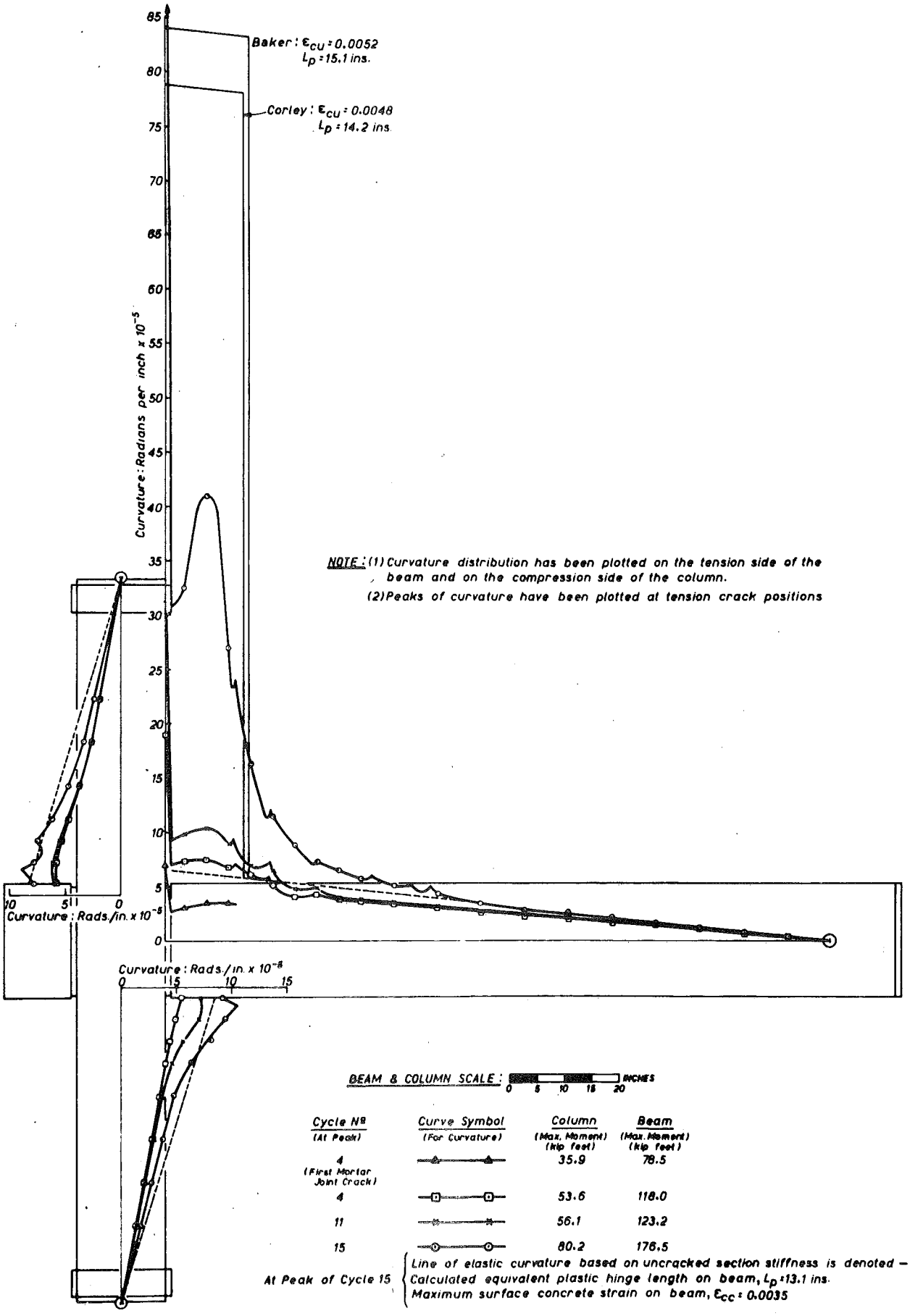

FIG. 3.19 : UNIT 1 CURVATURE DISTRIBUTION FOR DOWNWARD LOAD AT END OF BEAM.

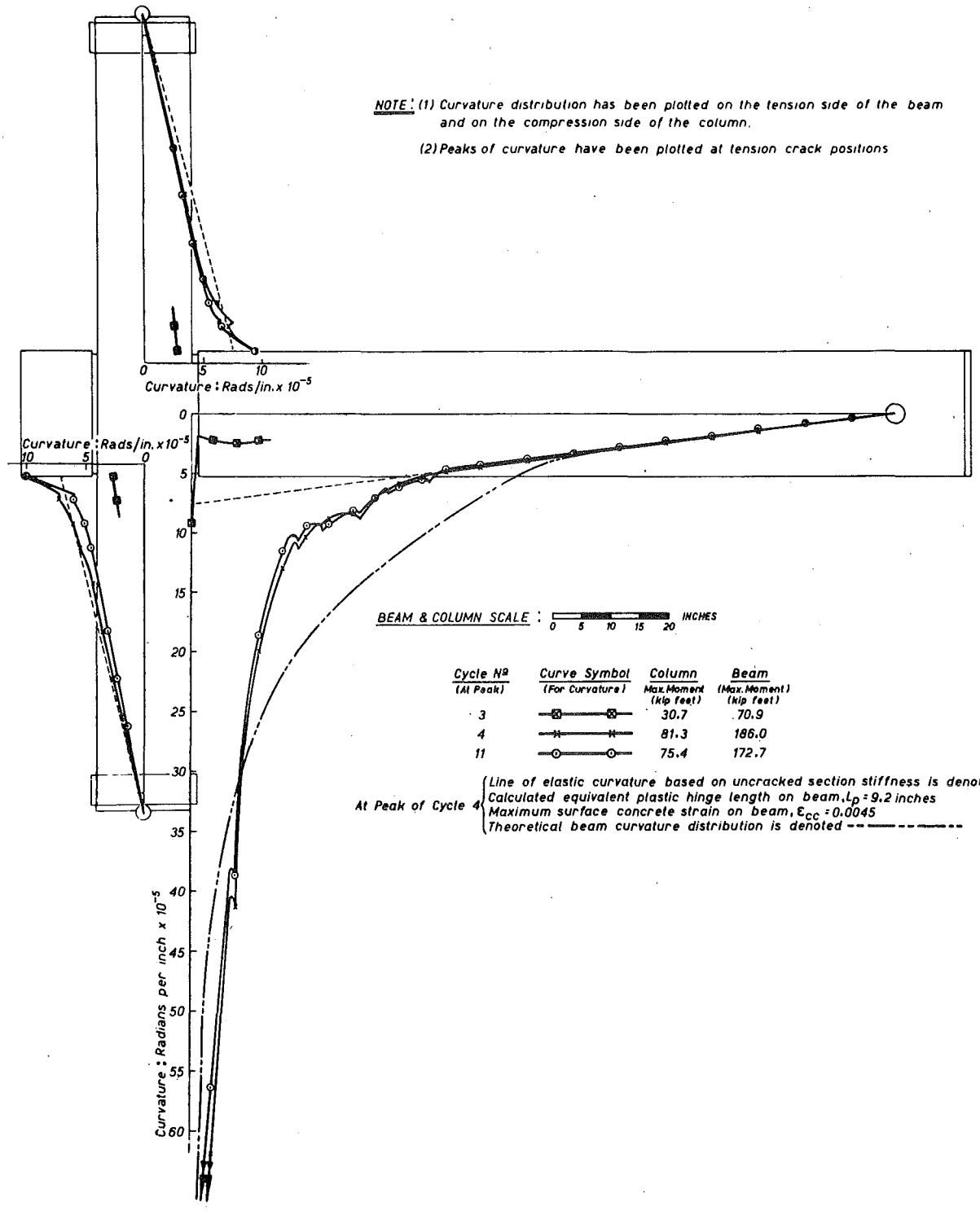

FIG. 3.20 : UNIT 2 CURVATURE DISTRIBUTION FOR UPWARD LOAD AT END OF BEAM

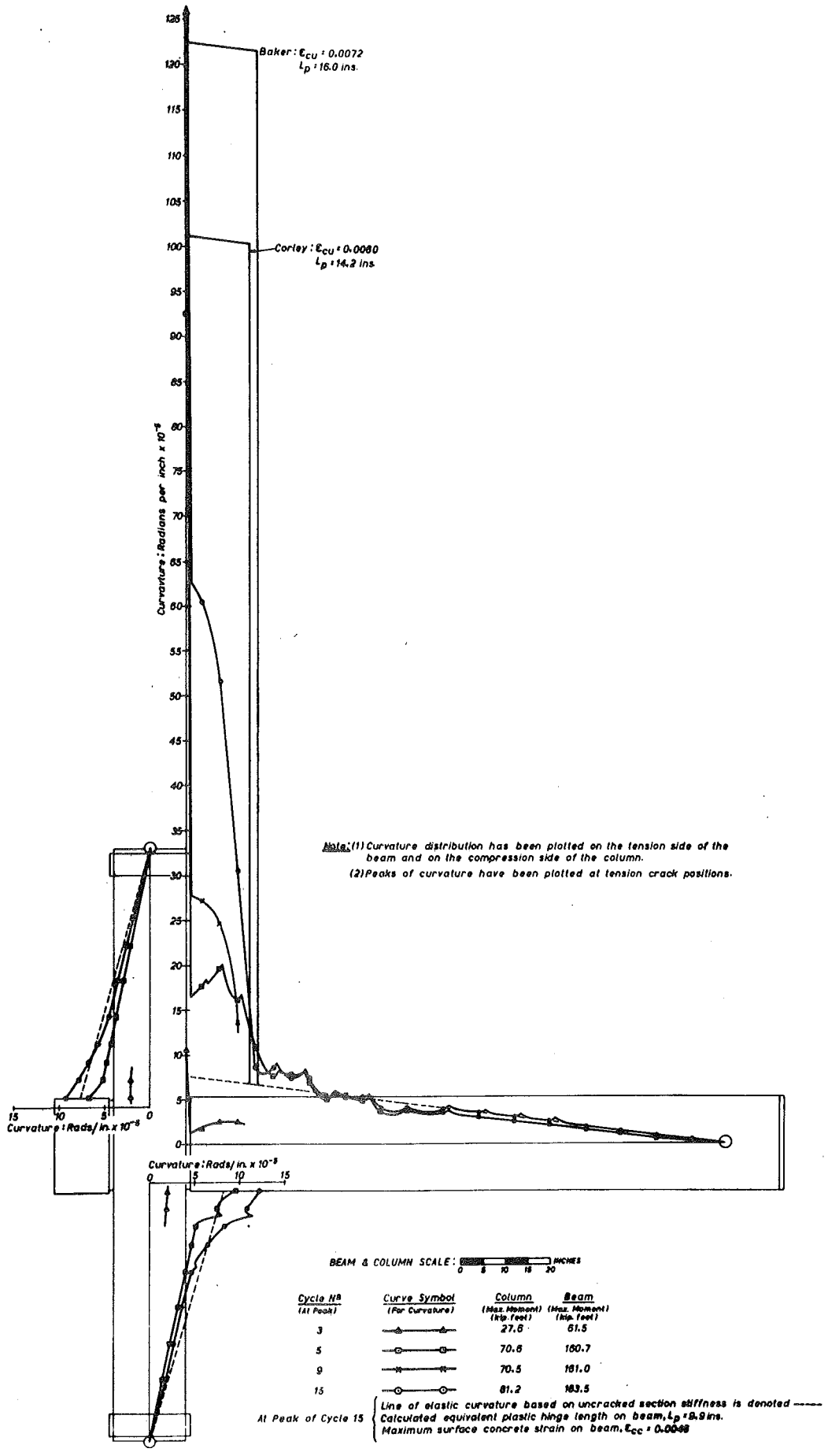

FIG. 3.21 : UNIT 2 CURVATURE DISTRIBUTION FOR DOWNWARD LOAD AT END OF BEAM

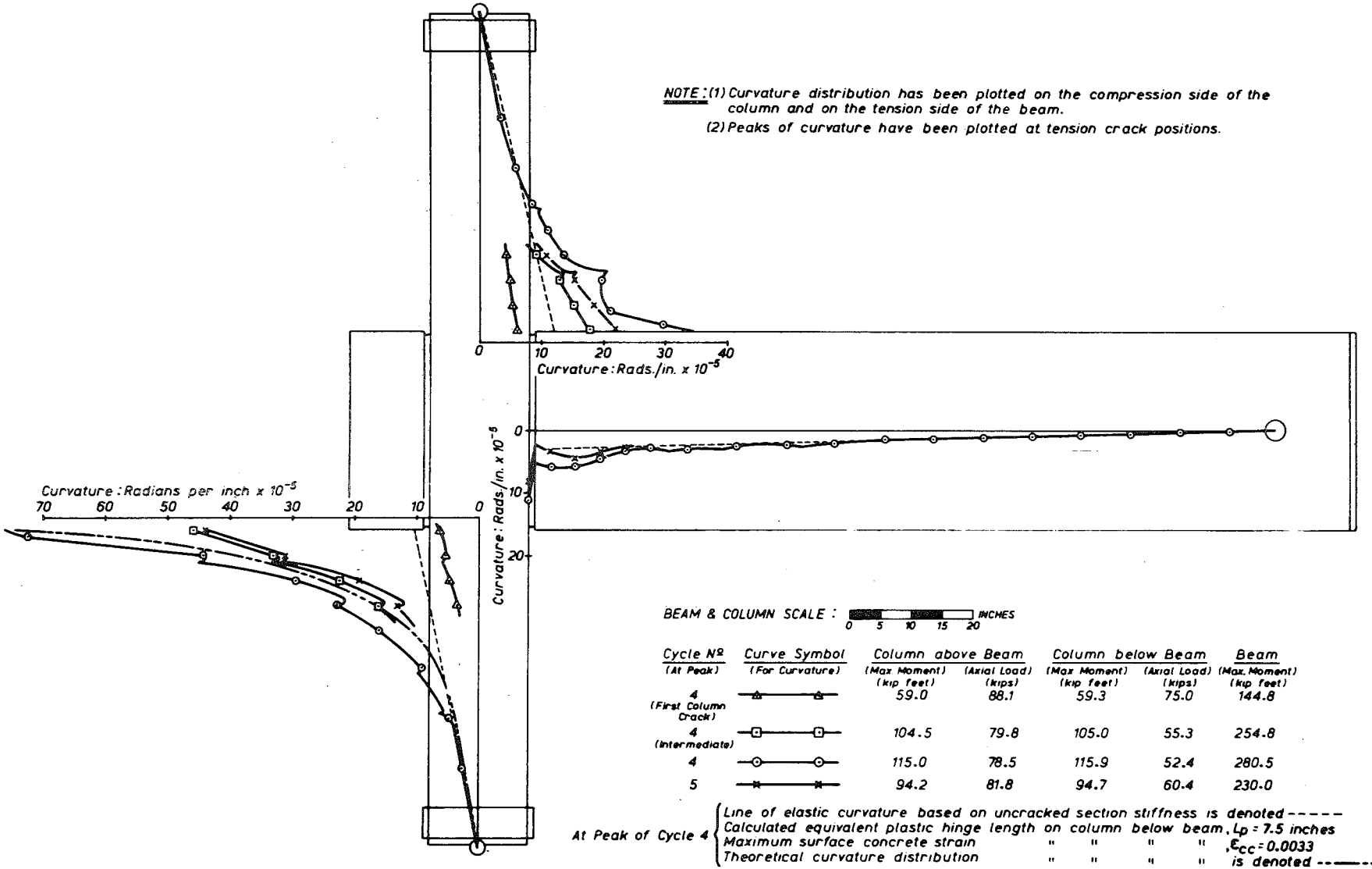

Cycle Nº (At Peak)	Curve Symbol (For Curvature)	Column above Beam (Max Moment) (kip feet)	Column above Beam (Axial Load) (kips)	Column below Beam (Max Moment) (kip feet)	Column below Beam (Axial Load) (kips)	Beam (Max. Moment) (kip feet)
4 (First Column Crack)		59.0	88.1	59.3	75.0	144.8
4 (Intermediate)		104.5	79.8	105.0	55.3	254.8
4		115.0	78.5	115.9	52.4	280.5
5		94.2	81.8	94.7	60.4	230.0

FIG. 3.22: UNIT 3 CURVATURE DISTRIBUTION FOR UPWARD LOAD AT END OF BEAM

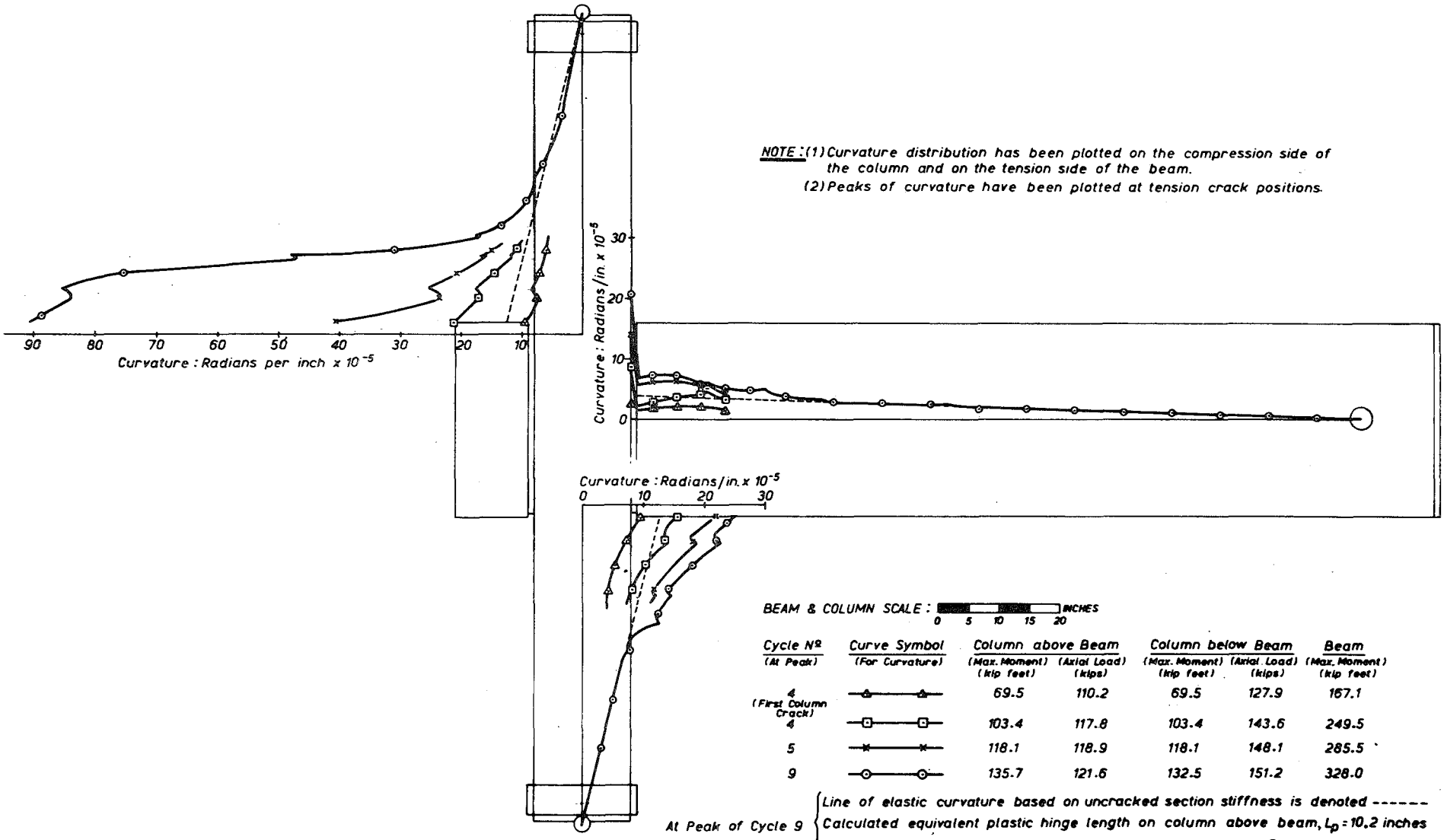

FIG. 3.23 : UNIT 3 CURVATURE DISTRIBUTION FOR DOWNWARD LOAD AT END OF BEAM

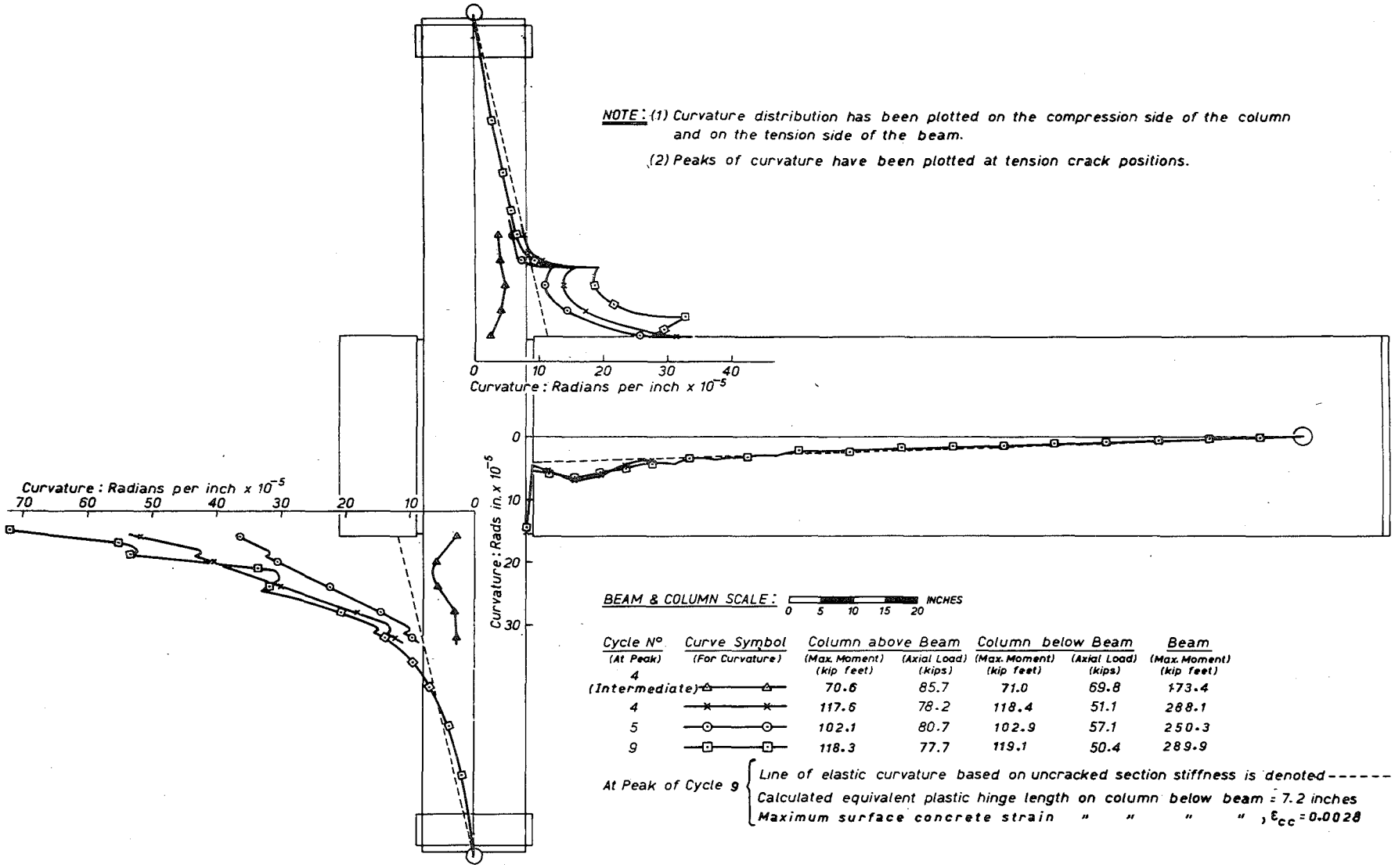

FIG. 3.24 : UNIT 4 CURVATURE DISTRIBUTION FOR UPWARD LOAD AT END OF BEAM

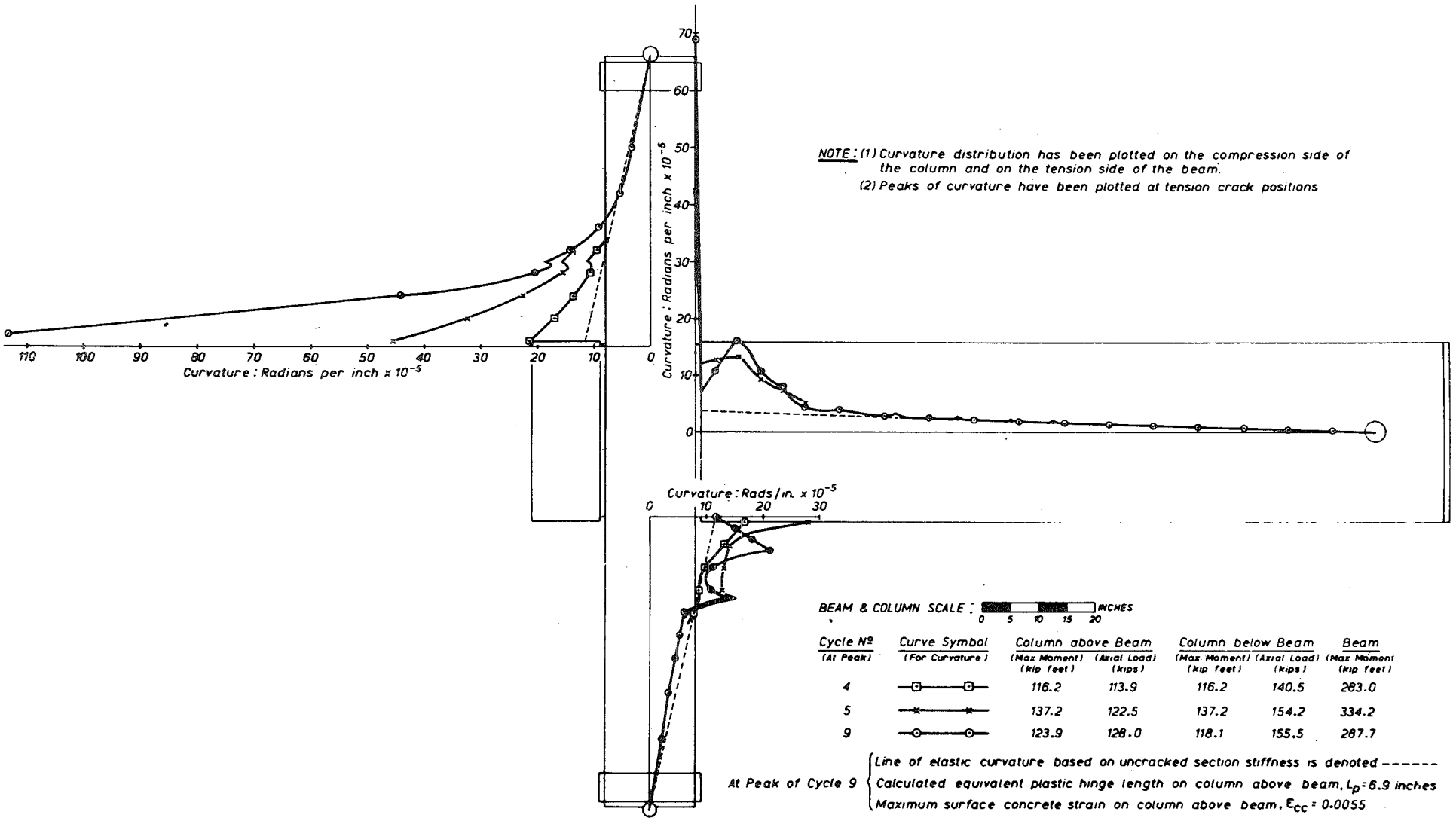

Cycle Nº (At Peak)	Curve Symbol (For Curvature)	Column above Beam (Max Moment) (kip feet)	Column above Beam (Axial Load) (kips)	Column below Beam (Max Moment) (kip feet)	Column below Beam (Axial Load) (kips)	Beam (Max Moment) (kip feet)
4	⊡—⊡	116.2	113.9	116.2	140.5	283.0
5	×—×	137.2	122.5	137.2	154.2	334.2
9	○—○	123.9	128.0	118.1	155.5	287.7

At Peak of Cycle 9:
- Line of elastic curvature based on uncracked section stiffness is denoted ------
- Calculated equivalent plastic hinge length on column above beam, L_p = 6.9 inches
- Maximum surface concrete strain on column above beam, ϵ_{cc} = 0.0055

FIG. 3.25 : UNIT 4 CURVATURE DISTRIBUTION FOR DOWNWARD LOAD AT END OF BEAM

correspond to tension crack positions. It is apparent that most of the inelastic rotations have occurred in the beams for Units 1 and 2 and in the columns for Units 3 and 4. Figs. 3.18 to 3.21 show that for Units 1 and 2 plastic curvature has not been solely concentrated at the mortar joints, but has extended over a good portion of the beam. The unusual effect shown in Fig. 3.19 of an apparent reduction in curvature in the beam near the column probably arises from the influence of the recessed mortar joint. Since the compressive stress paths in the beam must flow inwards through the reduced section, the surface concrete strains measured immediately adjacent to the recession may not be completely reliable. Figs. 3.22 to 3.25 show the much greater inelastic curvatures present in the particular column sections of Units 3 and 4 that were critical for moment capacity for a certain direction of loading. The slight differences in the moments noted for the two column hinges within a unit at some increments arises because of the eccentricity of the axial load when the joints deflected horizontally in the direction of the beam axis, after column plastic hinges had formed. This behaviour is illustrated in Section 3.3.5.

Theoretical Curvature Distribution

An analysis, which is presented in Chapter 4, was used to predict theoretically the curvature distribution on the members from their moment-curvature properties. Curves so obtained for the beams of Units 1 and 2 are plotted on Figs. 3.18 and 3.20. For the increment considered, the moment at a particular section is calculated and the corresponding theoretical curvature obtained. Because the theory applies to a cracked section, the resulting curve should be an envelope to the actual curve since the latter is influenced by variations of stress between cracks. An example of the relative theoretical and experimental curvature distributions for the columns is shown in Fig. 3.22. The theoretical curve is slightly conservative because the

inclined cracks in the column tend to spread the zone of plasticity more than that predicted. It is evident that fairly accurate representations of the curvature distributions may be obtained with this method.

Plastic Hinge Lengths

The area of the curvature diagram gives the rotation which occurs along the member. This area can be divided into a triangular region of elastic curvature plus a region of plastic curvature near the critical section as shown in Fig. 3.26. The plastic rotation, θ_p, can be conveniently expressed as:

$$\theta_p = (\varphi_{max} - \varphi_e) L_p \qquad \ldots (3.1)$$

where φ_{max} is the maximum curvature, φ_e is the maximum elastic curvature calculated assuming an uncracked section, and L_p is the equivalent plastic hinge length. The equivalent plastic hinge length, defined as above, was calculated for each test unit from the measured curvature distribution profiles at the peaks of major load cycles. In these calculations L_p was found from the area of plastic curvature $\div (\varphi_{max} - \varphi_e)$. The curvature in the mortar joints was conservatively ignored. The value of L_p, calculated for the curvature distribution obtained at the increment with maximum recorded surface concrete strains in each case, has been noted on the figures.

To date there has been no accurate method proposed for predicting the equivalent plastic hinge lengths in confined prestressed concrete members. It is evident from these tests that the value of L_p is dependent on the maximum surface concrete strain sustained, and on the degree of confinement of the members. However many more tests would have to be conducted to consider all the variables. In the absence of details for prestressed concrete, it is of interest to compare the equivalent plastic hinge lengths obtained with those recommended for

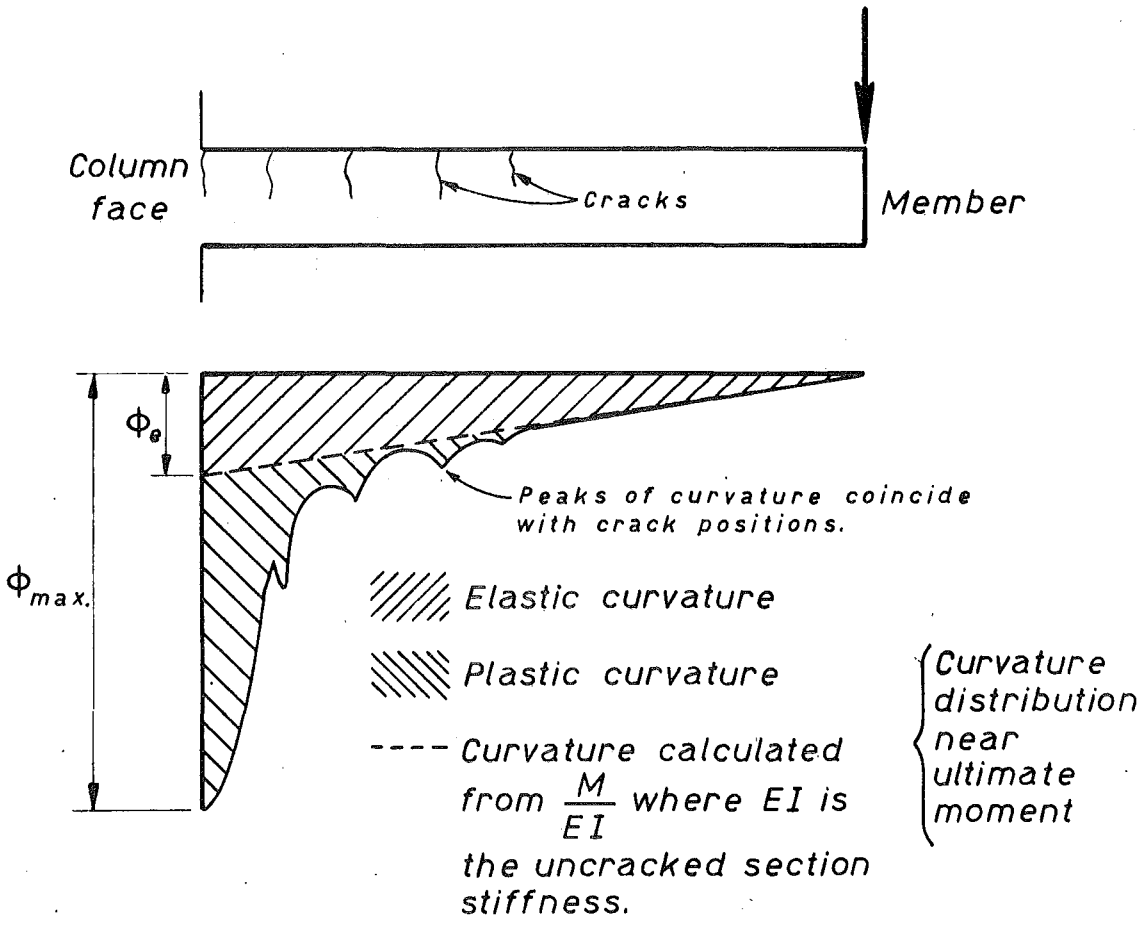

FIG. 3.26 : CURVATURE DISTRIBUTION ALONG A MEMBER

reinforced concrete by a number of investigators. The proposals of Baker and Amarakone[53] and Corley[54] were considered. Both are based on experiments with monotonically loaded beams. The values of "ultimate" curvature and plastic hinge length so calculated have been plotted for the beams of Units 1 and 2 on Figs. 3.19 and 3.21. In any comparison it should be noted that the experimental curvatures increased considerably beyond those plotted, but the surface concrete strains in the critical regions could not be recorded because of the onset of crushing. However, it does appear that the proposals for reinforced concrete are non-conservative when applied to prestressed concrete. One reason for this is that there were no diagonal tension cracks in the beams tested, whereas such cracks often allow a spread of plasticity in reinforced concrete beams.

Until suitable recommendations are presented for prestressed concrete, a rough approximation for equivalent plastic hinge length may be taken as one half of the overall depth of the member, when surface concrete strains in the critical zones are greater than 0.0035. For maximum concrete strains of the order of 0.002 the equivalent plastic hinge length may be taken as three quarters of the overall depth of the member.

3.3.5 Deflection Profiles

The deflection profiles for Units 1 to 4 for both upward and downward beam end loading are shown in Figs. 3.27 to 3.30. The deflections were measured relative to the initial condition where the beam was balanced by an upward load which gave zero moment at the joint. Most of the profiles were plotted at the peaks of selected cycles, but in some cases the profiles at first cracking, or at other intermediate points, have been plotted to cover the range of deflections. For Units 1 and 2 the maximum experimental deflections were considerably

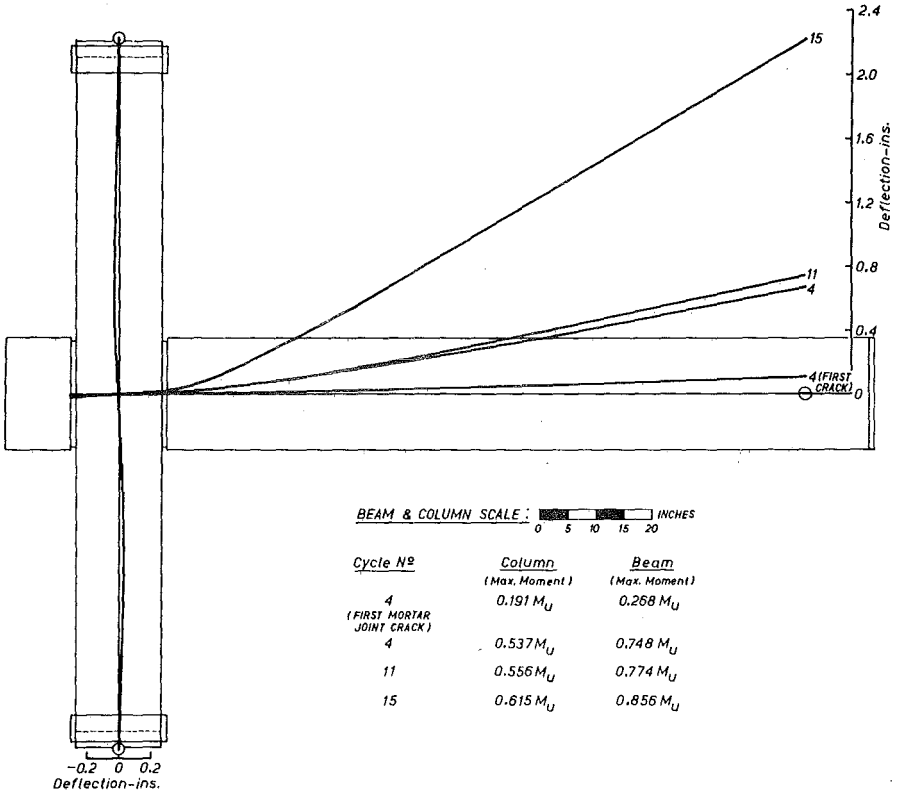

Cycle Nº	Column (Max. Moment)	Beam (Max. Moment)
4 (FIRST MORTAR JOINT CRACK)	$0.191\,M_u$	$0.268\,M_u$
4	$0.537\,M_u$	$0.748\,M_u$
11	$0.556\,M_u$	$0.774\,M_u$
15	$0.615\,M_u$	$0.856\,M_u$

(a) Upward Load at End of Beam

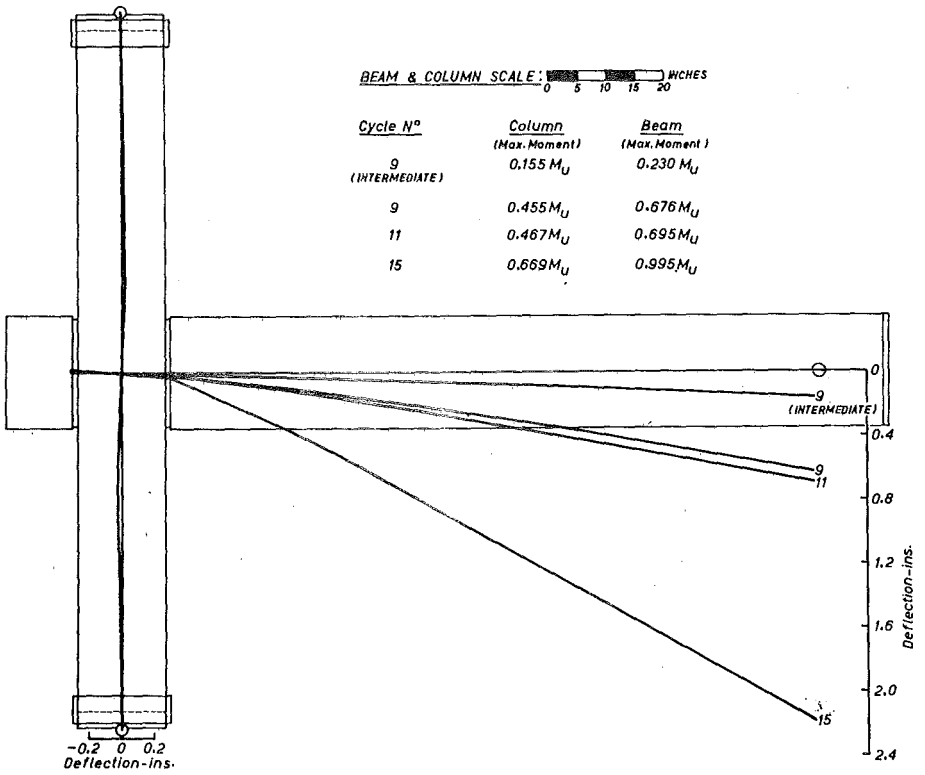

Cycle Nº	Column (Max. Moment)	Beam (Max. Moment)
9 (INTERMEDIATE)	$0.155\,M_u$	$0.230\,M_u$
9	$0.455\,M_u$	$0.676\,M_u$
11	$0.467\,M_u$	$0.695\,M_u$
15	$0.669\,M_u$	$0.995\,M_u$

(b) Downward Load at End of Beam

FIG. 3.27 : UNIT 1 DEFLECTION PROFILES

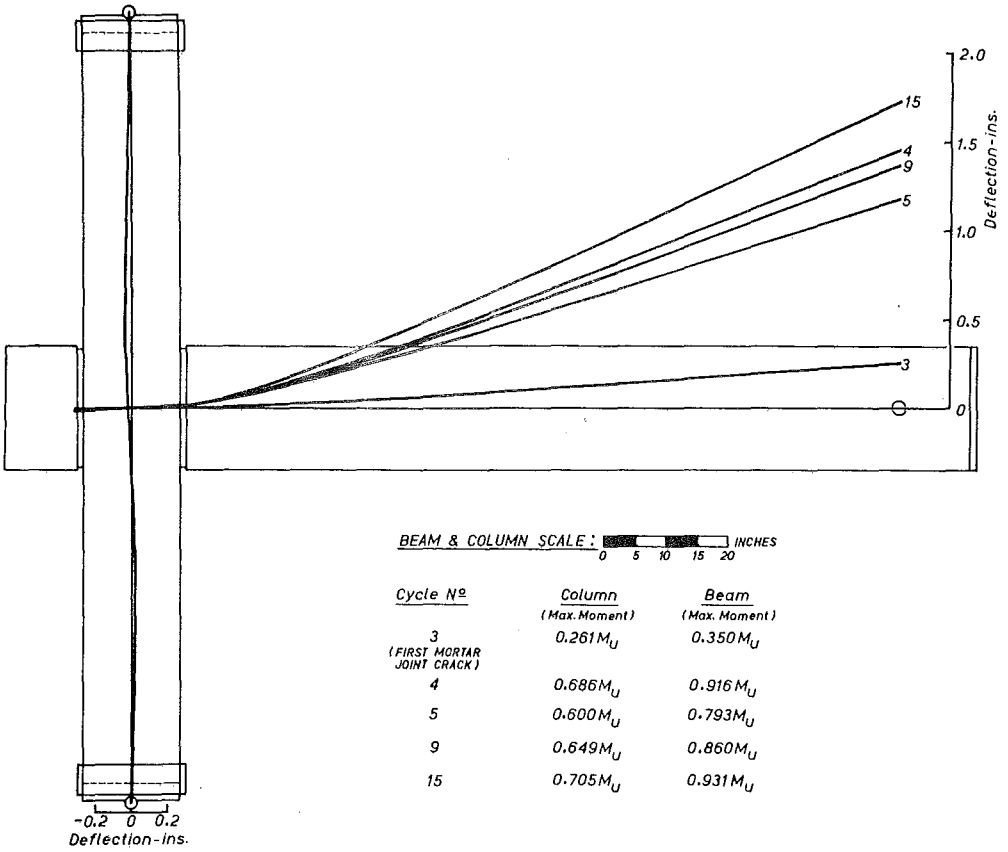

Cycle Nº	Column (Max. Moment)	Beam (Max. Moment)
3 (FIRST MORTAR JOINT CRACK)	$0.261M_U$	$0.350M_U$
4	$0.686M_U$	$0.916M_U$
5	$0.600M_U$	$0.793M_U$
9	$0.649M_U$	$0.860M_U$
15	$0.705M_U$	$0.931M_U$

(a) Upward Load at End of Beam

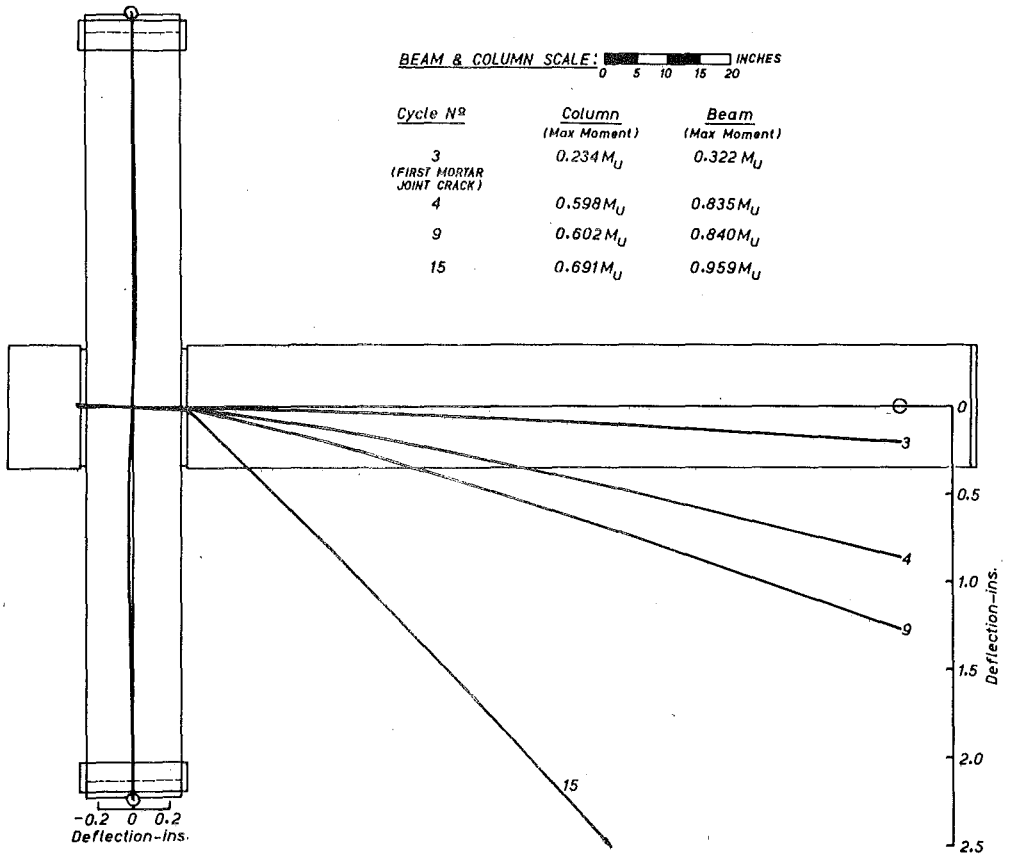

Cycle Nº	Column (Max Moment)	Beam (Max Moment)
3 (FIRST MORTAR JOINT CRACK)	$0.234M_U$	$0.322M_U$
4	$0.598M_U$	$0.835M_U$
9	$0.602M_U$	$0.840M_U$
15	$0.691M_U$	$0.959M_U$

(b) Downward Load at End of Beam

FIG. 3.28 : UNIT 2 DEFLECTION PROFILES

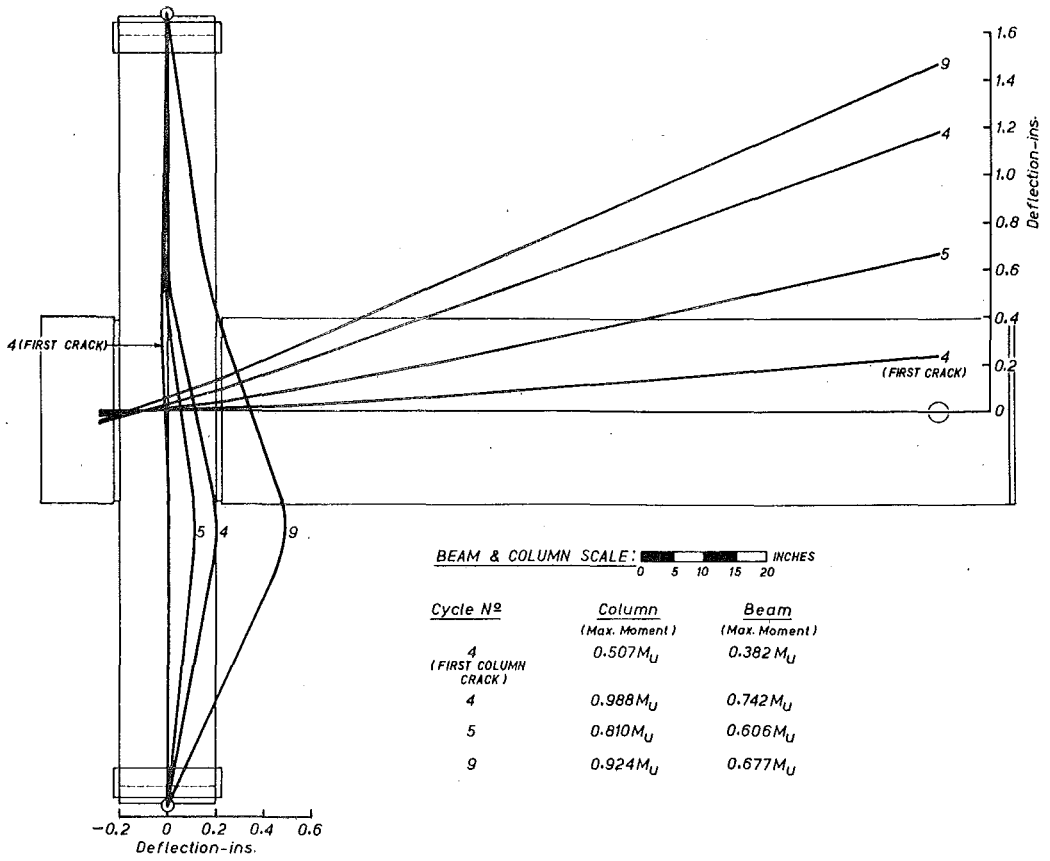

(a) Upward Load at End of Beam

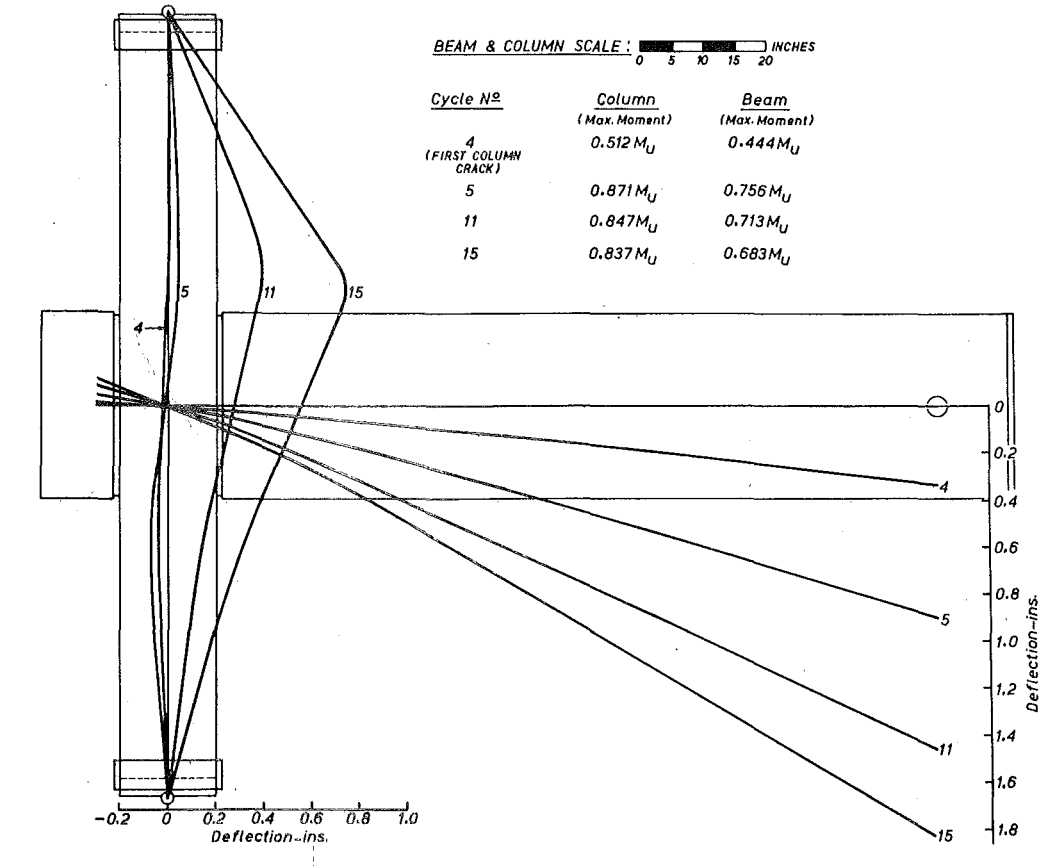

(b) Downward Load at End of Beam

FIG. 3.29 : UNIT 3 DEFLECTION PROFILES

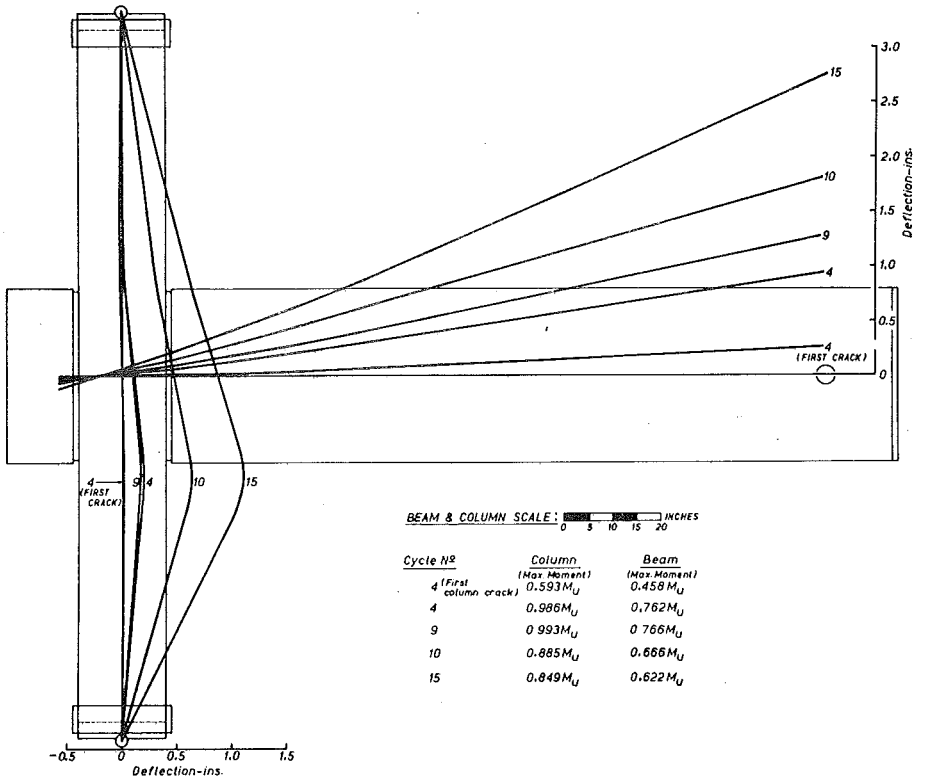

(a) Upward Load at End of Beam

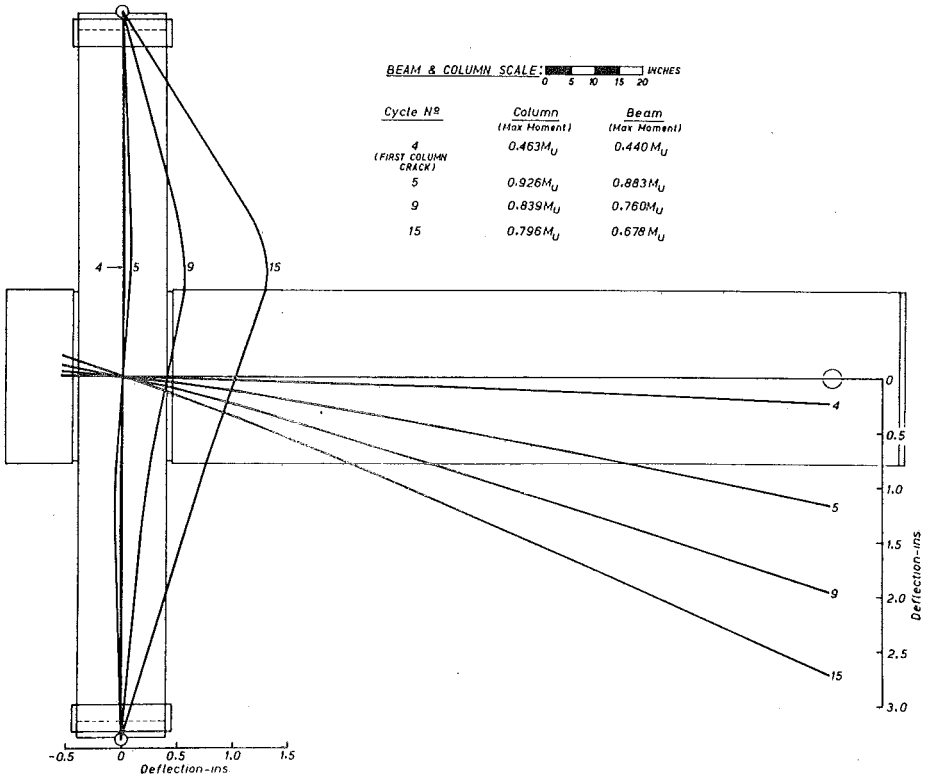

(b) Downward Load at End of Beam

FIG. 3.30 : UNIT 4 DEFLECTION PROFILES

greater than those for which the whole profile could be recorded, as the limits of the dial gauge extensions were exceeded. It should be noted that in Figs. 3.27 and 3.28 only one deflection profile for the column has been plotted (for the case of maximum deflections) as in these units all the column profiles were almost co-linear.

The significance of the curvatures in the zone of the mortar joint for Units 1 and 2 is apparent from the profiles. In Units 3 and 4 there was a horizontal translation at the joint in the direction of the beam axis of up to one inch, subsequent to plastic hinges forming in the column. The resulting moments due to the eccentricity of the axial load were relatively small, but were included in the experimental column moments listed. The discontinuity in the column profile at the plastic hinge is clearly evident in each case.

3.3.6 Deflection Components

The graphical results of the previous two sections can be summarised by tabulating the components of the beam end deflection for the four units as in Tables 3.3 and 3.4. For each direction of loading of a unit the components of deflection at the peaks of three major load cycles are presented. For Units 1 and 2, where the plastic hinge formed in the beam, the basic components considered were; the elastic deformation of the beam, the curvature of the column, the inelastic rotation at the beam hinge, and the shear distortion of the joint. The beam elastic deformation was calculated from the triangular area of elastic curvature on the appropriate curvature distribution plot. The component due to column curvature, which was predominantly elastic, was obtained from the deflection profile of the column for the increment considered. Inelastic beam rotations were measured over the 12 inches gauge length from the column face. The alternative use of curvature distributions to determine beam plasticity was not practicable

Table 3.3 COMPONENTS OF BEAM END DEFLECTION FOR UNITS 1 AND 2

Unit No.	Direction of beam end loading	Cycle No.	Max. beam moment kip ft.	Deflection Components at Beam End - inches					Measured deflection Δ_{test} inches	$\frac{\Delta_{comp.}}{\Delta_{test}}$	Deflection Component Percentages (of measured deflection)			
				Beam elastic	Column curvature	Joint shear distortion	Beam hinge inelastic	Total $\Delta_{comp.}$			Beam elastic	Column curvature	Joint shear distortion	Beam hinge inelastic
1	Upward	4	143.2	0.266	0.168	0.035	0.186	0.655	0.704	0.93	37.8	23.9	5.0	26.4
		9	143.5	0.266	0.211	0.038	0.210	0.725	0.738	0.98	36.0	28.6	5.2	28.5
		15	163.9	0.353	0.288	0.058	1.342	2.041	2.338	0.87	15.1	12.3	2.5	57.5
	Downward	4	-118.0	0.242	0.139	0.028	0.128	0.537	0.563	0.95	43.0	24.7	5.0	22.8
		9	-120.1	0.250	0.155	0.027	0.146	0.578	0.589	0.98	42.4	26.3	4.6	24.8
		15	-176.5	0.315	0.247	0.049	1.410	2.021	2.145	0.94	14.7	11.5	2.3	65.7
2	Upward	4	186.1	0.363	0.241	0.038	0.695	1.337	1.449	0.92	25.1	16.6	2.6	47.9
		9	174.4	0.346	0.240	0.041	0.730	1.357	1.364	0.99	25.4	17.6	3.0	53.5
		15	189.9	0.369	0.241	0.043	2.097	2.750	2.822	0.98	13.1	8.6	1.5	74.4
	Downward	4	-159.9	0.316	0.143	0.033	0.334	0.826	0.862	0.96	36.7	16.6	3.8	38.7
		9	-161.0	0.318	0.168	0.028	0.659	1.173	1.272	0.92	25.0	13.2	2.2	51.8
		15	-183.5	0.363	0.234	0.038	3.580	4.215	4.318	0.98	8.4	5.4	0.9	82.8

Table 3.4 COMPONENTS OF BEAM END DEFLECTION FOR UNITS 3 AND 4

Unit No.	Direction of beam end loading	Cycle No.	Max. column moment kip ft.	Deflection Components at Beam end - inches						Measured deflection Δ_{test} inches	$\frac{\Delta_{comp}}{\Delta_{test}}$	Deflection Component Percentages (of measured deflection)				
				Column elastic	Beam elastic	Joint shear distortion	Column inelastic	Beam hinge inelastic	Total Δ_{comp}			Column elastic	Beam elastic	Joint shear distortion	Column inelastic	Beam hinge inelastic
3	Upward	4	115.0	0.195	0.166	0.117	0.372	0.190	1.040	1.062	0.98	18.4	15.6	11.0	35.0	17.9
		5	94.2	0.160	0.136	0.067	0.164	0.120	0.647	0.654	0.99	24.5	20.8	10.2	25.1	18.3
		9	105.1	0.178	0.151	0.122	0.805	0.203	1.459	1.543	0.95	11.5	9.8	7.9	52.2	13.9
	Downward	5	-118.1	0.203	0.183	0.050	0.232	0.188	0.856	0.864	0.99	23.5	21.2	5.8	26.9	21.7
		11	-111.3	0.192	0.172	0.073	0.628	0.225	1.290	1.420	0.91	13.5	12.1	5.1	44.2	15.9
		15	-106.8	0.184	0.165	0.073	1.264	0.220	1.906	1.900	1.00	9.7	8.7	3.8	66.6	11.6
4	Upward	4	117.6	0.190	0.172	0.068	0.288	0.158	0.876	0.908	0.97	20.9	19.0	7.5	31.8	17.4
		9	118.3	0.191	0.173	0.066	0.463	0.224	1.117	1.238	0.90	15.4	14.0	5.3	37.4	18.1
		15	96.0	0.155	0.141	0.056	1.803	0.104	2.259	2.374	0.95	6.5	6.0	2.4	76.1	4.4
	Downward	5	-137.2	0.222	0.172	0.056	0.285	0.382	1.117	1.201	0.93	18.5	14.3	4.7	23.7	31.8
		9	-118.1	0.191	0.148	0.066	1.050	0.497	1.952	2.002	0.98	9.5	7.4	3.3	52.4	25.0
		15	-105.3	0.170	0.132	0.054	2.118	0.224	2.698	2.756	0.98	6.2	4.8	2.0	76.8	8.1

in all cases, as the onset of crushing denied the determination of curvature from surface concrete strains at the largest increments. The component of deflection due to shear distortion was calculated from surface concrete strain readings diagonally across the joint. The means of calculation is presented in Section B.7.

There is satisfactory correlation between the sum of the deflection components and the actual measured deflection. As would be expected, the former values are smaller as they do not include inelastic curvatures occurring outside the hinge gauge length. For this reason the individual components were calculated as percentages of the measured deflection in Tables 3.3 and 3.4. The good behaviour of the joint is reflected by the low percentage values for joint shear distortion. It is apparent that the dominant deflection component, particularly at large deflections, is that due to inelastic beam curvatures at the plastic hinge.

The basic deflection components considered for Units 3 and 4, where the plastic hinges formed in the column, were; column and beam elastic deformations, joint shear distortion, column hinge plasticity, and inelastic curvatures in the beam. The components due to elastic and plastic column curvature were calculated respectively from the triangular area of elastic curvature in the column, and from the column deflection profile at the increment considered. The other three components were calculated as for Units 1 and 2, except that the gauge length over which beam inelastic rotations were measured was 16 inches in this case. It is clear from Table 3.4 that a high proportion of the deflection at large deformations is due to plasticity in the hinges of the column. The values of the components for joint shear distortion are larger in these cases than for Units 1 and 2, because of the greater moments at the joint, but are still small relative to the total deflection. The component for joint shear distortion is greater for Unit 3 than for

the heavily bound column of Unit 4.

3.3.7 Transverse Steel Stresses

The strains in critical stirrups in the beam-column joint region were read from electrical resistance strain gauges throughout the tests. The steel stresses and strains sustained in the four units are shown in Figs. 3.31 to 3.34. For clarity only the stresses for upward loading to the maximum moment capacity during cycle 15 are shown in Fig. 3.31 for Unit 1. It must be recognised that the stresses in the legs of the stirrups will vary down their depths, particularly at points of horizontal cracking in the beam caused by flexing of the column. However, the gauges which are placed at the centre of the legs of the stirrups provide an indication of the stresses present. The stress in the beam stirrup closest to the joint approached yield, but the stresses elsewhere were low. Fig. 3.32 shows the pattern of strains at the centre of the critical beam stirrup of Unit 2, during the course of the 15 load cycles. Strains close to yield were sustained in the final cycle. Also included in this figure is the comparative strains of the beam stirrups during part of one cycle. The strains in the spirals of the column were not included as they were very low.

An indication of the stress levels in the ties and spirals of Units 3 and 4, at the peaks of selected cycles, may be seen in Figs. 3.33 and 3.34. It is significant that in Unit 3 the strain in the column tie gauge C2, in the compression zone, is comparable to the steel strain at mid-depth of the section, as shown by gauge C1. The maximum stresses recorded in the column steel were 33,100 psi and 19,500 psi for Units 3 and 4 respectively. In both cases this was well below yield stress.

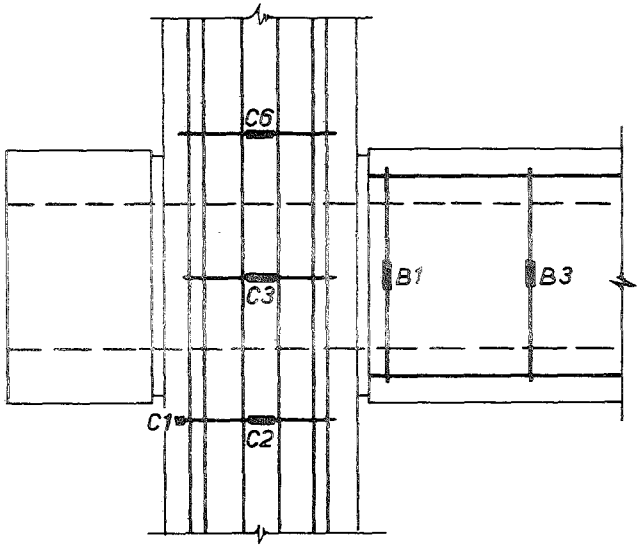

-STRAIN GAUGE POSITIONS-

NOTE: 1-Yield stress for transverse steel :-

Beam — f_y = 49,200 psi

Column — f_y = 49,400 psi

2-Positive stress is tensile.

3-Readings are for cycle 15, upward load increments to maximum moment capacity.

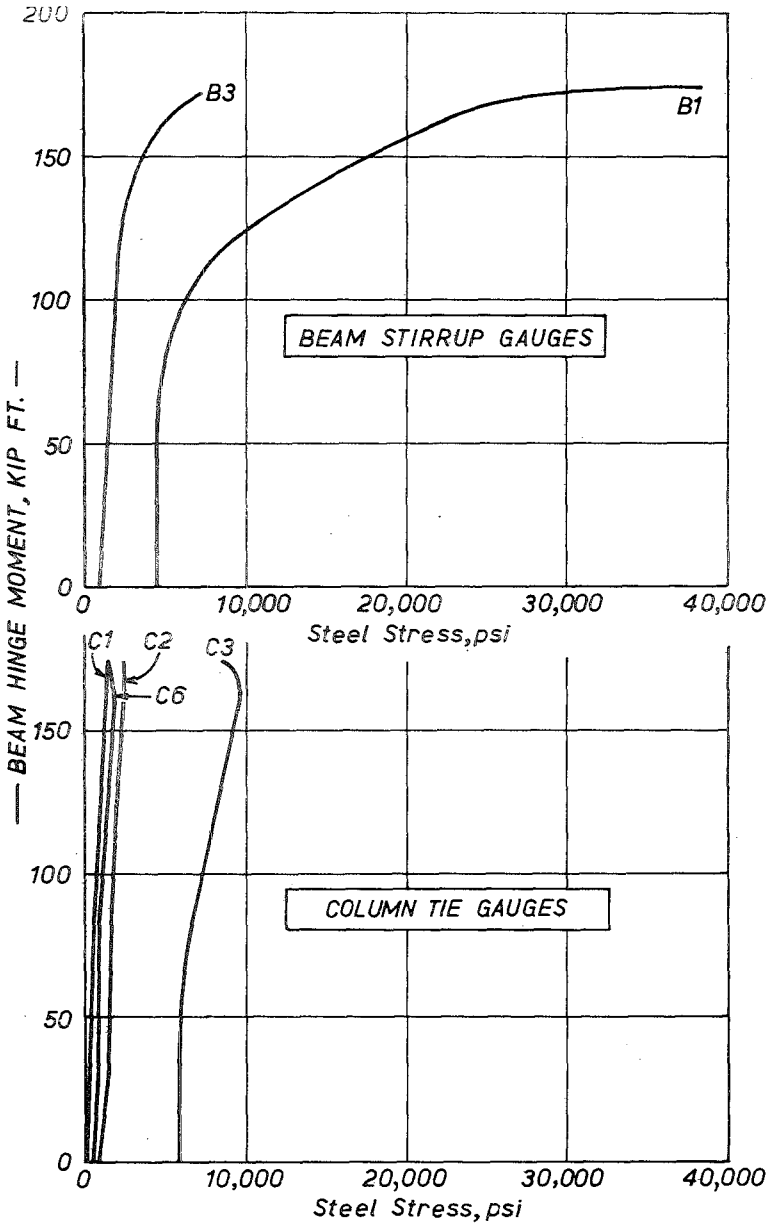

FIG. 3.31 : STRESSES IN STIRRUPS AND TIES OF UNIT 1

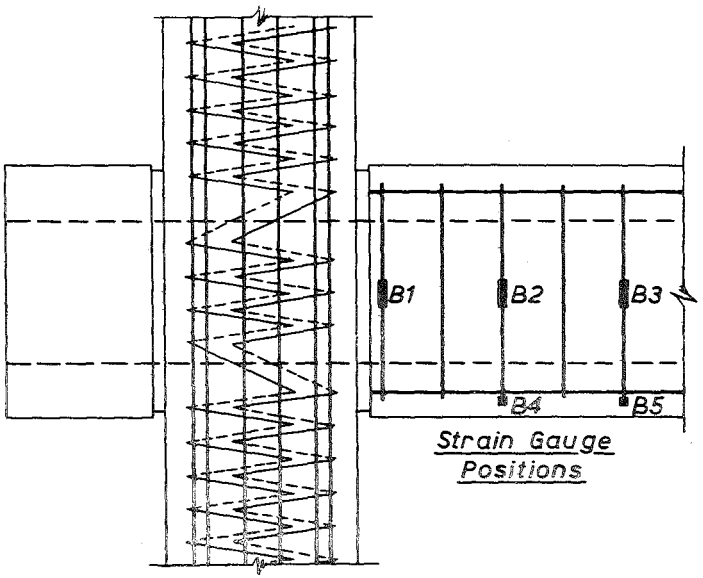

Strain Gauge Positions

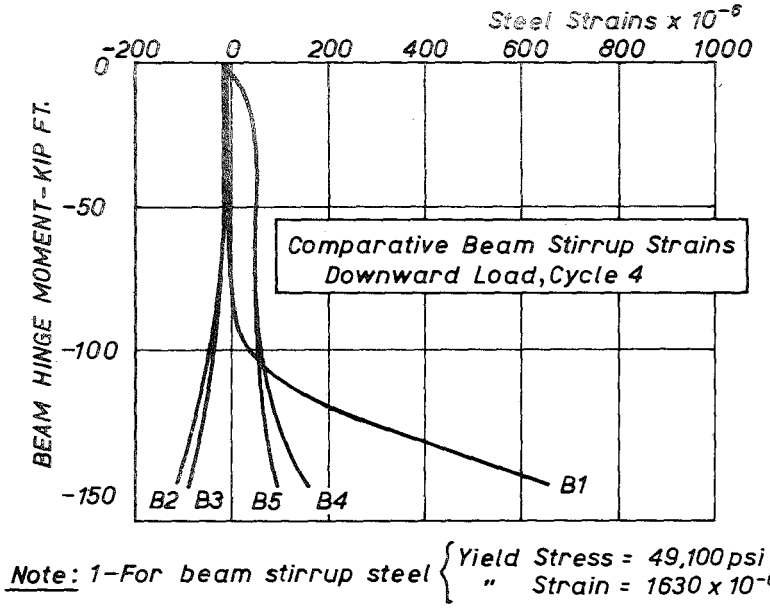

Note: 1-For beam stirrup steel { Yield Stress = 49,100 psi
" Strain = 1630 x 10⁻⁶

2-Positive strain is tensile.

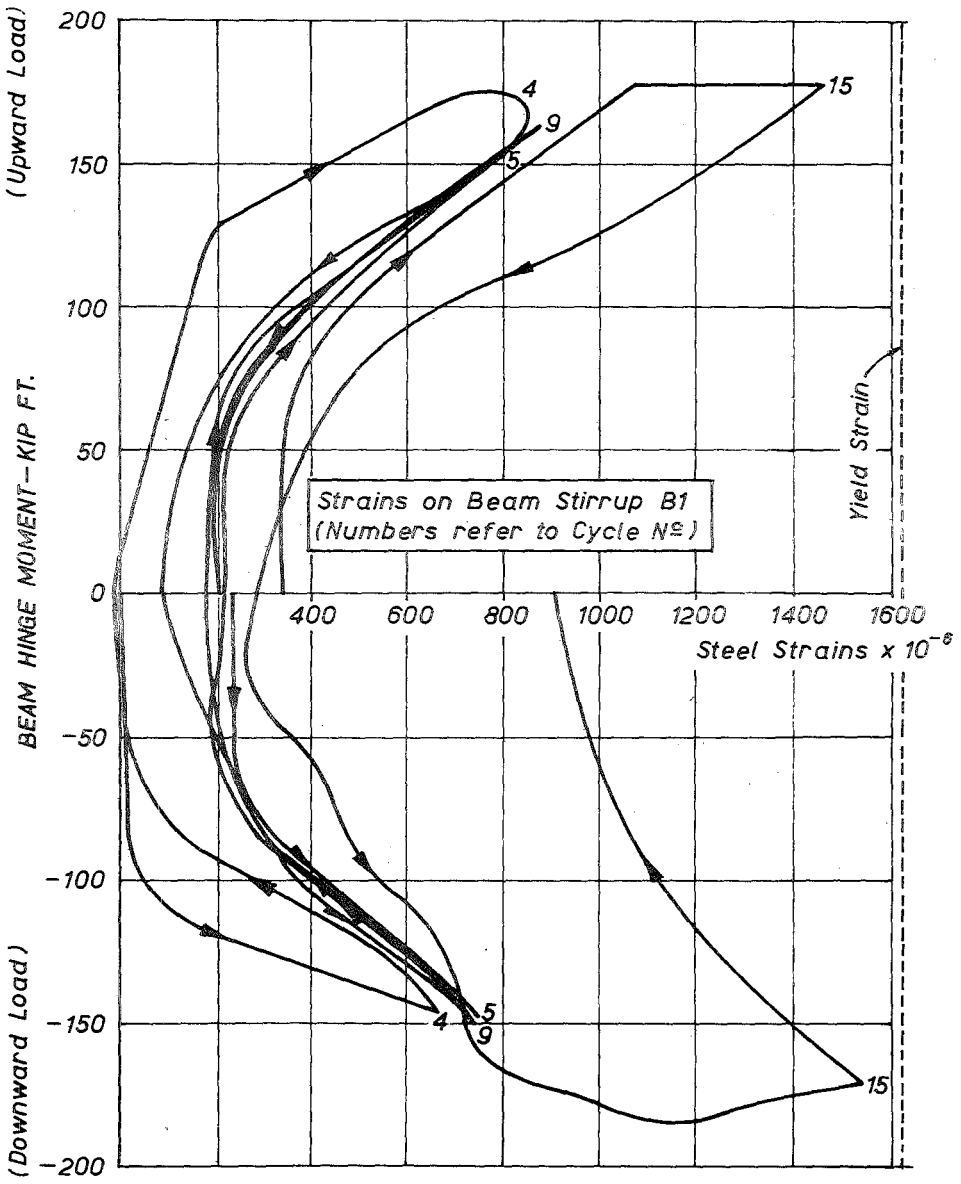

FIG. 3.32 : STRAINS IN STIRRUPS OF UNIT 2

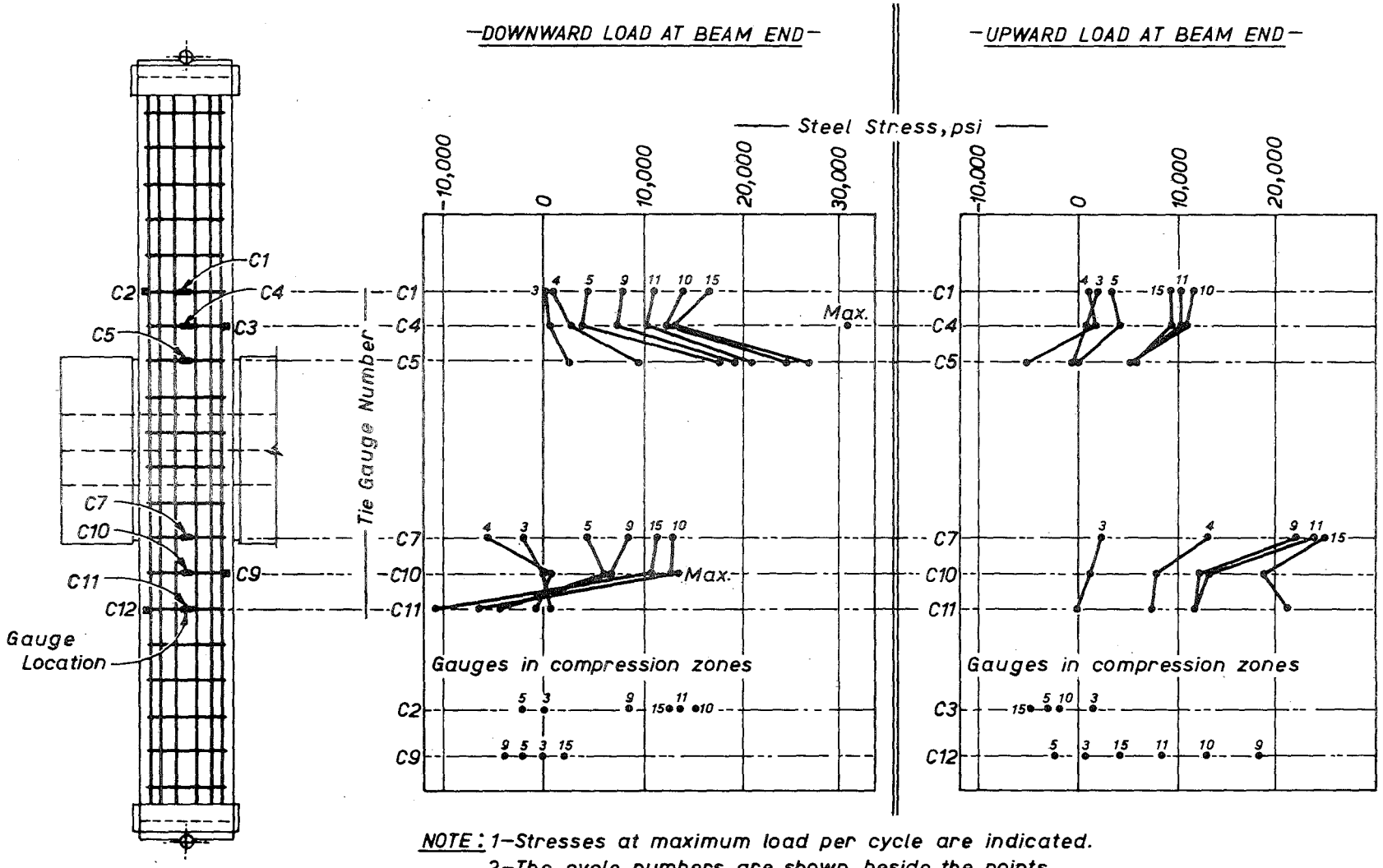

NOTE: 1—Stresses at maximum load per cycle are indicated.
2—The cycle numbers are shown beside the points.
3—Positive stress is tensile.
4—Yield stress of ties = 49,200 psi.

FIG. 3.33 — STRESSES IN COLUMN TIES OF UNIT 3

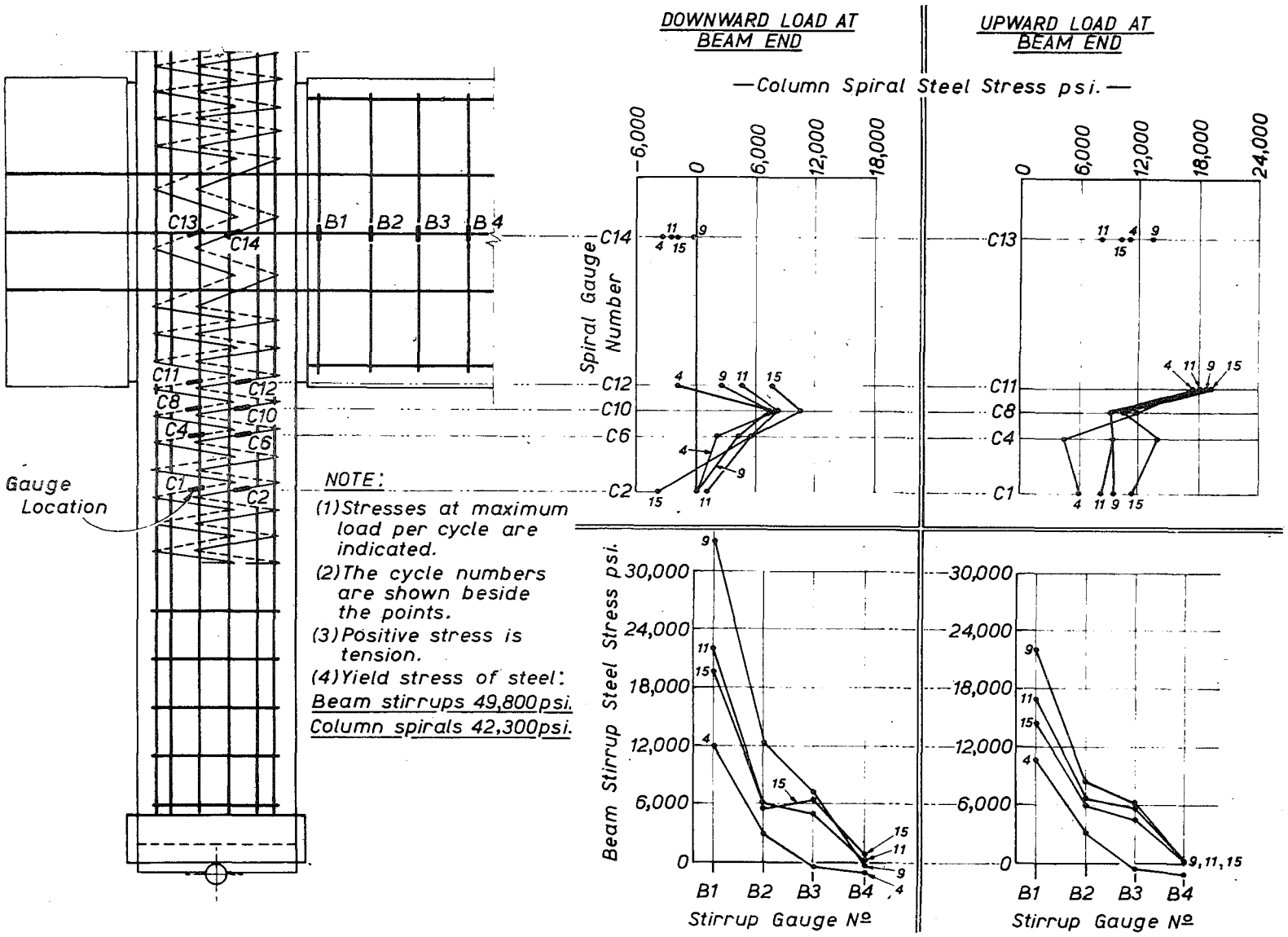

FIG. 3.34 : STRESSES IN STIRRUPS AND SPIRALS OF UNIT 4

3.4 DISCUSSION OF TEST RESULTS

The following points arise from the experimental results reported:

3.4.1 Energy Dissipation

The moment-rotation curves presented show that prestressed concrete members have little energy dissipation capacity while they remain in the cracked elastic range. However, the non-linear response analysis of Spencer[6] indicated that the member curvatures of a framed structure under an earthquake do not go beyond this range. If the maximum beam rotational ductility factor of 5 obtained in that study is generally correct, there would be little or no structural damage. If the rotational ductility factor required is greater than 5, there is a large reserve of energy dissipation available once the concrete has commenced to crush. However, at this stage the members have been structurally damaged with consequent difficulty of repair back to a fully prestressed condition.

3.4.2 Ductility

It was evident that large post-elastic deformations were available in all units. For these units there was no significant advantage in putting more transverse steel in the members than was required as shear reinforcement by normal prestressed concrete codes. The electrical resistance strain gauge measurements on the transverse steel in the columns of Units 3 and 4 showed that this steel did not yield as is commonly assumed, and in fact the stresses were quite low. This latter result is supported by recent research on columns confined by rectangular ties[55]. One rather undesirable effect of the heavy rectangular spirals was to precipitate the spalling of the cover concrete. The only advantage gained from the spirals in these tests was the prevention of a bond failure of the prestressing duct through the column at far

advanced strains. However, it should be noted when considering the effectiveness of the heavy spirals that the column loads were low. At higher axial loads there is more justification for including heavy hooping.

The tests showed the advantage of spreading the prestressing steel over the section. At high curvatures, after crushing of the concrete had commenced, the cables in the compression zone of the member acted as compression reinforcement and prevented a rapid deterioration of moment carrying capacity.

3.4.3 Bond Failure

The bond failure of the prestressing duct through the column, when the top cable of Unit 1 was in compression, is a point of concern at extremely large rotations under catastrophic loading. However, a more critical case would be that of an interior beam-column assembly, where the cable in the beam on one side of the column is in compression and on the other side of the column is in tension. The combined compressive and tensile force in the cable may be sufficient to break down the bond between the tendons and the duct, or the duct and the column, resulting in a reduction in moment carrying capacity of the beams when the tendons push through. It is therefore desirable that corrugated ducts be used through the columns for both interior and exterior beam-column assemblies to minimise the possibility of a bond failure between the duct and the column as occurred in Unit 1.

3.4.4 Joint Behaviour

There was little loss of mortar from the joint under cyclic load reversals, even when no internal binding was provided. The plastic curvature extended well along the beam and did not concentrate only at the mortar joint. Apart from a stress concentration in the compression zone caused by a recess of the mortar for architectural reasons, the

joint region behaved in a similar manner to that expected of a monolithic joint, except that cracking in the joint occurred earlier because of the lack of tensile strength.

3.5 CONCLUSIONS

This series of tests showed that prestressed concrete framed structures can be capable of resisting moderate earthquakes without structural damage, and of withstanding severe earthquakes although in this case structural damage may occur. Specific conclusions were as follows:

(a) Energy dissipation is relatively small prior to the commencement of crushing of the concrete, but substantial once crushing has occurred. Evidence is required from response analyses to show if this reserve of energy dissipation is necessary under severe earthquakes, and the actual ductility demands on the members.

(b) Large post-elastic deformations can be available in prestressed concrete members, even when the transverse reinforcement satisfies only normal prestressed concrete code requirements for shear. Heavy column spirals, satisfying the requirements of the SEAOC code for reinforced concrete for ductility, are felt to be unnecessary for the type of frame unit tested which had relatively low column loads.

(c) Substantial stiffness degradation is apparent for prestressed concrete members after high intensity cyclic loading.

(d) It is recommended that corrugated metal ducts be used for post-tensioning cables through columns for both interior and exterior beam-column assemblies. This precaution is to minimise the possibility of loss of moment capacity in the beams due to bond failure between the ducts and the column.

(e) Mortar joints between precast post-tensioned frame members can behave satisfactorily under high intensity load reversals.

CHAPTER 4

MOMENT-CURVATURE CHARACTERISTICS FOR PRESTRESSED CONCRETE MEMBERS UNDER MONOTONIC LOAD

SUMMARY

A theoretical determination of the moment-curvature relationships of prestressed concrete members under monotonic loading to failure is developed and tested against experimental results. The theory is used to present the effects on ductility of a number of practical section variables: steel area ratio, distribution of the prestressing steel within the section, degree of transverse reinforcement, and axial load. A comparison is made of the ductility available in comparable prestressed and reinforced concrete members. Finally, nomograms are presented for the determination of the curvature ratio at crushing for prestressed concrete members with varying steel area ratios and axial loads.

4.1 INTRODUCTION

It is shown in Chapter 5 that the monotonic loading (that is, loading in one direction) moment-curvature relationship is almost colinear with the envelope of cyclic loading curves, for a particular prestressed concrete member. Thus the monotonic load characteristics are a convenient measure of the ductility available in prestressed concrete members under seismic load. Previous theoretical analyses of prestressed concrete members under monotonic load, for example those by Priestley[56] and Sherbourne and Parameswar[57], determined moment-curvature curves up to a theoretical "ultimate" concrete compressive strain of 0.004. However deformations resulting in considerably greater strains than this may well be sustained under a severe earthquake. The existing

theory therefore needs to be extended to cover this eventuality.

Firm recommendations have been published for designers to attain fully ductile reinforced concrete members[50,51]. These were based on a history of earthquake behaviour and research information on this material. No such extensive guide exists yet for prestressed concrete. As a step towards overcoming this deficiency a study is made of the effect on ductility of a number of section variables, which would be of practical use to the design engineer.

4.2 THEORY FOR MONOTONIC LOADING ANALYSIS

4.2.1 Assumptions

The following assumptions are made:

(i) Plane sections remain plane after flexure

(ii) A stress-strain curve is assumed for the concrete (see below)

(iii) A stress-strain curve is assumed for the prestressing steel (see below)

(iv) It is assumed that no losses due to time dependent effects, such as creep, occur during the course of loading.

Two of these assumptions need to be presented in detail as follows:

(a) Concrete Stress-Strain Curve

Knowledge of the stress-strain characteristics of concrete is important for analysis of the behaviour of reinforced and prestressed concrete sections. A large number of stress-strain curves for concrete have been postulated by many investigators, for example[58,59,60,61,62,63,53,64,65]. These have been extensively reviewed by Kent[66] and more recently by Popovics[67], and consequently will not be discussed in detail here. Also, concrete compression is often represented by the stress block parameters of Hognestad, Hanson, and McHenry[68]. Rüsch[69] has shown that the shape of the stress-strain curve is influenced by such factors as concrete strength and rate of loading, and no single curve

will fit all cases. Furthermore many of these expressions have been evolved from load-deformation responses of specimens under axial load, but the validity of relating these to a member in which a flexural strain gradient exists across the section has been questioned[70]. It must be noted, however, that Hognestad et al[68] concluded that the general characteristics of stress-strain relationships for concrete in concentric compression were applicable also to flexure, and this has been supported by recent work of Ghosh and Handa[71]. The latter study separated the effects of strain gradient in a section under flexure and differential strain rate for different fibres, and showed that the former effect has very little influence on the stress-strain curves of concrete in compression. Fortunately any discrepancies in the expressions which have been proposed are not serious, as the moment curvature relationship of a prestressed concrete member is not greatly influenced by the exact shape of the stress-strain curve of the concrete.

It is important for this study that the concrete model chosen adequately represents the "falling" branch behaviour of the stress-strain curve. Yet it is in this region that mathematical expressions generally have been lacking. However one recent postulation by Kent and Park[72] was felt to be the most suitable representation of the complete stress-strain curve. The "falling" branch characteristics were based on an analysis of the results of several investigators' work on unconfined and confined concrete in compression. The resulting expression makes allowance for the influence of both the lateral confinement and the concrete strength on the slope of the "falling" branch. There are three regions for the curve in compression, as illustrated in Fig. 4.1. The expressions for each region are as follows:

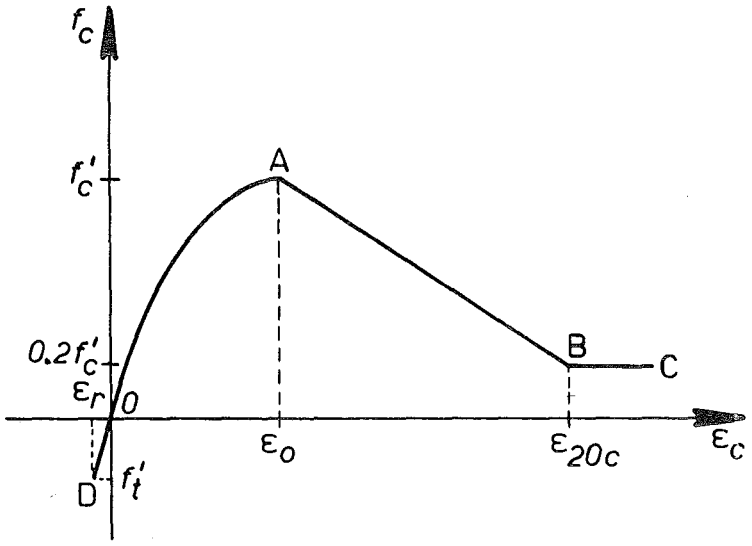

FIG. 4.1 : ASSUMED STRESS-STRAIN RELATION FOR CONCRETE

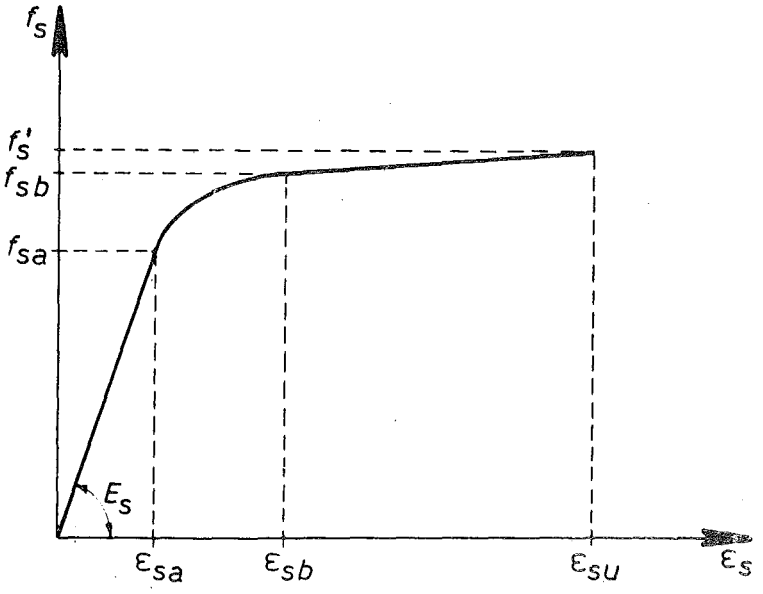

FIG. 4.2 : ASSUMED STRESS-STRAIN RELATION FOR PRESTRESSING STEEL

Region OA: $\epsilon_c \leq \epsilon_o$

$$f_c = f'_c \left[\frac{2\epsilon_c}{\epsilon_o} - \left(\frac{\epsilon_c}{\epsilon_o}\right)^2 \right] \quad \ldots (4.1)$$

Region AB: $\epsilon_o \leq \epsilon_c \leq \epsilon_{20c}$

$$f_c = f'_c \{1 - Z(\epsilon_c - \epsilon_o)\} \quad \ldots (4.2)$$

where Z is a parameter which defines the slope of the "falling" branch, and is derived from:

$$Z = \frac{0.5}{\epsilon_{50h} + \epsilon_{50u} - \epsilon_o} \quad \ldots (4.3)$$

where $$\epsilon_{50u} = \frac{3 + 0.002f'_c}{f'_c - 1000} \quad \ldots (4.4)$$

and $$\epsilon_{50h} = \frac{3}{4} p'' \sqrt{\frac{b''}{s}} \quad \ldots (4.5)$$

where p'' = binding steel ratio, b'' = minimum dimension of confined core, and s = spacing of transverse reinforcement.

Region BC: $\epsilon_{20c} \leq \epsilon_c$

$$f_c = 0.2f'_c \quad \ldots (4.6)$$

The stress-strain relationship in the tension region, OD , is assumed to follow the slope of the parabola of Region OA at the origin, and is given by:

$$f_c = \frac{2f'_c}{\epsilon_o} \epsilon_c \quad \ldots (4.7)$$

The maximum tensile strength of the concrete is assumed to be given by the expression:

$$f'_t = 7.5 \sqrt{f'_c} \quad \ldots (4.8)$$

in accordance with the recommendations of the A.C.I. 318-71 code[41].

(b) Steel Stress-Strain Curve

The stress-strain relation for the prestressing steel is assumed to be of a "linear-hyperbolic curve-linear" form as is illustrated in Fig. 4.2. The three regions which comprise the stress-strain relationship are expressed by:

$$\epsilon_s \leqslant \epsilon_{sa} \qquad f_s = \epsilon_s E_s \text{ , where } E_s = \frac{f_{sa}}{\epsilon_{sa}} \quad \ldots (4.9)$$

$$\epsilon_{sa} \leqslant \epsilon_s \leqslant \epsilon_{sb} \qquad f_s = \frac{f_{sb}\epsilon_{sb} - f_{sa}\epsilon_{sa}}{\epsilon_{sb} - \epsilon_{sa}} + \frac{\epsilon_{sa}\epsilon_{sb}(f_{sa} - f_{sb})}{\epsilon_s(\epsilon_{sb} - \epsilon_{sa})} \quad \ldots (4.10)$$

$$\epsilon_{sb} \leqslant \epsilon_s \qquad f_s = f_{sb} + \frac{\epsilon_s - \epsilon_{sb}}{\epsilon_{su} - \epsilon_{sb}}(f'_s - f_{sb}) \quad \ldots (4.11)$$

The hyperbolic assumption for the curved part of the stress-strain relation fits closely to experimental curves obtained for steel control specimens.

4.2.2 Development of Moment-Curvature Relationship

The theory enables moment-curvature relationships to be computed for sections with general dimensions, with or without axial load, and with the prestressing tendons distributed into up to five positions down the section. The moment-curvature relationship is obtained in three successive stages depending upon the position of the neutral axis, as illustrated in Fig. 4.3. For the purpose of a general illustration an eccentric prestressing force is assumed. It is to be noted that the

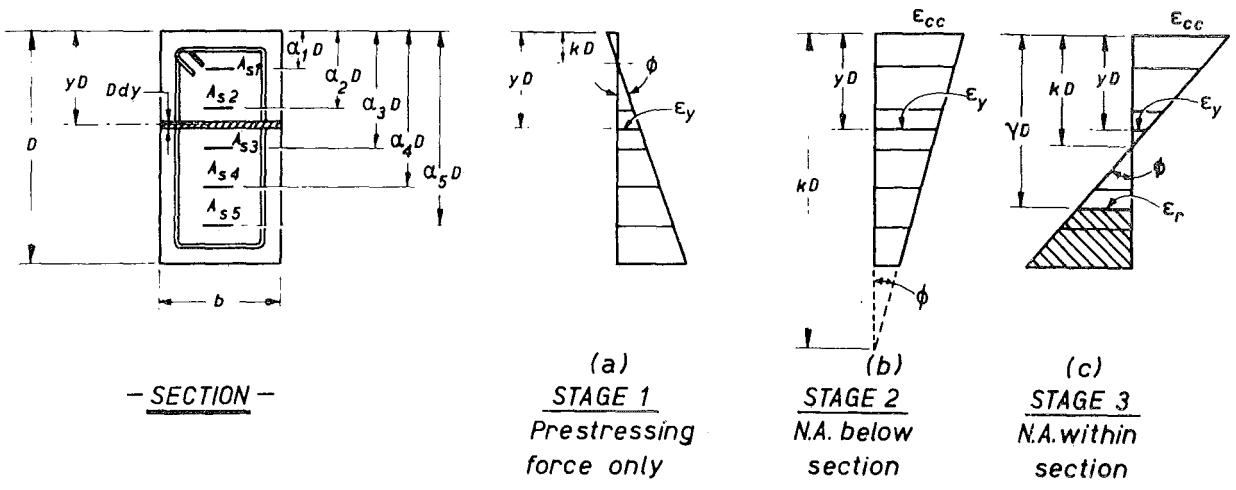

FIG. 4.3 : STRAIN PROFILES FOR THREE STAGES OF LOADING

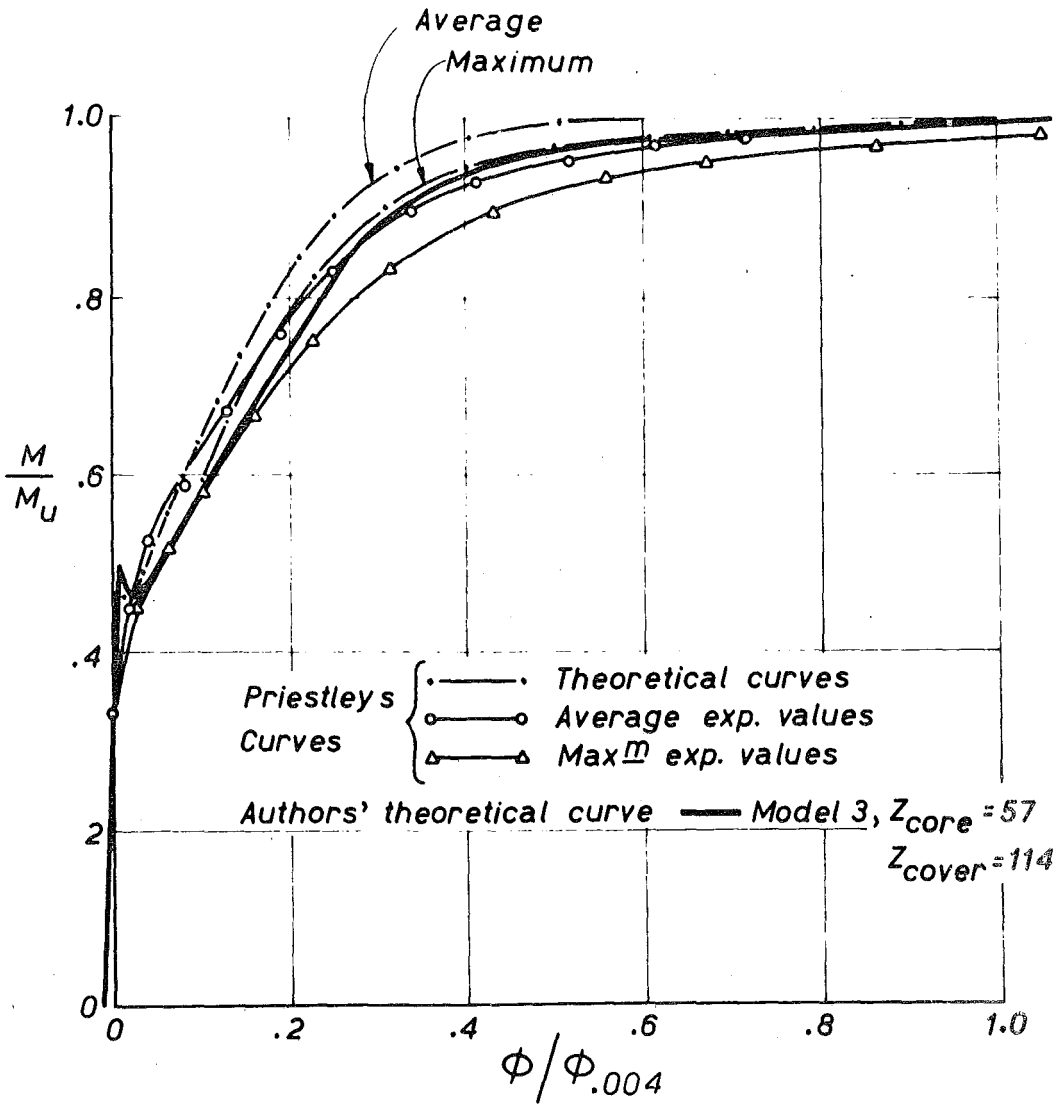

FIG. 4.4 : COMPARISON WITH PRIESTLEY'S[56] RESULTS

curvature is given by the angle φ in the figure. In this Chapter only a summary of the theoretical approach will be given. Details of the analysis are included in Appendix C.

(a) Stage 1 (Fig. 4.3a)

When the section is subjected to prestressing force only it will have a negative (hogging) curvature if the prestressing force has a downward eccentricity. The initial curvature may be calculated directly from the initial strain profile. If an increasing external positive moment is applied to the section the neutral axis will move upwards out of the section, until the next stage is reached.

(b) Stage 2 (Fig. 4.3b)

During this stage the whole section is under compression, and the neutral axis lies below the section.

The total compressive force in the concrete is given by,

$$C = \int_0^1 f_c b D . dy \qquad \ldots (4.12)$$

where f_c is the stress in the concrete fibre at a distance, yD, from the top.

The surface concrete strain is less than ϵ_o during this stage, and f_c may be represented by equation (4.1).

The steel strain at each tendon may be found from the sum of the initial steel strain due to prestress and the concrete strain at the level of the steel as determined from the neutral axis depth. The steel stresses are calculated from equation (4.9) as the steel strains are in the elastic range during this stage. By summation of the individual tendon forces the total tensile force, T_s, is calculated.

From equilibrium of forces on the section,

$$C = T_s + P \qquad \ldots (4.13)$$

where P is the external axial load ($P = 0$ in the case of a beam). The

substitution for C and T_s into equation (4.13) leads to a quadratic equation, from which the curvature corresponding to any value of neutral axis depth may be obtained. The corresponding moment can then be calculated.

Values of curvature and moment are determined for successively reducing values of neutral axis depth below the section.

(c) Stage 3 (Fig. 4.3c)

The neutral axis lies within the section during this stage. The bottom fibres are under tension and cracks form at strains beyond the limiting tensile strain. The compressive force in the concrete is given by:

$$C = -\int_k^0 f_c bD.dy \qquad \ldots (4.14)$$

where f_c is represented by equations (4.1), (4.2) and (4.6).

The tensile force in the concrete, T_c, depends on the existence of cracks. For the case where there are no cracks:

$$T_c = \int_k^1 f_c bD.dy \qquad \ldots (4.15)$$

where f_c is given by equation (4.7).

For the case where cracking has occurred:

$$T_c = \int_k^\gamma f_c bD.dy \qquad \ldots (4.16)$$

where γD is the distance from the extreme compression fibre to the top of the crack.

The total tensile force in the steel, T_s, is determined from the stresses in the prestressing steel at each level. Stresses for particular strains are found from the appropriate equation (4.9) to (4.11).

From force equilibrium,

$$C = T_s + T_c + P \qquad \ldots (4.17)$$

An iterative process was necessary for the solution of equation (4.17) because of the complex nature of the stress-strain relationships for the concrete and steel. For successive increments of surface concrete strain of 0.0001, the neutral axis depth was found and the corresponding curvatures and moments calculated.

The program time required on an IBM 360/44 computer, for analysis of the moment-curvature relationship of a member loaded to failure, was of the order of 2 minutes.

4.2.3 Models for Behaviour of Cover Concrete

Divergent opinions are held on the ability of the cover concrete in beams or columns to sustain stress at high curvatures. Four general approaches can be listed for consideration of the effectiveness of the cover concrete:

(i) It has been suggested that it would be appropriate to consider the cover concrete as following the same "falling" branch stress-strain relationship as the core concrete, without assigning a value of strain at which the cover concrete is assumed to be ineffective. Mattock[73] pointed out that the maximum concrete compressive strain in a reinforced concrete beam can be very much in excess of the usually assumed value of 0.003.

(ii) The second approach is to consider that the cover concrete spalls once it reaches a specified maximum compressive strain in the extreme compression fibre. Baker and Amarakone[53] recommended a limiting strain value for unbound concrete of 0.0035. Also, Blume, Newmark, and Corning[50] recommend a value of 0.004. Kent[66] chose a maximum allowable compressive strain for the cover concrete of 0.004, and considered this to be conservative in most cases.

(iii) Soliman and Yu[64] studied the stress-strain relationship of bound concrete in flexure. The variables in their test sequence included,

amongst others, the spacing of the transverse reinforcement and the cover outside the transverse reinforcement. A stress-strain expression was derived which applies to the whole concrete cross section while depending on the area of the cover concrete.

(iv) A further possible approach is to consider the cover concrete to follow a separate stress-strain relationship from that for the core concrete, beyond a strain of ϵ_o. Thus different slopes can be assigned to the "falling" branch relationship of the cover and core concretes to take into account their different degrees of confinement.

To determine the most suitable approach, the three following analytical models for the stress-strain relationship of the cover concrete were developed:

(a) Model 1. The cover concrete follows the same stress-strain relationship as the core concrete

(b) Model 2. The cover concrete follows the same stress-strain relationship as the core concrete up to a strain of 0.004, but subsequently any cover concrete at a strain greater than 0.004 is considered to have spalled and become ineffective.

(c) Model 3. The cover concrete can follow a separate stress-strain relationship from the core concrete at strains greater than ϵ_o.

One difficulty in the use of Model 3 should be noted. For a horizontal section in a member at a level below the top of the core, there may be different stresses in the adjacent cover and core concretes for a given strain. Thus a shear stress will arise at the outside of the core. This situation may well occur in an actual member, but its inclusion in this analysis was considered to be unwarranted because any effect due to this shear is probably within the limits of accuracy imposed by the concrete stress-strain idealization.

4.3 THEORETICAL STUDY OF BEAMS

4.3.1 Comparison of Theory and Experiment

For the beams studied, $\epsilon_o = 0.002$ is assumed in equations (4.1), (4.2) and (4.3) as used by Kent and Park[72], and as found in the concrete control cylinders of Units 1 and 2 ($f'_c = 6000$ psi).

(a) Priestley's Tests

Few experimental results have been published showing moment-curvature relations for prestressed concrete, and hence a comprehensive comparison of the theory with experimental results cannot be made. However, one well documented series of tests which could be used was those of Priestley[56]. Seven beams with an 8 inches x 4 inches cross section were tested simply supported over a span of 14 feet 9 inches. The beams were loaded by two point loads to give a constant moment zone over the central 6 feet of the span. Stirrups were included in the constant moment zone of only one of the beams (Beam MK5B) and hence only in this case can a direct comparison be made with the author's theory for confined compression zones. Also, readings were not taken beyond the stage of crushing of the compression fibres. A comparison of Priestley's and the author's curves are shown in Fig. 4.4. Priestley recorded experimentally both the average curvature over the length of the constant moment zone and the average of the maximum curvatures occurring at the tension crack positions within the constant moment zone. He also plotted moment-curvature relationships determined from his theory for both the curvature at a section which cracks in tension (that is, the "maximum" curvature), and for the "average" curvature which takes into account changes in stress conditions between cracks. To standardize the curves, all values of the moment, M, were divided by the theoretical "ultimate" moment, M_u, and the curvatures, φ, were divided by the theoretical "ultimate" curvature at a crack, $\varphi_{0.004}$. The

theoretical curves were calculated assuming an "ultimate" compressive strain in the concrete of 0.004.

The theoretical approach used by the author determined moments and curvatures at a section which cracks and therefore corresponds to Priestley's "maximum" experimental and theoretical curves. The Model 3 analytical curve with $Z_{cover} = 2 \times Z_{core}$ was chosen as providing the best representation of the concrete stress block. This assumption will be discussed more fully later. Correlation with Priestley's theoretical curve was good and related well to the shape and "ultimate" conditions of the experimental curve.

It will be noted that there is a difference in the behaviour at cracking between theory and experiment. On the author's theoretical curve there is a drop in load after cracking. Prior to flexural cracking, a tensile force is developed in the concrete at the bottom of the beam. When the beam cracks the tension force in the prestressing steel must increase to compensate for the loss of force in the concrete, and for a prestressed concrete beam with a low steel percentage a considerable steel strain may be required to reach equilibrium again. In the process a large crack height will be developed. During this stage there is a temporary reduction in moment resistance apparent on the theoretical curve. If all the cracks in the constant moment zone of Priestley's beam had formed simultaneously, a drop of load would have been expected at cracking because the deflection was held constant. As in fact the cracks did not appear simultaneously, the exact load at which cracking was initiated was not discernible and does not appear on the experimental plot.

In this study the theoretical approach based on maximum curvature will be compared with experimental readings of average curvature from gauge lengths up to 12 inches. The similarity between the author's theoretical curve and Priestley's experimental "average" curve justifies this approach. The large difference between the average and maximum

curvatures at a concrete strain of 0.004 in Priestley's test was because crushing occurred only above one or two cracks within the 6 feet length of the constant moment zone. However the much smaller gauge length used in the author's tests will result in a closer relationship between the average and maximum values.

(b) The Author's Tests

The results of the investigation described in Chapter 3 form a useful basis for testing the theory. Although the experiments involved cyclic loading of the members, the envelope of the moment-curvature curves so obtained for prestressed concrete is almost colinear with the monotonic curve, as shown in Chapter 5.

Fig. 4.5 makes a comparison for Unit 1 of a theoretical curve and the experimental moment-curvature curve from a 12 inch beam hinge gauge length. Experimental curvatures were not read beyond crushing, and thus a subsequent direct comparison was not possible. However a moment-deflection curve had been plotted and at large deformations this closely reflects the moment-curvature behaviour (see Section 6.3.3). To represent the behaviour of the cover concrete, Model 1 theoretical curve was chosen with the same Z value for the cover as for the core. The resulting theoretical post-crushing behaviour shown in Fig. 4.5 is very similar to that for Unit 1 in Fig. 3.10. The initial reduction in moment capacity after crushing was 15% both experimentally and theoretically. The discontinuity in the theoretical curve at large curvature occurs at the point of fracture of the tension steel at an assumed ultimate strain of 0.04. This represents a minimum value for prestressing wires, as strains of the order of 0.06 were recorded for some control specimens in this study.

The theoretical curve shows a greater initial stiffness than the experimental curve for the 12 inches gauge length adjacent to the column face. This is because the theoretical curves do not take into account

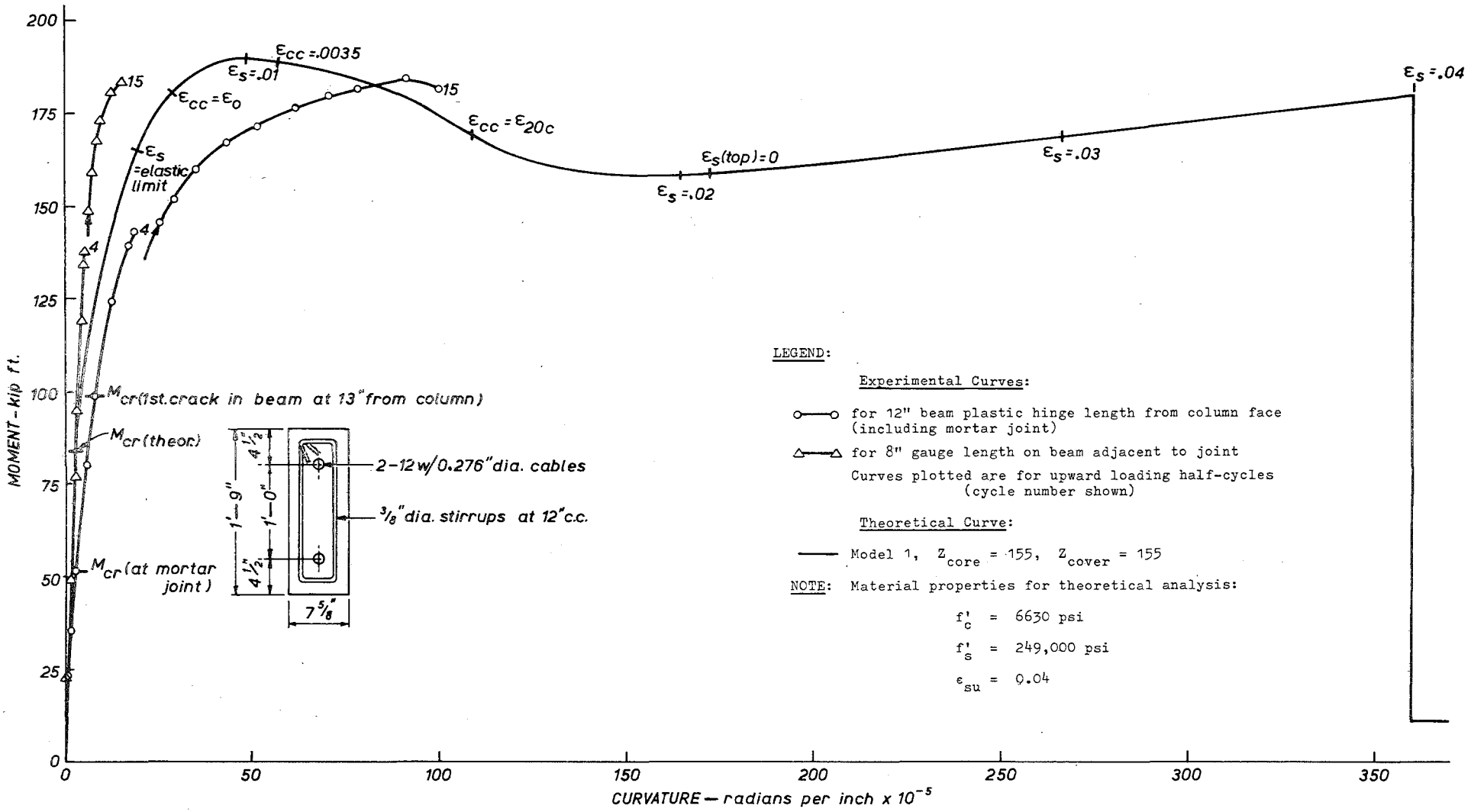

FIG. 4.5 : COMPARISON OF UNIT 1 BEAM & THEORETICAL MODEL

the smaller cross section of the $\frac{1}{2}$ inch recessed mortar joint at the column face. The reduced stiffness plus the lack of tensile strength across the mortar joint caused the first crack to occur in the joint at a lower moment than that predicted. For a further comparison, the experimental moment-curvature relationship for the 8 inches gauge length on the beam adjacent to the joint (but excluding the mortar joint) is also plotted in Fig. 4.5. The initial stiffness of this experimental curve corresponds exactly to the theoretical beam stiffness. However beyond the theoretical cracking moment the two curves diverge because no tension crack formed within the 8 inches gauge length.

Significant strains in the top compression fibre and in the bottom tendon have been plotted in the theoretical curve in Fig. 4.5. The curvature when the top tendon is reduced to zero stress under monotonic load has been noted (ϵ_s(top) = 0). This condition does not indicate that this tendon will suffer a permanent loss of prestress should the external moment be returned to zero (unless the concrete has crushed) because at no stage were the compressive strains very great and the steel would remain in the elastic range during both loading and unloading. The strain limits recommended by the F.I.P. Seismic Commission[38] for "moderate" and "severe" earthquakes (ϵ_s = elastic limit, ϵ_{cc} = 0.0035) have also been noted.

Experimental curvatures were read to higher values for Unit 2 than for Unit 1, and a more complete comparison of theory and experiment for behaviour after the onset of crushing was possible, as illustrated in Fig. 4.6. Experimental points are for two major cycles of upward load on the beam. The comparison made for Unit 1, between theory and experiment for initial stiffness, applies also in this case. All three theoretical models for the concrete stress block after maximum stress are presented in Fig. 4.6. Model 1, which allowed the cover concrete to follow the same stress-strain relationship as the core concrete, closely

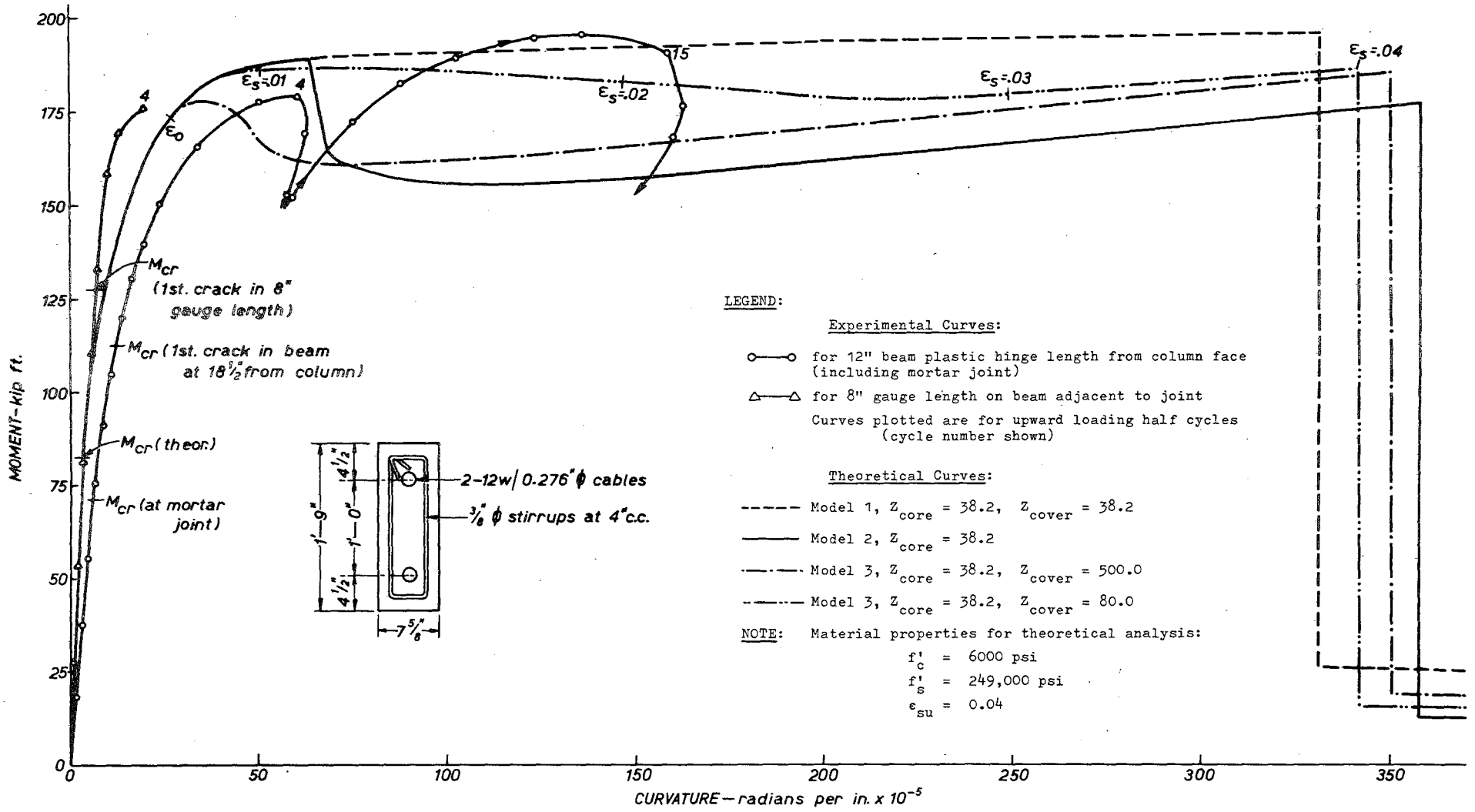

FIG. 4.6 : COMPARISON OF UNIT 2 BEAM & FOUR THEORETICAL MODELS

approximated the maximum moment capacity but made no allowance for reduction of moment with increasing curvature. Model 2, which considered all cover concrete at a strain greater than 0.004 to have spalled, underestimated the post-crushing moment resistance of the section. Various values of Z for the cover concrete were tried in Model 3 and the curve which gave the best fit to the experimental results had a Z value for the cover of 80 (i.e. approximately twice the Z value for the core). Also shown on Fig. 4.6 is the theoretical curve derived if the cover concrete is ascribed the Z value for unconfined concrete (Z = 500). It is clear that a very conservative estimation of the member's performance would result from this assumption.

It may be concluded that good correlation between experiment and theory may be obtained, but that no single stress block model will cover all experimental cases. Whereas the model which gave the best fit to the experimental curves for Unit 2 was Model 3 with $Z_{cover} = 2 \times Z_{core}$, the more lightly stirruped Unit 1 achieved the best fit with Model 1, $Z_{cover} = Z_{core}$. This result appears reasonable as intuitively one would expect that with a larger stirrup spacing the cover and core concrete would behave more monolithically.

4.3.2 Effect of Variation of Steel Area Ratio on Ductility

In order to study the effect of varying the steel area ratio on the moment-curvature relationships, a model of the dimensions shown on Fig. 4.7 was chosen, with eccentric prestressing at a steel depth of 0.8D. A representative Z value for the core of 80 was taken. This would be obtained for example from p" = 0.009, b"/s = 0.45, and f'_c = 6000 psi. Since this was intermediate between the case of Unit 2 (with $Z_{core} = 38$ and $Z_{cover} = 2 \times Z_{core}$) and that of Unit 1 (with $Z_{core} = 155$ and $Z_{cover} = Z_{core}$), a value of Z_{cover} of $1.5 \times Z_{core}$ was chosen. Curves for values of steel area ratio, $p = A_s/bD$, from

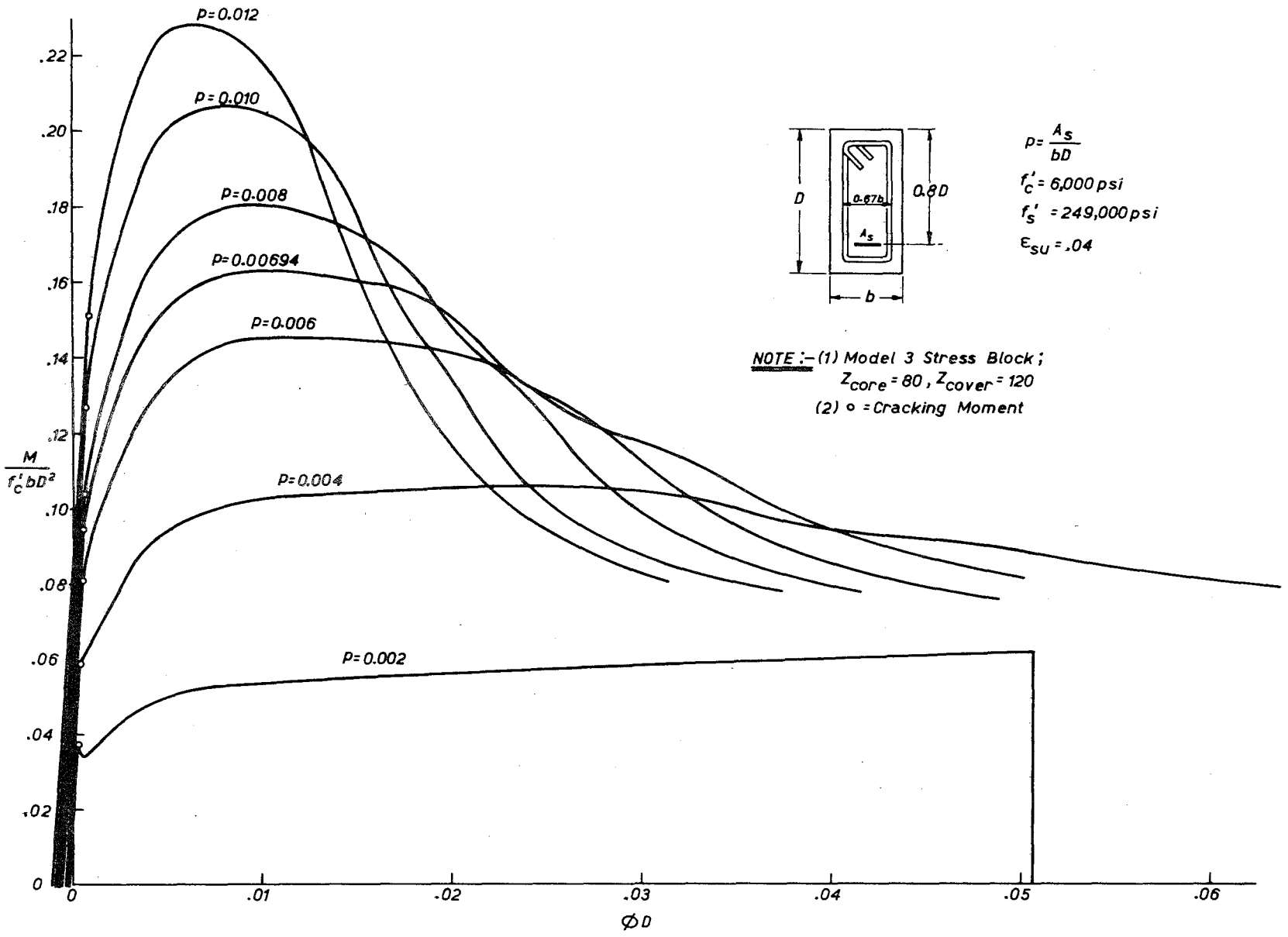

FIG.4.7 : EFFECT OF VARIATION OF STEEL AREA RATIO

0.002 to 0.012 are plotted on Fig. 4.7. Note that p is defined as the steel content as a proportion of the total area of the cross section. The general pattern of the curves shows an increase in moment capacity, but a decrease in ductility with increasing p.

The limitation on steel percentage specified in A.C.I. 318-63[40] and A.C.I. 318-71[41] is:

$$\frac{A_s f_{su}}{bd\ f'_c} \leqslant 0.3 \qquad \ldots (4.18)$$

where f_{su} is the prestressing steel stress at maximum moment. For the section studied, equation (4.18) required $p = A_s/bD \leqslant 0.00694$, where f_{su} was obtained from the theoretical analysis. The moment-curvature plot for this value of steel percentage is also shown in Fig. 4.7. The intention of the A.C.I. equation is to prevent a brittle failure from over-reinforcement. It is apparent that the curve for $p = 0.00694$ exhibits reasonable ductility but that for seismic design it may be necessary to restrict p to a smaller value than that given by the A.C.I. equation.

It is of interest to compare the analytically derived stress in the prestressing steel, at maximum strength of a member, with the A.C.I. code expression given for steel stress at ultimate load. For example, the comparison for a member with the limiting steel ratio is:

(i) From the theoretical moment-curvature plot:

At maximum moment ($\epsilon_{cc} = 0.00301$), $f_s = 211{,}200$ psi.

(ii) From A.C.I. 318-63[40] and the A.C.I. 318-71[41]:

$$f_{su} = f'_s \left(1 - 0.5 \cdot \frac{A_s}{bd} \cdot \frac{f'_s}{f'_c}\right) \qquad \ldots (4.19)$$

$$= 204{,}000 \text{ psi.}$$

The agreement is good and is even better at lower (more common) steel contents. The actual differences within the likely range of steel area ratios are as follows. At $p = 0.008$ the A.C.I. expression is 6% lower than the analytically derived value, at $p = 0.004$ it is $\frac{1}{4}$% higher, and

at $p = 0.002$ it is back to 5% lower. This variation arises because the expression for f_{su} varies linearly with p, whereas the steel strain and therefore stress at maximum strength varies in a hyperbolic manner with that term.

When the steel area ratio exceeds the limiting value, the A.C.I. code[40,41] specifies that the ultimate moment to be taken is not greater than:

$$M_u = \varphi(0.25 f'_c b d^2) \qquad \ldots (4.20)$$

This moment corresponds in Fig. 4.7 to:

$$100M/(f'_c b D^2) = \varphi \times 16.0 = 14.40$$

Before application of the capacity reduction factor of $\varphi = 0.9$, the maximum moment allowed is very close to the maximum moment for the limiting steel area ratio curve.

It should be noted at this point that equations (4.18) and (4.19) cannot be applied accurately to members prestressed concentrically with tendons in the top and bottom of the section, such as those required at the joints of frames subjected to seismic loading reversals. In this case the intent of the equations is satisfied if; $A_s/2$ is substituted for A_s, d denotes the depth to the bottom prestressing tendon (c.f. depth to the centroid of the steel[40,41]), and f_{su} denotes the stress in the bottom prestressing tendon at maximum strength of the member. This modified form of equation (4.19) was checked for a wide range of concentric prestressing steel areas and found to be accurate to within 3%.

It is concluded that the limit of steel percentage imposed by the A.C.I. code[40,41] does in fact result in reasonable ductility, but to ensure adequate ductility for seismic design it may be desirable to reduce the 0.3 on the right hand side of equation (4.18) to say 0.2. The value for f_{su} recommended by the A.C.I. code[40,41] results in a good approximation for the steel stress at maximum strength.

4.3.3 Effect of Distribution of Prestressing Steel in Member

Once a satisfactory steel area ratio is achieved for a member, a further important design criterion is the best distribution of the steel in the member. To study this question moment-curvature characteristics were computed for a section with a constant magnitude and line of action of the total prestressing force, but with a variable number and position of the tendons. An axial line of action of the total prestressing force was chosen because this configuration provides the best resistance to seismic load reversals. The steel area ratio and concrete stress block model conformed to those for the Unit 2 beam.

The results are shown plotted in Fig. 4.8. It is apparent that all curves are very similar apart from that for the single tendon position. In this case there is a lower maximum moment capacity and a subsequent substantial decline in moment resistance. The principal reason for the difference lies in the smaller value of lever arm, jD , within the section for the single tendon case. At maximum moment capacity the beam with one tendon has a slightly greater total steel force than the other cases, but a much smaller value of jD , and consequently it has a smaller maximum moment. At very large curvatures the neutral axis depth increases because of deterioration of the surface concrete, and this has a greater influence in reducing the moment capacity of the section for the single tendon because of its smaller value of jD. The reason for the curve for two positions of the tendons being lower than those for three, four or five positions was that the two tendons were not placed at the extremities of the section and therefore this was a slightly less favourable configuration than the others. This was done to provide a comparison with the practical case of Unit 2. The sharp drop in moment at a high curvature occurs when the bottom tendon reaches the tensile fracture strain.

It may be concluded that for seismic resistance of concentrically prestressed members it is advantageous to have the prestressing tendons

NOTE :-

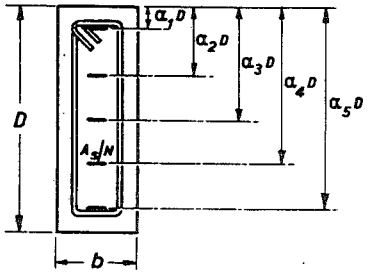

1. SECTION GEOMETRY

No. of tendon positions, N	1	2	3	4	5
α_1			0.1	0.1	0.1
α_2		0.2		0.367	0.3
α_3	0.5		0.5		0.5
α_4		0.8		0.633	0.7
α_5			0.9	0.9	0.9
A_s/N sq.ins.	1.435	0.718	0.478	0.359	0.287

p = 0.00896 for all cases.

2. MATERIAL PROPERTIES: f'_c = 6000 psi.
   f'_s = 249,000 psi.
   ε_{su} = 0.04

3. Model 3 stress block; Z_{core} = 38.2, Z_{cover} = 80.0

4. Analysis was based on $7\frac{5}{8}$" x 21" section with $1\frac{1}{2}$" cover to the stirrups.

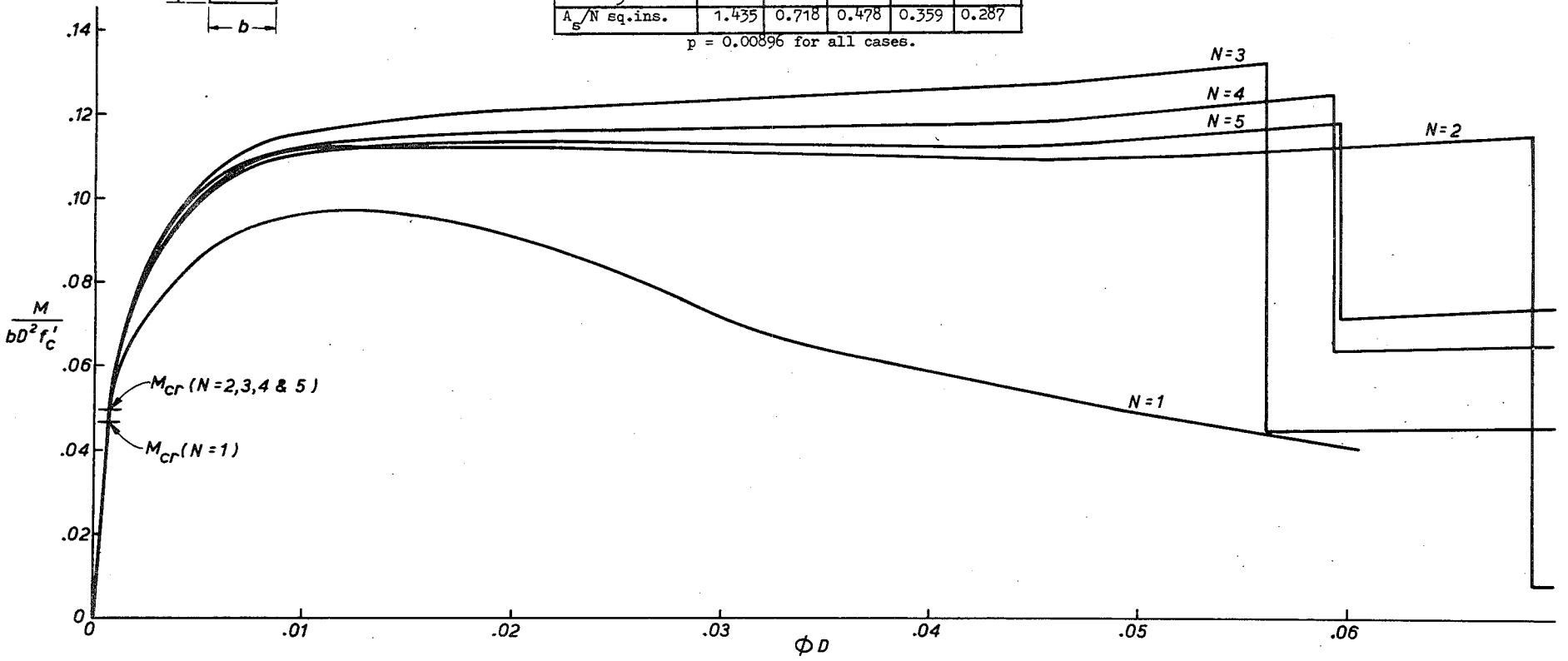

FIG. 4.8 : EFFECT OF DISTRIBUTION OF PRESTRESSING STEEL

distributed into more than one position within the section, but there is little difference in behaviour between sections with two or more positions of tendons for the same total prestressing force.

4.3.4 Effect of Transverse Reinforcement

For a given steel area ratio and tendon distribution, another important design consideration for ductility is the amount of transverse reinforcement. The differences shown in Section 4.3.1, between appropriate stress block models for varying degrees of lateral confinement, restricts a general study of the effect of transverse reinforcement on ductility. However a valuable guide may be obtained from comparing the practical cases of the beams of Units 1 and 2, because Unit 1 contained only sufficient stirrups for shear whereas Unit 2 contained additional stirrups for ductility. Fig. 4.9 illustrates the appropriate theoretical moment-curvature relationships for Units 1 and 2, plotted for the same value of concrete strength. Clearly the confined concrete of Unit 2 enables it to retain higher moments at large curvatures. However the curve for Unit 1 still shows adequate moment resistance, even at very high curvatures.

It is concluded that prestressed concrete beam sections, with sufficient transverse reinforcement to satisfy the shear requirements of codes, may be extremely ductile.

4.4 THEORETICAL STUDY OF COLUMNS

4.4.1 Comparison of Theory and Experiment

Figs. 4.10 and 4.11 show a comparison of the envelope of experimental cyclic moment-curvature relationships, obtained from the columns of Units 3 and 4 (see Chapter 3), and the appropriate theoretical monotonic loading curve. The experimental curves were plotted in each case for the column plastic hinge directly above the beam, since the

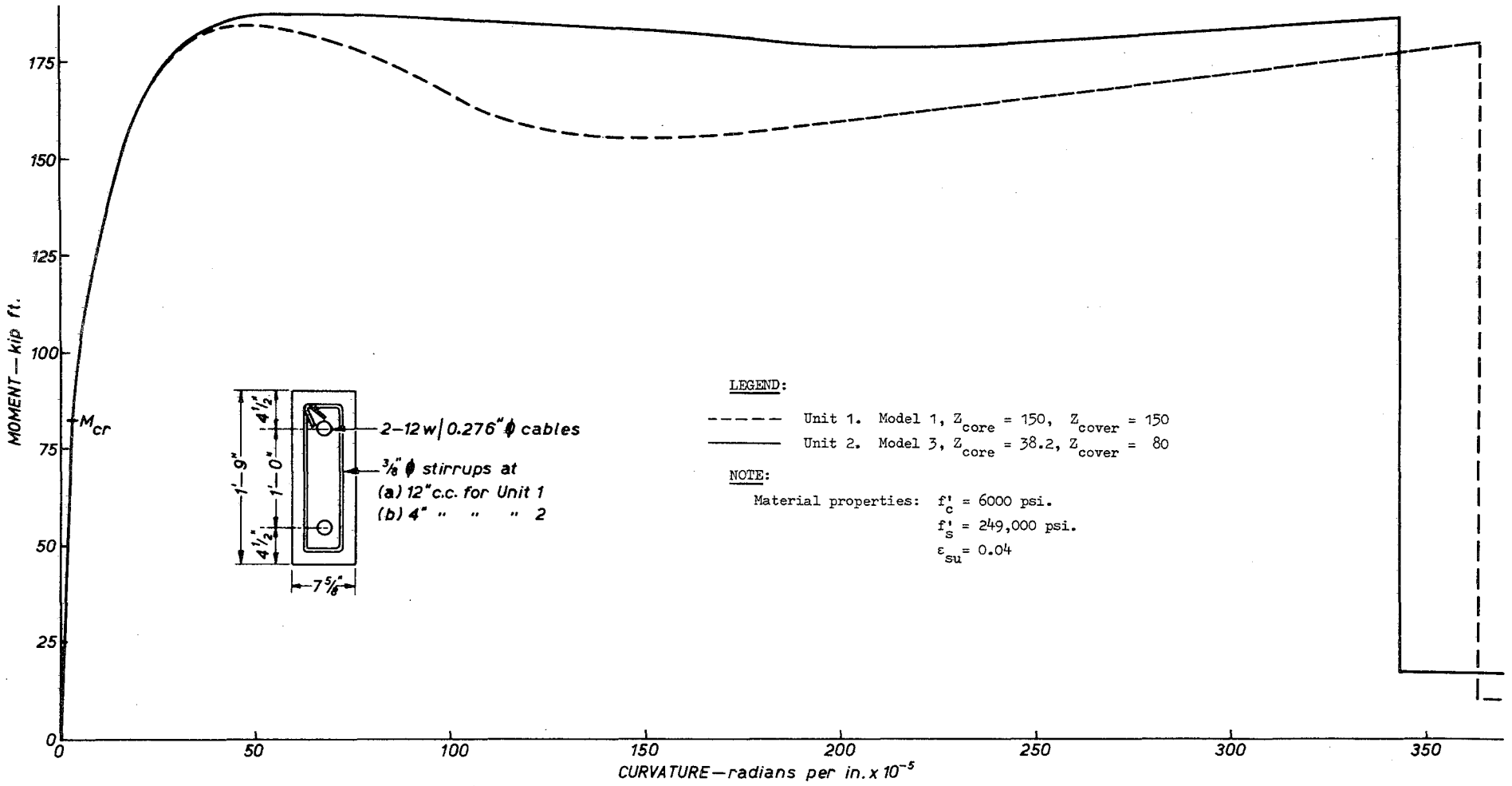

FIG. 4.9 : EFFECT OF TRANSVERSE REINFORCEMENT

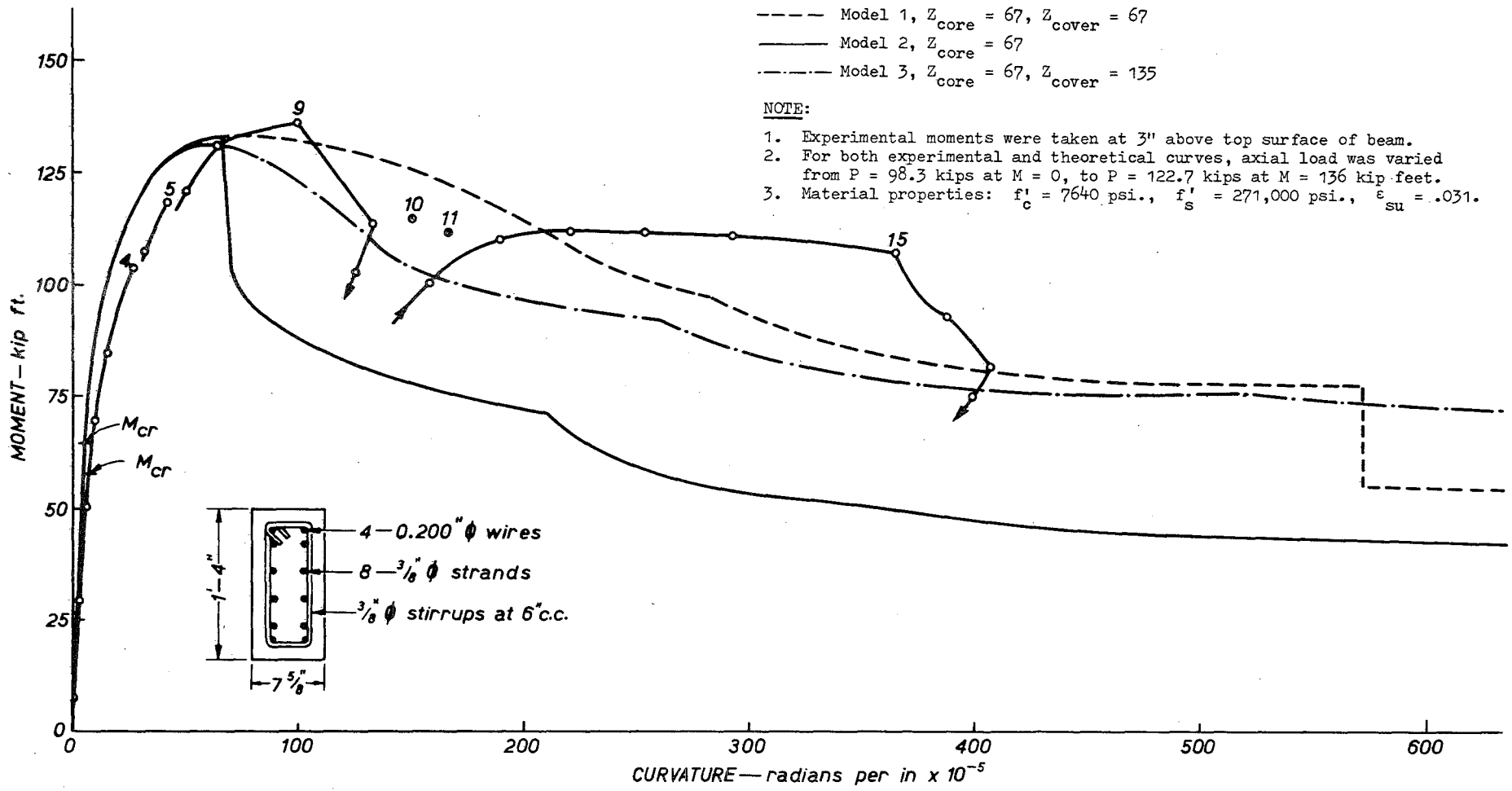

FIG. 4.10 : COMPARISON OF EXPERIMENTAL & THEORETICAL CURVES FOR UNIT 3

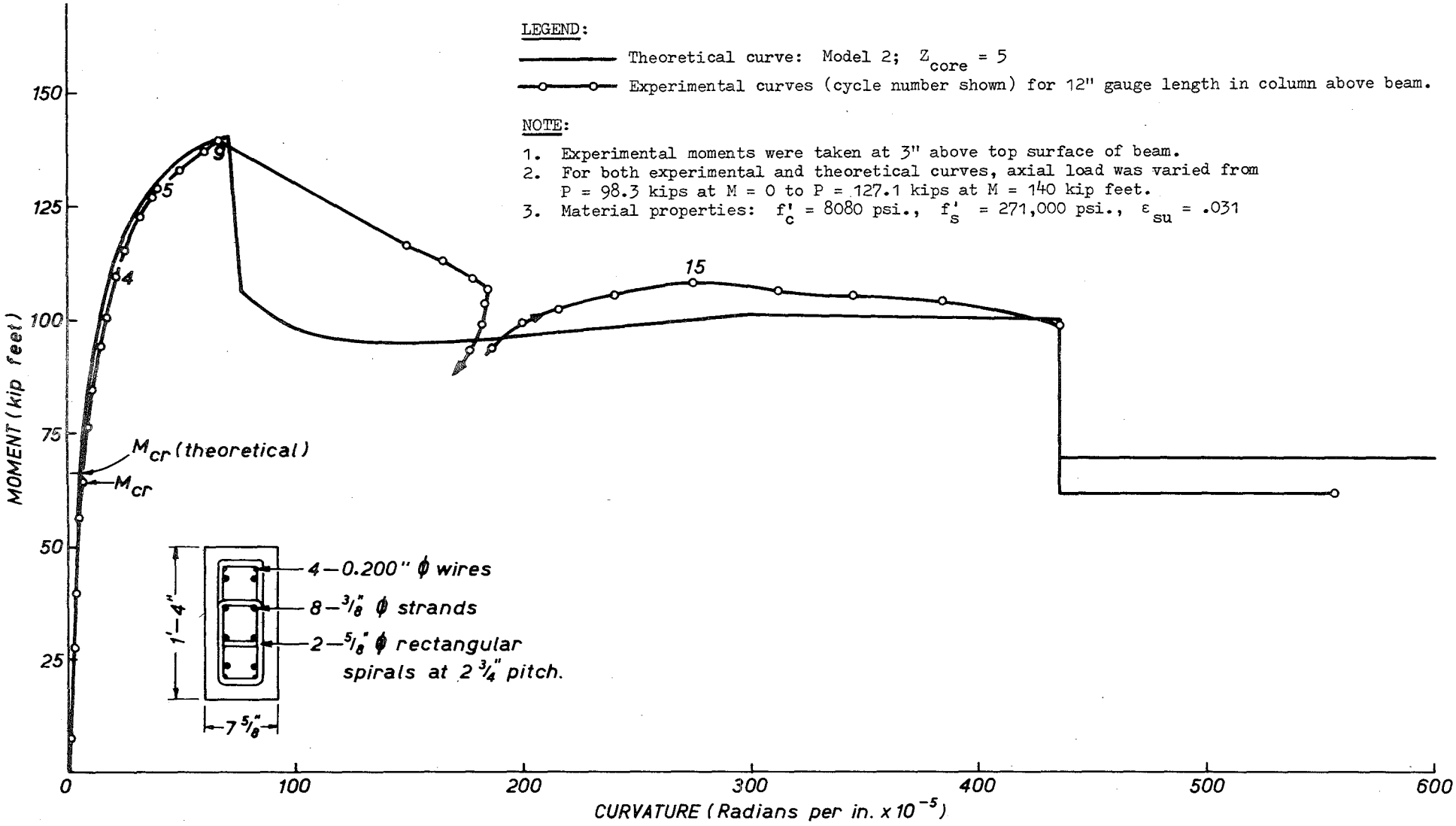

FIG.4.11 : COMPARISON OF EXPERIMENTAL & THEORETICAL CURVES FOR UNIT 4

largest values of curvature were recorded there. Moments were calculated at a section 3 inches above the top of the beam, as this corresponded to the critical section for crushing.

The theory assumed a value of $\epsilon_o = 0.0025$ for the concrete in these sections. This value was found from the concrete control tests on standard cylinders for Units 3 and 4. The greater value of ϵ_o in this case, relative to the beams of Units 1 and 2, arises because of the greater concrete strengths (f'_c = 8000 psi) in Units 3 and 4. This is consistent with the trend shown by Popovics[67] of an increase in ϵ_o with increasing f'_c. A further assumption was that the ultimate tensile strain of the $\frac{3}{8}$ inch prestressing strand was 0.031, based on control test results.

The experimental axial loads for the two cases considered were increased with increasing bending moment, and the same increasing axial load relationship was used in the theory. It was found in the theoretical analyses that at far advanced curvatures the strands in the compression zone attained quite large compressive strains. Little is known about the behaviour of prestressing tendons in compression within a flexural member. For reinforced concrete members it is generally assumed that the shape of the stress-strain curve for steel in tension will also apply in compression. Buckling is considered to be delayed by:

(a) the presence of some concrete around the bars.

(b) the necessity for a compression bar in a plastic hinge zone to undergo a reverse curvature to buckle during flexure.

However, prestressing wires or strands are more likely to buckle than reinforcing bars because of their higher stress levels and lower moments of inertia due to smaller diameters. For this reason the stress-strain relationship illustrated in Fig. 4.12 was assumed in this chapter for prestressing steel in compression. The tendon in compression is assumed to follow the elastic slope of the stress-strain

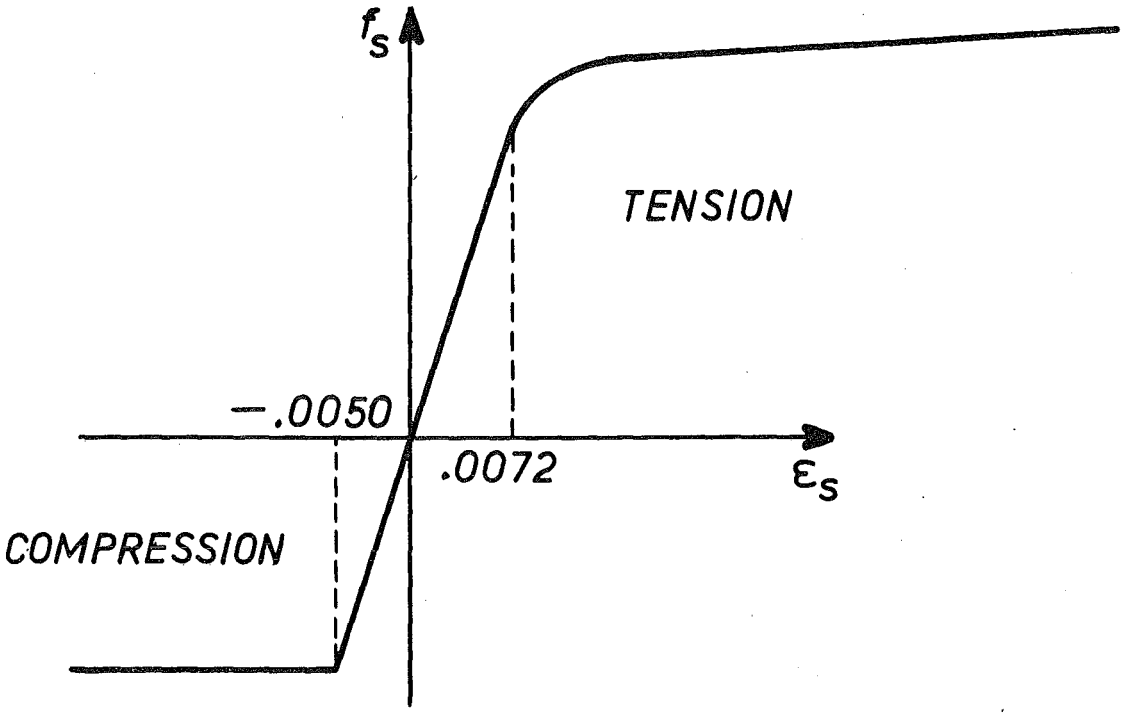

FIG. 4.12 : ASSUMED STEEL STRESS-STRAIN CURVE IN COMPRESSION

curve to a strain of -0.005 and then, in order to make some allowance for buckling, the tendon is assumed not to undergo further increase in stress with additional compressive strain. The theoretical member behaviour is only influenced by this assumption at large curvatures.

The column of Unit 3 contained ties which satisfied normal prestressed concrete code requirements for shear. The resulting value of Z for the core was 67. Three theoretical models for the compressed concrete are compared in Fig. 4.10. The closest correlation of theory with experiment for this column was obtained with Model 1. This is consistent with the observed gradual propagation of longitudinal cracking in the compression zone, rather than a sudden spalling of the cover concrete. It is apparent that Model 2 would underestimate considerably the moment capacity at large curvatures.

The column of Unit 4 contained heavy rectangular spirals, which resulted in a Z value for the core of 5. Since the cover concrete at the hinge spalled suddenly during testing it is not surprising that the best correlation with experiment was obtained from Model 2, which assumes that the cover concrete spalls at a strain greater than 0.004. The good agreement apparent in Fig. 4.11 justifies the assumed spalling strain. The sudden loss of moment at high curvature occurred at fracture of the bottom strands.

4.4.2 Variation of Ductility with Axial Load

The effect of axial load on ductility is important when considering the behaviour of prestressed concrete columns. A study was made of the effect of varying axial load on a section with transverse reinforcement satisfying normal prestressed concrete codes (for example, the best Unit 3 model). For comparison the behaviour of a section with special transverse reinforcement for confinement (for example, the best Unit 4 model) was also considered.

The shape of the moment-curvature relations for Unit 3 with varying

axial loads is shown in Fig. 4.13. Of the axial loads considered, a value of the dimensionless term, $P/f'_c bD$, of 0.12 results in the most ductile behaviour. This corresponds to the limit specified in the SEAOC code[51] for reinforced concrete of:

$$\frac{P}{A_g} \not> 0.12 f'_c \qquad \ldots (4.21)$$

above which the design must be such that plastic hinges will form in the beam rather than in the column at a particular joint.

Interaction and ductility curves are plotted for both cases of lateral confinement studied, in Figs. 4.14 and 4.15. It is apparent that the degree of confinement has only a small effect on both the interaction curves and the curvature at maximum moment. To give an indication of the ductility available after maximum moment, curvatures at one half of the maximum moment on the "falling" arm branch of the moment-curvature curve are also plotted. It may be seen that increasing the axial load from zero initially causes the curvature at half maximum moment to increase. This is because for low axial loads the moment drops to one half of its maximum value when the tension steel fractures, and the curvature at this point of fracture increases as the neutral axis depth increases with axial load. Eventually a discontinuity occurs because at higher axial loads the reduction of moment capacity to half of the maximum value is caused by deterioration of the concrete in compression, rather than fracture of the tension steel. These different characteristics are shown in Fig. 4.13.

The SEAOC[51] limit has been marked on the ductility curves of Figs. 4.14 and 4.15. A further comparison may be made with the recommendations of A.C.I. committee 315[74] for the seismic design of reinforced concrete frames. It is recommended that, where the design axial load exceeds 0.4 of the axial load at balanced conditions, special spirals or circular or rectangular hoops should be included in columns.

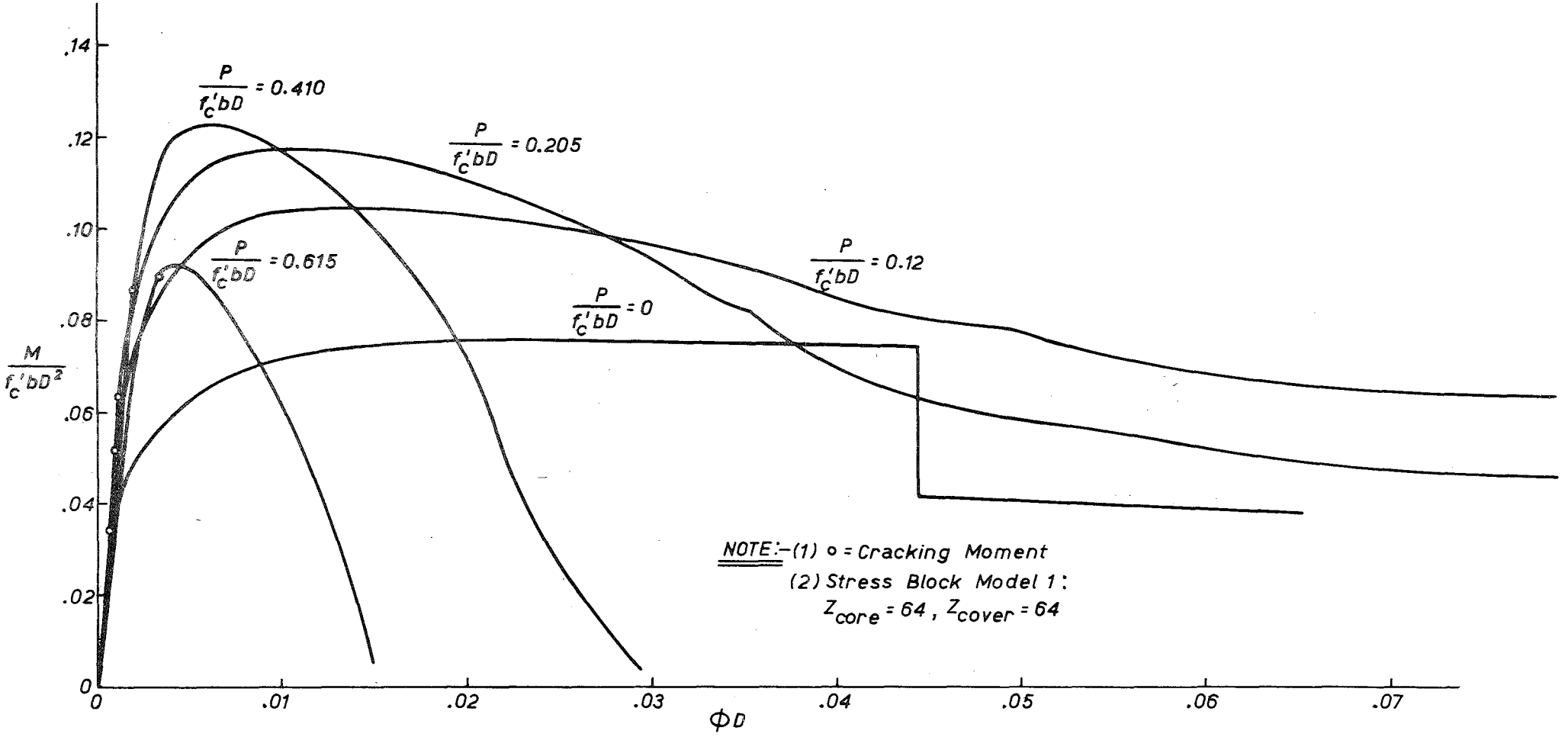

FIG.4.13: EFFECT OF VARIATION OF AXIAL LOAD ON UNIT 3 SECTION

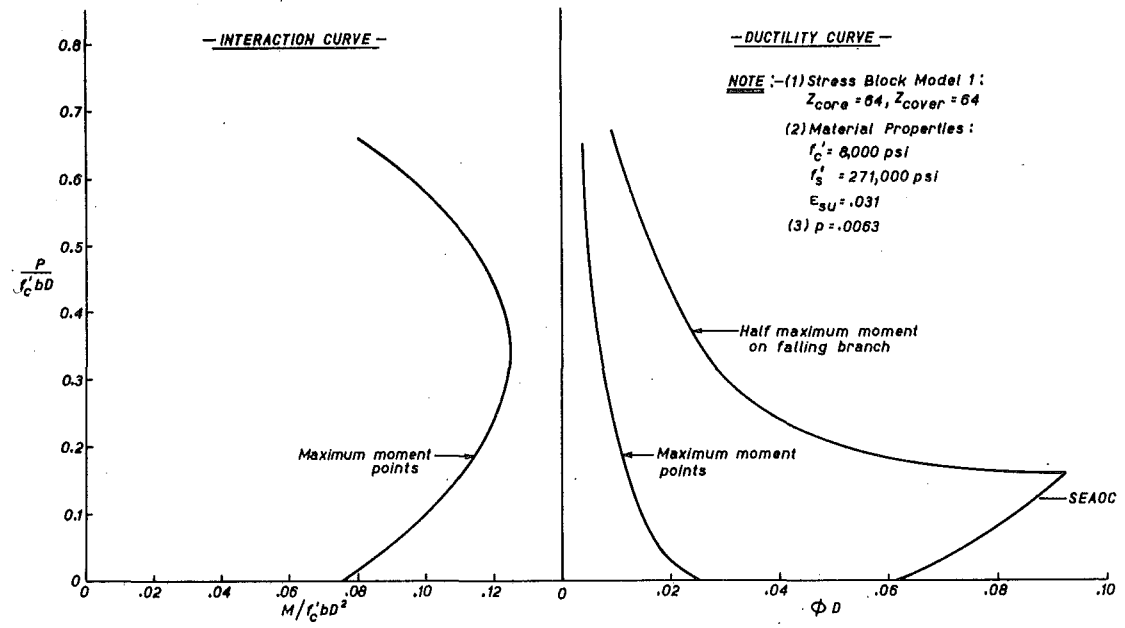

FIG. 4.14 : COLUMN WITH TRANSVERSE REINFORCEMENT FOR SHEAR

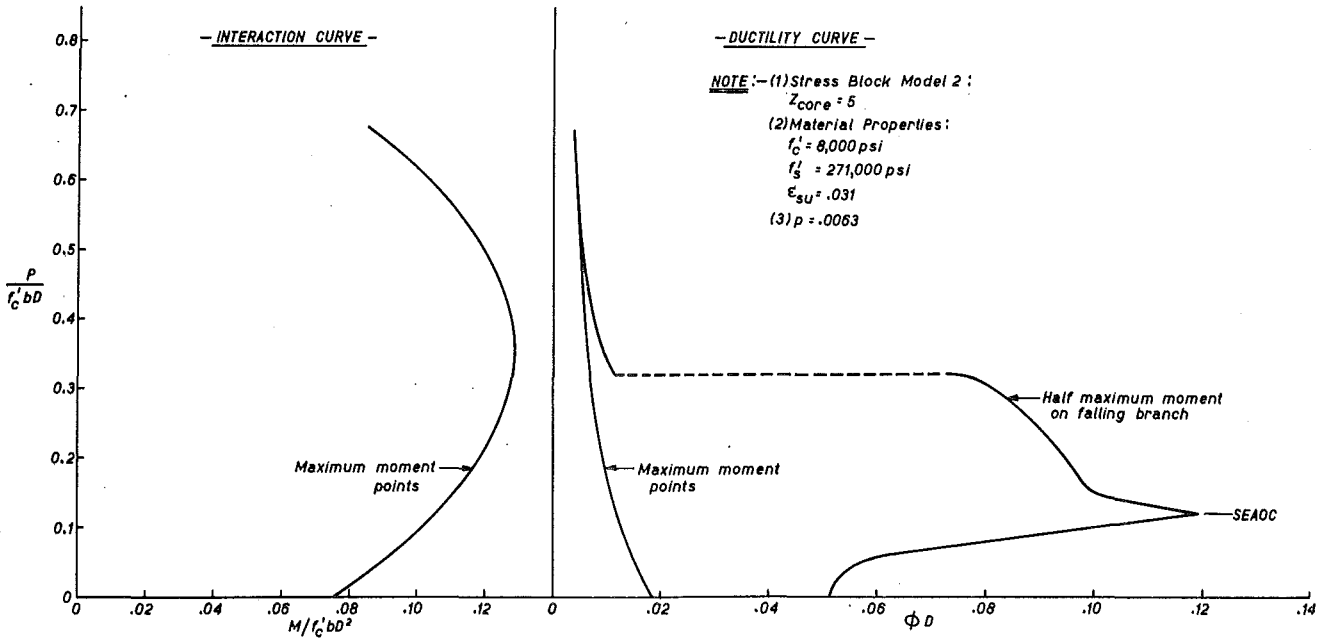

FIG. 4.15 : COLUMN WITH SPECIAL TRANSVERSE REINFORCEMENT FOR DUCTILITY

On the basis of the point on the interaction curve for prestressed concrete columns which is analagous to balanced conditions for reinforced concrete columns, the recommended limit occurs at $P/f'_c bD = 0.13$ on Figs. 4.14 and 4.15. This is very close to the SEAOC limit.

It may be concluded from Figs. 4.13 to 4.15 that special lateral reinforcement for confinement results in:

(a) a small increase in maximum moment capacity (approximately 3%) at all axial loads.

(b) a significant increase in maximum ductility available from the section.

(c) an increase in the range of axial load over which significant post-crushing ductility is available.

Further, the SEAOC code[51] limitation on axial load (equation 4.21) for reinforced concrete also serves as a valuable guide for prestressed concrete columns without special transverse reinforcement for confinement.

4.5 COMPARISON OF PRESTRESSED AND REINFORCED CONCRETE

Because more is known about the seismic behaviour of reinforced concrete structures, attempts are often made to compare prestressed concrete with reinforced concrete. It is therefore of value to study the moment-curvature characteristics of the two materials. Fig. 4.16 illustrates moment-curvature curves for typical reinforced concrete beam sections as determined in an analytical study by Kent[66], and for comparison typical prestressed concrete section responses. The same section geometry was used for both studies as shown in Fig. 4.16. The value of maximum concrete strength, f'_c, for the reinforced concrete study was 4000 psi, and a representative value of $f'_c = 6000$ psi was chosen for the prestressed concrete members.

The analytical model which had been used for the reinforced concrete study considered all cover concrete at a strain greater than

PRESTRESSED CONCRETE BEAMS							
	Z = 10				Z = 100		
No.	$\frac{A_s}{bd}$	$\frac{A_s f_{su}}{bd\ f'_c}$	$\frac{\varphi_{.004}}{\varphi_{cr}}$	No.	$\frac{A_s}{bd}$	$\frac{A_s f_{su}}{bd\ f'_c}$	$\frac{\varphi_{.004}}{\varphi_{cr}}$
P1	.0110	.389	4.3	P2	.0110	.386	4.1
P3	.0070	.255	10.5	P4	.0070	.253	10.0
P5	.0042	.158	26.4	P6	.0042	.157	25.1
P7	.0020	.083	96.1	P8	.0020	.083	93.5

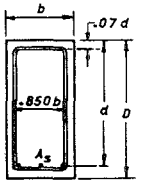

$D = 1.1 \times d$

$f'_c = 6{,}000$ psi

$f_{se} = 133{,}000$ psi

$f'_s = 249{,}000$ psi

REINFORCED CONCRETE BEAMS							
	Z = 10				Z = 100		
No.	$\frac{A_s}{bd}$	$\frac{A_s f_y}{bd\ f'_c}$	$\frac{\varphi_{.004}}{\varphi_y}$	No.	$\frac{A_s}{bd}$	$\frac{A_s f_y}{bd\ f'_c}$	$\frac{\varphi_{.004}}{\varphi_y}$
R5	.0375	.375	2.7	R6	.0375	.375	2.5
R9	.0250	.250	5.0	R10	.0250	.250	4.8
R13	.0125	.125	11.9	R14	.0125	.125	11.3

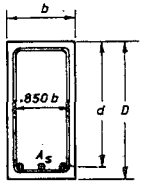

$D = 1.1 \times d$

$f'_c = 4{,}000$ psi

$f_y = 40{,}000$ psi

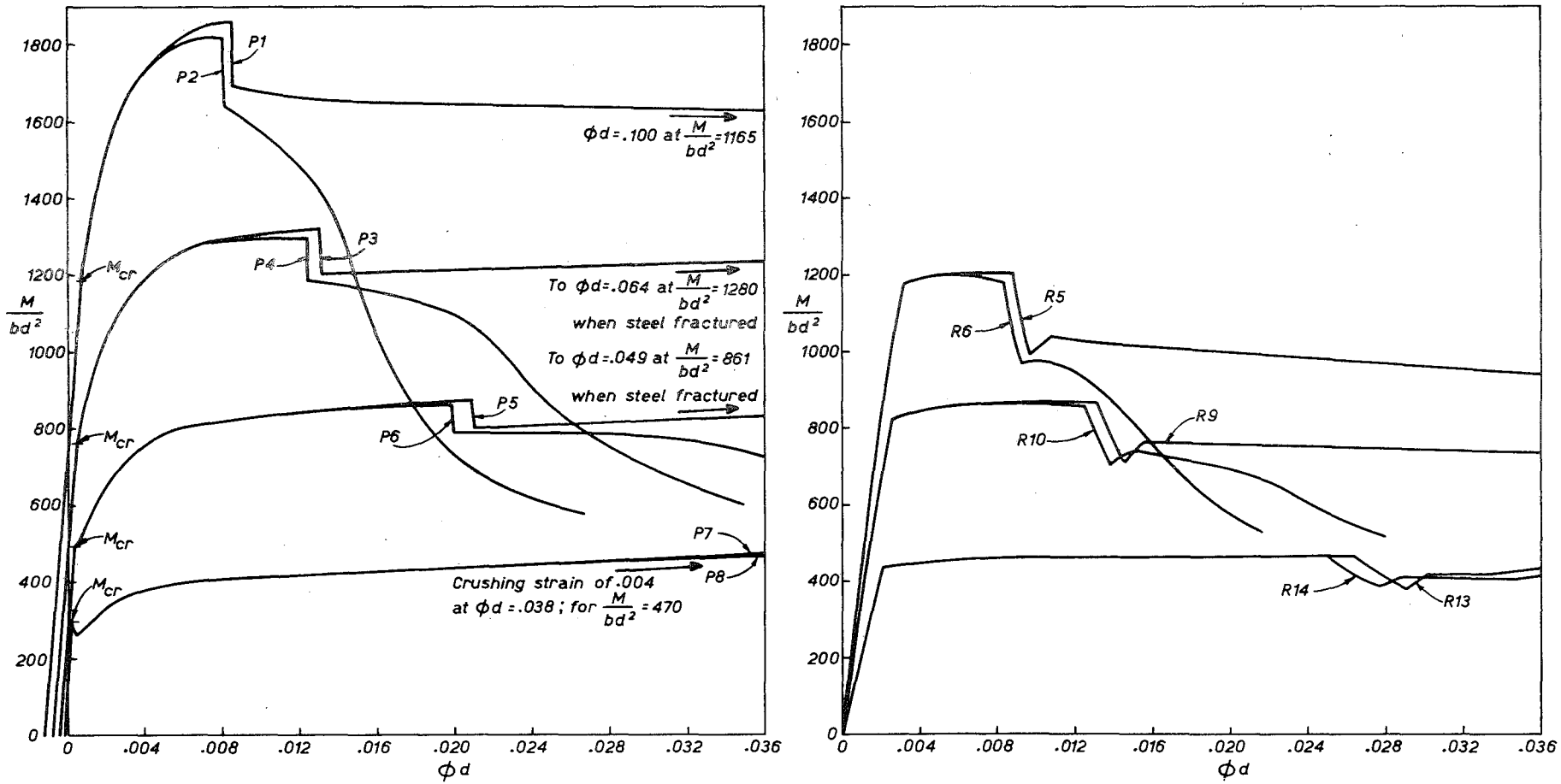

FIG. 4.16 : COMPARISON OF PRESTRESSED & REINFORCED CONCRETE MEMBERS

0.004 to be ineffective. For consistency the same model was used for prestressed concrete. It has been shown that this model provides good correlation with experiment at low values of Z , but is conservative for high values of Z at large curvatures. Curves for values of Z of 10 and 100 were plotted for both materials, thus covering a range of likely degrees of confinement in such beams. The validity of the assumption of a spalling strain of 0.004 was verified against experimental surface concrete strains, and further supported by the good correlation between theory and experiment in this Chapter for the Unit 4 column, the only member which spalled suddenly.

Rather than plot the curves to the dimensionless moment term, $M/(f'_c bd^2)$, the expression M/bd^2 was chosen as this allowed a direct comparison of prestressed and reinforced concrete members with the same size and maximum moment capacity (and therefore same design moment for an ultimate strength approach). For example, P6 and R10 have identical values of maximum moment from the expression, M/bd^2. A study of their respective curves show that P6 has a curvature at the crushing strain of 0.004 which is 1.6 times that of R10. (The point of crushing corresponds to the sharp drop in moment on the curves. The model used gives good results up to this point but underestimates the subsequent moment capacity for large Z values). The reasons for the difference in pre-crushing curvature may be seen from a comparison of the section behaviour at crushing, as shown in Table 4.1. The curvature when the extreme concrete fibre strain is 0.004 is dependent on the neutral axis depth. This depth is in turn dependent on the compressive force and the concrete strength, f'_c . Even though the values of compressive force are comparable in the two cases, the greater concrete strength for P6 allows a smaller neutral axis depth and therefore a larger curvature.

Alternatively, one may consider prestressed and reinforced concrete sections with the same curvatures at crushing, such as P4 and R10. The

Table 4.1

COMPARISON OF PRESTRESSED AND REINFORCED CONCRETE SECTIONS AT CRUSHING

	P6	R10
k	0.201	0.319
φd	0.01989	0.01253
$C=T=\frac{f_s A_s}{bd}$	945	1000
lever arm/D	0.910	0.859
$\frac{M}{bd^2}$	860	859

prestressed concrete member may have an ultimate strength 1.5 times that of the reinforced concrete member but still be capable of attaining the same crushing curvature.

The effect of the greater curvature at crushing for prestressed concrete members, than for reinforced concrete members of similar size, serves to help counteract the greater response of prestressed concrete structures to seismic motions when compared to reinforced concrete structures. The curvature and strength ratios, quoted above, compare favourably with the ratios of displacement or load found to be necessary by Rosenblueth[17] for prestressed and reinforced concrete structures with the same initial stiffness and damping ratio, as discussed in Section 2.3. However, if for comparable strength members the prestressed concrete section is smaller than that of the reinforced concrete section this advantage may be lost. The prestressed concrete section would require a greater steel area, with consequent greater neutral axis depth and lower curvature at crushing, in this case. For example, it was found that a prestressed concrete section with the same strength as P6, but with width and depth dimensions both reduced by a factor of 0.88, had

the same curvature at crushing as the reinforced concrete section R10 with the same strength and section size as P6. (The value of the expression $A_s f_{su}/bdf'_c$ increased from 0.157 for P6 to 0.263 for the section with reduced dimensions.)

It is of interest to compare the ductility factors as commonly defined for prestressed and reinforced concrete. The rotational ductility factor for prestressed concrete is usually defined as the ratio of rotation over a small increment of length to rotation over that length at first cracking, whereas for reinforced concrete the rotational ductility factor is taken as the ratio of rotation over a small increment of length to rotation over that length at first yield of the tension steel. The rotational ductility factors at the crushing strain of 0.004 have been tabulated on Fig. 4.16 for all the curves plotted. The rotational ductility factor terms for the prestressed concrete members are up to 6 times those of the reinforced concrete members for the same values of curvature. This illustrates why it is not possible to relate the ductility factor requirements as commonly defined for prestressed concrete members to those already known for reinforced concrete members.

A trend is apparent in Fig. 4.16 that prestressed concrete sections with higher steel area ratios show smaller curvatures at crushing but larger curvatures at the fracture strain of 0.04 for the tension steel. The explanation is simple. During flexure, the section with higher steel content has a greater steel force and therefore requires a greater neutral axis depth. This results in a lower curvature, for a given surface concrete strain, at crushing. On the other hand for a given ultimate bottom steel strain, the greater neutral axis depth for the beam with more steel results in a larger curvature at fracture.

It is concluded that generally a prestressed concrete beam will have a greater curvature at crushing than its reinforced concrete counterpart with the same section size, steel position and maximum moment capacity.

4.6 NOMOGRAMS FOR VARIATION OF CURVATURE RATIO AT CRUSHING

For prestressed concrete seismic design it is desirable to avoid crushing of the concrete in compression, because of the difficulty of repair of a structurally damaged member back to its fully prestressed condition. For this reason the curvature ratio at crushing (relative to first cracking) is an important parameter, and its likely values were determined for both beams and columns.

4.6.1 Beams

Fig. 4.17 shows the effect of steel area ratio and lateral confinement in beams, on the ratio of curvature at a surface concrete strain of 0.004 to that at first cracking. The cases of eccentric and concentric prestress are illustrated, and in each case curves are plotted for Z values of 10 and 100. In some cases of concentric prestress the tendons will be distributed at more than the two depths chosen for this section. However, it is shown in Section 4.3.3 that this case is general for moment-curvature relationships of sections with two or more positions of prestressing tendons. It was verified that the curves shown are independent of the ratio of section depth to width. In the dimensionless term for the abscissa, the ultimate steel stress, f'_s, was used rather than the more common value of stress at maximum strength, f_{su}. This was felt to be necessary as f_{su} is variable, particularly for the study of columns.

It is clear from Fig. 4.17 that the degree of confinement has little effect on the curvature ratio at crushing (although after crushing it would be significant). For concentric prestress the steel area ratio, p, includes the total steel area, but it is only the lower tendons which have a significant effect on the moment-curvature relationship beyond cracking. This is the principal reason for the difference in shape of the curves for concentric and eccentric prestress.

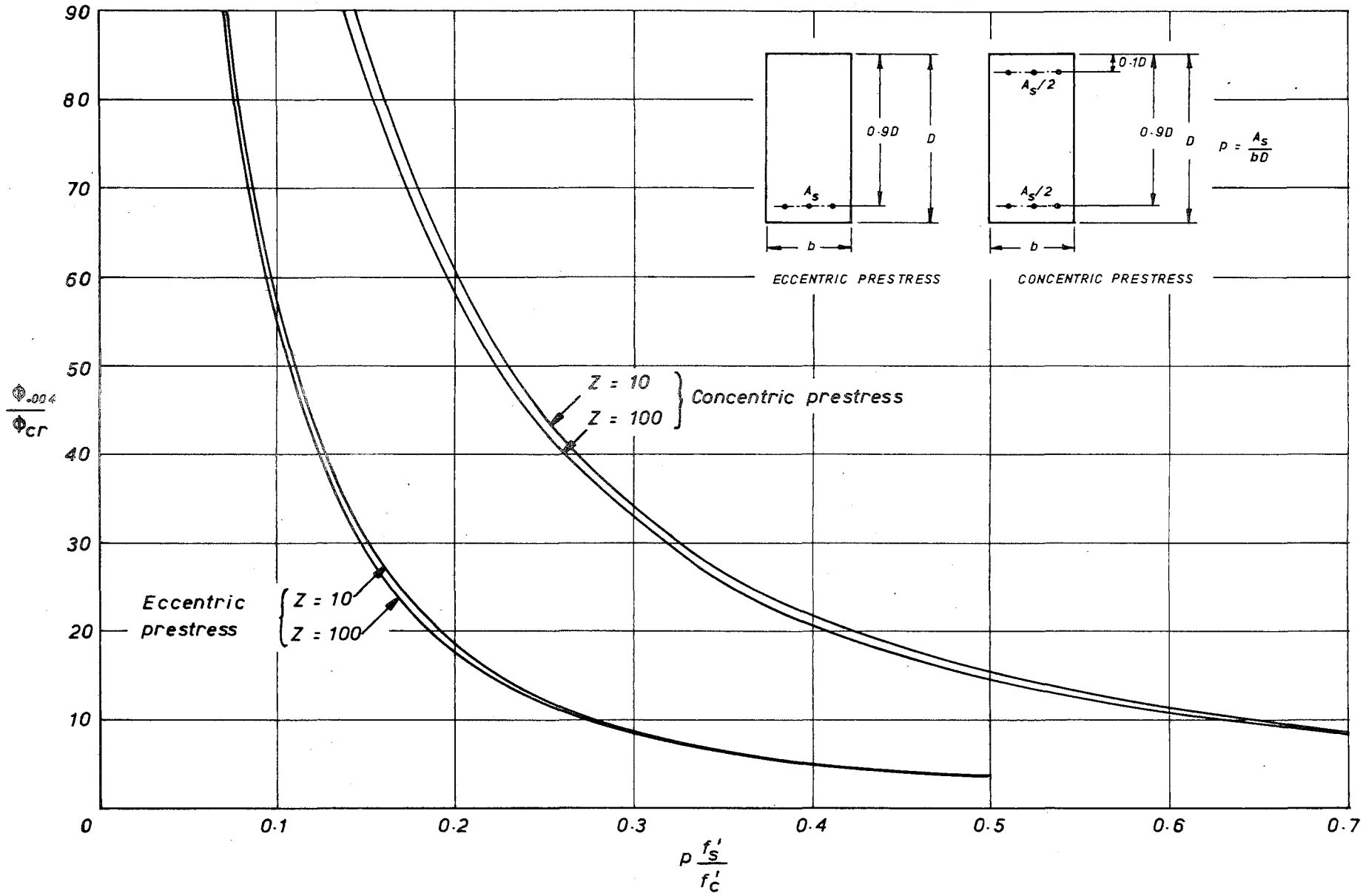

FIG. 4·17 : VARIATION OF CURVATURE RATIO AT CRUSHING FOR BEAMS

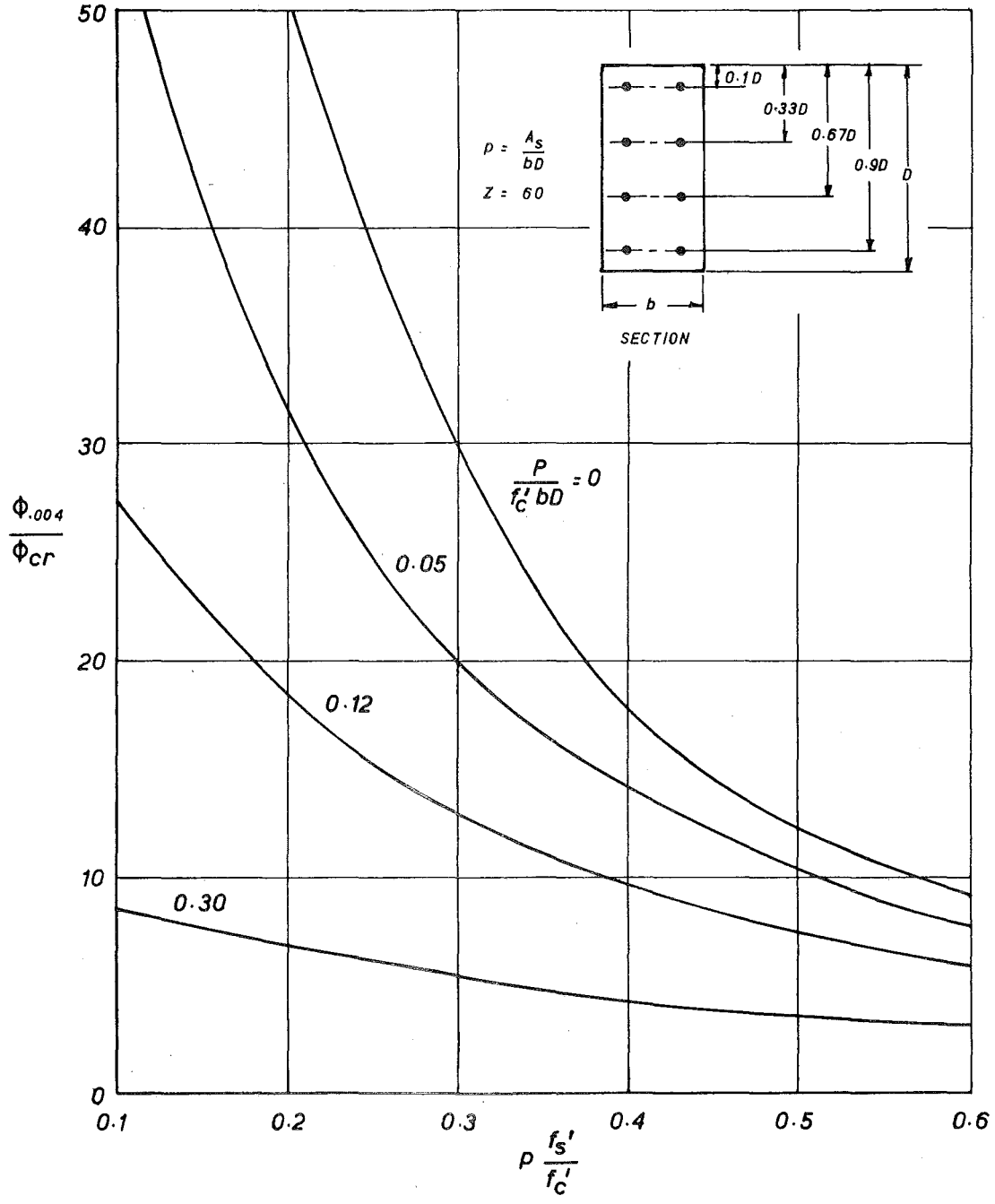

FIG. 4·18 : VARIATION OF CURVATURE RATIO AT CRUSHING FOR COLUMNS

4.6.2 Columns

The values of curvature ratio at crushing for columns with varying steel area ratios and axial loads may be read from Fig. 4.18. Only a section with concentric prestress was considered as this is a necessary configuration in a column subjected to seismic load reversals. Since it was shown in Fig. 4.17 that the degree of confinement has little effect on the curvature ratio at crushing, curves were plotted for only one value of Z, an intermediate figure of 60.

The curves presented for beams and columns allow a calculation of allowable curvatures prior to crushing, for the design of prestressed concrete members on the basis of their steel area ratio, lateral confinement, and axial load.

4.7 LIMITS FOR EFFECTIVENESS OF COVER CONCRETE

The various approaches to consideration of the effectiveness of the cover concrete, as discussed in Section 4.2.3, may be reviewed in the light of the results of this chapter. It is felt that the most accurate approach for a particular member depends on the degree of confinement of the core concrete. Approach (i) was suitable when the internal binding was not heavy, such as would occur when the transverse reinforcement satisfied normal prestressed concrete code requirements for shear. Approach (ii) was applicable in circumstances of heavy binding of the core concrete, such as that for small column sections satisfying special transverse steel requirements for ductility. In the latter case the cover concrete does tend to spall suddenly rather than by the gradual development of longitudinal cracks in the compression zone. For volumes of transverse steel intermediate between the above two cases Approach (iv) was found to be suitable.

Examination of the theoretical and experimental moment-curvature curves from this investigation indicate that the limits of binding steel

ratio, p" , for which the above approaches are valid are as follows:

$p'' \leq 0.0125$	$Z_{cover} = Z_{core}$	(Approach (i))
$0.0125 < p'' \leq 0.10$	$Z_{cover} = 2 \times Z_{core}$	(Approach (iv))
$0.10 < p''$	cover concrete at strain > 0.004 spalls	(Approach (ii))

It should be emphasised that the above findings are for sections of the size tested in this investigation. For larger sections these limits may not apply accurately, but it should be noted that the effect of cover concrete is less for larger sections where the cover thickness remains constant.

4.8 COMPUTER PROGRAM

The listing of the computer program developed in this Chapter appears in Appendix A.

Program 4.1 ("MOROAN"): Monotonic loading of prestressed concrete members with or without axial load, and with up to five positions of prestressing tendons. Analysis is based on an assumed stress-strain relation for prestressing steel, and a concrete stress-strain relation which allows for the effect of lateral confinement and includes three possible models for the behaviour of the cover concrete.

4.9 CONCLUSIONS

Specific conclusions have already been given at the end of each section. It has been shown that adequate ductility can be achieved in prestressed concrete members provided appropriate limits of steel area ratio and axial load are observed. For a concentrically prestressed member, a distribution of the tendons into two locations near the top and bottom of the section results in considerably greater ductility than for a single large tendon at the centre.

However there is little difference in behaviour for sections with two or more tendon locations for the same steel area. A member with normal lateral reinforcement, not specially detailed for ductility, can achieve large ductilities provided it satisfies the constraints outlined above. Finally, it was concluded that a prestressed concrete member will generally show larger curvatures at crushing than a comparable reinforced concrete member with the same size and strength.

CHAPTER 5

MOMENT-CURVATURE CHARACTERISTICS FOR PRESTRESSED CONCRETE MEMBERS UNDER CYCLIC LOAD

SUMMARY

A theory is presented to determine the moment-curvature characteristics of general prestressed concrete sections under reversed cycles of load. The analysis is based on the stress-strain relations for concrete and prestressing steel under cyclic loading. An idealization is also postulated to represent the moment-curvature characteristics of prestressed concrete members under cyclic load, for use in dynamic earthquake analyses of framed structures. Both the theory and the idealization are tested against seven experimental moment-curvature plots of both beams and columns subjected to high intensity cyclic loading. Finally, a comparison is made between the theoretical moment-curvature relations of cyclically loaded prestressed concrete and reinforced concrete beams with the same size and strength.

5.1 INTRODUCTION

A study of the characteristics of prestressed concrete members under monotonic load, such as that in the previous chapter, provides a means of determining available ductility in such members. However, it is also necessary to know their performance under cyclic load to assess the ability of prestressed concrete framed structures to withstand seismic load reversals. Such cyclic load characteristics as energy dissipation and stiffness degradation of the members will have a significant effect on the response of the structure to seismic

motions.

The only attempt known of by the author, to predict theoretically the cyclic load behaviour of prestressed concrete members, was carried out by Paranagama and Edwards[75]. They considered repeated load cycles with the load acting in one direction only. In that study it was found to be necessary to vary the factor representing bond between the steel and the concrete, in order to achieve correlation between theory and experiment. The work described in this chapter extends existing work in providing a means of analysis of general prestressed concrete sections subjected to cycles of load in both directions, and including an allowance for varying degrees of confinement of the concrete.

Because of the considerable computer time and storage required to derive moment-curvature curves theoretically, an idealization of the cyclic loading moment-curvature characteristics is necessary for the dynamic earthquake analyses of large frames. Spencer[6] used a bilinear elastic moment-curvature idealization for prestressed concrete members, which was adequate for the low curvature demands that he obtained. The idealization presented in this chapter is more general in that it allows for much higher curvatures and includes stiffness degradation after crushing for high intensity cyclic loading.

5.2 THEORETICAL MOMENT-CURVATURE ANALYSIS

The analysis developed allows determination of the moment-curvature properties of a general prestressed concrete section with any number of tendon positions, with or without external axial load, and for cycles of load in both directions. It can also be used for monotonic load analysis. The effectiveness of the cover concrete may be represented by either of Models 1 and 2 in Section 4.2.3. The effect of shear force on the moment-curvature response is not

considered, as it is felt to be of relatively small significance for a prestressed concrete section.

5.2.1 Stress-Strain Model for Cyclically Loaded Concrete

Many investigators have studied the stress-strain relations of concrete under monotonic loading and a correspondingly large number of analytical curves have been postulated, as reviewed briefly in Chapter 4. For the study of seismic load effects, or even the effect of repeated loads, it is necessary to know the behaviour of concrete under cyclic or fluctuating loads. Sinha, Gerstle, and Tulin[76] and Karsan and Jirsa[77] studied the behaviour of plain concrete subjected to repetitions of compressive stress. In both cases expressions for the loading and unloading stress-strain relationships were derived. Some curves obtained experimentally by Sinha et al are shown in Fig. 5.1. A comparable investigation for confined concrete has not as yet been carried out but in the meantime the curves shown serve as a valuable guide.

In this thesis an idealized stress-strain response is assumed for repeated and cyclic load and is illustrated in Fig. 5.2. The envelope curve is the same as that derived by Kent and Park[72], and used in Chapter 4 for monotonic load. Equations (4.1), (4.2) and (4.6) give expressions for the regions OA, AB, and BC.

For analysis, a member is considered as being composed of small but discrete concrete elements. If the maximum strain sustained in such an element is less than ϵ_o, as for example at point E, the unloading path follows a line ED with a slope equal to the initial tangent modulus of elasticity E_c. If the element has not cracked it is capable of carrying tensile stress to point F. If the element has previously cracked, or if it cracks during the course of unloading, the stress will return to zero. It will then in the course of reloading have to return to point D before compressive stress can be

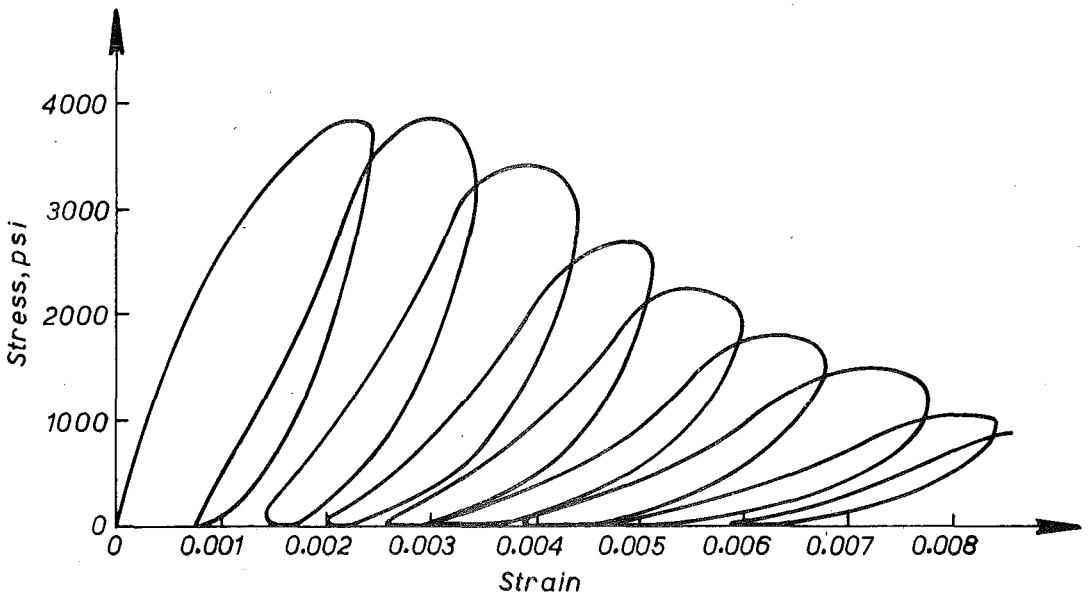

FIG. 5.1 : EXPERIMENTAL STRESS STRAIN CURVES FOR CONCRETE, AFTER SINHA et al [76]

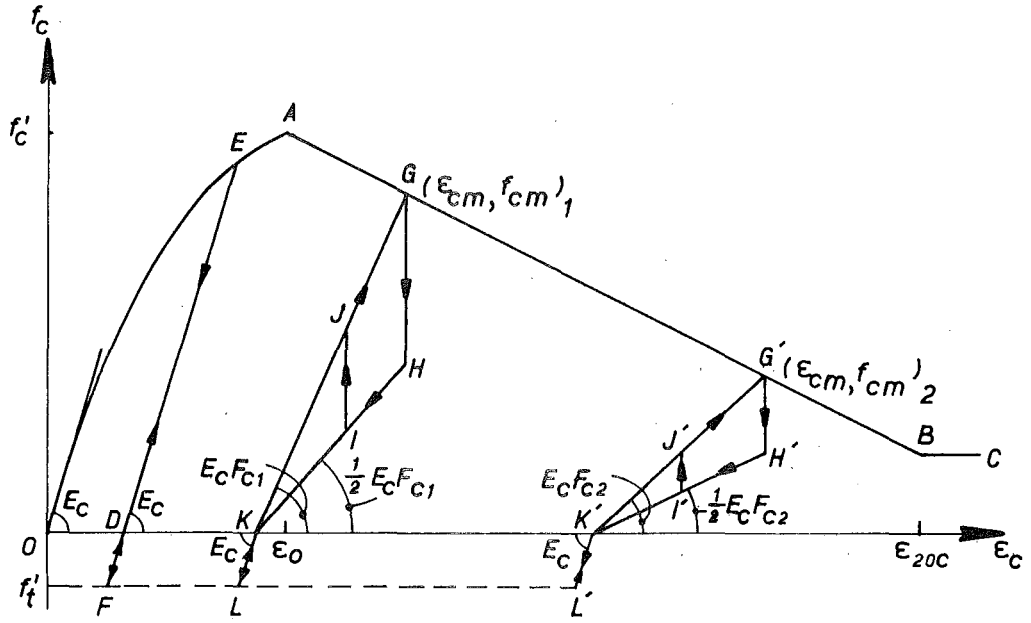

FIG. 5.2 : STRESS-STRAIN IDEALIZATION FOR CYCLIC LOADING OF CONCRETE.

sustained once more. The reloading path is identical to that for unloading.

It is apparent from Fig. 5.1 that for strains greater than ϵ_o there is a successive degradation of stiffness of both the unloading and reloading curves, for increasing values of maximum strain. In order to represent this behaviour, a reduction factor is introduced to apply to the term E_c to represent successively reducing stiffness. This factor has the form:

$$F_c = 0.8 - \frac{(\epsilon_{cm} - \epsilon_o)0.7}{\epsilon_{20c} - \epsilon_o} \qquad \ldots (5.1)$$

where F_c is the Modulus of Elasticity Concrete Factor and ϵ_{cm} is the current maximum concrete strain sustained. Hence F_c varies from 0.8 at a strain just greater than ϵ_o, to a minimum of 0.1 at a strain of ϵ_{20c} or greater.

The stress-strain loops for $\epsilon_{cm} > \epsilon_o$ were idealized by a linear path for increasing strain and a bilinear path for decreasing strain as shown in Fig. 5.2. On unloading from a point G it is assumed that 50% of the stress at G is lost without decrease of strain, and thereafter unloading follows a linear path of slope $\frac{1}{2}E_cF_c$ to point K. As previously, if the element has not cracked it may carry tensile stress to point L with a slope E_c. Once the element has cracked it must regain point K before compressive stress can be once more sustained. From K the line KG with slope E_cF_c is followed back to the stress-strain envelope. If reloading commences before unloading reaches zero stress, one of the infinite number of reloading paths parallel to HG between H and K is followed. One of these paths GHIJG is shown in Fig. 5.2.

It should be noted that the derivation of the stress-strain model for concrete assumes that the envelope curve for cyclic loading coincides with the stress-strain curve for a specimen under monotonic

loading. This assumption was substantiated in the tests of Karsan and Jirsa[77].

It was felt that the more complex expressions which have been proposed for unloading and reloading curves for concrete[76,77] were unwarranted for this study, because of the relatively small effect that the shape of the concrete stress-strain curves has on the moment-curvature characteristics. It has been found by Kent[66] for reinforced concrete and verified in this study for prestressed concrete that the characteristics under reversed loading are predominantly affected by the steel behaviour.

5.2.2 Stress-Strain Model for Cyclically Loaded Prestressing Steel

The stress-strain model chosen for repeated and cyclic loading of prestressing steel was based on some tests carried out on 0.276 inch diameter prestressing wires. Experimental details are included in Appendix D. One set of experimental curves obtained is illustrated in Fig. 5.3.

Points worthy of note from Fig. 5.3 are:

(1) Hysteresis was evident on reloading of the specimen, particularly at high strains. This is contrary to the normally accepted idea that the reloading curve coincides with the unloading curve. The area within the hysteresis loops increased for increasing values of maximum strain before unloading.

(2) There was a continual reduction in the slope of the unloading line with increasing maximum strain before unloading. The slope of the linear region of each unloading curve in Fig. 5.3 was as follows:

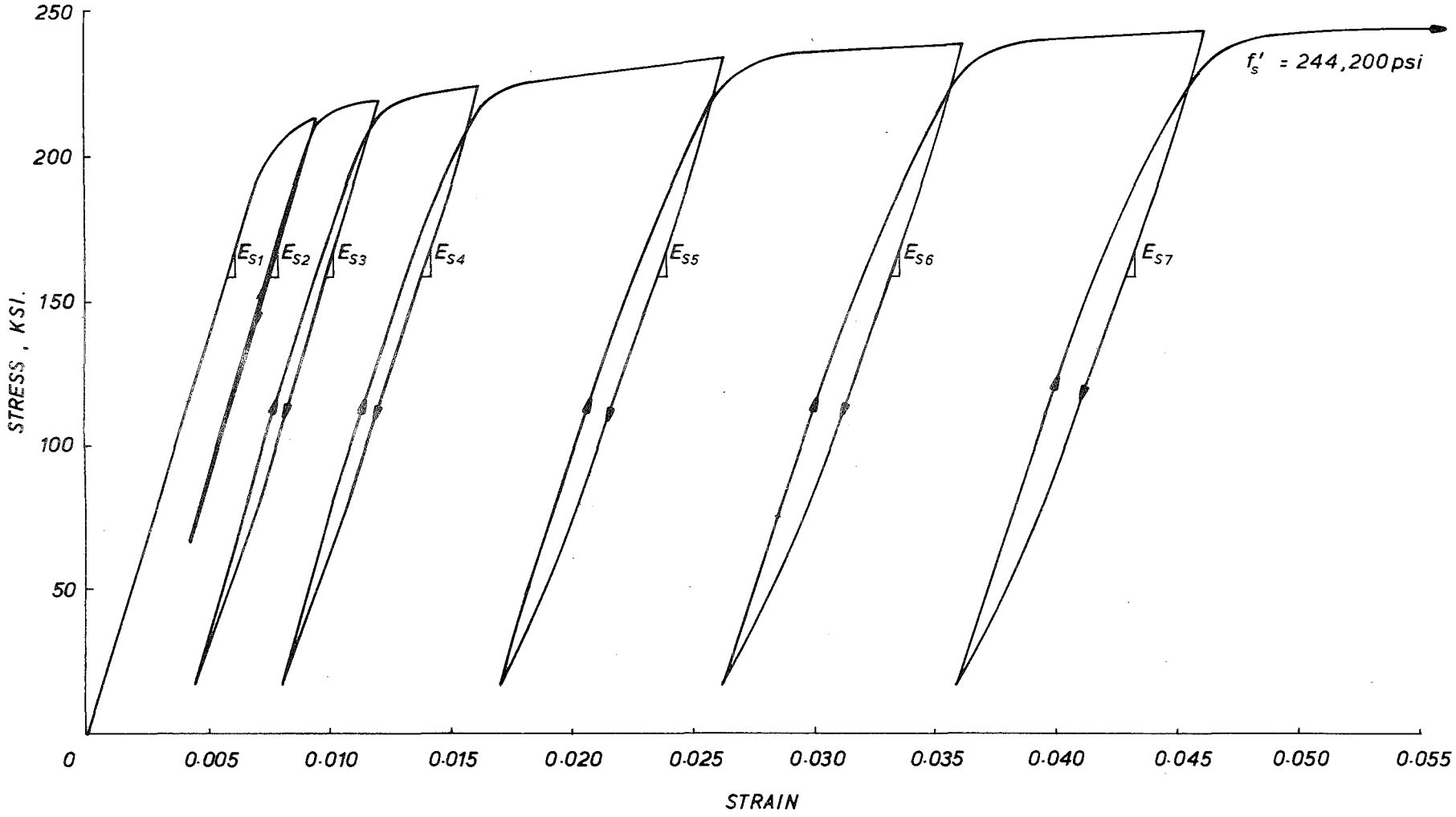

FIG. 5·3 : REPEATED LOAD TEST ON 0·276 INCH DIAMETER PRESTRESSING WIRE.

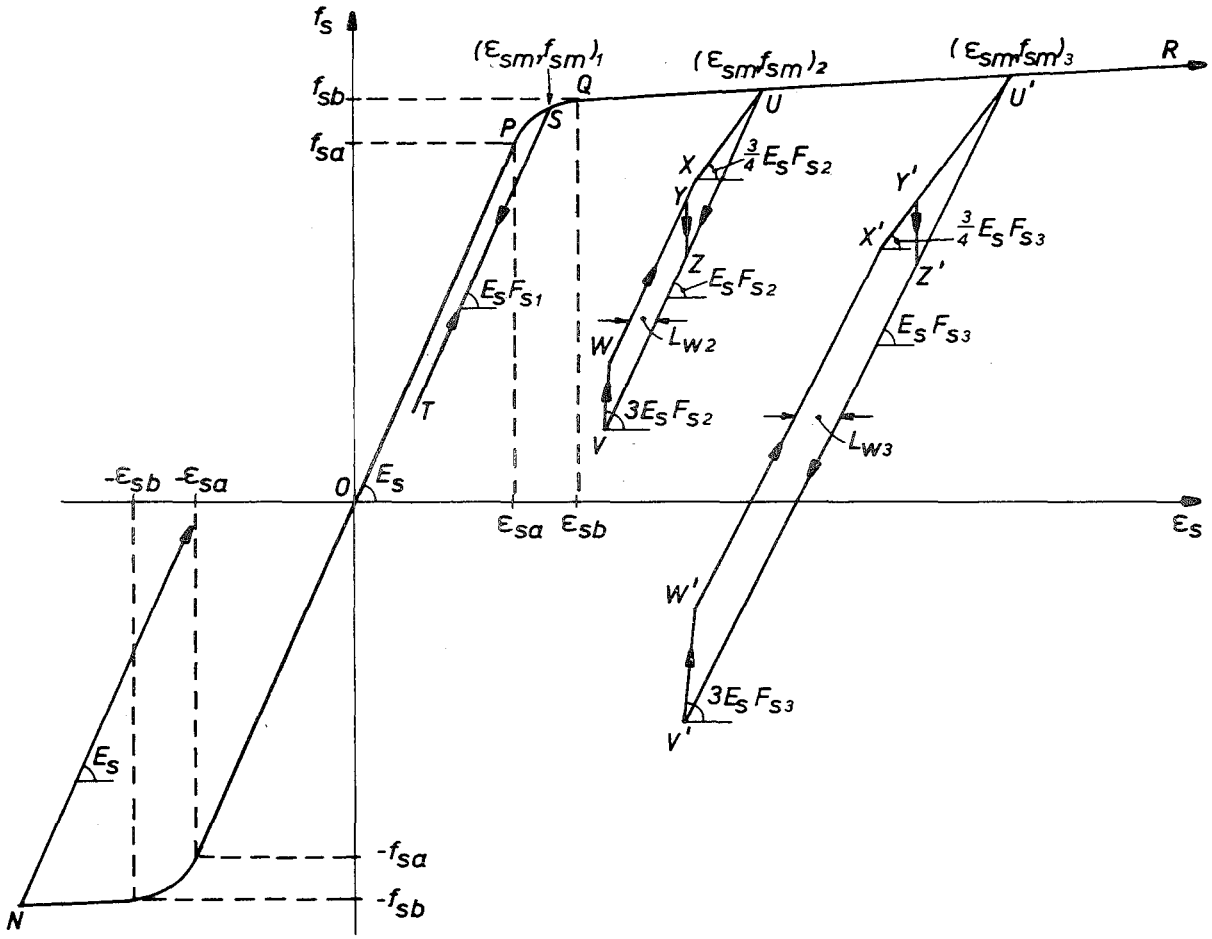

FIG. 5·4 : STRESS-STRAIN IDEALIZATION FOR CYCLIC LOADING OF PRESTRESSING STEEL.

$$E_{s1} = 28.0 \times 10^6 \text{ psi}$$
$$E_{s2} = 28.2 \times 10^6 \text{ psi}$$
$$E_{s3} = 28.4 \times 10^6 \text{ psi}$$
$$E_{s4} = 26.1 \times 10^6 \text{ psi}$$
$$E_{s5} = 25.8 \times 10^6 \text{ psi}$$
$$E_{s6} = 25.2 \times 10^6 \text{ psi}$$
$$E_{s7} = 25.1 \times 10^6 \text{ psi}$$

At the bottom of each unloading curve the slope further reduced giving the appearance of the beginning of a Bauschinger-type effect. It is probable that if the load had been reversed and compression applied, the subsequent area within the hysteresis loop would have been considerably greater.

Two parameters were obtained from the experimental curves for use in an idealization of the steel stress-strain characteristics:

(a) Loop Width Value, L_w

Measurements were taken of the width of the loop at points where the unloading and reloading curves were linear. The following Loop Width Values, L_w, were obtained:

$$\text{If } \epsilon_{sm} \leqslant 0.009, \quad L_w = 0.0 \qquad \ldots (5.2a)$$
$$\text{If } \epsilon_{sm} > 0.009, \quad L_w = 0.045\, \epsilon_{sm} \qquad \ldots (5.2b)$$

where ϵ_{sm} is the current maximum steel strain sustained.

(b) Modulus of Elasticity Steel Factor, F_s

Slopes were measured on the linear part of the unloading curve as this represented the most important section for the moment-curvature response. The following Modulus of Elasticity Steel Factors, F_s, were appropriate for multiplication of the modulus of elasticity of the steel to give the slope of the unloading curve:

$$\text{if } \epsilon_{sm} \leqslant 0.012, \quad F_s = 1.0 \qquad \ldots (5.3a)$$
$$\text{or } \epsilon_{sm} > 0.012, \quad F_s = 1.0 - (\epsilon_{sm} - 0.012)7.7 \qquad \ldots (5.3b)$$

The idealization for the steel characteristics is shown in Fig. 5.4. The envelope curve is assumed to be a "linear-hyperbolic curve-linear" relationship as for monotonic loading. Expressions for the regions OP, PQ, and QR on Fig. 5.4 are given by equations (4.9), (4.10), and (4.11). On unloading, a linear path of slope $E_s F_s$ is followed, where F_s is given by equation (5.3). The reloading path depends on the Loop Width Value, which is defined by equation (5.2). Fig. 5.4 shows three unloading and reloading curves, for one of which L_w is zero. (The scale of the width of the loops is exaggerated on the figure for clarity). On reloading from the minimum strain at V, a line VW of slope $3E_s F_s$ is followed. This line intersects with the line WX parallel to the unloading line. For a given stress the strain on the reloading line is less than that on the unloading line by a value of L_w. The final section of the reloading curve is represented by XU and has a slope of $\frac{3}{4}E_s F_s$. Should the steel tendon unload before reaching its previous maximum strain from any point such as Y, the vertical line YZ is followed back to the previous linear unloading path.

The stress-strain envelope relationships for tension are assumed to apply also in compression and a curve such as ON would be followed. This was felt to be valid as the assumption made in Chapter 4, that the tendons in compression would buckle before attaining their maximum strength, resulted in an underestimation of the moment capacity of the section at very large curvatures.

5.2.3 Method of Analysis

It was apparent in the monotonic load study of Chapter 4 that the calculation of a concrete force for a given strain profile became very complex, because of the number of possible cases for the compressive stress block that had to be considered. For example, in the analysis of sections for which cover concrete at a strain greater than 0.004 is

considered to have spalled it was necessary to include seven possible stress blocks in the analysis. For the cyclic stress-strain relationship shown in Fig. 5.2 there would be numerous possible stress blocks, and this approach to the solution becomes prohibitively complex.

It is clear that another mode of solution is necessary for cyclic loading. The approach used in this chapter is to consider a member as being composed of a number of discrete horizontal elements, and to compute strains and stresses for each of the elements in turn. This approach is similar to that used by Kent[66] for reinforced concrete beams.

The concrete section is divided into N_e discrete elements, each of depth D/N_e and each extending across the whole width of the section. The arrangement is illustrated in Fig. 5.5. If there are five positions of the prestressing tendons at depths of $\alpha_1 D$, $\alpha_2 D$, $\alpha_3 D$, $\alpha_4 D$, $\alpha_5 D$, the corresponding elements in which the tendons reside are $\alpha_1 N_e$, $\alpha_2 N_e$, $\alpha_3 N_e$, $\alpha_4 N_e$, and $\alpha_5 N_e$.

For a strain in the top fibre of ϵ_{cc} and a neutral axis depth of kD (where k may be negative), the average strain in concrete element, i, is given by:

$$\epsilon_{ci} = \epsilon_{cc} \frac{kN_e - i + 0.5}{kN_e} \qquad \ldots (5.4)$$

The strain in the steel at each level is found from the sum of the concrete strain at that level, as determined from the strain profile, and the initial strain due to "effective prestress" (as defined in Section C.2.1). It is assumed in this analysis that the tendons are fully bonded.

For a given strain in the top concrete fibre, the neutral axis depth must be found by an iterative method. This results in the analysis being relatively slow. On the other hand the method has advantages, for example when dealing with complex stress distributions, when making allowance for the reduction of element forces in the case

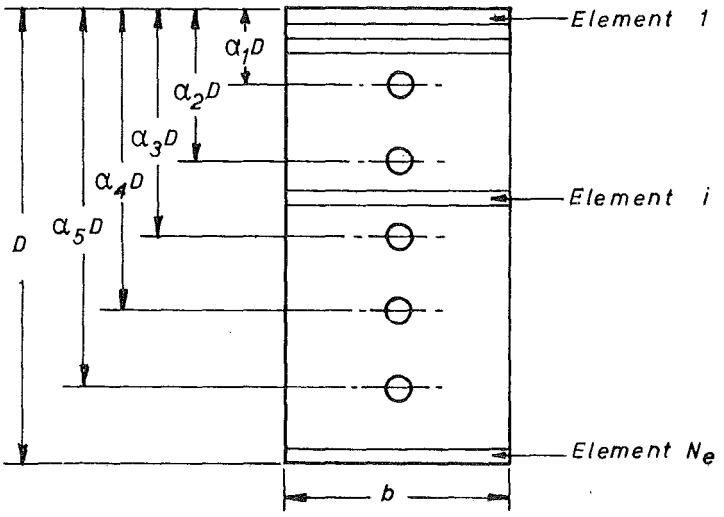

FIG. 5·5 : DISCRETE HORIZONTAL ELEMENTS

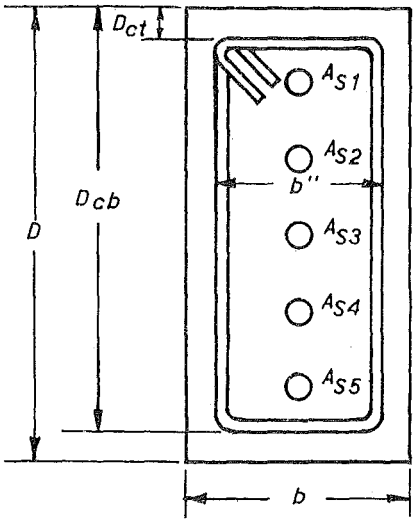

FIG. 5·6 : SECTION DIMENSIONS

of spalling of the cover concrete, and for recording of those elements which have cracked.

5.3 DEVELOPMENT OF COMPUTER PROGRAM FOR THEORETICAL ANALYSIS

A computer program was developed for the analysis of prestressed concrete members under cyclic load. It computes moment, curvature, and energy dissipation for cycles with specified curvature limits. A general section is considered with any number of positions of prestressing tendons, and with or without external axial load. The axial load may be varied during the course of loading. The algebra of the analysis can be found in the listing of Program 5.1 in Appendix A.

The input requirements are: section properties (b, D, b", D_{ct}, D_{cb}, α_1, α_2 etc., A_{s1}, A_{s2}, etc., N_e) as shown in Figs. 5.5 and 5.6; concrete properties (f'_c, ϵ_o, Z); prestressing steel properties (ϵ_{sa}, ϵ_{sb}, ϵ_{su}, f_{sa}, f_{sb}, f'_s, ϵ_{se1}, ϵ_{se2}, etc.) If axial load is required, the initial axial load and a factor for variation of axial load with moment are read in. Finally, the curvature limits for each cycle are read. From this input various other properties are determined for both the steel and concrete stress-strain relationships.

5.3.1 Iterative Technique

The following of the moment-curvature relationship requires calculations of moments and curvatures for successive increments of the top fibre strain, ϵ_{cc}. Positive or negative adjustments are made to ϵ_{cc} according to whether it is desired to increase or decrease the curvature respectively. For a particular value of ϵ_{cc}, the neutral axis depth ratio, k , is first chosen as -20000 and all concrete and steel strains and their corresponding stresses are computed. From a force compatibility check for this strain profile it can be established if the actual neutral axis depth is positive or negative according to whether ϵ_{cc}(Σ compression forces - Σ tension forces -

axial force) is positive or negative respectively. If it is found to be positive, k is set equal to +10, if negative k is set equal to -10, and the concrete and steel strains and stresses are then recomputed. For subsequent adjustments of the neutral axis depth, expressions are used which provide a fairly rapid close on the value of k for force compatibility. The appropriate expression depends on the strain profile configuration. Five general cases for the profile are illustrated in Fig. 5.7. For each case a suitable expression was derived by trial and adjustment, and is similar to that used by L.L. Jones[78].

For cases Fig. 5.7(a),(b) and (e):

$$k = \frac{k}{12.0}\left[10.0 + 2.0\,\frac{(\Sigma T + P)}{\Sigma C}\right] \qquad \ldots (5.5)$$

where ΣT is the sum of the tensile forces in steel and concrete

P is the axial load

ΣC is the sum of the compressive forces in concrete, and steel (if any)

Note that in case (e) compression is provided by the steel alone rather than the concrete. This means that for a beam section the moment is due solely to the action of a steel couple.

For cases Fig. 5.7(c) and (d):

$$k = \frac{k}{12.0}\left[10.0 + 2.0\,\frac{\Sigma C}{(\Sigma T + P)}\right] \qquad \ldots (5.6)$$

In using equations (5.5) and (5.6) iteration is continued until a force equilibrium error of less than (bD/5) lbs is reached.

In some circumstances the above iterative method becomes unstable, and if after 100 trial values of k equilibrium of forces has not been obtained the following alternative approach has to be used. During previous iterations a variable a is assigned the value of k which resulted in the least equilibrium error for $\Sigma C > \Sigma T + P$, and a variable b is assigned the value of k for the least equilibrium

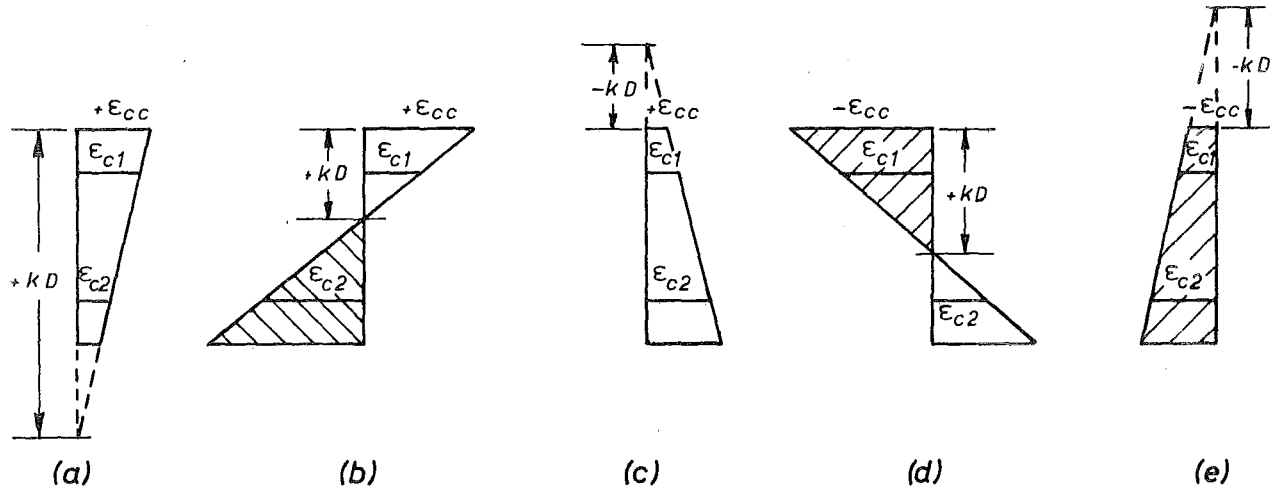

NOTE: Shaded regions denote tensile strain.

FIG. 5·7 : TYPICAL STRAIN PROFILES

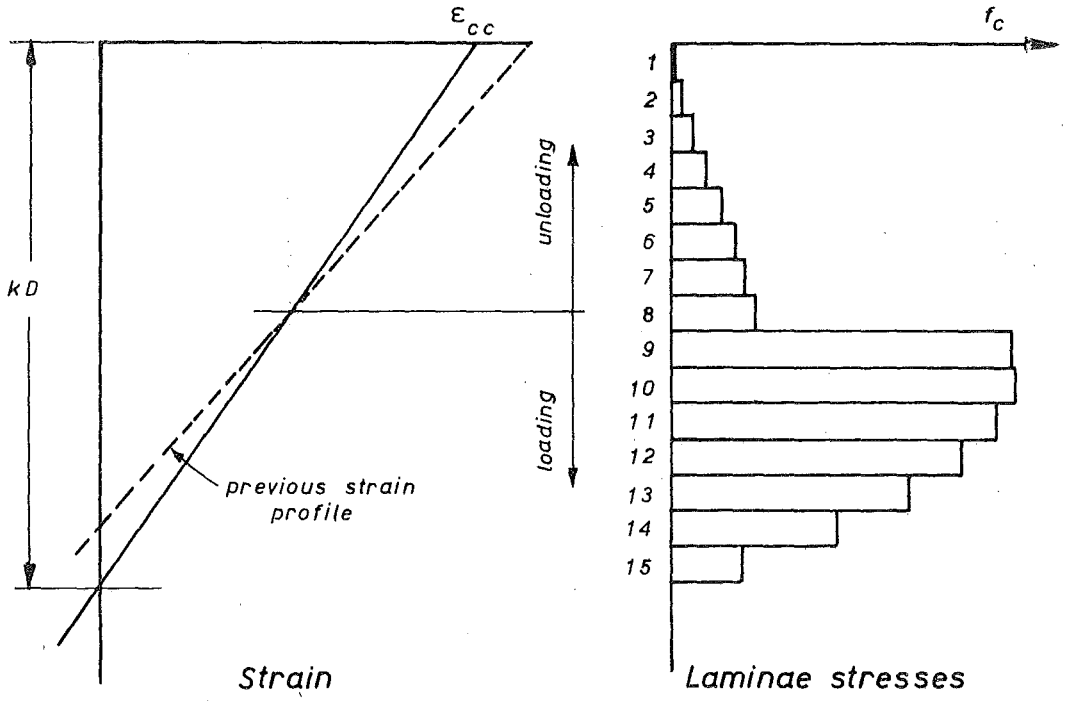

FIG. 5·8 : LAMINA COMPRESSIVE STRESS CONFIGURATION

error when $\Sigma C < \Sigma T + P$. A new value of k is tried half way between a and b. If now $\Sigma C > \Sigma T + P$, then a is set equal to this new value of k, or if $\Sigma C < \Sigma T + P$, then b is set equal to this value of k. A new value of k half way between the new limits is then tried. This process is continued until a value of k is obtained which gives force equilibrium to within (bD/5) lbs.

However in some situations even this refinement will not give force equilibrium. The problem is illustrated in Fig. 5.8. The strain profile is drawn for unloading of the section, and ϵ_{cc} has been decremented from its previous value. However, because the neutral axis has dropped part of the section under compression will be at a higher compressive strain than for the previous strain profile, and part will be at a lower compressive strain. Thus some of the laminae will be loading while others are unloading. The situation may arise where, for a given value of ϵ_{cc}, a very small change in neutral axis depth is sufficient to make the difference between a lamina such as 8 in Fig. 5.8 having a loading or an unloading strain. It may well be that, to achieve the necessary concrete force to balance steel force and axial load, a stress is required in lamina 8 part way between that for loading and unloading. In such a case the iterative techniques outlined above will not achieve force equilibrium. When this occurs a linear interpolation is made to obtain the required concrete force for equilibrium, and the moment due to this force is then calculated.

Once equilibrium has been attained the moment and curvature are calculated. For column sections with a varying axial load relationship in accordance with the moment on the section, the appropriate value of axial load for this moment is calculated and then applied to a further series of iterations to obtain new values of moment and curvature for that particular value of ϵ_{cc}. It was found that analysis with the

axial load at the first new level gave sufficient accuracy for this investigation. Thus only one cycle of change of axial load with moment was necessary at each increment.

If at this stage it is found that the computed curvature is greater than the input curvature for the cycle being considered, a linear relationship is assumed between the ϵ_{cc} and computed curvature of the previous increment, and the ϵ_{cc} and computed curvature of the current increment, to obtain an ϵ_{cc} that will produce the required input curvature. This method was successful in achieving the desired curvature limits.

After satisfactory completion of moment and curvature calculations for a particular increment, the parameters which record the progress along the stress-strain paths for all concrete elements and pre-stressing tendons are updated.

5.3.2 Concrete Model

The following operations must be carried out for each concrete element. Firstly it must be determined if the strain is greater than a previous maximum value. If this is the case, stress may be calculated from the appropriate equation of (4.1), (4.2) or (4.6). If strain is less than a previous maximum it may be in one of the following states: unloading or reloading in compression, loading or unloading in tension, or with zero stress. In all cases the basic parameter required to determine the stress in the element is the current maximum concrete strain, ϵ_{cm}, and from this is calculated both the strain at zero stress for the cycle and the Modulus of Elasticity Concrete Factor, F_c. If the element has a strain indicating compression it is necessary to know the strain at the previous increment to determine if the element is in an unloading or reloading compressive state. On the other hand, if the strain indicates tensile stress it must be determined whether the element can sustain the stress, that is

if f_t' is not exceeded or if the element has not previously cracked.

Finally, a correction is made if necessary to allow for spalling, and the summation of forces and bending moments about the top surface of the section due to all concrete elements is computed. An alteration is applied to force and moment calculations to allow for the section area taken by the prestressing tendons.

5.3.3 Prestressing Steel Model

The stress in each prestressing tendon is determined as follows. As for the case of the concrete model the first check is whether the strain is greater than a previous maximum value. If it is the stress may be determined from the appropriate equation of (4.9), (4.10) or (4.11), or will be zero if the ultimate tensile strain is or has been previously exceeded (that is, the steel has fractured). If the strain is less than a previous maximum, the tendon may either be unloading or reloading. In these cases the basic parameter necessary to determine stress is the current maximum steel strain, ϵ_{sm}, and from this is determined the Modulus of Elasticity Steel Factor, F_s, the Loop Width Value, L_w, and the strain at zero stress for the cycle. The strain at the previous increment is also necessary to ascertain whether the tendon is loading or unloading. If on unloading the linear elastic range is exceeded in compression, expressions are applied to determine stress for the "hyperbolic", and "upper branch" portions of the curve in compression.

Forces and moments due to all the prestressing tendons are then summed. Moments are taken about the top surface of the section by multiplying the forces by the tendon depths, $\alpha_1 D$, $\alpha_2 D$ etc.

5.3.4 Operation of Computer Program

Because the operation of this program is relatively slow, attempts were made to minimise program times. The initial strain values used for incrementing ϵ_{cc} were 0.0002. However, subsequent to significant stiffness degradation occurring, strain increments of as high as 0.0012 gave quite acceptable results for plotting the curves. Another factor which has a significant effect on the computing time required for the analysis is the number of elements that the section is divided into. It was decided to use an element depth of one half of an inch so that if the cover thickness above the core was in increments of half an inch it would be represented by a whole number of elements. This was necessary for accuracy in the case of a section in which the cover concrete was considered to have spalled. The result was 32 elements for column section analyses of Units 3 and 4 and 42 elements for the beams of Units 1 and 2. A comparison was made for sections with 100 and 200 elements and there were only very minor differences in output. These differences were too small to plot. Calculation of theoretical moment-curvature characteristics corresponding to the 15 cycles of loading for beam members took in the order of 10 minutes, while column analyses took in the order of 15 minutes on an I.B.M. 360/44 computer.

The analyses were programmed so that results could be automatically plotted.

5.4 MOMENT-CURVATURE IDEALIZATION

An idealization of the moment-curvature characteristics of pre-stressed concrete members under cyclic load was developed by fitting curves to experimental results. The basic model includes three stages as shown in Fig. 5.9. Stage 1 corresponds to cycles in the post-cracking range but before the concrete in the member has crushed.

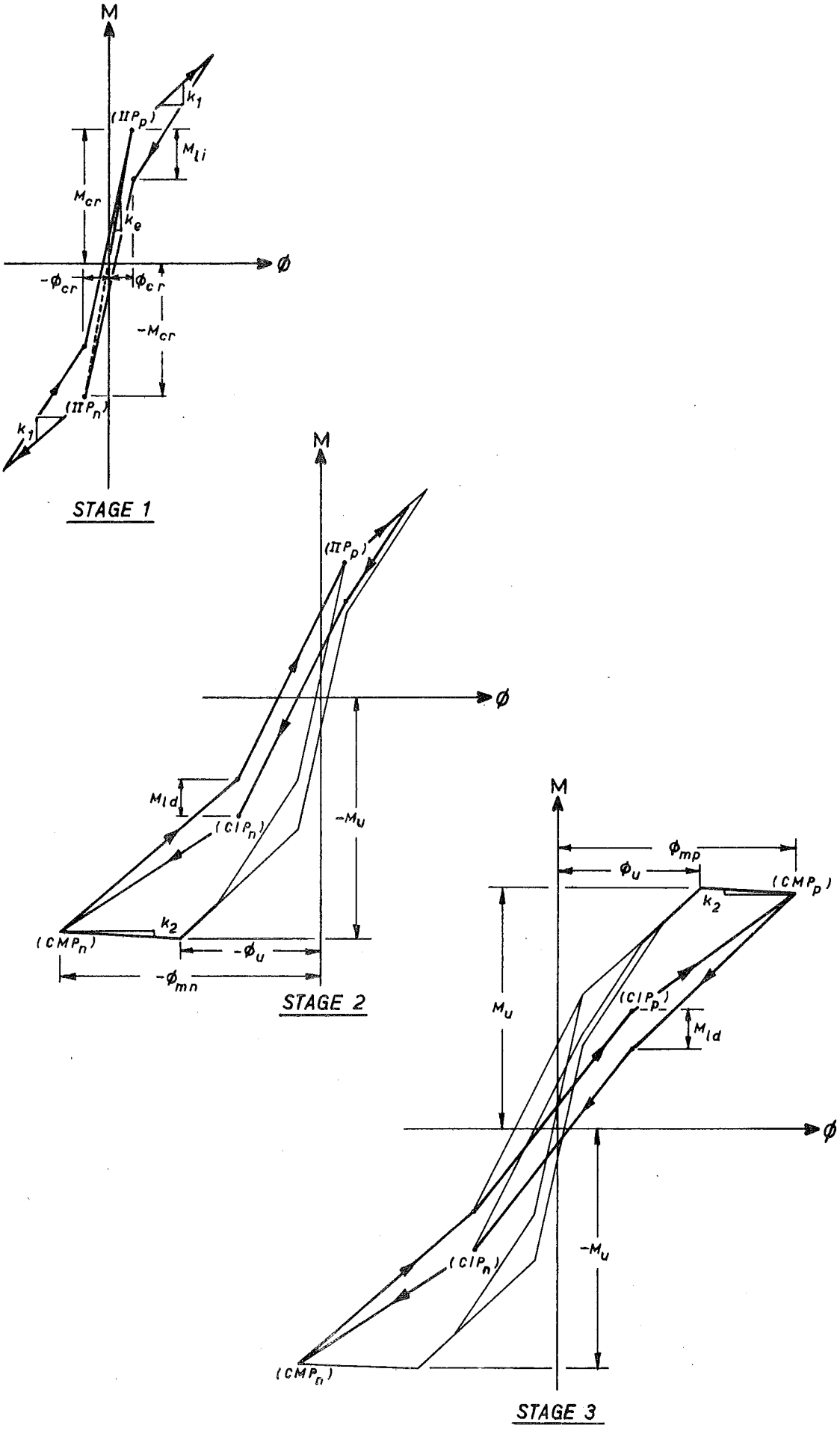

FIG. 5.9 : MOMENT-CURVATURE IDEALIZATION

Stiffness degradation first occurs during Stage 2 when the member has crushed for one direction of loading only, and Stage 3 represents the situation when the member has crushed during cycles in both directions of loading.

5.4.1 Definition of System

The basic parameters which define the system are: the elastic stiffness, k_e; the maximum moment capacity, M_u; the ratio, γ_1, of the post-cracking stiffness, k_1, to k_e; the ratio, γ_2, of the post-crushing stiffness, k_2, to k_e; and the ratio, γ_{LF}, of M_u to the cracking moment, M_{cr}.

5.4.2 Cyclic Loading Sequence

(a) Stage 1

On initial loading in Stage 1, the elastic stiffness, $k_e = M_{cr}/\varphi_{cr}$, is followed to the Initial Positive Inelastic Point, IIP_p. Further loading beyond IIP_p follows the upper branch line with a stiffness k_1. On unloading, the stiffness is defined by two points on the moment-curvature plot: (1) the point from which unloading commenced, and (2) a point with co-ordinates $(M_{cr} - M_{li})$, φ_{cr}, where M_{li} is the Initial Loop Depth Moment value. This latter point together with the Initial Negative Inelastic Point, IIP_n, serves to define the stiffness for the completion of unloading and the commencement of negative loading. From IIP_n, the negative loading, unloading, and positive reloading to IIP_p repeats the previously described corresponding phases in the cycle.

(b) Stage 2

Should the curvature during loading reach $\pm \varphi_u$, corresponding to the points of maximum strength, $\pm M_u$, and hence the commencement of crushing in the member, the "falling" branch stiffness will be k_2. For example, Stage 2 in Fig. 5.9 illustrates the case where the

initial post-crushing loading was in the negative direction. On reloading from the Current Negative Maximum Point CMP_n, the hysteresis loop for cyclic loading has a similar shape to that for Stage 1. However, M_{1i} is replaced by the Degraded Loop Depth Moment value, M_{1d}, and for the case shown IIP_n is replaced by the Current Negative Inelastic Point, CIP_n. The co-ordinates of CIP_n are determined from an expression given in the next section, which is dependent on the curvature, φ_{mn}, of CMP_n. The slope of the upper branch of the negative loading curve is no longer equal to k_1, but rather is defined by the two points, CIP_n and CMP_n. The situation would be analogous if curvatures greater than φ_u had first occurred in the positive direction.

(c) Stage 3

After curvatures greater than φ_u have been sustained in both directions the idealized behaviour is represented by Stage 3. Both IIP_p and IIP_n have now been replaced by CIP_p and CIP_n respectively, and the loop depth moment value is M_{1d}.

5.4.3 Numerical Values of Parameters

Numerical values of the parameters for the moment-curvature idealization were obtained from an analysis of the experimental moment-curvature curves of Units 1 to 4. They are as follows:

Parameter	Numerical Value
$\gamma_{LF} = M_u/M_{cr}$	1.8
$\gamma_1 = k_1/k_e$	0.15
$\gamma_2 = k_2/k_e$	beams: -0.003
	columns: -0.009
M_{1i}/M_u	0.21
M_{1d}/M_u	0.16

During Stages 2 and 3 the co-ordinates of CIP_p are given by:

$$M = 0.5\ M_u \qquad \ldots (5.7)$$

and,

$$\text{for } \varphi_u < \varphi_{mp} \leq 10\varphi_u, \qquad \varphi = \varphi_{mp}\left(0.23 + \frac{\varphi_{mp}}{\varphi_u}\,0.05\right) \qquad \ldots (5.8a)$$

$$\text{and } \varphi_{mp} > 10\varphi_u, \qquad \varphi = 0.7\varphi_{mp} \qquad \ldots (5.8b)$$

where φ_u is the curvature at maximum strength, M_u, and φ_{mp} is the current maximum positive curvature. Similarly, the numerical values of the negative M and φ of CIP_n are found from equation (5.7) and from substitution of $|\varphi_{mn}|$ for φ_{mp} in equation (5.8).

The values of the parameters would be expected to depend on factors which normally affect moment-curvature curves, for example steel area ratio, transverse reinforcement, and axial load. However, it was found that for the range of these variables included in the experimental beams and columns, a close fit to all experimental curves was obtained by both the parameters nominated for the shape of the loading curves prior to crushing and the expressions for recovery on unloading. Only the parameter γ_2, describing the "falling" branch curve past the point of crushing, was significantly affected by both transverse reinforcement and axial load. For this reason values of γ_2 have been given for both beams and columns, the experimental values being within $\pm$ 0.001 of those listed.

5.5 COMPARISON OF EXPERIMENTAL, THEORETICAL AND IDEALIZED MOMENT-CURVATURE CHARACTERISTICS

From the experimental programme outlined in Chapter 3, seven sets of moment-curvature curves for cyclic loading were available to test the theoretical derivation and idealization presented in this Chapter. Figs. 5.10 to 5.16 present the experimental, theoretical, and idealized curves for three beam plastic hinge lengths and four column hinge

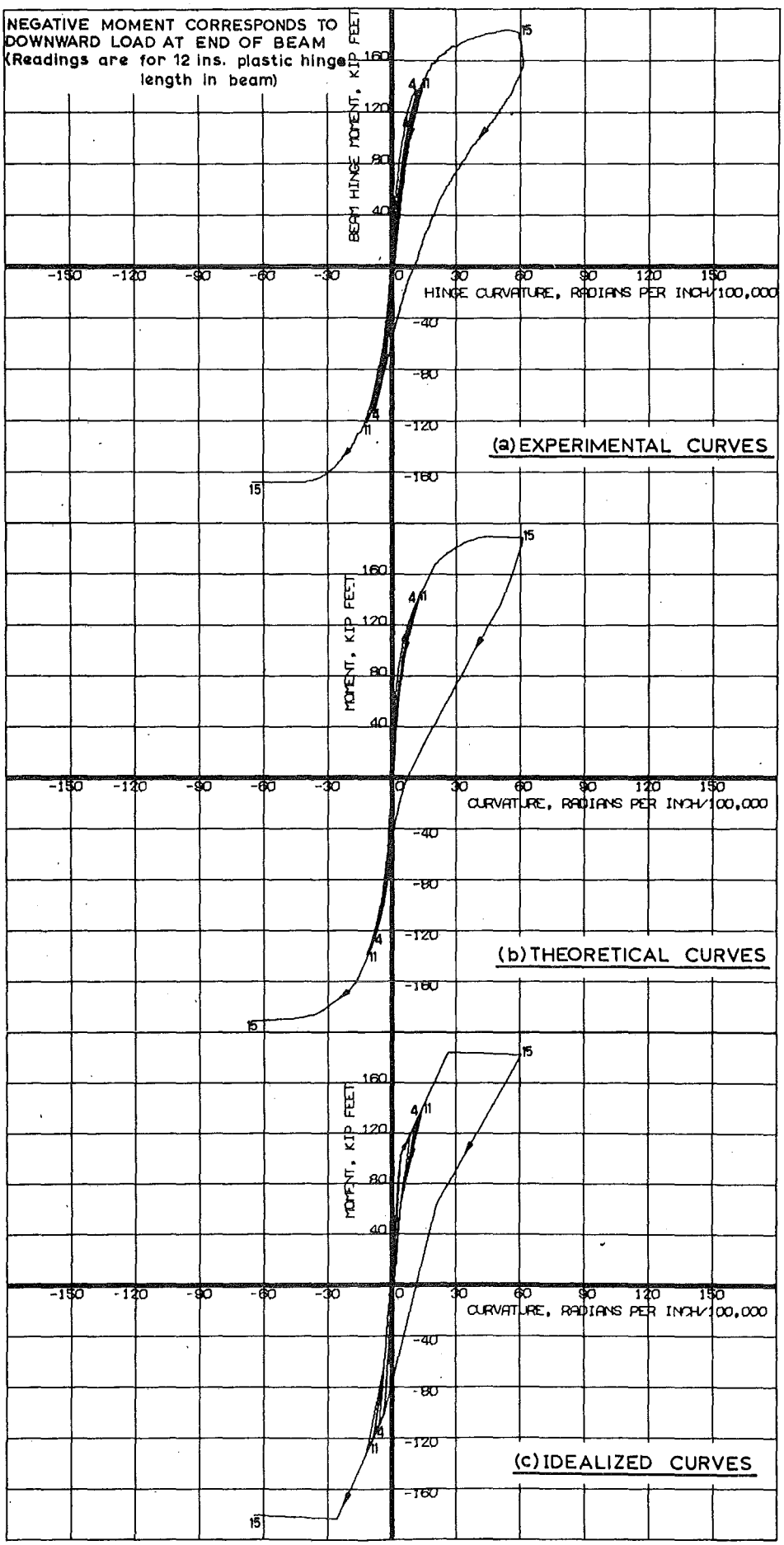

FIG. 5·10 : MOMENT-CURVATURE CURVES FOR UNIT 1 BEAM.

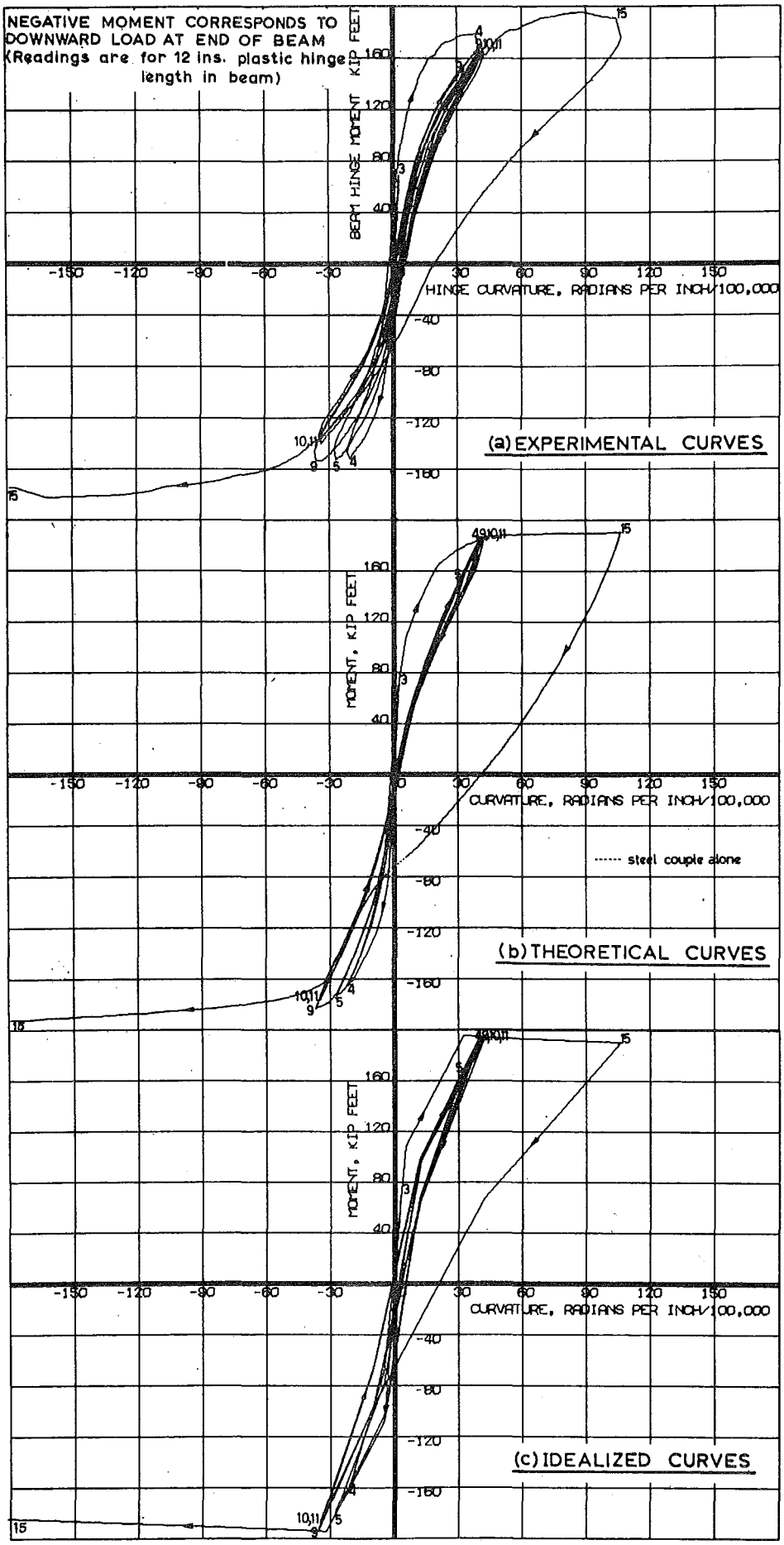

FIG. 5·11 : MOMENT-CURVATURE CURVES FOR UNIT 2 BEAM.

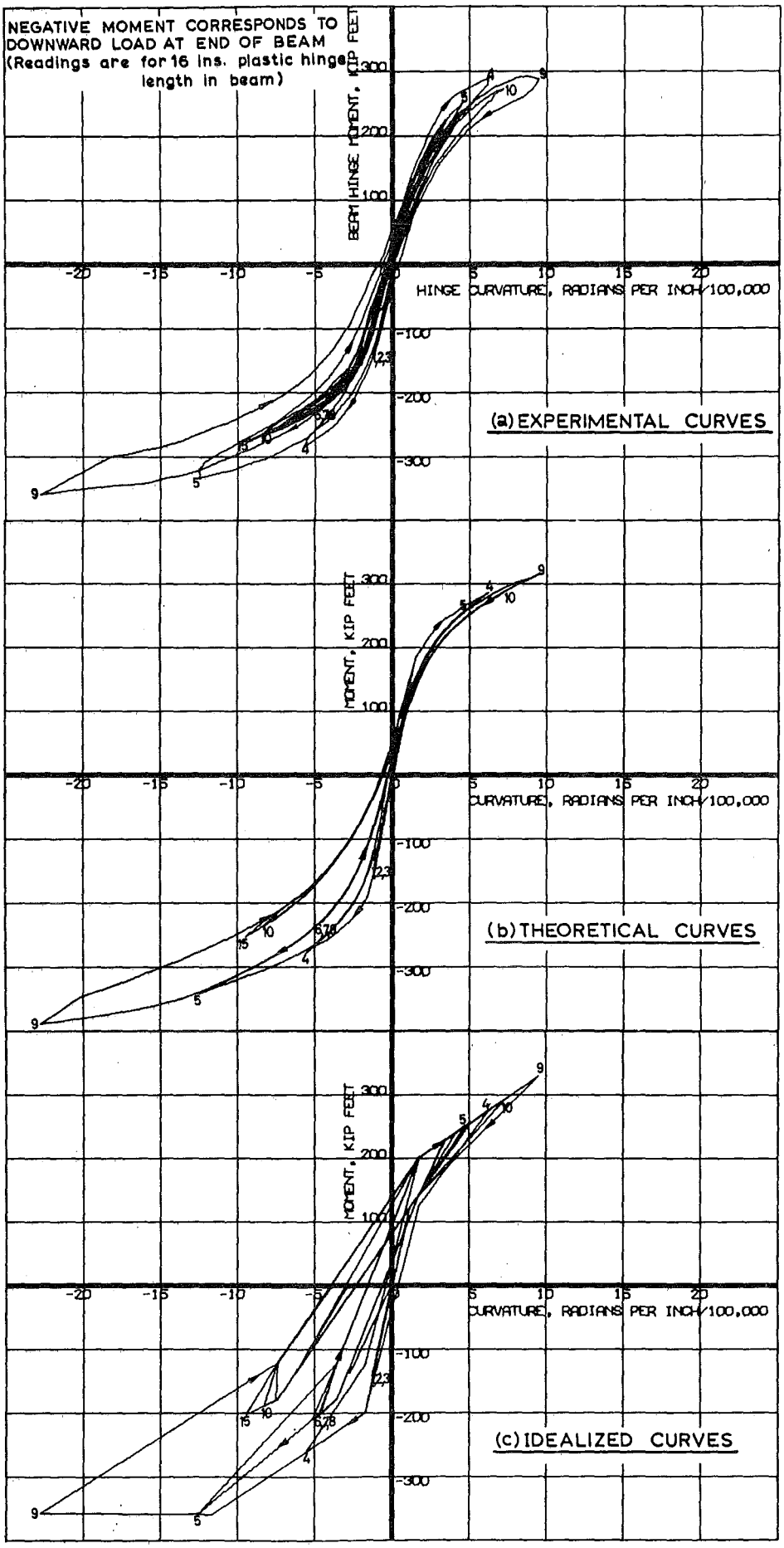

FIG. 5·12 : MOMENT CURVATURE CURVES FOR UNIT 4 BEAM.

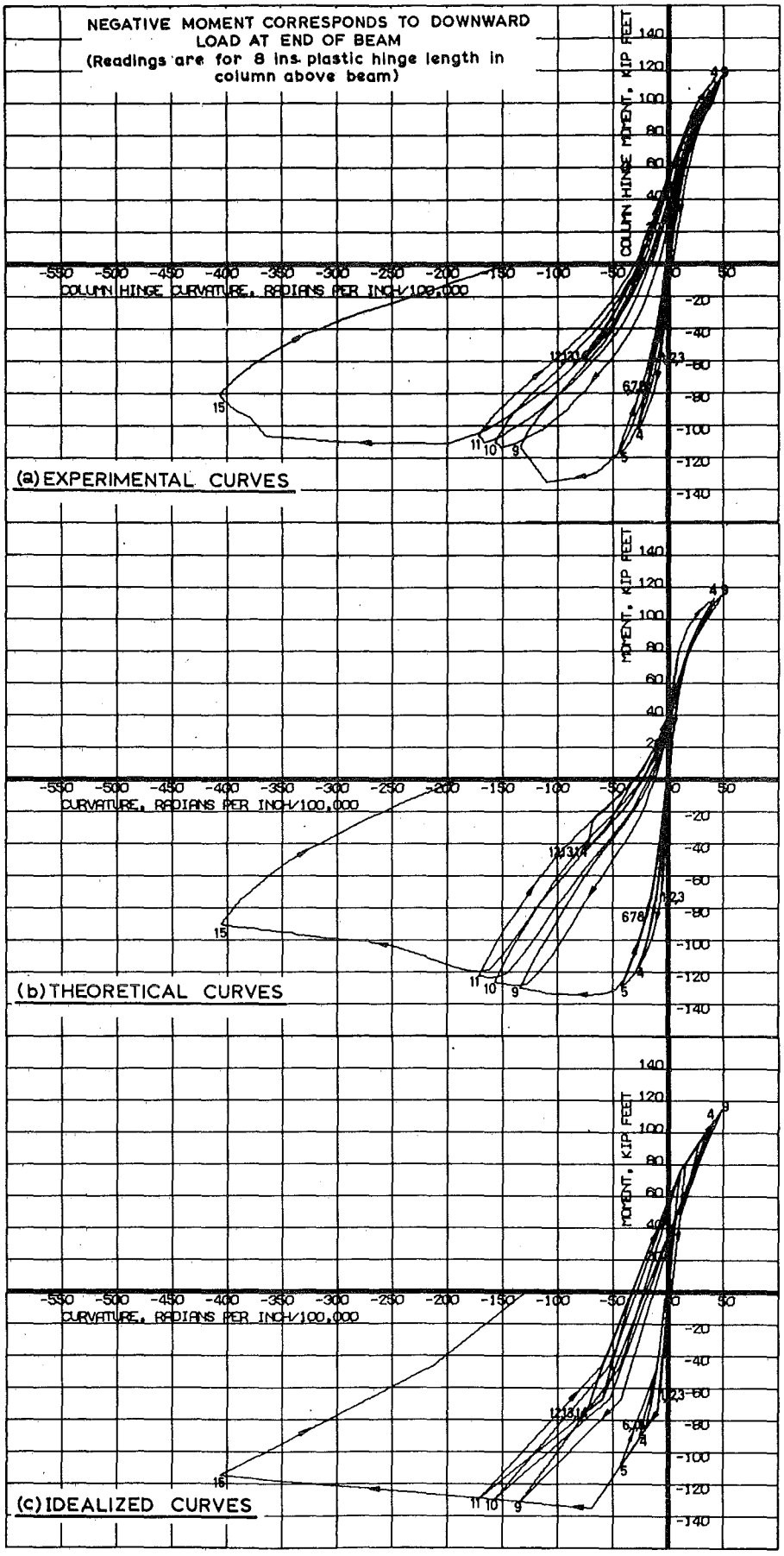

FIG. 5·13 : MOMENT CURVATURE CURVES FOR UNIT 3 COLUMN ABOVE BEAM.

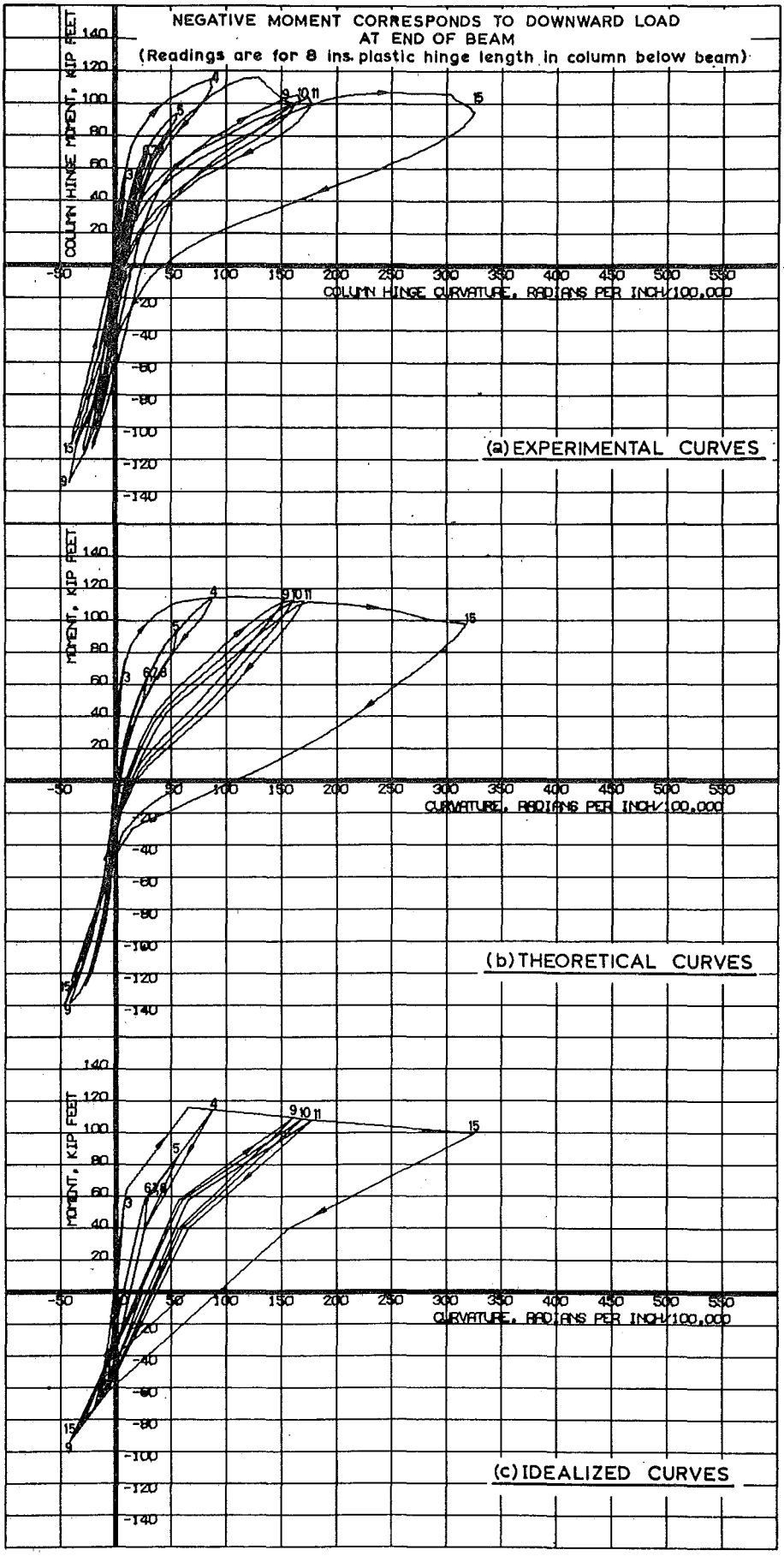

FIG. 5·14 : MOMENT-CURVATURE CURVES FOR UNIT 3 COLUMN BELOW BEAM.

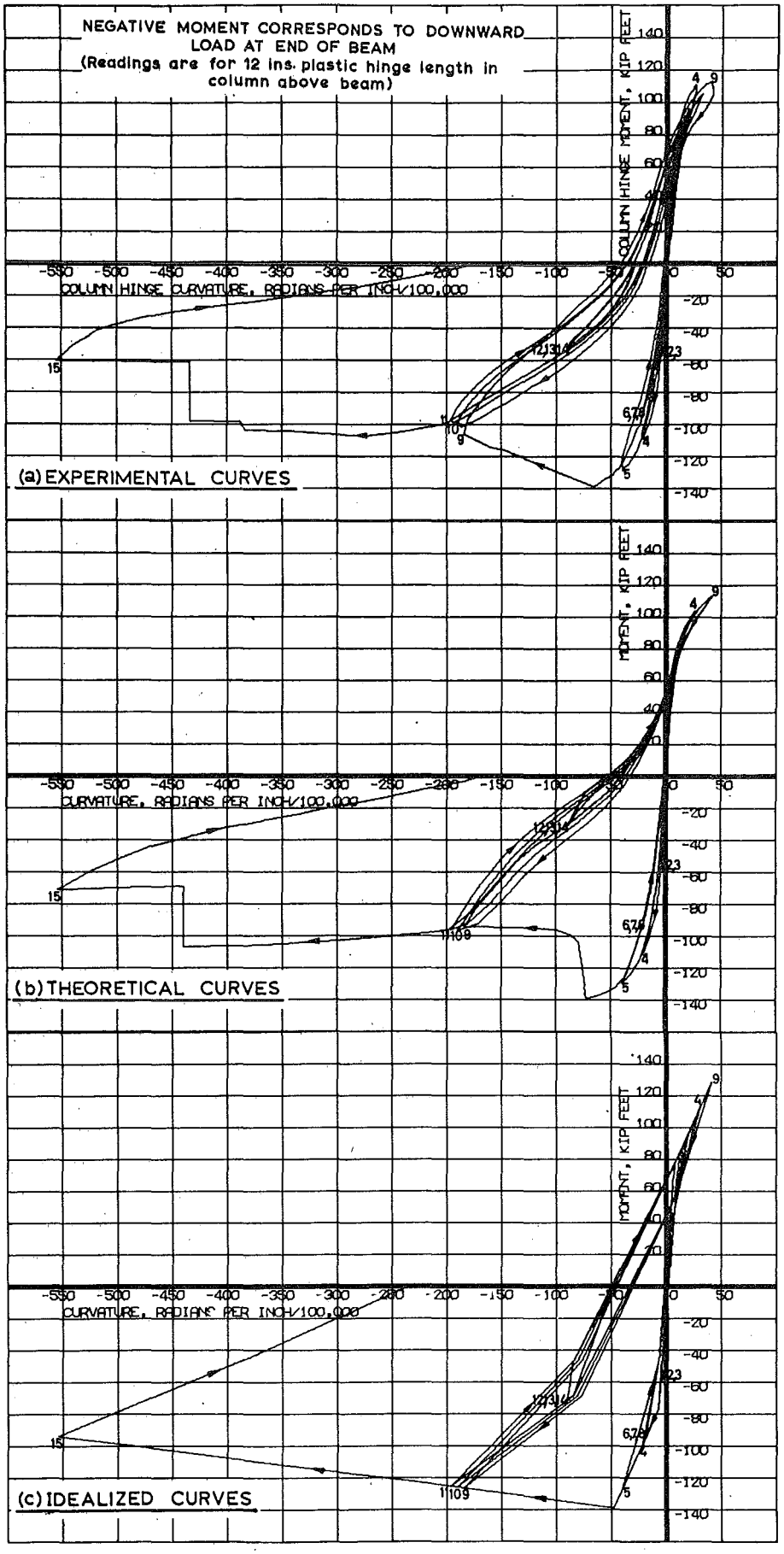

FIG. 5·15 : MOMENT-CURVATURE CURVES FOR UNIT 4 COLUMN ABOVE BEAM.

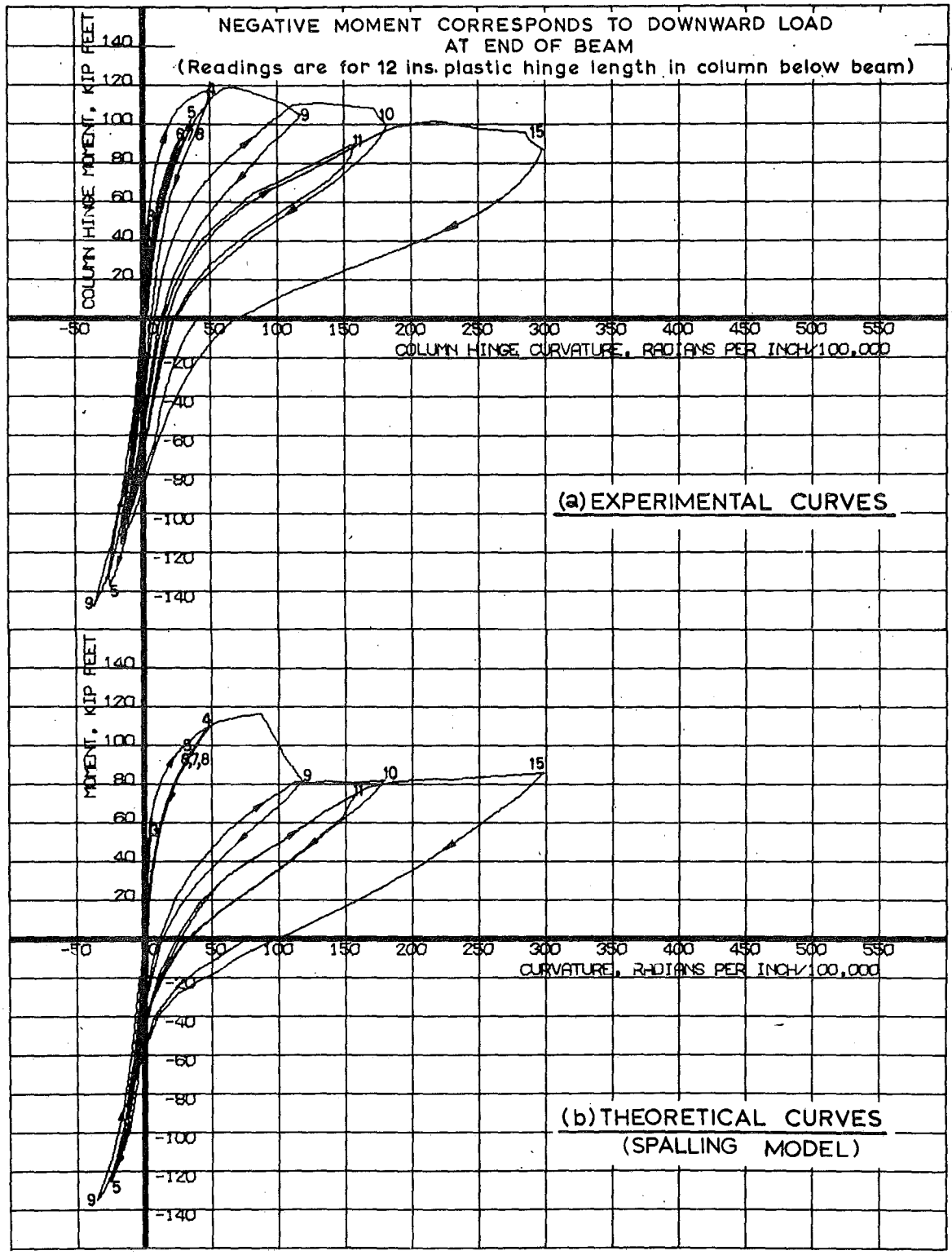

FIG. 5·16 : MOMENT-CURVATURE CURVES FOR UNIT 4 COLUMN BELOW BEAM.

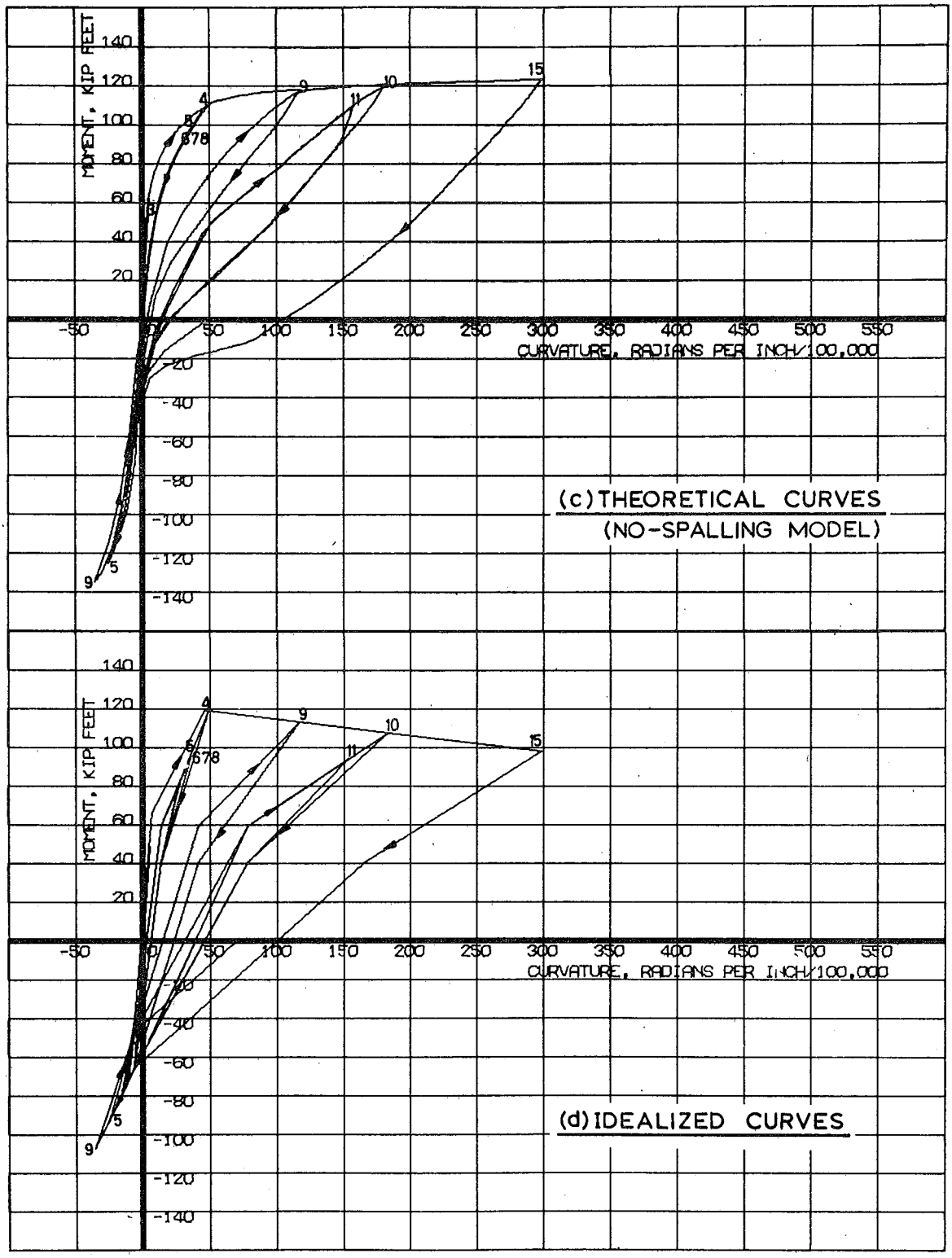

FIG. 5·16 : MOMENT-CURVATURE CURVES FOR UNIT 4 COLUMN BELOW BEAM.

lengths, each subjected to 15 cycles of high intensity cyclic loading. Experimental details of these tests are included in Chapter 3 and Appendix B. The theoretical and idealized curves are determined between the same curvature limits as the experimental curves. For the beam hinges there was some discrepancy between curvatures measured over a 12 inch gauge length at the joint, firstly by dial gauges attached to frameworks around the beam, and secondly by the strain measurements from Demec gauges. This arose because of small opposing inaccuracies in both means of measurement (arising from the special stress conditions due to the mortar joint), which would not affect the shape of the curves but do affect the magnitude of the curvature. The curvature limits taken were those determined from the Demec gauge analysis, as it was felt that these were the most accurate.

The theoretical analyses assumed spalling of any cover concrete at a strain greater than 0.004 only in the case of the column hinges of Unit 4. (Model 2 in Section 4.2.3). This column had heavy internal binding, and for the hinge in the column above the beam this seemed to precipitate a sudden spalling of the cover concrete. For all other hinges during the tests there was a gradual formation of longitudinal cracks in the compression zone, and in the theory it was assumed that the cover concrete did not spall but followed the same stress-strain relation as the core concrete. (Model 1 in Section 4.2.3).

5.6 DISCUSSION OF RESULTS

5.6.1 Accuracy of Theoretical Analysis

In general there is good agreement between theoretical and experimental moment-curvature curves. However, two points where agreement is not so good should be discussed.

The first of these is apparent in Fig. 5.15. The experimental curves for downward load half-cycles 10 and 11 have rather more area

within the hysteresis loops than do the theoretical curves. It is apparent that for downward beam end loading in these half-cycles the experimental moments are greater for a given curvature than their theoretical counterparts. This may well be explained by the fact that on reloading, after sustaining wide cracks in tension, the cracks on a real member may close earlier than predicted theoretically by the assumption of a "clean" crack. For example, small shear displacements along the crack may mean that peaks on one side of a crack do not fit neatly back into the corresponding recess on the other side. Hence the two sides of the crack come into contact earlier than is predicted theoretically. Also, particles of concrete may flake off during cracking and by filling the cracks cause them to effectively close more quickly. The latter case would be more significant in a beam, where cracks are vertical, than in a column. These two phenomena would increase the area within the hysteresis loops.

The second deviation of theory from experiment concerns the elastic recovery apparent for Unit 2 beam after upward load in half-cycle 15, as shown in Fig. 5.11. In this case the theoretical elastic recovery was not as large as the experimental recovery. In contrast all other curves showed good correlation for elastic recovery. It may well be that there is some substance in the suggestion of Paranagama and Edwards[75] of the occurrence of bond slip, as this could explain the greater experimental recovery. However, because Units 1 and 4 beams showed good correlations for rather smaller maximum steel strains, the differences shown by Unit 2 would seem to be significant only at very large steel strains. This point is further illustrated in that the columns of Units 3 and 4 showed good agreement with theory. In these cases slip would not be expected because of the greater bond resistance of their pretensioning strands relative to the grouted wire cables of the beams.

It is of interest to study the accuracy of the model assumed to represent the cover concrete. The assumption, for all cases except the column hinges of Unit 4, that the cover concrete did not spall, gave good correlation with experiment at large curvatures for these members. There was a slight difference in behaviour of Unit 3 column at the peak of downward load half-cycle 9, as shown in Fig. 5.13. In reality there was some spalling, but application of the spalling theoretical model would have considerably underestimated the subsequent moment capacity of the section. However, use of the spalling model in the analysis of the upper column hinge of Unit 4 resulted in the envelopes of the experimental and theoretical curves being almost identical, as shown in Fig. 5.15. The situation was not quite so clear for the lower column hinge of Unit 4, as although the concrete gave signs of crushing in this region it did not spall. This may be seen from the photograph in Fig. 3.17. Figs. 5.16(b) and (c) show analyses using spalling and no-spalling models respectively. Comparison with Fig. 5.16(a) shows that the real situation is part way between these two extremes.

Only in one section of the theoretical curves did the situation represented by Fig. 5.7(e) occur, that is, there was an open crack throughout the depth of the section and moment resistance was provided by a steel couple alone. This occurred for Unit 2 as illustrated in Fig. 5.11(b) for a small section of the curve for downward load half-cycle 15.

5.6.2 Accuracy of Moment-Curvature Idealization

Inspection of Figs. 5.10 to 5.16 shows the accuracy of the proposed idealization. In Fig. 5.12 the elastic recovery of the beam is underestimated, but generally the idealization closely represents the shape, energy dissipation, and stiffness degradation characteristics of the experimental curves.

5.6.3 Accuracy of Stress-Strain Models for Concrete and Steel

It may be assumed from the good correlation between the theoretical and experimental results that the stress-strain idealizations for concrete and prestressing steel under cyclic loading do closely represent the actual behaviour of these materials. It should be noted that although the inclusion of hysteresis in the cyclic loading idealization for prestressing steel may appear fastidious, it did in fact help correlation with experiment. An initial steel model was used in the analysis based on the usual assumption that the reloading line coincides with the unloading line. However, the theoretical moment-curvature curves resulting did not show the hysteresis for large curvature cycles that were evident experimentally. Subsequent cyclic testing of prestressing wires, and the use of an idealization based on the hysteresis apparent in these tests, resulted in good correlation with experiment.

5.6.4 Comparison of Theoretical Curves for Monotonic and Cyclic Loading

On loading of a section the reverse situation to that depicted in Fig. 5.8 occurs. That is, the neutral axis rises on successive increments of ϵ_{cc}, and part of the concrete under compression is in a loading state and part in the unloading state shown in Fig. 5.2. This situation is not taken into account in most theories determining moment-curvature relationships of prestressed concrete, including that in Chapter 4, for monotonic loading. It is usual to assume the stress block for loading of concrete applies over all the compression area, and indeed it is necessary to use an approach akin to the lamina analysis presented in this chapter to take this repeated loading into account. However, although this is an interesting matter of principle it has little effect on the moment-curvature response, mainly because of the small influence of the concrete stress representation. For example, a comparison of Figs. 5.15(b) and 4.11, for the column hinge

of Unit 4, shows very close correlation between the theoretical monotonic curve and the envelope of the cyclic curves. In fact there is less than ½% difference in the maximum moment capacities of the section for the two approaches.

5.7 COMPARISON OF PRESTRESSED AND REINFORCED CONCRETE SECTIONS UNDER CYCLIC LOADING

Any attempted comparison of the expected seismic response of prestressed and reinforced concrete structures must take into account the relative energy dissipation capacities of these two materials under cyclic loading. Fig. 5.17 illustrates a comparison of a reinforced and a prestressed concrete member both with the same section sizes and transverse reinforcement properties, and the same maximum moment capacities (and therefore some design moments for an ultimate strength approach). Both members have equivalent steel areas in the top as at the bottom of their respective sections. The curves for the reinforced concrete section were obtained by Kent[66] for the first two post-elastic cycles of a theoretical cyclic load analysis. His theoretical curves showed very good correlation with previously determined experimental moment-curvature points. The curves for prestressed concrete were obtained using the author's theory, between curvature limits of the two cycles for the reinforced concrete section.

Initially the two sections have the same stiffness, but for the prestressed concrete member tension cracking is delayed relative to the reinforced concrete member by the presence of the prestressing force. However, the most significant difference between the two sets of curves is the greater elastic recovery exhibited by the prestressed concrete section. This is shown clearly by the respective energy dissipations represented by the areas within the hysteresis loops. For the two cycles considered, the prestressed concrete section had a hysteretic energy dissipation of 0.4 times that for reinforced concrete.

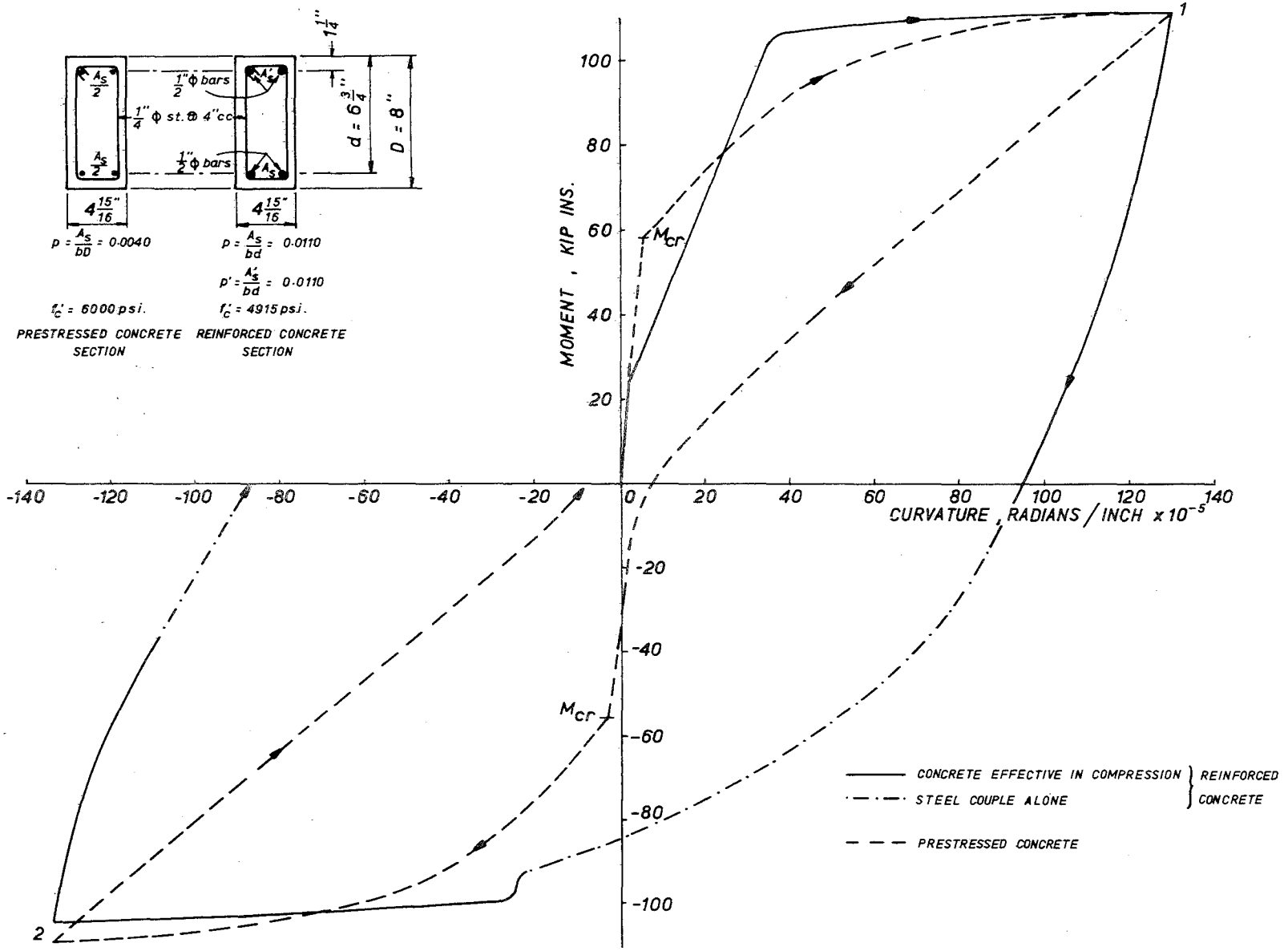

FIG. 5·17 : COMPARISON OF REINFORCED AND PRESTRESSED CONCRETE SECTIONS UNDER CYCLIC LOADING.

To study the reasons for the greater elastic recovery of prestressed concrete, the values of parameters affecting moment and curvature for both sections are shown in Table 5.1, firstly at the peak of half-cycle 1, and secondly at points on the return curves where ϵ_{cc} has been decremented to a similar value. The sign convention is compression force negative and tension force positive. It should be remembered that the strain in the prestressing steel includes the initial strain due to effective prestress.

Table 5.1

COMPARISON OF REINFORCED AND PRESTRESSED CONCRETE MEMBERS UNDER CYCLIC LOADING

	At peak of half-cycle 1		A few decrements after peak of half-cycle 1	
	Reinforced Concrete	Prestressed Concrete	Reinforced Concrete	Prestressed Concrete
ϵ_{cc}	0.00179	0.001862	0.00120	0.00116
bottom steel, ϵ_s	0.00697	0.01153	0.00549	0.00783
concrete force, lbs	-15,980	-26,697	-1,830	-18,116
top steel force, lbs	-1,864	9,880	399	9,821
bottom steel force, lbs	17,900	16,810	1,431	8,490
k	0.204	0.179	0.179	0.225
φ, rads/in. x 10^{-5}	129.8	129.8	99.0	64.5
M, Kip ins.	111.5	112.1	9.3	56.1

While the strains in the top compression fibre have decreased by similar amounts in each case, the steel and concrete forces have reduced to a very much lower value for the reinforced concrete member than for the prestressed concrete member. This arises because although the steel for both members is well into the inelastic range before reversal, the prestressing steel has a much higher stress level and consequently

a smaller required steel area for a comparable moment capacity. Therefore, a given strain reduction will cause a greater force reduction for the reinforced concrete member, because of its smaller initial stress level and greater steel area. The ensuing higher steel force for the prestressed concrete member relative to the reinforced concrete member, after a few decrements, has a dual effect. Firstly, it requires a greater neutral axis depth because of the greater consequent concrete compression, thus causing a lower curvature for a given value of ϵ_{cc}. Secondly, it results in a greater moment resistance. It is significant that, between the two load stages studied, the neutral axis depth for reinforced concrete has decreased while that for prestressed concrete has increased. This was a continuous trend on unloading of the two sections. In the case of the reinforced concrete section a crack formed over the full depth of the section, on loading in the reverse direction, and moment was provided by a steel couple due to the top steel in tension, and the bottom steel in compression. In the prestressed concrete section, on the other hand, all cracks closed and the section returned to its initial stiffness for loading in the reverse direction.

It should be noted that this comparison presents the maximum likely differences between the energy dissipations of prestressed and reinforced members. In practice a prestressed concrete member may have a smaller section size than a reinforced concrete member with the same strength. Therefore, a greater prestressing steel area would be required and from the argument above the elastic recovery would not be so large.

5.8 COMPUTER PROGRAM

A listing of the computer program written for the analysis in this chapter appears in Appendix A.

Program 5.1 ("CYCLOPS"): Cyclic loading of prestressed concrete members with up to 12 positions of prestressing tendons, and using up to 200 discrete elements to determine force in the concrete. The analysis uses stress-strain models for the cyclic behaviour of concrete and prestressing steel. The section may be without or with a constant, or variable, axial load.

5.9 CONCLUSIONS

The results presented in this Chapter have shown that the models proposed, to represent the cyclic loading of concrete and prestressing steel, can be successfully used to determine the moment-curvature relationships of a prestressed concrete member under cyclic load. The theoretical characteristics obtained show good correlation with experimentally derived curves. The analysis developed could usefully be employed to study the cyclic load characteristics of particular prestressed concrete sections under a wide range of imposed curvatures.

An idealization for the moment-curvature characteristics of prestressed concrete members, under high intensity cyclic loading, has also been presented for use in seismic analyses of framed structures. The idealization closely represents the available experimental curves from this study.

For prestressed concrete members the theoretical monotonic loading moment-curvature curve is very close to the envelope of curves for cyclic loading. Also, the maximum moment capacity for members subjected to cyclic loading is almost identical with that for monotonic loading.

The elastic recovery of prestressed concrete members is a feature of special significance for seismic resistance. For prestressed and reinforced concrete members with comparable size and strength and loaded well into the inelastic range, the energy dissipation capacity of the prestressed concrete member is less than half of that of the

reinforced concrete member. This difference will not be so pronounced where the prestressed concrete section is smaller than that of a reinforced concrete member with the same strength.

CHAPTER 6

EARTHQUAKE RESPONSE OF PRESTRESSED CONCRETE STRUCTURES AND COMPARISON WITH REINFORCED CONCRETE STRUCTURES

SUMMARY

A comparative study is made of the earthquake responses of prestressed concrete and reinforced concrete single-degree-of-freedom portal frame structures. Three non-linear idealizations for load-displacement characteristics are used; a prestressed concrete system, a degrading stiffness system, and an elasto-plastic system. Relative maximum displacements and energy dissipations for the three systems are tabulated for varying values of period of vibration and viscous damping ratio. The effect of the level of design strength on the response of the prestressed concrete system is considered and the significance of the results for section curvature requirements is discussed.

6.1 INTRODUCTION

It has been recognised for some time that the inertia loads from theoretical elastic response analyses for strong earthquakes are much greater than the lateral loads recommended for seismic design by building codes. Hence it is clear that buildings designed to these code lateral forces will be loaded beyond the elastic limit. Previous chapters have demonstrated the ability of properly designed prestressed concrete sections to sustain large post-elastic curvatures. However, the actual ductility demands on members of prestressed concrete frames under seismic loading are not as yet clear. Quantitative values may be obtained from inelastic response analyses of such structures, yet apart from one study by Spencer[6] little research on these lines has been

undertaken.

Because more is known about the behaviour of reinforced concrete structures in earthquakes, intuitive comparisons are often attempted between the responses of prestressed and reinforced concrete frames. It is generally argued that the response of a prestressed concrete structure will be greater than that of a comparable reinforced concrete structure because of the smaller energy dissipation and lower viscous damping properties usually assumed for prestressed concrete. This investigation sets out to make such a comparison quantitative, and for this purpose only simple single-degree-of-freedom structures are considered.

The traditional moment-curvature or load-displacement characteristics assumed for reinforced concrete have been elasto-plastic. In recent years more sophisticated representations have been suggested. Clough[79] postulated a "degrading stiffness" idealization and compared the response of this system with that of an elasto-plastic system for a single-degree-of-freedom structure. Ramberg-Osgood functions have also been suggested for reinforced concrete[80]. An idealization for the moment-curvature characteristics of prestressed concrete members has been presented in Section 5.4, and in this Chapter the idealization is extended to provide a load-displacement function for use in the seismic analysis of a single-degree-of-freedom system.

There is little experimental evidence of the viscous damping ratio which may be applied to prestressed concrete framed structures. Many dynamic loading tests have been made on reinforced concrete structures and in a review of these Katayama[81] shows that the average viscous damping ratio is of the order of 8%. Apparently the general acceptance that a lower damping ratio is applicable to prestressed concrete framed structures is based largely on the results of dynamic tests of members, for example[1,25,26]. Yet it is interesting to note

that James, Lutes, and Smith[82] found little difference in damping ratio for prestressed and reinforced concrete beams. Further, a factor tending to equalize damping ratios for frames is that non-structural elements may have a significant influence on damping independent of the frame component material. However, factors which would lead to a lower damping ratio for prestressed concrete structures are firstly, damping due to foundation compliance may be less for a prestressed concrete frame as it is likely to be more flexible than its reinforced concrete counterpart, and secondly, for medium amplitude vibrations the members of the prestressed concrete frame may not be cracked whereas those of the reinforced concrete frame will be. Thus the common assumption for prestressed concrete structures of a damping ratio approximately one half of that for reinforced concrete structures appears to be a reasonable figure until more experimental evidence becomes available.

6.2 DYNAMIC RESPONSE ANALYSIS

6.2.1 Equations of Motion

The structural system which was considered for this analysis is illustrated in Fig. 6.1. It consists of a rigid girder of mass, M, weightless columns with a total lateral stiffness, k, and a viscous damping mechanism, c. The elastic properties of the system may be described in terms of the period of vibration, T, and the damping ratio, λ:

$$\text{where} \qquad T = 2\pi\sqrt{\frac{M}{k}} \qquad \ldots (6.1)$$

$$\text{and} \qquad \lambda = \frac{c}{c_{cr}} = \frac{c}{2\sqrt{Mk}} \qquad \ldots (6.2)$$

The background to these equations, and other basic dynamics used in the analysis, is presented by Biggs[83] and others.

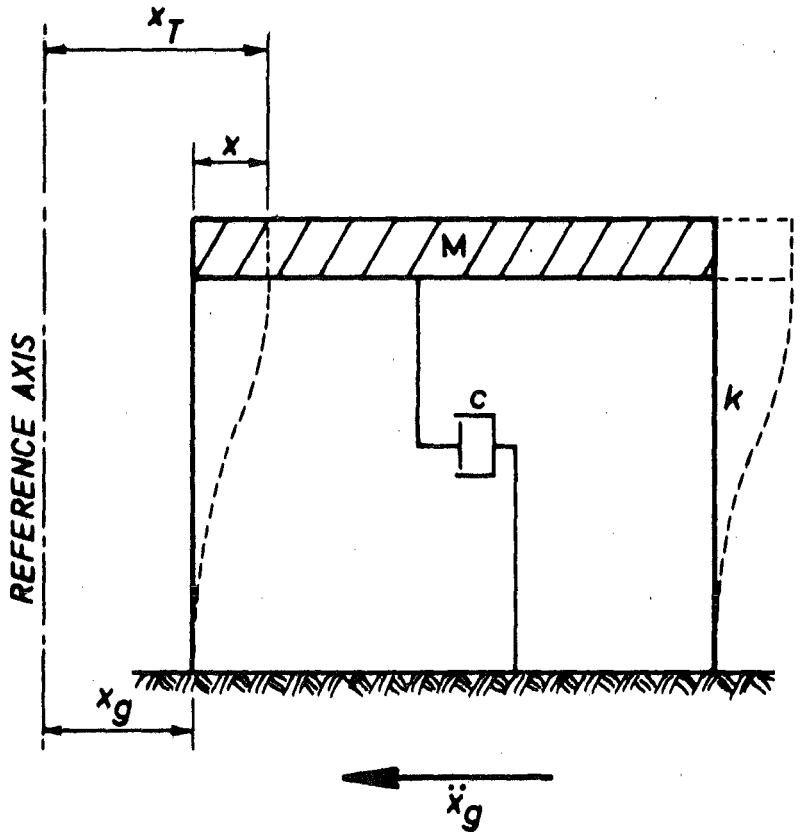

FIG. 6.1 : STRUCTURAL SYSTEM

At a time, t, the incremental forces acting on the mass, M, are given by:

$$\text{inertia force,} \qquad (\Delta F_I)_t = M(\Delta \ddot{x}_T)_t$$

$$\text{damping force,} \qquad (\Delta F_D)_t = c(\Delta \dot{x})_t$$

$$\text{spring resistance,} \qquad (\Delta V)_t = k(\Delta x)_t$$

where $\ddot{x}_T$ is the total acceleration, and $\dot{x}$ and x are the velocity and displacement relative to the ground.

The equation for dynamic equilibrium of the system is:

$$(\Delta F_I)_t + (\Delta F_D)_t + (\Delta V)_t = 0 \qquad \ldots (6.3)$$

It should be noted that the total acceleration, $\ddot{x}_T$, may be expressed as the sum of the ground acceleration, $\ddot{x}_g$, plus the relative acceleration, $\ddot{x}$. Substituting in equation (6.3) leads to:

$$M(\Delta \ddot{x})_t + c(\Delta \dot{x})_t + k(\Delta x)_t = -M(\Delta \ddot{x}_g)_t \qquad \ldots (6.4)$$

Dividing equation (6.4) by M and introducing the relationships:

$$\frac{k_e}{M} = \frac{4\pi^2}{T^2}, \quad \text{where } k_e \text{ is the elastic stiffness}$$

$$\text{and} \qquad \frac{c}{M} = \frac{4\pi}{T}\lambda$$

gives an expression which involves only the fundamental parameters; period of vibration, T, and damping ratio, λ:

$$(\Delta \ddot{x})_t + \frac{4\pi}{T}\lambda\,(\Delta \dot{x})_t + \frac{4\pi^2}{T^2}(\Delta x)_t = -(\Delta \ddot{x}_g)_t \qquad \ldots (6.5)$$

The stiffness at time, t, will depend on the position on the appropriate non-linear load-displacement response, but may be expressed as a proportion of the elastic stiffness.

The displacement response was calculated from equation (6.5) using step-by-step numerical integration. The assumption was made that the

acceleration varies linearly during each time increment.

6.2.2 Ultimate Lateral Strength

An important property for the analysis is the ultimate strength for each system, defined as the maximum load on the load-displacement curve. For a given period of vibration all three systems have the same ultimate strength, V_u, being:

$$V_u = L.F. \times V_d \qquad \ldots (6.6)$$

where V_d = design earthquake load from NZSS 1900 Chapter 8[84]

L.F. = load factor for earthquake loading from the NZS 3101 code[85].

The New Zealand design load code[84] has a trilinear spectrum of seismic coefficients, with varying intensities for the three seismic zone divisions within the country. It also has provision for higher coefficients for important public buildings. The New Zealand Code[85] for reinforced concrete is based on the ACI 318-63 code[40].

For this study the same load factors are used for prestressed concrete as for reinforced concrete and consequently the structures have the same lateral strength for an ultimate strength design approach. The choice of an appropriate load factor is based on the following reasoning:

The code[85] design capacity which will be critical in most cases is:

$$U = 1.25 (D + L_e + E) \qquad \ldots (6.7)$$

From equation (6.7) it is apparent that the actual strength of the member available to resist earthquake loading is given by:

$$U = 1.25 (D + L_e + E) - (D + L_e) \qquad \ldots (6.8)$$

If it is assumed that at the hinge points in a frame the sum of the dead and seismic live load moments is equal to three fifths of the design earthquake moment, M_e, the ultimate moment, M_u, may be obtained from equation (6.8):

$$M_u = 1.25\ (0.6M_e + M_e) - 0.6M_e = 1.4M_e \qquad \ldots (6.9)$$

On this basis a load factor of 1.4 is appropriate to apply to the design earthquake loads to obtain the actual lateral strength. It should be noted that this will give a minimum actual strength level, as capacity reduction factors included in the design would probably result in the actual member strengths being rather greater than those required for the design loads.

It is convenient to express the lateral load as a ratio of the weight of the structure. Thus the strength ratio, β , which is defined as the ratio of the ultimate lateral strength of the structure to the weight of the structure, becomes for this study:

$$\beta = \frac{V_u}{W} = \frac{1.4CW}{W} = 1.4\ C \qquad \ldots (6.10)$$

where C is the appropriate seismic coefficient, and W is the weight of the structure.

6.3 NON-LINEAR IDEALIZATIONS FOR STRUCTURAL BEHAVIOUR

The solution of the equations of motion for the systems requires a knowledge of the stiffness, k , at any particular time. This may be determined from the relationship between lateral force, V , and the displacement, x. Three non-linear load-displacement characteristics are considered:

6.3.1 Elasto-Plastic Model

The elasto-plastic model is characterised by the load-displacement relationship illustrated in Fig. 6.2. The two basic properties which define the shape of the relationship are the yield strength level, V_y, which also corresponds to the ultimate strength, and the elastic stiffness, k_e. After the elastic limit deflection, x_y , is exceeded for loading from zero, the system has zero stiffness. On unloading, the initial elastic stiffness is followed. The same yield strength level applies to both directions of loading.

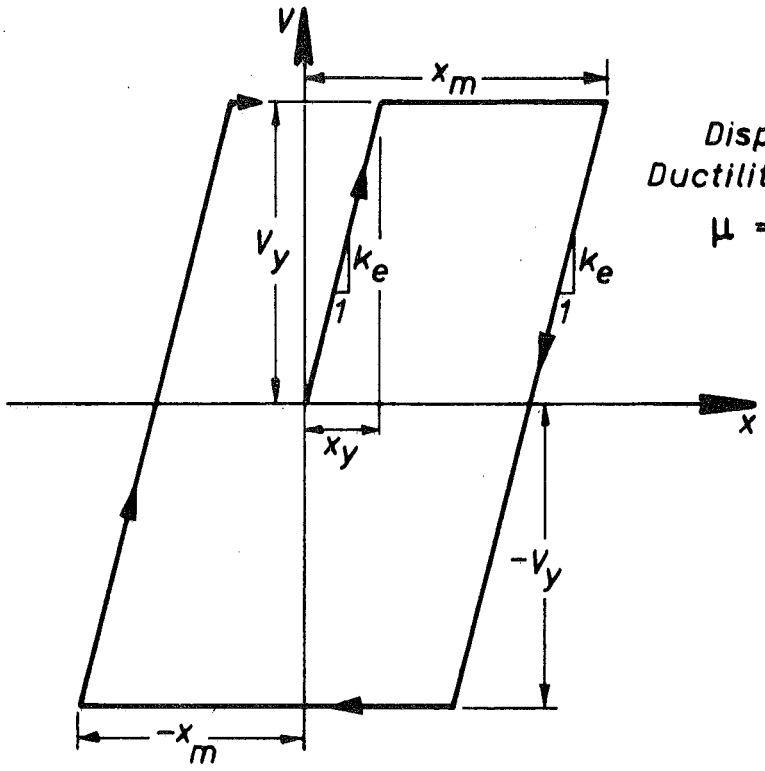

FIG. 6.2 : ELASTO-PLASTIC MODEL

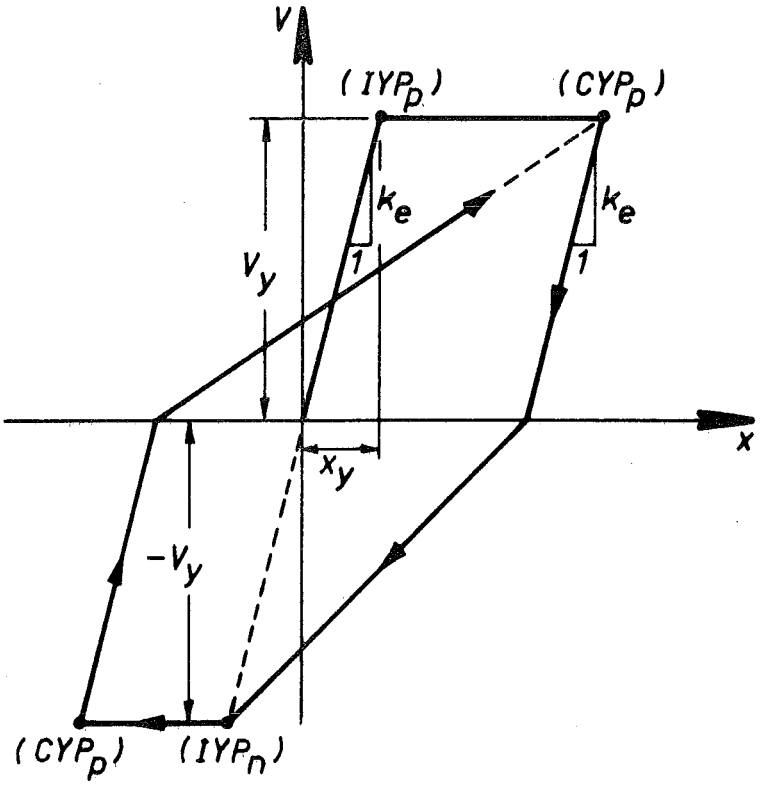

FIG. 6.3 : CLOUGH'S DEGRADING STIFFNESS MODEL

A convenient expression for the amount of displacement in either direction is the displacement ductility factor, μ , which is defined on Fig. 6.2 as:

$$\mu = \frac{x_m}{x_y}$$

where x_m = maximum displacement from zero in either direction

and x_y = initial yield displacement.

6.3.2 Degrading Stiffness Model

The degrading stiffness model proposed by Clough[79] is shown in Fig. 6.3. The initial behaviour is identical with that of the elasto-plastic model and is characterised by the same basic parameters: yield strength, V_y , and elastic stiffness, k_e. However, after loading, yielding, and unloading the behaviour differs. Negative loading follows a stiffness defined by two points on the load-displacement response: (1) the displacement at which positive unloading terminated at zero load, and (2) the current negative yield point, CYP_n. For the initial negative loading cycle, the current negative yield point is called the initial negative yield point, IYP_n, and is at a hypothetical point of negative yield for an initial loading in this direction. However, after negative yielding has taken place, the CYP_n is defined by the maximum negative displacement which has occurred previously and by the negative yield force.

The negative unloading phase follows the initial elastic stiffness in the same manner as the elasto-plastic system. However on positive reloading the degrading stiffness property is again in evidence, and is once more defined by two points on the load-displacement response in exact similarity with the negative loading case.

For this model the definition of displacement ductility factor is the same as that given in Section 6.3.1.

6.3.3 Prestressed Concrete Model

A moment-curvature idealization for prestressed concrete members was presented in Section 5.4. The load-displacement idealization, which is used in this Chapter for the single-degree-of-freedom analysis (see Fig. 6.4), utilizes the same basic model but employs different

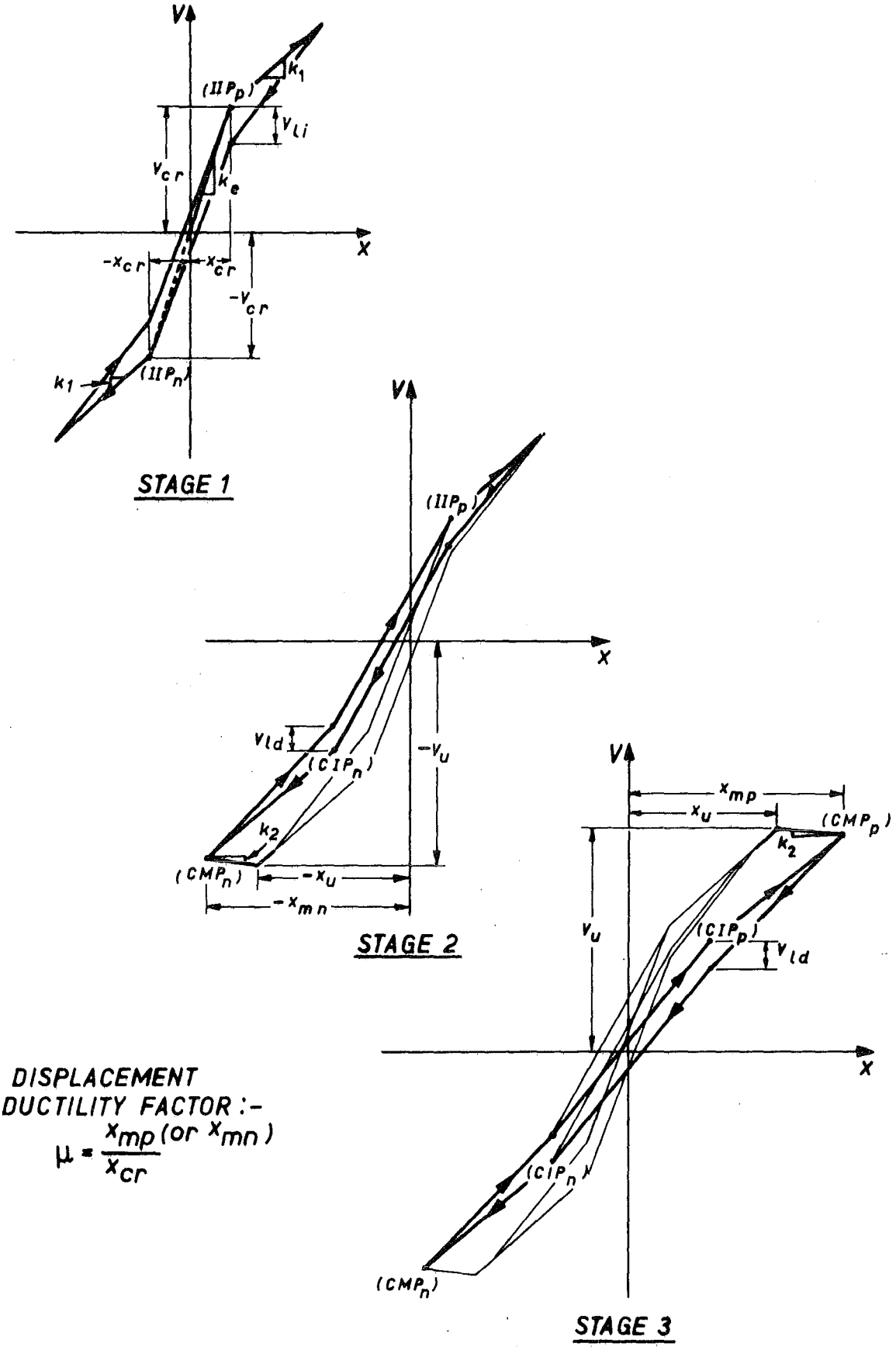

DISPLACEMENT DUCTILITY FACTOR :-

$$\mu = \frac{x_{mp} \text{ (or } x_{mn})}{x_{cr}}$$

FIG.6.4 : PRESTRESSED CONCRETE MODEL

numerical values of the parameters which describe it.

(a) Definition of System

Fig. 6.4 shows the three stages of loading within the load-displacement model, corresponding respectively to post-cracking cycles, cycles after crushing in the members for one direction of load, and cycles after crushing during both directions of loading. The basic parameters which define the system are the elastic stiffness, k_e ; the ultimate strength V_u ; the ratio, γ_1 , of the post-cracking stiffness, k_1 , to k_e ; the ratio γ_2 of the post-crushing stiffness, k_2 , to k_e ; and the ratio, γ_{LF} , of V_u to the cracking strength V_{cr} . The sequence for following curves on the idealization has already been described in detail in Section 5.4.2.

The displacement ductility factor, μ , which will be used in this study is defined with reference to Fig. 6.4 as:

$$\mu = \frac{x_{mp} \text{ (or } x_{mn})}{x_{cr}}$$

where x_{mp} is the current maximum positive displacement

x_{mn} is the current maximum negative displacement

x_{cr} is the displacement at first cracking.

(b) Numerical Values of Parameters

The numerical values of the parameters describing the shape of the load-displacement curves were determined from an analysis of the experimental results of Units 1 and 2. In these units the displacement at the end of the beam was due principally to deformations within that member, as the deflection component due to column curvature was small. The values are as follows:

Parameter	Numerical Value
$\gamma_{LF} = V_u/V_{cr}$	1.8
$\gamma_1 = k_1/k_e$	0.3
$\gamma_2 = k_2/k_e$	-0.007
V_{li}/V_u	0.15
V_{ld}/V_u	0.12

The relationship to determine the co-ordinates, V , x , of the Current Positive Inelastic Point, CIP_p , is as follows:

$$V = 0.5V_u \qquad \ldots (6.11)$$

for $x_u < x_{mp} \leq 7x_u$, $\quad x = x_{mp}\,(0.24 + \frac{x_{mp}}{x_u}\,0.09)$ $\qquad \ldots (6.12a)$

and $x_{mp} > 7x_u$, $\quad x = 0.8x_{mp}$ $\qquad \ldots (6.12b)$

Similarly, the numerical values of the negative V and x of the Current Negative Inelastic Point, CIP_n , are determined from equation (6.11) and from substitution of $|x_{mn}|$ for x_{mp} in equation (6.12).

(c) Accuracy of Load-Displacement Idealization

Figs. 6.5 and 6.6 allow a comparison of the experimental load-displacement characteristics at the end of the beam of Unit 2 and the idealized curves plotted between the same displacement limits. Fig. 6.5 shows the curve shapes for displacements up to twice the displacement at first crushing, and Fig. 6.6 includes two very large displacement half-cycles as well as the previously shown cycles all plotted to a smaller scale. In both cases the idealization closely follows the experimental characteristics. The idealization does not include a nominated failure deflection, so that actual ductility demands may be ascertained in each case. Instead, the values of displacement ductility factor required in the seismic analysis may be compared with the maximum available in this unit of 37 (at the failure deflection of 12.5 inches

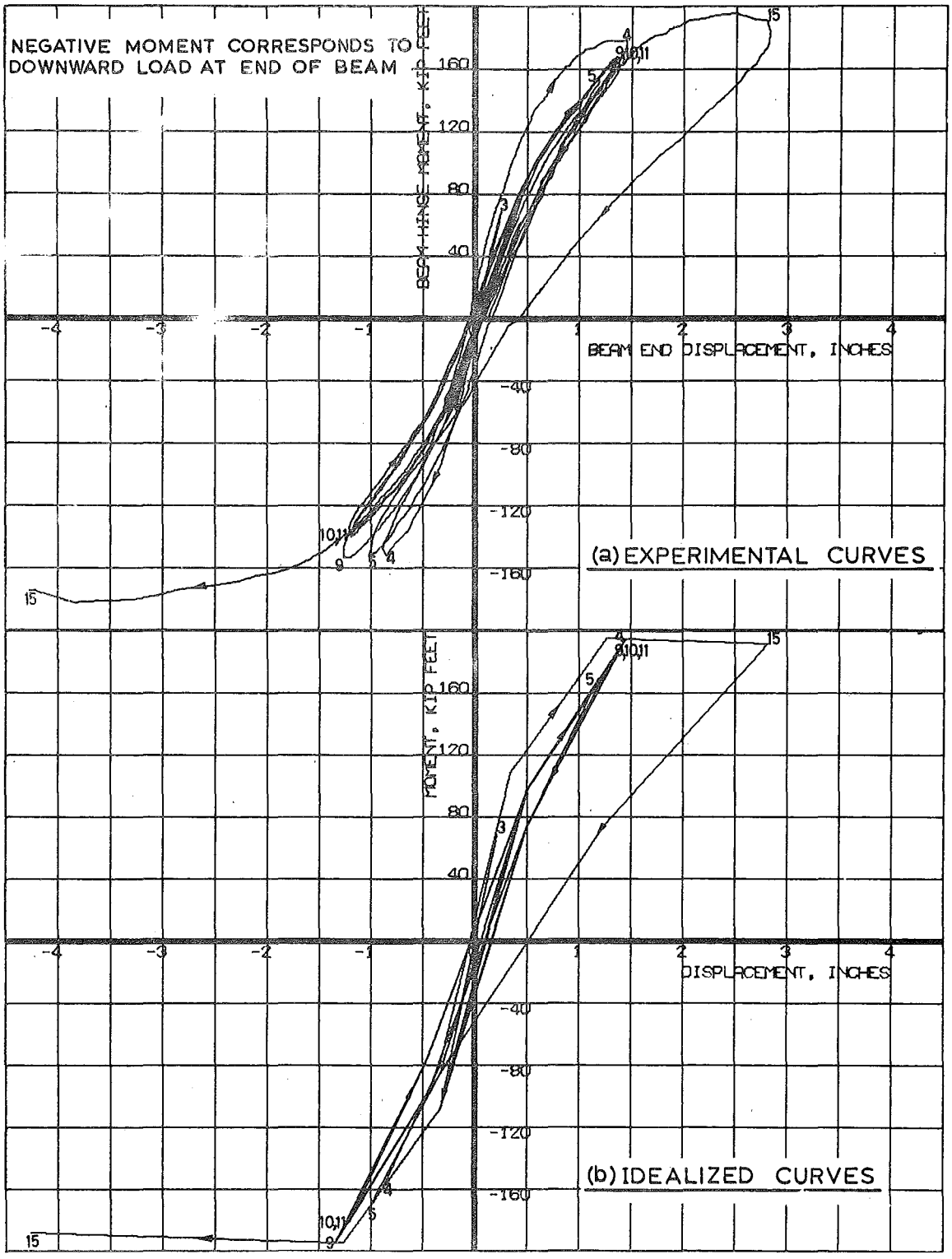

FIG. 6·5 : MOMENT-DISPLACEMENT CURVES FOR 15 CYCLES OF UNIT 2.

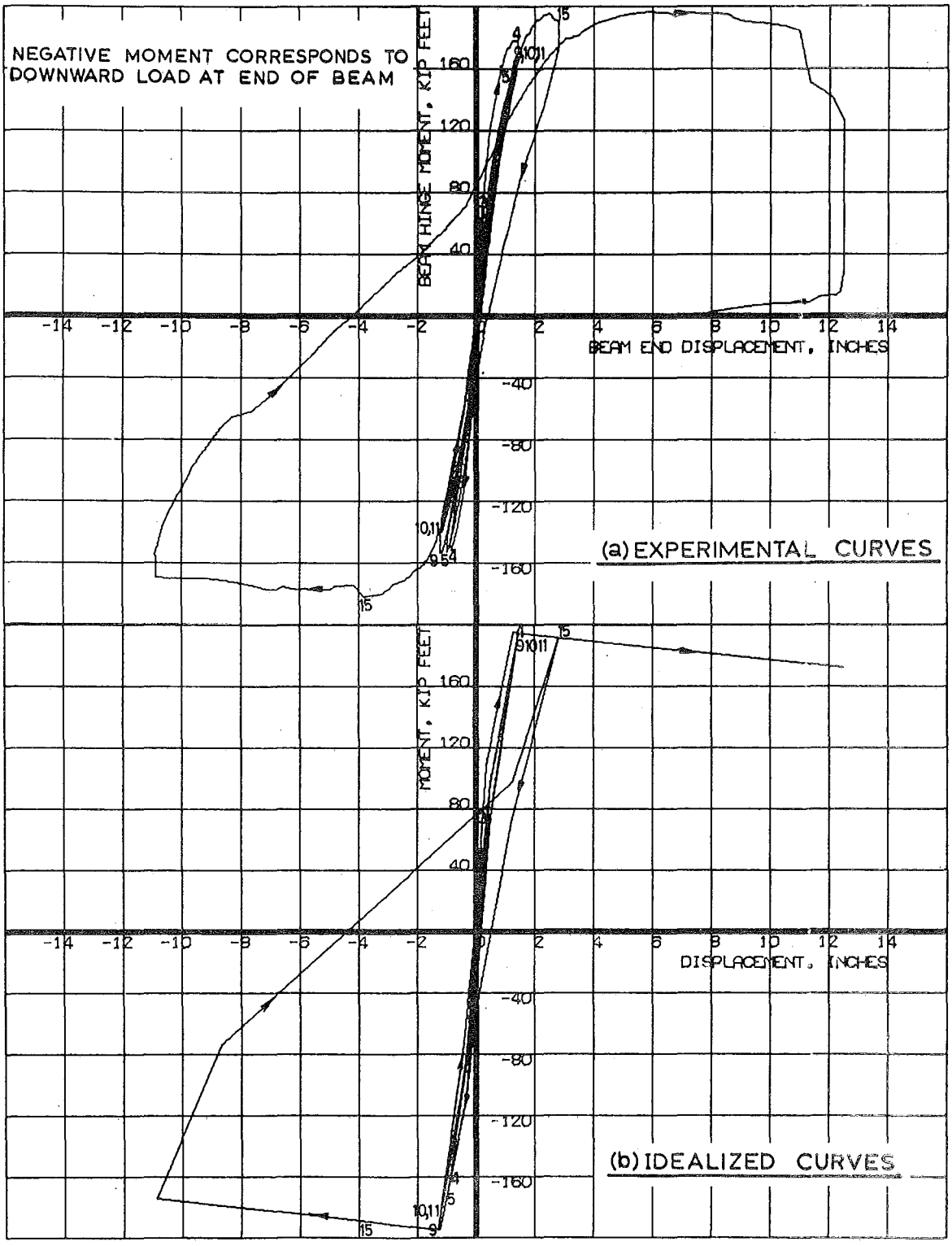

FIG. 6·6 : MOMENT-DISPLACEMENT CURVES FOR LARGE AMPLITUDE CYCLES OF UNIT 2.

on upward loading).

A comparison of the load-displacement curves of Unit 1 and the idealization may be made from Figs. 3.10 and 6.6(b), since the downward displacement limit is the same in each case. The idealization does not make special allowance for the phenomenon of bond failure of the ducts of the post-tensioning cables of the beam as they passed through the column, which caused gradual failure on final upward loading of Unit 1, as provisions to avoid this have already been suggested in Section 3.4.3.

The justification for use of the same basic model for both moment-curvature and load-displacement plots may be found in a comparison of Figs. 5.11(a) and 6.5(a). Clearly, there is a similarity of shape between the moment-curvature characteristics at the plastic hinge in the beam of Unit 2, and the load-displacement curves at the end of the beam. At the maximum positive displacement in half-cycle 15, the component of deflection at the end of the beam due to inelastic curvature over the hinge length was 75% of the total deflection, which explains the interrelationship of the two characteristics.

6.4 OPERATION OF COMPUTER PROGRAMS

Three computer programs were developed for this analysis, one for each of the three non-linear load-displacement idealizations. From a digitised earthquake record and specified system properties, the programs will compute acceleration, velocity, displacement, ratio of lateral force to weight, energy dissipation from viscous damping and energy dissipated by hysteresis. Provision is included for automatic plotting of displacement-time and load-displacement responses. Details of the analyses appear in the listings of Programs 6.1 to 6.3 in Appendix A.

6.4.1 Basic Cycle of Operations

The expressions for the basic cycle of operations for all programs may be derived from equation (6.5) and with use of the linear acceleration method of numerical integration as outlined by Biggs[83]. They are as follows:

$$Q = -(\Delta\ddot{x}_g) - \frac{4\pi}{T}\lambda\,(\ddot{x})\,\Delta t - \frac{k}{M}\left[(\dot{x})\,\Delta t + (\ddot{x})\,\frac{\Delta t^2}{2}\right]$$

$$P = 1 + \frac{2\pi}{T}\lambda\,\Delta t + \frac{k}{M}\,\frac{\Delta t^2}{6}$$

$$(\Delta\ddot{x}) = Q/P$$

$$(\Delta\dot{x}) = (\ddot{x})\,\Delta t + (\Delta\ddot{x})\frac{\Delta t}{2}$$

$$(\Delta x) = (\dot{x})\,\Delta t + (\ddot{x})\,\frac{\Delta t^2}{2} + (\Delta\ddot{x})\frac{\Delta t^2}{6}$$

$$x = x + \Delta x$$

$$\dot{x} = \dot{x} + \Delta\dot{x}$$

$$\ddot{x} = \ddot{x} + \Delta\ddot{x}$$

Calculate k for next increment

Read $\Delta\ddot{x}_g$

The difference between the programs lies in the determination of k from the current position on the appropriate load-displacement idealization.

6.4.2 Procedure for Change of Stiffness

The basic cycle of operations was interrupted at points of change of stiffness. The two general cases are; change of stiffness during an increment for displacements in a particular direction, and change of direction of displacement during an increment. The procedure for these situations is illustrated in Fig. 6.7 for the prestressed concrete

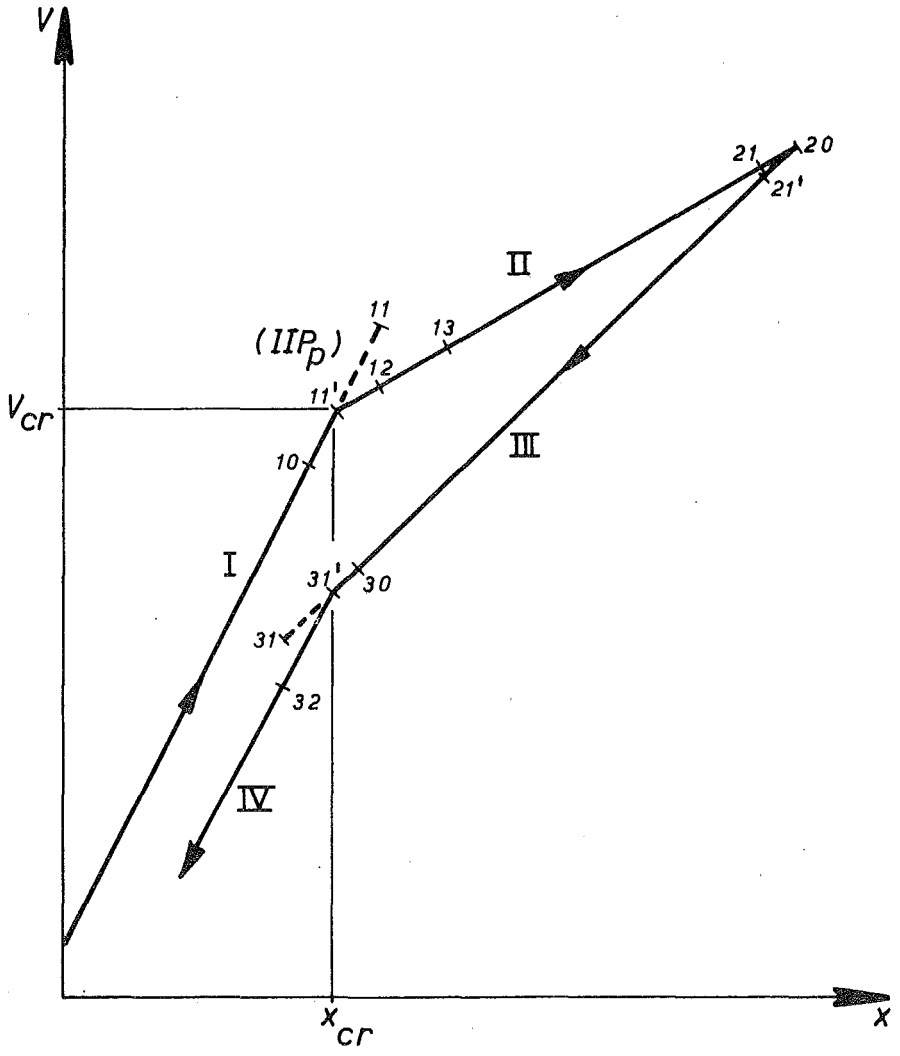

FIG. 6.7 : CHANGE OF STIFFNESS DURING CYCLE

system, considering four stiffness regimes.

The first case occurs when the member is being loaded with a stiffness k_I and the displacement of IIP_p is exceeded, for example during increment 11. A linear relationship is assumed between time interval and incremental displacement, and a new time interval is found by interpolation to give the required displacement at IIP_p. The equations of motion are recalculated for this new increment, 11'. The next increment, 12, is calculated with stiffness k_{II} and a time interval equal to the complement of the original and previous time intervals. Subsequent increments have the original time interval. An identical procedure is followed for change of stiffness between regimes III and IV. For all cases studied this procedure closely followed the required behaviour.

An example of the occurrence of the second case is shown in Fig. 6.7 for the increment 21, when the member has stiffness k_{II}. On computation of the computer cycle for this increment it is found that the displacement has decreased from that for the previous increment. It is assumed that the displacement at the previous increment, 20, represents the peak. The sequence of operations for increment 21 is now repeated using the original time increment as before, but changing the stiffness to k_{III} rather than k_{II}. Subsequent increments proceed with stiffness k_{III}. There will usually be a slight error in this approach if the peak displacement occurs during increment 21 and has a value greater than that at the end of increment 20. However, because of the small time intervals used this error is negligible.

6.4.3 Time Interval

The value of the time interval used was such that it could be represented as a binary number and hence be ascribed its exact value in hexadecimal arithmetic for machine calculations. The principal value used for the time interval was $\frac{1}{64}$ second. For a structure

with the minimum period considered of 0.3 seconds, a comparison was made of responses with $\frac{1}{64}$ second and $\frac{1}{128}$ second intervals. The two responses were found to be almost identical. Using an interval of $\frac{1}{64}$ second the time taken to compute 35 seconds of earthquake response was approximately 8 minutes on an IBM 360/44 computer. However for most analyses only the first 10 seconds of response history was obtained as this was ample to include the maximum displacement cycles.

6.5 SCHEDULE OF CASES STUDIED

In order to compare the behaviour of the three structural systems a wide range of periods and damping ratios was considered. Combinations of all the following properties were analysed:

Damping Ratio; λ = 2, 5, 10 per cent.

Period of Vibration; T = 0.3, 0.6, 0.9, 1.2, 1.5, 1.8, 2.1 and 2.7 secs.

Design Load Level; Zone A Non-Public Buildings[84].

Earthquake Record; El Centro 1940, North-South Component[86].

For each period and damping ratio the elastic response was also computed as a standard for comparison.

A further study was made of the effect of the level of the design lateral load on the seismic response for the prestressed concrete structural system.

The variables considered were:

Damping Ratio; λ = 2, 5, 10 per cent.

Period of Vibration; T = 0.3, 0.6, 0.9, 1.5, and 2.1 seconds.

Design Load Level; Zone A Public Buildings, Zone C Non-Public Buildings[84].

Earthquake Record; El Centro 1940, North-South Component[86].

6.6 RESULTS OF COMPARATIVE ANALYSES

The important structural details for these analyses are shown in Table 6.1. Also included are the ratios of maximum elastic response force to the ultimate lateral strength of the non-linear systems, and the maximum displacement ductility factors. These will be discussed in detail subsequently.

6.6.1 Comparison of Response Curves

The clearest means of comparison of the three non-linear systems considered is through their displacement-time responses. These represent the history of the displacement of the mass of the structure relative to the ground during the course of the earthquake. Figs. 6.8 to 6.10 present three examples of responses for different values of period of vibration, but each designed to the lateral load requirements of Zone A Non-Public Buildings and with a damping ratio of 2%.

(a) 2.1 Second Period

Fig. 6.8 illustrates the relative displacement responses for the elastic system and three non-linear systems with periods of 2.1 seconds. This is a relatively long period structure. For all non-linear systems post-elastic displacements occurred in many of the vibration cycles. The earthquake ground motion ceased at 30 seconds and thus the last 5 seconds of the response history represents the residual damped free vibration response.

It is apparent that both the prestressed concrete and elasto-plastic systems behave in a similar manner to harmonic oscillators, with typical vibratory response. However the degrading stiffness system loses its vibrating characteristics after the first few post-elastic cycles. The main effect of yielding on the elasto-plastic response appears to be to limit the amplitude of vibration. The vibration continues at approximately the elastic free vibration frequency. The load-displacement relationships for the prestressed concrete system,

Table 6.1

RESPONSE OF PRESTRESSED CONCRETE, DEGRADING STIFFNESS, AND ELASTO-PLASTIC SYSTEMS
(Zone A Non-Public Buildings, El Centro 1940 N-S Earthquake)

PERIOD seconds	$\beta = \frac{V_u}{W}$	MAX.ELASTIC RESPONSE FORCE / ULT.LATERAL STRENGTH (V_u)			x_{cr} ins	x_y ins	MAXIMUM DISPLACEMENT DUCTILITY FACTORS								
							PRESTRESSED CONCRETE			DEGRADING STIFFNESS			ELASTO-PLASTIC		
		λ=10%	λ=5%	λ=2%			λ=10%	λ=5%	λ=2%	λ=10%	λ=5%	λ=2%	λ=10%	λ=5%	λ=2%
0.3	0.168	3.55	4.35	4.76	0.084	0.151	16.43	27.5	38.3	7.58	8.58	11.24	4.57	8.21	9.42
0.6	0.151	3.65	4.96	6.07	0.300	0.540	8.36	11.33	14.63	4.09	4.28	5.76	3.41	4.41	5.26
0.9	0.118	2.94	4.68	6.90	0.526	0.947	5.64	6.69	7.34	3.81	4.37	6.09	3.77	4.64	5.33
1.2	0.084	2.36	3.12	4.15	0.671	1.21	4.60	5.07	5.65	4.04	4.89	5.28	3.55	3.89	4.01
1.5	0.084	1.98	2.43	2.81	1.05	1.89	3.84	5.42	7.90	2.16	2.35	2.48	2.18	2.42	2.62
1.8	0.084	1.47	1.64	2.20	1.51	2.72	5.45	6.63	7.42	2.13	2.53	2.70	2.09	2.31	2.57
2.1	0.084	1.77	2.19	2.99	2.05	3.70	4.06	5.24	6.77	2.09	2.32	2.53	2.34	2.84	2.93
2.7	0.084	2.01	2.61	3.10	3.40	6.11	3.28	4.36	4.94	1.57	1.84	2.05	1.57	1.84	2.05

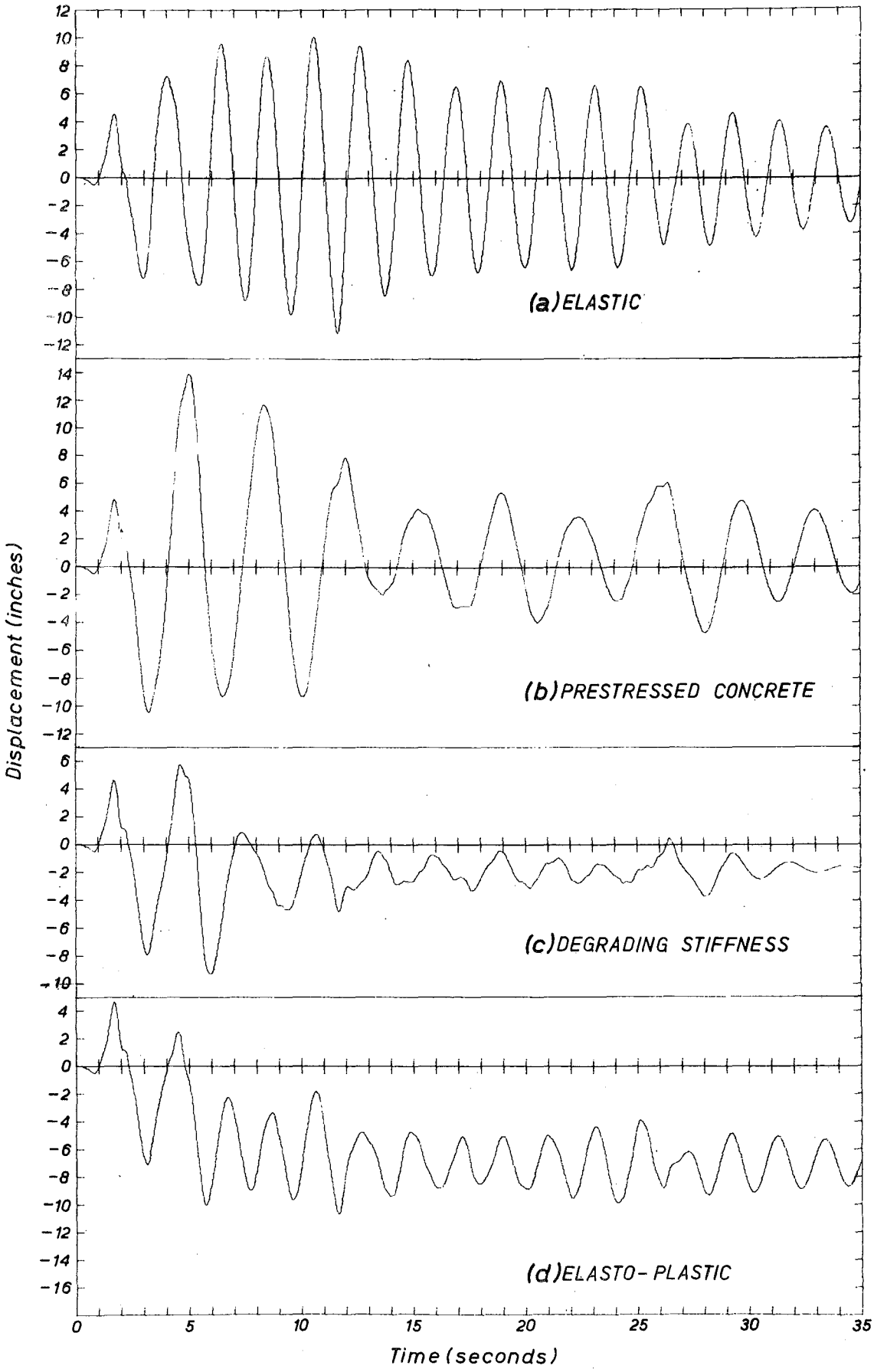

FIG. 6.8 : EARTHQUAKE DISPLACEMENT RESPONSES
(T = 2.1 seconds, λ = 2%, Zone A Non-Public Buildings)
El Centro 1940 N-S Earthquake

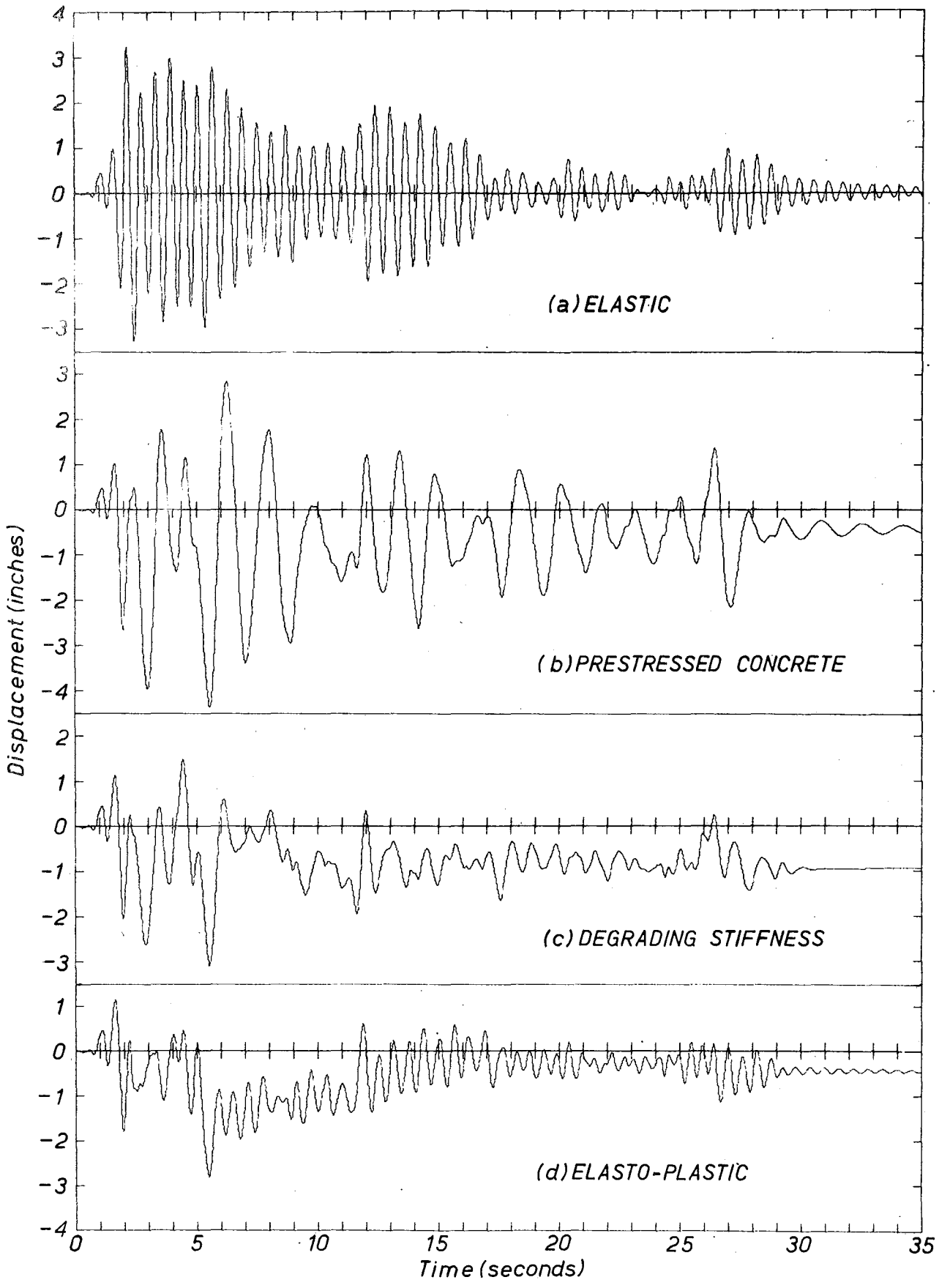

FIG.6.9 : EARTHQUAKE DISPLACEMENT RESPONSES
(T = 0.6 seconds, λ = 2%, Zone A Non-Public Buildings)
El Centro 1940 N-S Earthquake

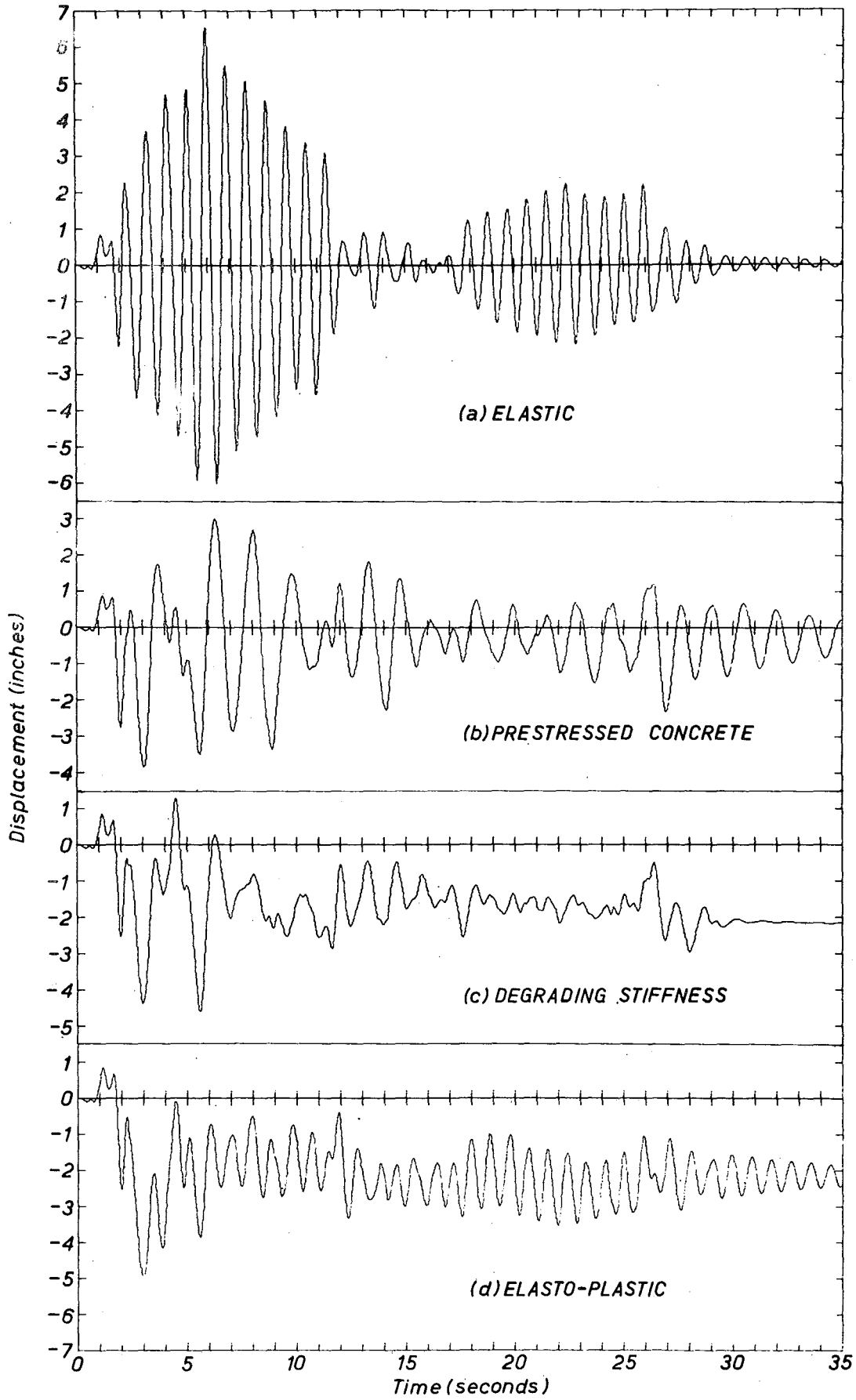

FIG. 6.10 : EARTHQUAKE DISPLACEMENT RESPONSES
(T = 0.9 seconds, λ = 2%, Zone A Non-Public Buildings)
El Centro 1940 N-S Earthquake

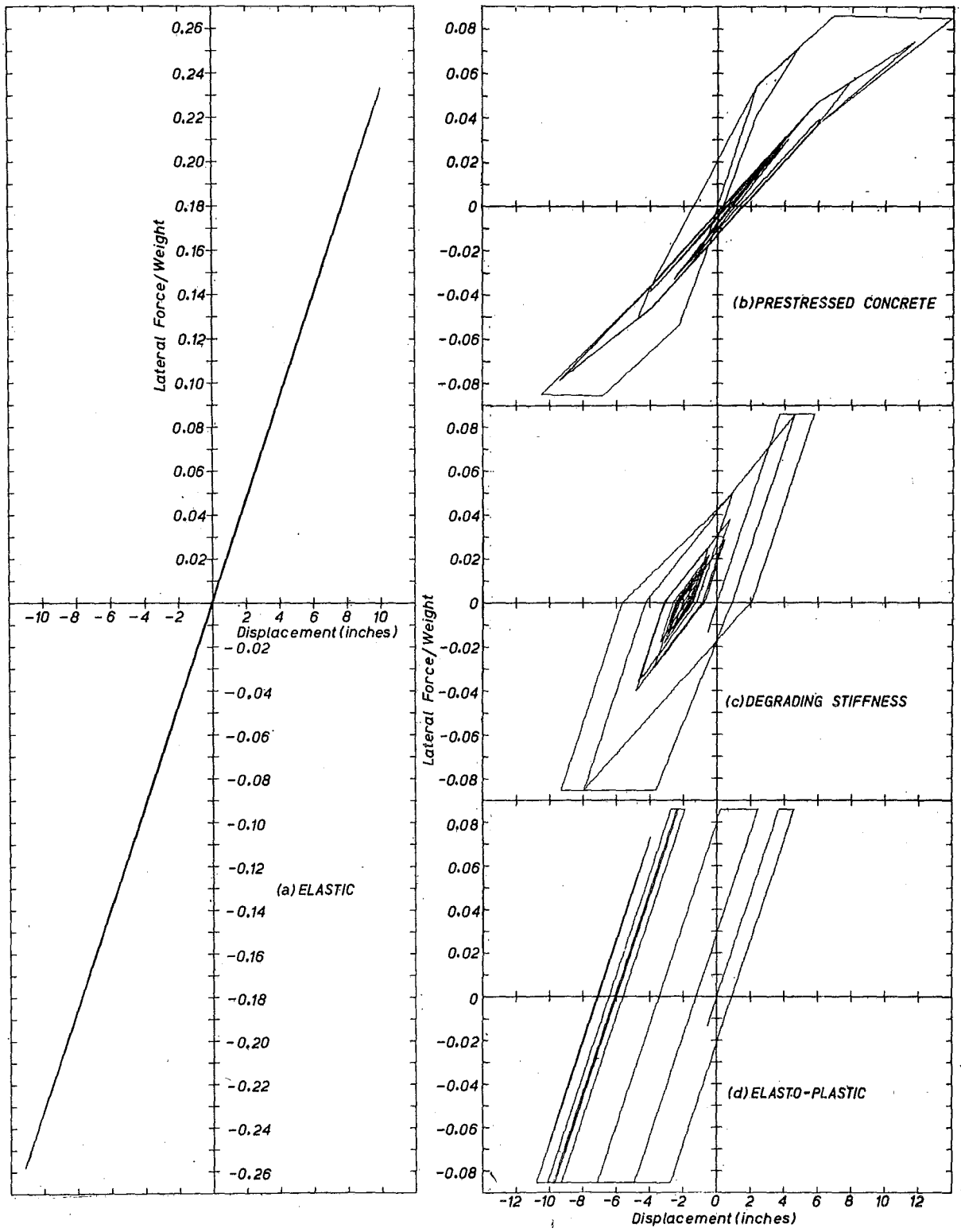

FIG. 6.11 : LOAD–DISPLACEMENT RELATIONSHIPS
(T = 2.1 seconds, λ = 2 %, Zone A Non-Public Buildings)
El Centro 1940 N-S Earthquake

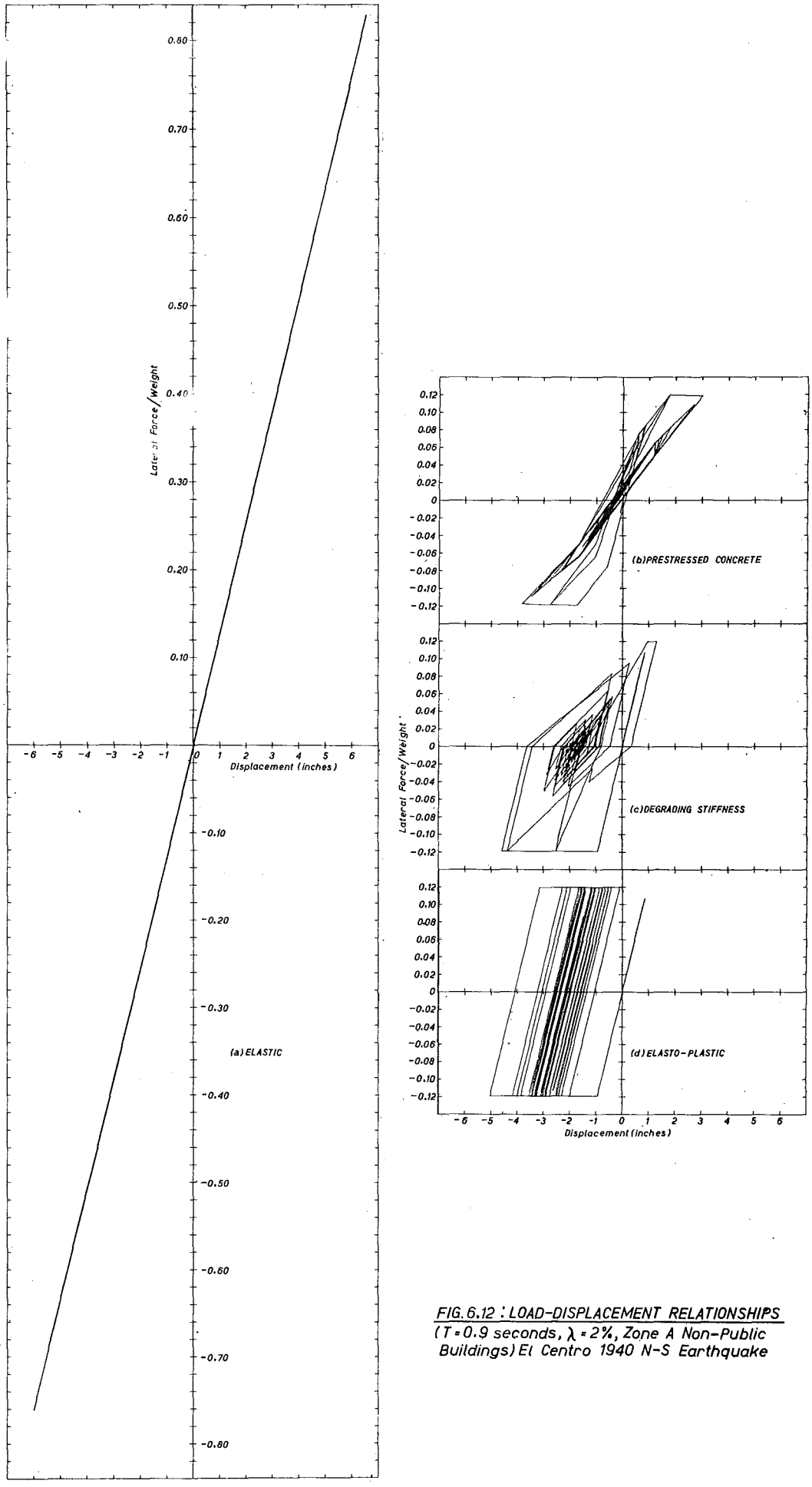

FIG. 6.12 : LOAD-DISPLACEMENT RELATIONSHIPS
(T = 0.9 seconds, λ = 2%, Zone A Non-Public Buildings) El Centro 1940 N-S Earthquake

however, result in an effective period of vibration $1\frac{1}{2}$ times that for elastic free vibrations. Greater maximum displacements are also apparent for this system. The load-displacement responses for the four systems are compared in Fig. 6.11.

(b) 0.6 Second Period

The next example is for a short period structure. Fig. 6.9 compares the displacement responses for the four systems with periods of 0.6 seconds. As previously the prestressed concrete system has a greater effective period of vibration and is subjected to greater amplitudes of vibration than the other two non-linear systems. In comparison with the longer period structures the maximum displacement ductility factors (as defined in Section 6.3) for each model are twice those for their 2.1 second period counterparts, indicating a greater excitation from the earthquake.

(c) 0.9 Second Period

This case is of particular interest as one would expect the period of a prestressed concrete portal frame to be in this vicinity. The relative displacement responses of the four systems with periods of 0.9 seconds are shown in Fig. 6.10. Similar response characteristics to the previous cases are apparent, except that for this period the maximum displacement of the prestressed concrete system is less than that for the elasto-plastic and degrading stiffness systems. This arises because of the characteristic tendency of single-degree-of-freedom structures represented by the latter two models to form a new axis of vibration away from the zero displacement line, after a large initial displacement. The prestressed concrete system is not so susceptible to this phenomenon because of the inherent greater elastic recovery. Thus differences arise in a comparison based on zero initial displacement. However this can be allowed for in a comparison of the response histories by determining a mean axis of vibration.

The load-displacement characteristics have also been presented for this case in Fig. 6.12 as these curves clearly show the reduction in response through inelastic deformations for the three non-linear systems.

6.6.2 Maximum Displacement Ductility Factors

For design considerations, the most important results from the analyses are the maximum displacements which the structures are subjected to during the course of the earthquake. These can be conveniently presented in terms of the maximum displacement ductility factor, μ. Table 6.1 details values of μ for the three non-linear systems for varying values of period and damping ratio, but all with lateral load design levels conforming to Zone A Non-Public Buildings. The results are shown graphically in Fig. 6.13. There is a general trend, for all systems, of decreasing ductility factor requirements with increasing period of vibration. This occurs even though the shorter period structures have higher ultimate strength levels in compliance with code design coefficients. It is apparent from Table 6.1 that for longer period structures the lateral strength derived from code requirements is higher relative to the maximum elastic response force than for short period structures. This is a contributory factor to the above trend. Damping ratio is also seen to have a significant effect on results. The maximum available displacement ductility factor of 37 for Unit 2 is only exceeded in the case of a prestressed concrete structure with a period of 0.3 seconds and a damping ratio of 2%.

In making any comparison between the ductility factor requirements of the three systems for a given period, it must be recognised that the definition of this term depends on the displacement at cracking for the prestressed concrete system, whereas that for the elasto-plastic and degrading stiffness systems depends on the higher value of displacement at first yield.

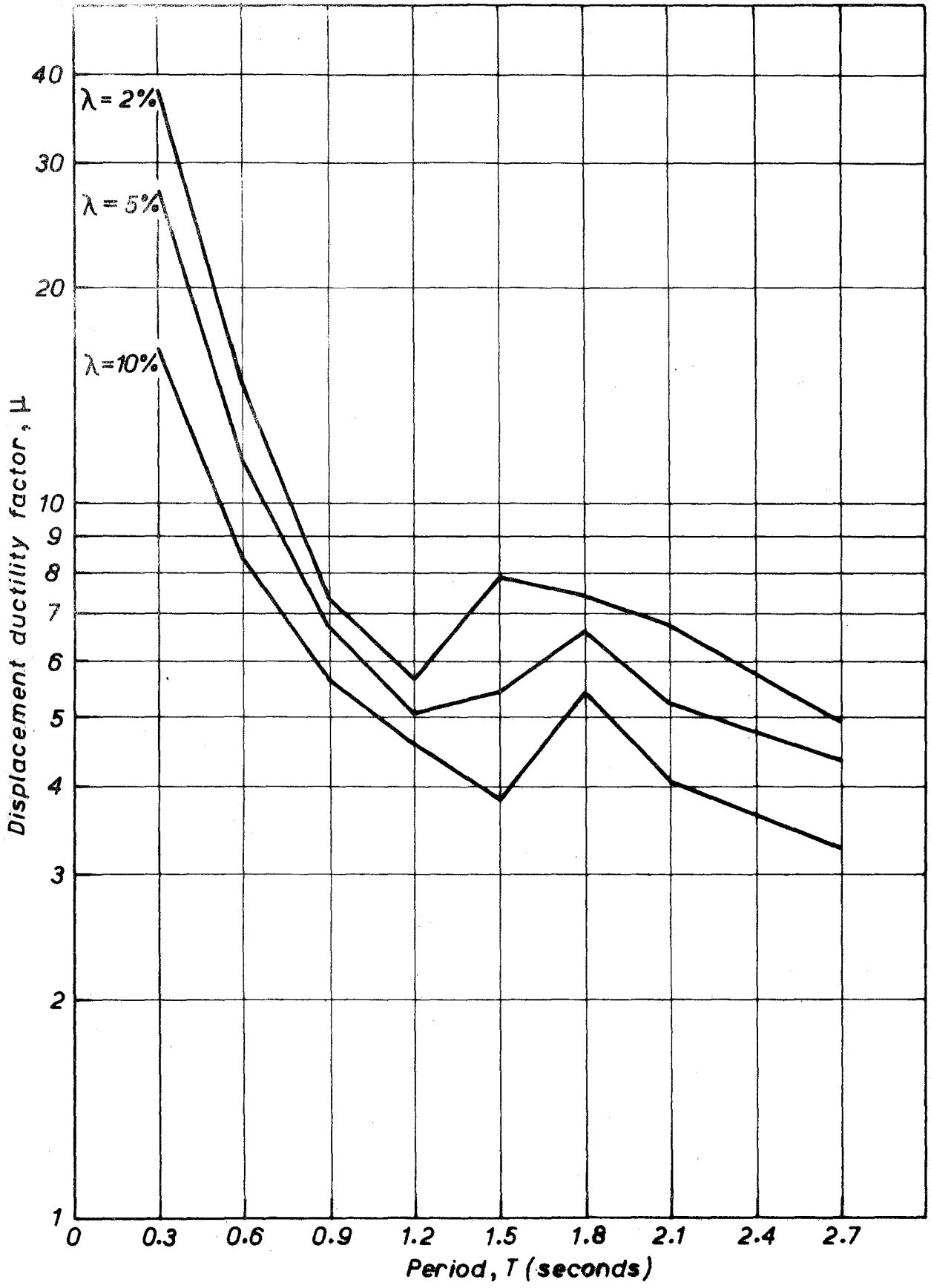

(a) Prestressed Concrete System

FIG. 6.13 : MAXIMUM DISPLACEMENT DUCTILITY FACTORS

(Zone A Non-Public Buildings, El Centro 1940 N-S Earthquake)

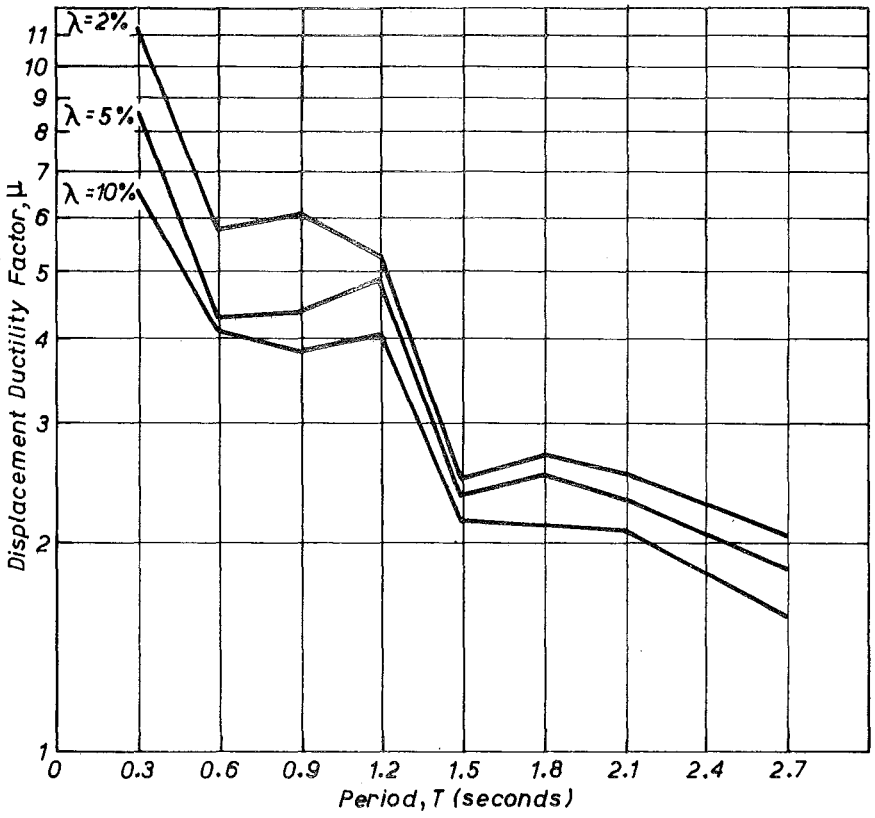

(b) Degrading Stiffness System

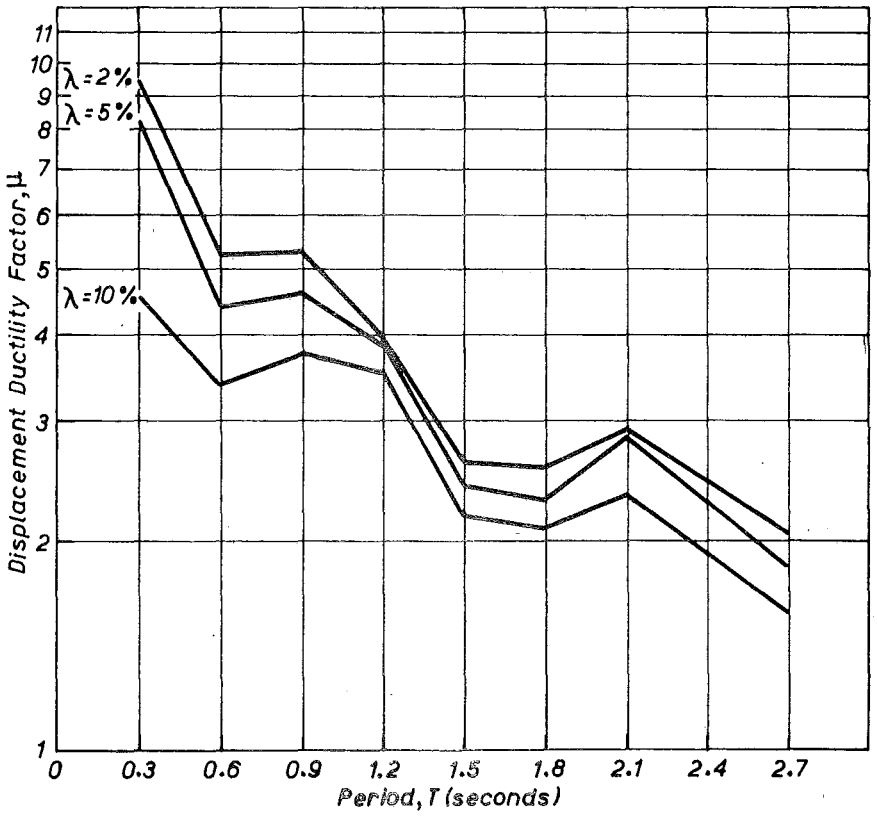

(c) Elasto-Plastic System

FIG. 6.13 : MAXIMUM DISPLACEMENT DUCTILITY FACTORS
(Zone A Non-Public Buildings, El Centro 1940 N-S Earthquake)

6.6.3 Relative Maximum Displacements

A general comparison of the maximum seismic responses of the four systems can be made by tabulating the ratios of maximum displacements of the elastic, prestressed concrete, and degrading stiffness systems to those of the elasto-plastic system with the same period and damping ratio, as in Table 6.2. It will be noted that there is a large variation in the ratios over the range of periods considered. This is in part due to the particular characteristics of the earthquake record chosen. The comparison for a period of 0.3 seconds is perhaps of academic interest only as this represents a very short period for a portal frame structure. A contributing factor to the high ratio for prestressed concrete at this period is the loss of strength with increased loading after crushing ("falling" branch behaviour) of the prestressed concrete system. It has been shown[79] that the response of very short period structures is very sensitive to this behaviour. The displacement ratios of less than unity for the prestressed concrete systems of periods 0.9 and 1.2 seconds are attributable to the displacement of the centre of vibration for the elasto-plastic response history. Even allowing for this effect the maximum displacement ratios for these periods are 1.3 or less.

For all analyses shown in Table 6.2, if displacements are measured from the mean axis of vibration rather than initial zero displacement the displacement ratios are between 1.2 and 1.9. However, no consistent trend exists relating these displacement ratios with period. They are a minimum between 0.9 and 1.2 seconds and a maximum near both ends of the range of periods studied.

The basis of comparison of prestressed and reinforced concrete structures may be questioned, that is, to compare such structures with the same period and damping ratio. In practice a prestressed concrete building is likely to have smaller member sizes than a comparable

Table 6.2

RATIO OF MAXIMUM DISPLACEMENT OF SYSTEM TO MAXIMUM DISPLACEMENT OF ELASTO-PLASTIC SYSTEM WITH SAME PERIOD AND DAMPING RATIO
(Zone A Non-Public Buildings, El Centro 1940 N-S Earthquake)

PERIOD	ELASTIC			PRESTRESSED CONCRETE			DEGRADING STIFFNESS		
seconds	λ=10%	λ=5%	λ=2%	λ=10%	λ=5%	λ=2%	λ=10%	λ=5%	λ=2%
0.3	0.78	0.53	0.51	2.31	2.16	2.62	1.66	1.04	1.19
0.6	1.07	1.13	1.16	1.36	1.43	1.54	1.20	0.97	1.09
0.9	0.78	1.01	1.30	0.83	0.84	0.76	1.01	0.94	0.87
1.2	0.66	0.80	1.04	0.72	0.73	0.78	1.14	1.25	1.32
1.5	0.91	1.01	1.07	0.98	1.25	1.67	0.99	0.97	0.95
1.8	0.71	0.71	0.86	1.50	1.59	1.60	1.02	1.09	1.05
2.1	0.76	0.77	1.03	0.96	1.02	1.28	0.89	0.82	0.92
2.7	1.29	1.42	1.52	1.16	1.32	1.32	1.00	1.00	1.00

Table 6.3

RATIO OF HYSTERETIC ENERGY DISSIPATION BY SYSTEM TO HYSTERETIC ENERGY DISSIPATION OF ELASTO-PLASTIC SYSTEM WITH SAME PERIOD AND DAMPING RATIO
(Zone A Non-Public Buildings, El Centro 1940 N-S Earthquake)

PERIOD	PRESTRESSED CONCRETE			DEGRADING STIFFNESS		
seconds	λ=10%	λ=5%	λ=2%	λ=10%	λ=5%	λ=2%
0.3	0.59	0.64	0.72	1.59	1.50	1.49
0.6	0.37	0.54	0.68	1.05	1.04	0.96
0.9	0.29	0.35	0.36	1.05	0.89	0.82
1.2	0.32	0.39	0.38	1.04	1.05	1.05
1.5	0.44	0.64	0.84	1.22	1.21	1.12
1.8	0.67	0.77	0.85	1.19	1.12	1.06
2.1	0.56	0.71	0.68	1.28	1.14	1.16
2.7	0.44	0.50	0.56	0.91	0.98	1.00

reinforced concrete building, and therefore to be more flexible. Furthermore, as discussed in Section 6.1 a lower damping ratio is generally assumed for prestressed concrete. Because of the uncertainty of these differences of period and damping ratio, a comparison was not attempted on that basis. However their effects may cancel each other. The trend shown in Table 6.1 and Fig. 6.13 of decreasing displacement ductility factor with increasing period represents an advantage to prestressed concrete in these comparisons, which may well be sufficient to compensate for the lower damping ratio. For example, Table 6.2 shows a displacement ratio of 1.54 for prestressed concrete and elasto-plastic systems with periods of 0.6 seconds and damping ratios of 2%. If instead the elasto-plastic system is considered to have a damping ratio of 5% with the same period of 0.6 seconds, the equivalent displacement ratio is obtained from a prestressed concrete system with a damping ratio of 2% and a period of 0.68 seconds. That is, more than doubling the damping ratio for the elasto-plastic system is compensated for if the prestressed concrete system has a 13% greater period. Other similar comparisons could be made from Fig. 6.13.

6.6.4 Energy Considerations

The energy dissipation capacity of a vibrating structure has a major influence on the ensuing earthquake response. The sources of energy dissipation can be classified as either that represented by viscous damping, or that arising from hysteresis under cyclic load in the structural members. The relative amounts of hysteretic energy dissipated by the three non-linear systems is presented in Table 6.3. Results are presented for the first 10 seconds of earthquake response, but from checks of some cases the ratios were found to be representative for the full response history. As one would expect from the intrinsic shape of the hysteresis loops for prestressed concrete, the hysteretic energy dissipation is lower than that for the elasto-plastic system.

The difference is made less severe by the fact that the vibration cycles of the prestressed concrete system have greater amplitudes than those for the corresponding elasto-plastic system, and therefore have more opportunity for energy dissipation. This is also true of the degrading stiffness system and explains their hysteretic energy ratios greater than unity.

Although the hysteretic energy dissipation of a prestressed concrete system is lower than that of the elasto-plastic system with the same period and damping ratio, the energy dissipated by viscous damping in the prestressed concrete response is generally between 1.5 and 2.0 times that of its elasto-plastic counterpart with the same damping ratio. The reason for this is that the greater vibration amplitudes for the prestressed concrete system increased the energy dissipation from the velocity dependent viscous damping.

6.6.5 Discussion of Comparative Analyses

The higher displacements obtained for the prestressed concrete system in the comparative analyses with reinforced concrete systems may be attributed to:

(1) the influence of the effective period of vibration after post-elastic cycles (post-cracking cycles for prestressed concrete), and

(2) the lower inherent energy dissipation capacity of prestressed concrete.

The first factor bears further discussion. It was apparent from the response histories presented in Section 6.6.1 that although the systems may have the same initial frequency, after the occurrence of cracking or yielding the prestressed concrete system is more flexible than its elasto-plastic counterpart. The difference is due to the respective shapes of the load-displacement characteristics. The increase of

period for prestressed concrete can have two effects: (a) it will diminish the response activity expected from response spectra considerations, and (b) the greater flexibility will lead to increased amplitudes of displacement. The displacement for each period depends on the combination of these mutually opposing effects. A study was made of the effect of varying the slope, k_1 , of the upper branch of the load-displacement model (and consequently varying the resulting period) for prestressed concrete. The results showed that effect (b) is dominant for periods greater than 0.9 seconds, and effect (a) dominates the response for periods less than 0.9 seconds. This would have been expected from the much lower slope of the response spectrum for this earthquake subsequent to a period of 0.9 seconds.

The displacement ratios obtained (from 1.2 to 1.9) may be related to a similar comparison made in a mathematical study by Rosenbleuth[17]. His expression was based on a rather approximate bilinear elastic load-displacement function with zero slope for the upper branch. For the range of ductility factors for which the above ratios were determined in this study, Rosenbleuth's expression gives displacement ratios between 1.1 and 1.5.

6.7 EFFECT OF DESIGN LOAD LEVEL ON RESPONSE FOR PRESTRESSED CONCRETE SYSTEM

The choice of appropriate seismic design coefficients, or debate on the adoption of higher load factors for prestressed concrete, require a knowledge of the influence of design lateral load level on response. A study was made of the maximum displacements for prestressed concrete systems designed to the seismic coefficients of Zone A Public Buildings, and Zone C Non-Public Buildings[84]. The results are presented in Table 6.4(a). The large difference between displacement ductility factor requirements for the two design cases indicates the significance of this variable. Disregarding the very short period structures, the displacement

Table 6.4

PRESTRESSED CONCRETE SYSTEM ANALYSIS
(El Centro 1940 N-S Earthquake)

(a) Maximum Displacement Ductility Factors

PERIOD secs	ZONE A PUBLIC BUILDINGS					ZONE C NON-PUBLIC BUILDINGS				
	$\beta = \frac{V_u}{W}$	x_{cr} ins	μ			$\beta = \frac{V_u}{W}$	x_{cr} ins	μ		
			λ=10%	λ=5%	λ=2%			λ=10%	λ=5%	λ=2%
0.3	0.224	0.114	12.00	15.25	27.7	0.112	0.057	28.6	66.7	91.4
0.6	0.201	0.400	5.35	7.94	9.85	0.100	0.200	13.10	24.4	31.2
0.9	0.157	0.701	3.64	4.77	5.54	0.078	0.351	11.23	11.80	13.84
1.5	0.112	1.397	2.61	2.72	2.96	0.056	0.699	8.60	12.58	15.83
2.1	0.112	2.738	3.30	4.30	4.84	0.056	1.370	6.72	8.02	9.54

(b) Ratio of Hysteretic Energy Dissipation to Total Energy Dissipation (i.e. Hysteretic + Viscous Damping)

(Total Energy Dissipation in Parentheses - lb.ins/lb_{weight})

PERIOD secs	ZONE A PUBLIC BUILDINGS			ZONE C NON-PUBLIC BUILDINGS		
	λ=10%	λ=5%	λ=2%	λ=10%	λ=5%	λ=2%
0.3	0.17 (1.830	0.31 (2.112)	0.43 (2.023)	0.14 (1.691)	0.26 (1.532)	0.44 (1.206)
0.6	0.21 (2.184)	0.35 (1.945)	0.60 (1.791)	0.23 (1.503)	0.40 (1.297)	0.51 (1.133)
0.9	0.19 (1.448)	0.37 (1.313)	0.60 (1.175)	0.23 (1.117)	0.39 (0.907)	0.63 (0.635)
1.5	0.26 (0.970)	0.40 (0.774)	0.58 (0.568)	0.27 (1.346)	0.45 (1.289)	0.67 (1.082)
2.1	0.24 (1.670)	0.42 (1.834)	0.65 (1.565)	0.29 (1.496)	0.45 (1.251)	0.67 (0.964)

ductility factor requirements for Zone A structures appear reasonable, while those for Zone C appear dangerously high for the El Centro 1940 N-S earthquake.

The ratios of hysteretic to total (that is, hysteretic plus viscous damping) energy dissipation for the study are shown in Table 6.4(b). It is apparent that this ratio is largely independent of design level and period even though the total energy dissipated, as shown in parentheses, does vary between these cases.

6.8 DETERMINATION OF SECTION CURVATURE REQUIREMENTS

In order to make the displacement ductility factor results for the prestressed concrete systems of Table 6.4(a) meaningful, it is necessary to have an indication of what they represent in terms of section curvature requirements in the members of the frame. To make such a comparison an approach was used essentially the same as that of Park[47] in a study of reinforced concrete frames. Although a portal frame cannot strictly be represented by the single-degree-of-freedom model used, such a representation will give a good indication of the likely response. The portal frame considered is shown in Fig. 6.14 under both gravity and seismic loading. The analysis is necessarily approximate in that the simplifying assumption is made that plastic hinges form at all the critical sections at the same load and at sufficient sections to form a mechanism. The assumed shape of the moment-curvature relationship for the prestressed concrete sections is shown in Fig. 6.15. The maximum available lateral deflection depends on which of the two possible mechanisms form. These will now be discussed.

6.8.1 Elastic Conditions

The curvature in the columns at incipient cracking in the frame is shown in Fig. 6.16. Since the moments are still in the initial linear

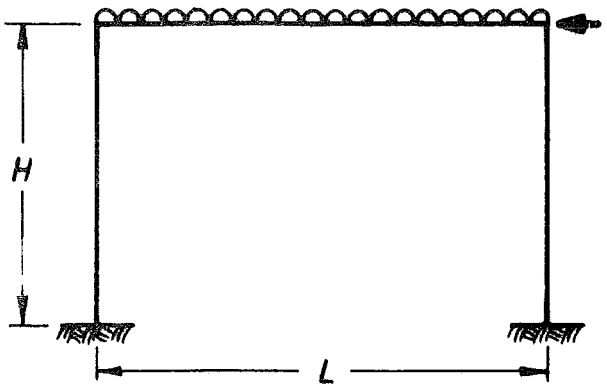

FIG. 6.14 : PORTAL FRAME UNDER GRAVITY & SEISMIC LOADING

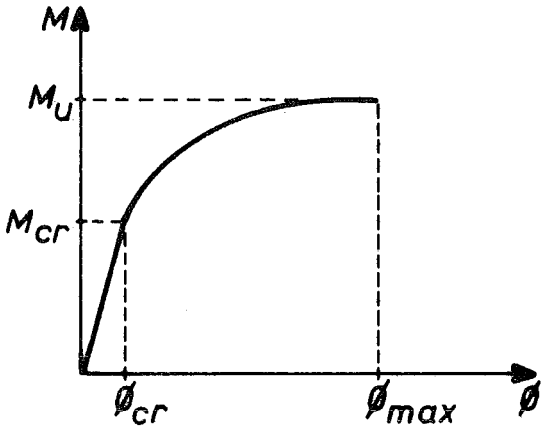

FIG. 6.15 : ASSUMED SECTION MOMENT-CURVATURE RELATIONSHIP

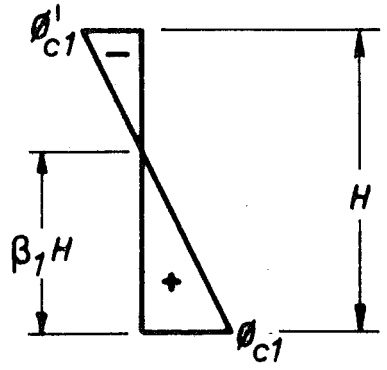

FIG. 6.16 : CURVATURE DISTRIBUTION IN COLUMNS AT FIRST CRACKING IN FRAME

section of the moment-curvature curves this curvature distribution follows the shape of the bending moment diagram. From application of the moment area method, the lateral deflection at the top of the frame relative to the ground, at first cracking, may be calculated. Assuming that β_1 , which represents the position of the point of contraflexure, has a value of 0.6 the deflection is:

$$\Delta_{cr} = 0.222\ \varphi_{c1} H^2 \qquad \ldots (6.13)$$

where φ_{c1} is the curvature at the bottom of the column at first cracking in the frame.

6.8.2 Column Sidesway Mechanism

For the case of a frame in which the columns are rather more flexible than the beams, the critical column sections may reach a moment of M_u before significant post-elastic curvature has occurred in the beam sections. Thus a column sidesway mechanism is formed as shown in Fig. 6.17. In such a case cracking will occur first in the frame at the critical sections in the columns and φ_{c1} will be equal to the curvature at first cracking of the column, φ_{crc}. If it is assumed that when the maximum allowable curvatures are reached at both plastic hinges in the column the point of contraflexure will be at the mid-height of the column, the resulting curvature distribution at this stage will be as shown in Fig. 6.18. The inelastic rotation available at the column hinges, θ_{pc} , is either $(\varphi'_{maxc} - \varphi'_{ec})\ L'_{pc}$ or $(\varphi_{maxc} - \varphi_{ec})\ L_{pc}$, whichever is least.

where φ_{maxc} is the maximum available curvature in the member, φ_{ec} is the maximum elastic curvature assuming an uncracked section, and L_{pc} is the plastic hinge length in the column.

The lateral deflection at the top of the frame when the maximum allowable curvature is reached in the columns for this mechanism is:

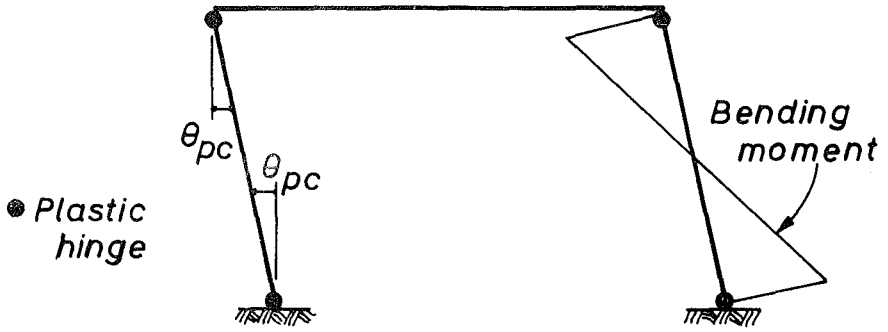

FIG. 6.17 : COLUMN SIDESWAY MECHANISM

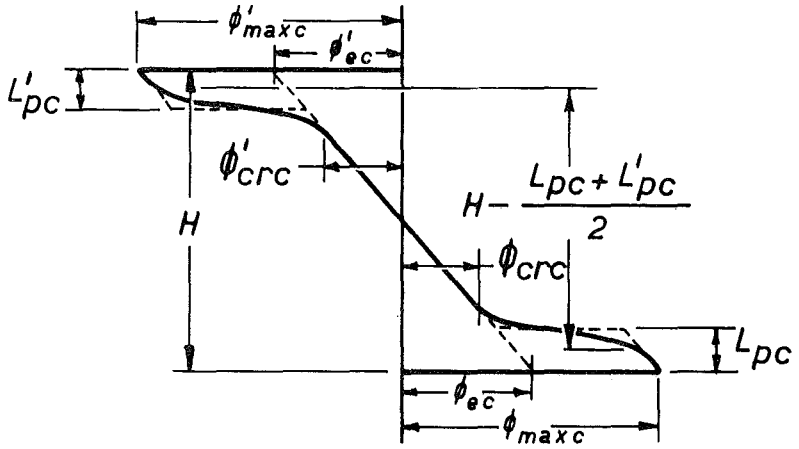

FIG. 6.18 : CURVATURE DISTRIBUTION IN COLUMN

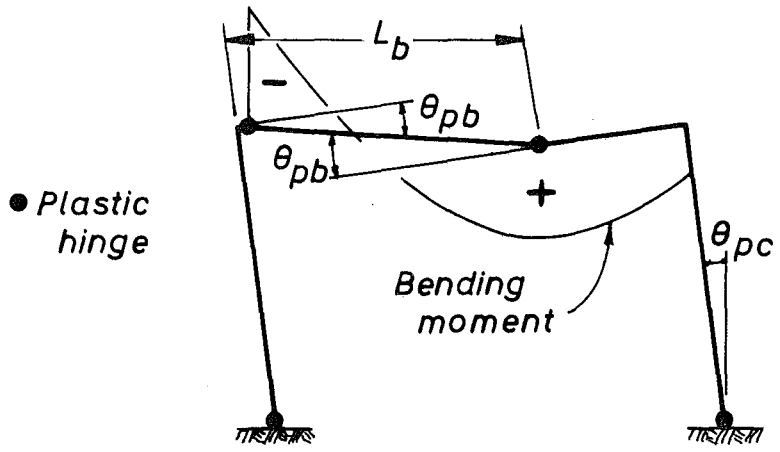

FIG. 6.19 : BEAM SIDESWAY MECHANISM

$$\Delta_{max} = \Delta_e + \theta_{pc} \{H - 0.5 (L_{pc} + L'_{pc})\} \quad \ldots (6.14)$$

where Δ_e is the deflection corresponding to the elastic area of the curvature distribution profile at maximum deflection.

From moment area:

$$\Delta_e = 0.180 \varphi_{ec} H^2 \quad \ldots (6.15)$$

The maximum displacement ductility factor is given by:

$$\mu = \frac{\Delta_{max}}{\Delta_{cr}} \quad \ldots (6.16)$$

From equation (6.14):

$$\mu = \frac{\Delta_e}{\Delta_{cr}} + \frac{\theta_{pc}}{\Delta_{cr}} \{H - 0.5 (L_{pc} + L'_{pc})\} \quad \ldots (6.17)$$

where Δ_{cr} is given by equation (6.13), and Δ_e is given by equation (6.15).

To determine the likely section curvature requirements for a portal frame, values of $\varphi_{maxc}/\varphi_{crc}$ were calculated for the range of displacement ductility factors from Table 6.4(a) for buildings designed as Zone A Public Buildings, and with a conservatively low damping ratio of 2%. For the solution of equation (6.17) the following values were assumed: $L_{pc} = L'_{pc} = 0.6D$, $\beta_1 = 0.6$, $\varphi_{ec}/\varphi_{crc} = 1.5$, and H = 10D (and 16D). The results are presented in Table 6.5 for values of μ of 4, 6, 8, and 10.

6.8.3 Beam Sidesway Mechanism

A second possible case is that of a beam sidesway mechanism, as shown in Fig. 6.19. This occurs when moments at the critical sections of the beam reach ultimate and the mechanism is completed by the formation of plastic hinges at the bases of the columns. From the geometry of the deformations and following the procedure used by Park[47], the displacement ductility factor for the frame at the maximum allowable section curvatures may be written in terms of the rotation of the beam

Table 6.5

SECTION CURVATURE RATIOS

DISPLACEMENT DUCTILITY FACTOR μ	COLUMN SIDESWAY MECHANISM		BEAM SIDESWAY MECHANISM			
	COLUMN CURVATURE RATIO $\varphi_{maxc}/\varphi_{crc}$		BEAM CURVATURE RATIO $\varphi_{maxb}/\varphi_{crb}$		COLUMN CURVATURE RATIO $\varphi_{maxc}/\varphi_{crc}$	
	H = 10D	H = 16D	H = 8D	H = 14D	H = 8D	H = 14D
4	12.5	18.5	13.0	21.4	9.2	14.7
6	20.3	30.8	22.2	37.2	15.4	25.3
8	28.2	43.0	31.5	53.1	21.5	35.9
10	36.1	55.3	40.7	69.0	27.7	46.5

hinges (and from equation (6.16)) as:

$$\mu = \frac{\Delta_e}{\Delta_{cr}} + \frac{(H - \frac{L_{pc}}{2})\, L_b}{L} \frac{\theta_{pb}}{\Delta_{cr}} \qquad \ldots (6.18)$$

where θ_{pb} is either $(\varphi'_{maxb} - \varphi'_{eb})\, L'_{pb}$ or $(\varphi_{maxb} - \varphi_{eb})\, L_{pb}$, whichever is least, Δ_{cr} is given by equation (6.13), and Δ_e takes the following value:

$$\Delta_e = 0.222\, \varphi_{ec} H^2 \qquad \ldots (6.19)$$

assuming that β_1 remains equal to 0.6, since a plastic hinge has formed in the column only at the base.

The section curvature requirements for varying values of ductility factor are presented for this mechanism also in Table 6.5. The values of $\varphi_{maxb}/\varphi_{crb}$ are determined for the following assumptions: $L_b = \frac{2}{3}L$, $L_{pb} = L_{pc} = 0.6D$, $\beta_1 = 0.6$, $\varphi_{ec}/\varphi_{crc} = 1.5$, $\varphi_{eb}/\varphi_{crb} = 1.5$, $\varphi_{c1} = \varphi_{crb}$, and $H = 8D$ (and $14D$). The requirement for $\varphi'_{maxb}/\varphi'_{crb}$ at the positive moment hinge will not be so severe as that for $\varphi_{maxb}/\varphi_{crb}$, because there is a greater plastic hinge length available at the positive moment hinge.

In addition, the ductility factor in terms of the hinges at the base of each column is:

$$\mu = \frac{\Delta_e}{\Delta_{cr}} + (H - \frac{L_{pc}}{2}) \frac{\theta_{pc}}{\Delta_{cr}} \qquad \ldots (6.20)$$

where $\theta_{pc} = (\varphi_{maxc} - \varphi_{ec})\, L_{pc}$, Δ_{cr} is given by equation (6.13), and Δ_e is given by equation (6.19).

Values of $\varphi_{maxc}/\varphi_{crc}$ are tabulated for the following assumptions: $L_{pc} = 0.6D$, $\beta_1 = 0.6$, $\varphi_{crc} = \varphi_{c1}$, $\varphi_{ec}/\varphi_{crc} = 1.5$, $H = 8D$ (and $14D$).

6.8.4 Discussion of Section Curvature Requirements

The results of Table 6.5 may be compared with the curves relating curvature ratio at crushing against steel area ratio for beams and columns as shown in Figs. 4.17 and 4.18. For example a frame of period 0.9 seconds and damping ratio 2%, designed as a Zone A Public Building with the same load factor as for reinforced concrete[85], will have a displacement ductility factor of 6 from Table 6.4(a). Considering the column sidesway mechanism and assuming properties for the column of $pf'_s/f'_c = 0.25$ and $P/f'_cbD = 0.05$, crushing would not be expected if $H = 10D$ but would occur if $H = 16D$. For the same column and a beam with $pf'_s/f'_c = 0.3$ the beam sidesway mechanism would cause crushing in the members only for the greater height frame considered. Since the larger of the two heights considered is more likely for a portal frame of this period, crushing would be expected in the members of such a structure under an earthquake of the intensity of El Centro 1940 N-S.

Although crushing would be expected in the members of a frame for approximately half of the curvature ratio requirements in Table 6.5, a catastrophic member failure would not occur even for the largest values recorded. This is evident from the large ductilities shown for properly designed beams and columns in Chapter 4.

6.9 COMPUTER PROGRAMS

Listings of the three principal computer programs used for this chapter appear in Appendix A.

Program 6.1 ("EQANEP"): Seismic analysis of a single-degree-of-freedom system with elasto-plastic load-displacement characteristics. Any digitised earthquake acceleration record may be used. Analysis is performed by step-by-step numerical integration assuming the acceleration of the system to vary linearly during each time increment.

Program 6.2 ("EQANDS"): As for Program 6.1 but using a degrading stiffness load-displacement characteristic.

Program 6.3 ("EQANPSM"): As for Program 6.1 but using a model representing the load-displacement characteristics of prestressed concrete.

6.10 CONCLUSIONS

It has been shown in the first part of this study that prestressed concrete structures (represented by a postulated load-displacement model) have significantly different earthquake response characteristics from reinforced concrete structures (represented by elasto-plastic and degrading stiffness systems). For single-degree-of-freedom models with periods greater than half a second, a prestressed concrete system undergoes maximum displacements about a mean axis of vibration of between 1.2 and 1.9 times those of an elasto-plastic system with the same strength, initial stiffness, and damping ratio. Low, stiff frames with periods of less than half a second will have high ductility demands for both prestressed concrete and reinforced concrete, even though they are designed to higher lateral load coefficients, and therefore warrant further study for seismic resistant design. The reasons for the greater displacements of the prestressed concrete system relative to its elasto-plastic counterpart are; firstly, an increase of period of vibration (and consequent greater flexibility) arising from the load-displacement characteristics of prestressed concrete, and secondly, the lower inherent hysteretic energy dissipation capacity for prestressed concrete.

The comparative results which have been quoted from these single-degree-of-freedom analyses serve to show trends as to the likely relative responses of multistorey structures. However it would be difficult to predict ductility factor requirements for a multistorey prestressed concrete structure on the basis of its single-degree-of-

freedom counterpart. Nevertheless it should be noted that, provided any drift of the axis of vibration is taken into account, the single-degree-of-freedom systems will accentuate any differences between the prestressed and reinforced concrete models. It may well be that, in the complex response behaviour of a multistorey frame, the relative moment-curvature characteristics at the points where plastic hinges form assume less significance than the relative load-displacement characteristics of a single-degree-of-freedom system.

The second part of this study showed the significance of the design lateral load level on the magnitude of response for the prestressed concrete structural system. For the load factor used, the structure considered would have behaved satisfactorily under an El Centro type earthquake if it had been designed as a Public Building in Zone A of the New Zealand Basic Design Loads Code[84], but may have been close to collapse if it had been built as a Non-Public Building in Zone C.

The results of both parts of this investigation have a bearing on suitable load factors for prestressed concrete seismic design. On the basis of the greater response displacements of prestressed concrete structures relative to comparable reinforced concrete structures of the same strength, initial stiffness, and percentage critical viscous damping, as shown in this study and others[6,17], a greater design lateral load for prestressed concrete structures relative to reinforced concrete structures appears to be warranted. Rather than specify separate, higher seismic coefficients for prestressed concrete design, it is preferable to increase the ultimate strength design seismic load factor for prestressed concrete structures. To this end, the recommendations of the N.Z.P.C.I.[42] which effectively require a 20% increase in the earthquake load part of the ultimate strength design loads for prestressed concrete structures over that for reinforced concrete structures, appear reasonable.

CHAPTER 7

SUGGESTED FUTURE RESEARCH AND CONCLUSIONS

7.1 SUGGESTED FUTURE RESEARCH

It has been evident from this study that several important areas, relating to the seismic resistance of prestressed concrete, require further research.

7.1.1 Response Analyses

Response analyses of multistorey prestressed concrete framed buildings are needed to clarify the actual ductility demands on the members under strong earthquakes. The idealization proposed in Chapter 5 may be used to represent the moment-curvature characteristics at the plastic hinges. It is suggested that in such analyses an earthquake acceleration record with greater maximum accelerations and a longer period of intense shaking than that for the El Centro 1940 N-S earthquake be tried. The pseudo-earthquakes of Jennings[87] appear to be suitable.

The single-degree-of-freedom analyses of Chapter 6 could profitably be extended to cover a range of earthquake acceleration records, as the trends obtained are no doubt influenced to some extent by the characteristics of the record chosen. These analyses did serve to show particular seismic design problems associated with low stiff prestressed concrete buildings, a topic that warrants further research.

7.1.2 Tests for Analytical Work

Although this investigation enabled the postulation of a moment-curvature relationship for prestressed concrete members, more information is needed on the following characteristics affecting response analyses:

(a) Shaking tests of prestressed concrete buildings will lead to a better understanding of their damping performance, and consequent greater accuracy in response analyses.

(b) Since it has been shown that expressions[53,54] for determination of equivalent plastic hinge lengths in confined reinforced concrete members are not appropriate for prestressed concrete, a detailed experimental investigation is required to formulate suitable expressions for prestressed concrete members. An analytical approach could also be employed on the basis of the theoretical curvature distribution analysis presented in Section 3.3.4.

7.1.3 Experimental Cyclic Loading Studies

The following experimental projects on prestressed concrete elements under cyclic loading should be given attention:

(a) Internal beam-column assemblies present a more severe bond problem than that found for external joints at large deformations, and warrant study of their performance under high intensity cyclic load.

(b) Dynamic load testing of beam-column assemblies would be useful to test the validity of results obtained from static cyclic loading.

(c) A study is needed of the behaviour of prestressed concrete flat slab-column connections under cyclic load.

(d) The possible benefits of including mild steel at the joints of frames to increase energy dissipation under seismic load reversals should be investigated. Viable connection details incorporating mild steel need to be presented for precast construction.

7.2 SUMMARY OF RESULTS

The discussion and conclusions at the end of each chapter may be summarized as follows:

An investigation was made of the behaviour of four precast prestressed concrete beam-column assemblies under high intensity cyclic load. The section sizes were based on those of an already constructed two storey prestressed concrete framed structure. It is shown that the energy dissipation of prestressed concrete members is low prior to crushing of the cover concrete, but that there is a reserve of energy dissipation available should greater curvatures be sustained. For all members tested large post elastic deformations were available, and there was no significant advantage in putting more transverse steel in the members than was required as shear reinforcement by normal prestressed concrete codes. However, special transverse steel for confinement may be warranted at higher axial loads. The occurrence of a bond failure in the post-tensioning cable duct through the column at high deformations, and the satisfactory behaviour of the mortar joint are other results of importance for design considerations.

An analysis was developed to determine the moment-curvature relationships of prestressed concrete members under monotonic load to failure. The theory is tested against experimental results, and then used to determine the effects on ductility of a number of practical section variables. A limit of steel area ratio rather lower than the ACI code[40,41] requirements is suggested for ductility in seismic design. Distribution of the prestressing tendons into at least two positions near the top and bottom of the member is shown to be desirable, and the high ductilities possible in members with transverse reinforcement satisfying only shear requirements is further demonstrated. The SEAOC[51] code limitation on axial load is concluded to be applicable also to prestressed concrete members. Finally in this section, it is shown that prestressed concrete members will have greater curvatures at crushing than comparable reinforced concrete members with the same size and strength.

From postulated cyclic load stress-strain curves for concrete and prestressing steel, an analysis was evolved to determine the moment-curvature relationships of a general prestressed concrete section under cyclic load. An idealization for the moment-curvature characteristics of prestressed concrete members is also presented, for use in seismic analyses of multistorey framed structures. Good correlation is obtained with experimental results for both the theoretical and idealized curves. The theory is then used to show the smaller energy dissipation capacity under cyclic load of a prestressed concrete section relative to a reinforced concrete section of the same strength.

A comparative study is made of the earthquake responses of prestressed concrete and reinforced concrete single-degree-of-freedom portal frame structures. Elasto-plastic, degrading stiffness, and prestressed concrete idealizations are used for the load-displacement relationships. For a given strength, period of vibration, and damping ratio, it is found that a prestressed concrete structure sustains maximum displacements about the mean axis of vibration of between 1.2 and 1.9 times those of a comparable reinforced concrete structure, over the likely range of periods. The significance of maximum lateral strength upon the seismic response of the prestressed concrete system is also demonstrated.

7.3 CONCLUSIONS

The design of prestressed concrete structures for seismic resistance has in the past been based on comparative considerations of the well documented behaviour of reinforced concrete structures under earthquakes. Until a sufficient history of research information and observation under earthquake conditions has been compiled to consider prestressed concrete quantitatively in its own right, such comparative analyses form a useful guide to the design engineer. The results of

this study and other investigations[6,17] suggest that a prestressed concrete frame when responding to a typical earthquake will generally have a maximum displacement of about 1.4 times that of a reinforced concrete frame with the same strength, initial stiffness, and percentage critical viscous damping. In practice a prestressed concrete structure is likely to have a lower percentage critical viscous damping than its reinforced concrete counterpart, a factor which will tend to increase the above displacement ratio. However this may be counteracted by the greater flexibility of the prestressed concrete frame (due to smaller member sizes), which results in reduced ductility demands even if the design strength decreases with increasing period of vibration in accordance with code requirements[84]. Also if the section sizes do happen to be similar, prestressed concrete members may undergo greater curvatures before crushing of the concrete members, because of the smaller neutral axis depth due to higher strength concrete.

In the light of these considerations a higher lateral design load for prestressed concrete structures over that for reinforced concrete structures appears to be warranted, so that the prestressed concrete structure will undergo similar displacements to its reinforced concrete counterpart in a particular earthquake. Rather than formulating higher seismic coefficients for prestressed concrete, the ultimate strength design seismic load factors should be increased. To this end the recommendations of the N.Z.P.C.I., which effectively require a 20% increase in the earthquake load part of the ultimate strength design loads for prestressed concrete structures over that for reinforced concrete structures, appear reasonable. If future response analyses can substantiate Spencer's[6] results, or if additional experimental work can verify that prestressed concrete structures can sustain greater deflections before collapse than reinforced concrete structures, this increased load factor would not be necessary.

It is felt that the rather stringent strain limits specified by the F.I.P. Seismic Commission[38] would require greater load factors for design than is being advocated here, because they will allow little reduction of response through post-elastic deformations. It is therefore felt that more realistic criteria would be to limit the concrete strains to avoid the concrete crushing under a moderate earthquake (since crushing of the concrete rather than steel permanent set represents significant structural damage in prestressed concrete members), and to ensure that collapse does not occur under a severe earthquake. It has been shown in this study that provided suitable limits of steel area ratio, transverse steel, and axial loads are observed, prestressed concrete members may sustain very large post-crushing deformations, thus satisfying the latter criterion.

LIST OF REFERENCES

1. NAKANO, K., "Experiment on Behaviour Under Lateral Force of Prestressed Concrete Portal Frames", Occasional Report No. 21, Building Research Institute, Ministry of Construction, Japanese Government, Sept. 1964, 15pp.

2. DESPEYROUX, J. "On the Use of Prestressed Concrete in Earthquake Resistant Design", Proceedings of the Third World Conference on Earthquake Engineering, New Zealand, Jan. 1965, Vol. III, pp. IV-203 to 215.

3. GUYON, Y. "Energy absorption by Prestressed Concrete Beams", Proceedings of the Third World Conference on Earthquake Engineering, New Zealand, Jan. 1965, Vol. III, pp. IV-216 to 223.

4. SUTHERLAND, W.M., "Prestressed Concrete Earthquake Resistant Structures - Development, Performance, and Current Research", Proceedings of the Third World Conference on Earthquake Engineering, New Zealand, Jan. 1965, Vol. III, pp. IV-463 to 494.

5. LIN, T.Y., "Prestressed and Precast Concrete Structures", Chapter 19, "Earthquake Engineering", co-ordinating editor Robert L. Wiegel, Prentice Hall Inc., 1970.

6. SPENCER, R.A., "The Nonlinear Response of a Multistorey Prestressed Concrete Structure to Earthquake Excitation", Proceedings of the Fourth World Conference on Earthquake Engineering, Chile, Jan. 1969, Vol. II, pp. A4-139 to 154.

7. FREYSSINET, E., "A Revolution in the Technique of the Utilization of Concrete", The Structural Engineer, Vol. 14, No. 5, May 1936, pp.242-262.

8. HUNT, D.S., "A Dynamic Study of Structural Concrete", M.E. Thesis, University of Canterbury, New Zealand, 1966, 189pp.

9. JACOBS, M.L., "The Fatigue of Prestressed Concrete Beams Under Reversed Cyclic Loading", Ph.D. Thesis, University of Auckland, New Zealand, 1968, 269pp.

10. ELLISON, W.H. and LIN, T.Y., "Parking Garage Built for $5.28 per sq.ft.", Civil Engineering (N.Y.), Vol. 25, No. 6, June 1955, pp.37-40.

11. LIN, T.Y., "Revolution in Concrete", New Zealand Concrete Construction, Vol. 6, No. 9, Sept. 1962, pp.156-159.

12. BAN, S., "Rigid Building Frames of Post-Tensioned Prestressed Concrete in Active Earthquake", Proceedings of the World Conference on Prestressed Concrete, San Francisco, July 1957, pp. A22-1 to 4.

13. GLOGAU, O.A., "1st Chilean Conference on Earthquake Engineering. Building Damage 1960 Chilean Earthquake. Recent Trends in Earthquake Resistant Design", Report on Overseas Visit, Structural Design Office, Ministry of Works, New Zealand, August 1963, 31pp.

14. LIN, T.Y., "Design of Prestressed Concrete Buildings for Earthquake Resistance", Journal of the Prestressed Concrete Institute, Vol. 9, No. 6, Dec. 1964, pp.15-31.

15. ROSENBLEUTH, E., Discussion on paper by T.Y. Lin "Design of Prestressed Concrete Buildings for Earthquake Resistance", Journal of the Structural Division, A.S.C.E., Vol. 92, No. ST1, Feb. 1966, pp.502-504.

16. ROSENBLEUTH, E., "On Earthquake-Resistant Design", New Zealand Engineering, Vol. 21, No. 9, Sept. 1966, pp.371-386.

17. ROSENBLEUTH, E., Private Communication, 1968.

18. ALLARDICE, N.W., "Engineering Aspects of the Arts and Library Building, Victoria University of Wellington", New Zealand Engineering, Vol. 21, No. 12, Dec. 1966, pp.501-508.

19. BRISAC, M., "The Sheds at Piraeus: an Earthquake-Proof Building in Prestressed Concrete", Construction, Vol. 22, No. 3, March 1967, pp.108-110 (In French).

20. KORCHINSKII, I.L., "Prestressed Concrete for Seismic Construction", Beton i Zhelezobeton, No. 1, 1965, pp.13-16 (In Russian).

21. BERG, G.V., "The Skopje, Yugoslavia Earthquake", American Iron and Steel Institute, 1964, 78pp.

22. KUNZE, W.E., SBAROUNIS, J.A. and AMRHEIN, J.A., "Behaviour of Prestressed Concrete Structures During the Alaskan Earthquake", Journal of the Prestressed Concrete Institute, Vol. 10, No. 2, April 1965, pp.80-91.

23. INOMATA, S., "A Report on the Behaviour of Structures Employing Prestressed Concrete During Niigata Earthquake", Journal of Japan Prestressed Concrete Engineering Association, Vol. 6, No. 5, Oct. 1964, pp.38-42.

24. FINTEL, M., "Behaviour of Structures in the Caracas Earthquake", Civil Engineering (U.S.A.), Feb. 1968, pp.42-46.

25. HISADA, T. and NAKAGAWA, K., "Vibrations of Buildings in Japan", Part II, Proceedings of World Conference on Earthquake Engineering, California, 1956, pp. 7_{II} - 1 to 10.

26. PENZIEN, J., "Damping Characteristics of Prestressed Concrete", Journal of the A.C.I., Vol. 61, No. 9, Sept. 1964, pp.1125-1147.

27. NAKANO, K., "Experiment on Behaviour of Prestressed Concrete Four Storeyed Model Structure Under Lateral Force", Proceedings of the Third World Conference on Earthquake Engineering, New Zealand, Jan. 1965, Vol. III, pp. IV-572 to 590.

28. INOMATA, S., "Comparative Study on Behaviour of Prestressed and Reinforced Concrete Beams Subjected to Reversed Loading", Journal of Japan Prestressed Concrete Engineering Association, Vol. 11, No. 1, March 1969.

29. JOINT F.I.P.-C.E.B. COMMITTEE, "Practical Recommendations for the Design and Construction of Prestressed Concrete Structures", London, Fédération Internationale de la Précontrainte, June 1966, 82pp.

30. ENTRICAN, G.C., "Reinforced Concrete Frames With Prestress. Behaviour Under Repeated Reversed Loading Beyond the Yield", Private Communication, New Zealand, March 1969, 16pp.

31. OLADAPO, I.O., "Rate of Loading Effect on Moment-Curvature Relation in Prestressed Concrete Beams", Journal of the A.C.I., Vol. 61, No. 7, July 1964, pp.871-886.

32. SPENCER, R.A., "The Damping and Flexural Properties of Prestressed Concrete Members Subjected to Reversed Cyclic Loading", Ph.D. Thesis, University of Auckland, New Zealand, 1966.

33. ZAVRIEV, K.S., "Dynamics and Earthquake Resistance of Prestressed Reinforced Concrete Structures", Proceedings of the Third World Conference on Earthquake Engineering, New Zealand, Jan. 1965, Vol. II, p. IV-645.

34. HOGNESTAD, E., "Research on Prestressed Concrete Outside of Europe and U.S.S.R.", Le Genie Civil, Tome 143, No. 24, Dec. 1966, pp.523-524 (In French).

35. LIGTENBERG, M., "Research on Prestressed Concrete in Eastern Europe", Le Genie Civil, Tome 143, No. 22, Nov. 1966, p.472 (In French).

36. GVOZDEV, A.A., "Research on Prestressed Concrete in U.S.S.R. and Neighbouring Countries", Le Genie Civil, Tome 143, No. 22, Nov. 1966, pp.472-474 (In French).

37. F.I.P., "General Principles of Earthquake Resistant Design of Prestressed Concrete Structures", Report of the F.I.P. Commission on Prestressed Concrete Seismic Structures, Proceedings of the Fifth Congress of La Fédération Internationale de la Précontrainte, Paris, 1966, London, Cement and Concrete Association, 1967, pp.101-105.

38. F.I.P., "Report of the F.I.P. Commission on Seismic Structures", Proceedings of the Sixth Congress of La Fédération Internationale de la Précontrainte, Prague, 1970, 6pp.

39. P.C.I. SEISMIC COMMITTEE, "Principles of the Design and Construction of Earthquake Resistant Prestressed Concrete Structures", Journal of the P.C.I., Vol. 11, No. 3, June 1966, pp.18-22.

40. A.C.I. COMMITTEE 318, "Building Code Requirements for Reinforced Concrete", American Concrete Institute, 1963, 144pp.

41. A.C.I. COMMITTEE 318, "Proposed Revision ofA.C.I. 318-63: Building Code Requirements for Reinforced Concrete", Journal of the A.C.I., Vol. 67, No. 2, Feb. 1970, pp.77-186.

42. N.Z.P.C.I., "Seismic Design Recommendations for Prestressed Concrete", New Zealand Prestressed Concrete Institute, Sept. 1966.

43. HANSON, N.W. and CONNER, H.W., "Seismic Resistance of Reinforced Concrete Beam-Column Joints", Journal of the Structural Division, A.S.C.E., Vol. 93, No. ST5, Oct. 1967, pp.533-560.

44. ATCHLEY, W.L. and FURR, H.L., "Strength and Energy Absorption Capabilities of Plain Concrete Under Dynamic and Static Loadings", Journal of the A.C.I., Vol. 64, No. 11, Nov. 1967, pp.745-756.

45. A.C.I. COMMITTEE 439, "Effect of Steel Strength and of Reinforcement Ratio on the Mode of Failure and Strain Energy Capacity of Reinforced Concrete Beams", Journal of the A.C.I., Vol. 66, No. 3, March 1969, pp.165-173.

46. TAKEDA, T., SOZEN, M.A., and NIELSEN, N.W., "Reinforced Concrete Response to Simulated Earthquakes", Journal of the Structural Division, A.S.C.E., Vol. 96, No. ST12, Dec. 1970, pp.2557-2573.

47. PARK, R., "Ductility of Reinforced Concrete Frames Under Seismic Loading", New Zealand Engineering, Vol. 23, No. 11, Nov. 1968, pp.427-435.

48. P.C.I., "Prestressed Concrete Building Code Requirements", American Prestressed Concrete Institute, 1961.

49. C.P.115: 1959, "The Structural Use of Prestressed Concrete in Buildings", British Standards Institution, 1959, 44pp.

50. BLUME, J.A., NEWMARK, N.M. and CORNING, L.H., "Design of Multi-Storey Reinforced Concrete Buildings for Earthquake Motions", Portland Cement Association, Skokie, 1961, 318pp.

51. S.E.A.O.C., "Recommended Lateral Force Requirements", Seismology Committee, Structural Engineers Association of California, 1968, 100pp.

52. JOINT F.I.P.-C.E.B. COMMITTEE, "International Recommendations for the Design and Construction of Concrete Structures", London, La Fédération Internationale de la Précontrainte, June 1970, 80pp.

53. BAKER, A.L.L. and AMARAKONE, A.M.N., "Inelastic Hyperstatic Frames Analysis", Flexural Mechanics of Reinforced Concrete, Proceedings of the International Symposium, Miami, Fla., 1964, pp.85-135.

54. CORLEY, W.G., "Rotational Capacity of Reinforced Concrete Beams", Journal of the Structural Division, A.S.C.E., Vol. 92, No. ST5, Oct. 1966, pp.121-146.

55. BURDETTE, E.G. and HILSDORF, H.K., "Behaviour of Laterally Reinforced Concrete Columns", Journal of the Structural Division, A.S.C.E., Vol. 97, No. ST2, Feb. 1971, pp.587-602.

56. PRIESTLEY, M.J.N., "Moment Redistribution in Prestressed Concrete Continuous Beams", Ph.D. Thesis, University of Canterbury, New Zealand, 1966, 189pp.

57. SHERBOURNE, A.N. and PARAMESWAR, H.C., "Limit Analysis of Continuous Prestressed Beams", Journal of the Structural Division, A.S.C.E., Vol. 94, No. ST1, Jan. 1968, pp.19-40.

58. HOGNESTAD, E., "A Study of Combined Bending and Axial Load in Reinforced Concrete Members", The Reinforced Concrete Research Council of the Engineers' Foundation, Bulletin No. 1, June 1951.

59. SMITH, G.M. and YOUNG, L.E., "Ultimate Theory in Flexure by Exponential Function", Journal of A.C.I., Vol. 52, No. 3, Nov. 1955, pp.349-360.

60. CHAN, W.W.L., "The Ultimate Strength and Deformation of Plastic Hinges in Reinforced Concrete Frameworks", Magazine of Concrete Research, Vol. 7, No. 21, Nov. 1955, pp.121-132.

61. KRIZ, L.B. and LEE, S.L., "Ultimate Strength of Over-Reinforced Beams", Journal of the Engineering Mechanics Division, A.S.C.E., Vol. 86, No. EM3, June 1960, pp.95-105.

62. LIEBENBERG, A.C., "A Stress-Strain Function for Concrete Subjected to Short-Term Loading", Magazine of Concrete Research, Vol. 14, No. 41, July 1962, pp.85-90.

63. DESAYI, P. and KRISHNAN, S., "Equations for the Stress-Strain Curve of Concrete", Journal of the A.C.I., Vol. 61, No. 3, March 1964, pp.345-350.

64. SOLIMAN, M. and YU, C.W.,"The Flexural Stress-Strain Relationship of Concrete Confined by Rectangular Transverse Reinforcement", Magazine of Concrete Research, Vol. 19, No. 61, Dec. 1967, pp.223-238.

65. SARGIN, M., "Stress-Strain Relationship for Concrete and the Analysis of Structural Concrete Sections", Ph.D. Thesis, University of Waterloo, Canada, 1968, 334 pp.

66. KENT, D.C., "Inelastic Behaviour of Reinforced Concrete Members With Cyclic Loading", Ph.D. Thesis, University of Canterbury, New Zealand, 1969, 246pp.

67. POPOVICS, S., "A Review of Stress-Strain Relationships for Concrete", Journal of the A.C.I., Vol. 67, No. 3, Mar. 1970, pp.243-248.

68. HOGNESTAD, E., HANSON, N.W. and McHENRY, D., "Concrete Stress Distribution in Ultimate Strength Design", Journal of the A.C.I., Vol. 52, No. 4, Dec. 1955, pp.455-479.

69. RÜSCH, H., "Researches Towards a General Flexural Theory for Structural Concrete", Journal of the A.C.I., Vol. 57, No. 1, July 1960, pp.1-28.

70. STURMAN, G.M., SHAH, S.P. and WINTER, G., "Effects of Flexural Strain Gradients on Microcracking and Stress-Strain Behaviour of Concrete", Journal of the A.C.I., Vol. 62, No. 7, July 1965, pp.805-821.

71. GHOSH, S.K. and HANDA, V.K., "Strain Gradient and the Stress-Strain Relationship of Concrete in Compression", Highway Research Record, Washington, D.C., No. 324, 1970, pp.44-53.

72. KENT, D.C. and PARK, R., "Flexural Members With Confined Concrete", Journal of the Structural Division, A.S.C.E., Vol. 97, No. ST7, July 1971.

73. MATTOCK, A.H., "Rotational Capacity of Hinging Regions in Reinforced concrete Beams", Flexural Mechanics of Reinforced Concrete, Proceedings of the International Symposium, Miami, Fla., 1964, pp.143-181.

74. A.C.I. COMMITTEE 315, "Seismic Details for Special Ductile Frames", Journal of the A.C.I., Vol. 67, No. 5, May 1970, pp.374-379.

75. PARANAGAMA, D.D.O. and EDWARDS, A.D., "Moment-Deformation Characteristics of Pretensioned Concrete Beams Subject to Fluctuating Loads", Journal of the P.C.I., Vol. 14, No. 4, Aug. 1969, pp.62-74.

76. SINHA, B.P., GERSTLE, K.H. and TULIN, L.G., "Stress-Strain Relations for Concrete Under Cyclic Loading", Journal of the A.C.I., Vol. 61, No. 2, Feb. 1964, pp.195-211.

77. KARSAN, I.D. and JIRSA, J.O., "Behaviour of Concrete Under Compressive Loadings", Journal of the Structural Division, A.S.C.E., Vol. 95, No. ST12, Dec. 1969, pp.2543-2563.

78. JONES, L.L., "The Ultimate Flexural Strength of Reinforced and Prestressed Concrete Beams", Cement and Concrete Association Technical Report, TRA/304, Nov. 1958, 35pp.

79. CLOUGH, R.W., "Effect of Stiffness Degradation on Earthquake Ductility Requirements", University of California Structural Engineering Laboratory, Report No. 66-16, Oct. 1966, 66pp.

80. KENT, D.C. and PARK, R., "Inelastic Behaviour of Reinforced Concrete Members With Cyclic Loading", Bulletin of the New Zealand Society for Earthquake Engineering, Vol. 4, March 1971, pp.108-125.

81. KATAYAMA, T., "A Review of Theoretical and Experimental Investigations of Damping in Structures", UNICIV Report, University of New South Wales, No. I-4, July 1965, 29pp.

82. JAMES, M.L., LUTES, L.D. and SMITH, G.M., "Dynamic Properties of Reinforced and Prestressed Concrete Structural Components", Journal of the A.C.I., Vol. 61, No. 11, Nov. 1964, pp.1359-1382.

83. BIGGS, J.M., "Introduction to Structural Dynamics", McGraw-Hill Book Company, 1964.

84. New Zealand Standard Model Building Bylaw, N.Z.S.S. 1900, Chapter 8, "Basic Design Loads", Dec. 1965, 39pp.

85. NZS 3101: 1971, "Code of Practice for Reinforced Concrete Design", Standards Association of New Zealand.

86. University of Canterbury, Civil Engineering Department, Computer Program Library.

87. JENNINGS, P.C., HOUSNER, G.W. and TSAI, N.C., "Simulated Earthquake Motions for Design Purposes", Proceedings of the Fourth World Conference on Earthquake Engineering, Chile, Jan. 1969, Vol. I, pp. A1-145 to 160.

88. ASTM Designation: C31-62T, "Tentative Method for Making and Curing Concrete Compression and Flexure Test Specimens in the Field".

89. ASTM Designation: C39-64, "Standard Method of Test for Compressive Strength of Moulded Concrete Cylinders".

90. ASTM Designation: C78-64, "Standard Method of Test for Flexural Strength of Concrete (Using Simple Beam With Third-Point Loading)".

91. NZSR 32: 1968, "Prestressed Concrete", Standards Association of New Zealand, 1968, 63pp.

92. NZSS 197: 1949, "Rolled Steel Bars and Hard Drawn Steel Wire for Concrete Reinforcement", New Zealand Standards Institute.

93. NZSS 2129: 1967, "Sands for Mortars, Plasters, and External Renderings", New Zealand Standards Institute.

APPENDIX A

COMPUTER PROGRAMS

A.1 COMPUTER FACILITIES

Throughout this investigation the University of Canterbury's principal computer was an I.B.M. 360 Model 44. The machine had 128^K bytes core storage and a peripheral storage comprising two 2315 disc drives, each capable of storing one million bytes. Execution speeds were very rapid, facilitated by the use of floating point hardware.

A facility was also available for automatic plotting of graphs. This consisted of a CALCOMP 11 inch drum plotter attached to an I.B.M. 1620 computer, which ran off-line to the 360/44 computer.

A.2 PROGRAM LISTINGS

Listings of programs developed for the theoretical analyses of this thesis are included in this appendix. Programs were also written to reduce the experimental data of the beam-column tests to the required form, but since these are not likely to be of general use they have not been included.

Output from the programs is self explanatory. The input requirements are set out below.

Program 4.1 - "MOROAN"

Input:

FCD = concrete cylinder strength, f'_c (psi)

EO = concrete strain at maximum stress, ϵ_o

Z = Z value for core concrete, as defined by equation (4.3)

Z1 = Z value for cover concrete

ESP = concrete strain at spalling, ϵ_{sp}

ECU = limiting concrete strain for termination of analysis

MODEL = number of model for behaviour of cover concrete (see Section 4.2.3)

ESA = steel strain, ϵ_{sa} (see Fig. 4.2)

ESB = steel strain, ϵ_{sb} (see Fig. 4.2)

ESU = ultimate steel strain, ϵ_{su}

FSA = steel stress, f_{sa} (psi) (see Fig. 4.2)

FSB = steel stress, f_{sb} (psi) (see Fig. 4.2)

FSU = ultimate steel stress, f'_s (psi)

ESO1, ESO2,... = steel strains at datum of zero concrete strain for tendons 1,2,...

F1, F2,... = bond factor for tendons 1,2,... (equal to unity if bond is perfect)

B = overall width of section, b (ins.)

D = overall depth of section, D (ins.)

ABDD = width of the confined core, b" (ins.)

DCT = depth, D_{ct}, from the top of the section to the top of the core

ALPHA1, ALPHA2,... = depth ratio α_1, α_2,... of distance to tendon position 1,2,... from extreme compression fibre/D

AS1, AS2,... = area of steel, A_{s1}, A_{s2},... at tendon positions 1,2,... (sq.ins.)

PO = initial axial load (lbs)

AXVAR = factor for variation of axial load with moment (lbs/lb.ins.)

E = eccentricity of axial load (ins.)

Program 5.1 - "CYCLOPS"

The following input requirements for this program are the same as for Program 4.1:

FCD, EO, Z, ESP, MODEL, ESA, ESB, ESU, FSA, FSB, FSU,

B, D, ABDD, DCT, PO, AXVAR

Other input requirements are:

ECC1 = initial strain in concrete at extreme compression fibre

SMALLP = steel area ratio, $p = A_s/bD$

NSP = number of tendon positions

ESO(1), ESO(2),... = steel strains at datum of zero concrete strain for tendons 1,2,...

SF(1), SF(2),... = bond factor for tendons 1,2,...

DCB = depth, D_{cb}, from the top of the section to the bottom of the core

NEL = number of concrete elements, N_e

NCR = number of curvature readings for analysis

HL = plastic hinge length for rotation output

ALPHA(1), ALPHA(2)... = depth ratios α_1, α_2...

AS(1), AS(2),... = steel areas, A_{s1}, A_{s2},... (sq.ins.)

KOAX = 1 for constant axial load, 2 for variable axial load

CR(1), CR(2),... = curvature limits 1,2,... (rads./in.)

Program 6.1 - "EQANEP"

Input:

PERIOD = period of vibration, T (seconds)

XLAMDA = damping ratio, λ

ADT = time interval, Δt (seconds)

NCARD = number of cards in digitised earthquake record

CMAX = maximum seismic coefficient for particular zone[84] (short periods)

CMIN = minimum seismic coefficient for particular zone[84] (long periods)

Program 6.2 "EQUANDS"

Input: As for Program 6.1

Program 6.3 - "EQUANPSM"

Input: As for Program 6.1 with the following additions:

GAMMA1 = ratio, γ_1, of post-cracking stiffness to elastic stiffness

GAMMA2 = ratio, γ_2, of post-crushing stiffness to elastic stiffness

CLF = ratio, γ_{LF}, of V_u to V_{cr}

VLI = initial loop depth load ratio, V_{li}/V_u

VLD = degraded loop depth load ratio, V_{ld}/V_u

```
C     ********************************************************************
C
C     MOMENT-CURVATURE RELATIONSHIPS FOR PRESTRESSED CONCRETE MEMBERS
C     UNDER MONOTONIC LOADING
C
C     JULY 1970
C
C     ********************************************************************
      COMMON ESA,ESB,ESU,FSA,FSB,YMS,YMSUB,FSHYP,A,ALPHA,BETA,ZETA,PSI,E
     1TA,XNU,XI,CHI,BDD,EO,ECC,E20C,E20C1,DK,FCC,Z,Z1,B,D,PHID,DCT,ABDD,
     2ESP
      WRITE(6,101)
      WRITE(6,102)
C
C     READ CONCRETE PROPERTIES
      READ(5,102) FCD,EO,Z,Z1,ESP,ECU,MODEL
      ER=7.5*SQRT(FCD)*EO/(2.0*FCD)
      E20C=EO+.8/Z
      E20C1=EO+.8/Z1
C
C     READ STEEL PROPERTIES
      READ(5,103) ESA,ESB,ESU,FSA,FSB,FSU
      READ(5,104) ES01,ES02,ES03,ES04,ES05
      READ(5,105) F1,F2,F3,F4,F5
      FSHYP=(FSB*ESB-FSA*ESA)/(ESB-ESA)
      A=ESA*ESB*(FSA-FSB)/(ESB-ESA)
      YMS=FSA/ESA
      YMSUB=(FSU-FSB)/(ESU-ESB)
C
C     READ BEAM GEOMETRY
      READ(5,106) B,D,ABDD,DCT
      READ(5,107) ALPHA1,ALPHA2,ALPHA3,ALPHA4,ALPHA5
      READ(5,108) AS1,AS2,AS3,AS4,AS5
      DEL=B*D/5.
      SMALLP=(AS1+AS2+AS3+AS4+AS5)/(B*D)
C
C     READ AXIAL LOAD VARIABLES
      READ(5,109) PO,AXVAR,E
C
C     INPUT DATA LIST AND RESULTS HEADINGS
      WRITE(6,110)
      WRITE(6,111) YMS,FCD,B
      WRITE(6,112) YMSUB,Z,D
      WRITE(6,113) AS1,Z1,ALPHA1
      WRITE(6,114) AS2,MODEL,ALPHA2
      WRITE(6,115) AS3,ALPHA3
      WRITE(6,116) AS4,ALPHA4
      WRITE(6,117) AS5,ALPHA5
      WRITE(6,118) ESU,SMALLP
      WRITE(6,119) PO
      WRITE(6,120)
      WRITE(6,121)
      WRITE(6,122)
C
C     NEUTRAL AXIS BELOW SECTION
C
C     SOLUTION OF QUADRATIC FOR CURVATURE
```



```
      P=PO
      DK=21.0
    3 IF(DK-1.0) 1,2,2
    2 C1=((-3./(B*D))*(YMS*EO/FCD)*(F1*AS1*(DK-ALPHA1)+F2*AS2*(DK-ALPHA2
     1)+F3*AS3*(DK-ALPHA3)+F4*AS4*(DK-ALPHA4)+F5*AS5*(DK-ALPHA5))-3.0*(2
     2.*DK-1.0))/(3.0*DK**2-3.0*DK+1.0)
      C2=((3.*YMS*(AS1*ES01+AS2*ES02+AS3*ES03+AS4*ES04+AS5*ES05)/(B*D*EC
     1D))+3.0*P/(FCC*B*D))/(3.0*DK**2-3.0*DK+1.0)
      SQD=SQRT(C1**2-4.0*C2)
      X1=(-C1+SQD)/2.0
      X2=(-C1-SQD)/2.0
      PHI=(X2*EO/D)*1.E5
      PHID=X2
C
C     CALCULATE MOMENT
      C3=-6.*DK**2+8.*DK-3.
      C4=12.*DK-8.
      C5=-YMS*D*EO*(F1*AS1*(DK-ALPHA1)*ALPHA1+F2*AS2*(DK-ALPHA2)*ALPHA2+
     1F3*AS3*(DK-ALPHA3)*ALPHA3+F4*AS4*(DK-ALPHA4)*ALPHA4+F5*AS5*(DK-ALP
     2HA5)*ALPHA5)
      C6=YMS*D*(AS1*ES01*ALPHA1+AS2*ES02*ALPHA2+AS3*ES03*ALPHA3+AS4*ES04
     1*ALPHA4+AS5*ES05*ALPHA5)+P*(0.5*D+E)
      BMTCT=-((FCD*B*D**2)/12.0)*(PHID**2*C3+PHID*C4)+PHID*C5+C6
      P=PO+AXVAR*BMTCT
      BMOM=BMTOT*1.E-3/12.0
      DMOM=(BMOM*100.0/(B*D**2*FCD))*1.E3*12.0
      ECC=(DK*PHID*EO)*1.E6
      ECT=(DK-1.0)*PHID*EO*1.E6
      ES1=-(DK-ALPHA1)*PHID*EO*F1+ES01
      ES5=-(DK-ALPHA5)*PHID*EO*F5+ES05
      WRITE(6,123) BMOM,PHI,DMOM,PHID,P,DK,ECC,ECT,ES1,ES5
      DK=DK-1.0
      GO TO 3
    1 WRITE(6,124)
      EC1=ECC
C
C     NEUTRAL AXIS WITHIN SECTION
C
      WRITE(6,121)
      WRITE(6,122)
C
C     COMMENCEMENT OF COMPUTATION OF MOMENT AND CURVATURE AT FIRST
C     CRACKING
      WRITE(6,125)
      DK=0.85
      N=0
  502 ECT=ER
      ECC=ECT*DK/(1.0-DK)
      PHID=ECC/(DK*EO)
      GO TO 4
C
C     COMMENCEMENT OF COMPUTATION FOR SUCCESSIVE INCREMENTS OF ECC
  601 ECC=EC1*1.E-6+.00005
      DK=1.0-0.04
      KOUNT=0
   28 PHID=ECC/(DK*EO)
      ECT=(1.0-DK)*PHID*EO
```

```
C
C     CALCULATE TENSILE FORCE IN CONCRETE
      IF(ECT-ER) 4,4,5
    5 GAMMA=DK+(1.0-DK)*ER/ECT
      TC=2.0*FCD*B*D*PHID*(-0.5*DK**2+DK*GAMMA-0.5*GAMMA**2)
      GO TO 6
    4 TC=2.0*FCD*B*D*PHID*(-0.5*DK**2+DK-0.5)
C
C     CALCULATE PRESTRESSING STEEL STRAINS,STRESSES AND FORCES
    6 IF(AS1-0.) 7,7,8
    7 FS1=0.
      ES1=0.
      GO TO 9
    8 ES=-(DK-ALPHA1)*PHID*E0*F1+ES01
      ES1=ES
      CALL STSTR(ES,FS)
      FS1=FS
    9 IF(AS2-0.) 10,10,11
   10 FS2=0.
      GO TO 12
   11 ES=-(DK-ALPHA2)*PHID*E0*F2+ES02
      CALL STSTR(ES,FS)
      FS2=FS
   12 IF(AS3-0.) 13,13,14
   13 FS3=0.
      GO TO 15
   14 ES=-(DK-ALPHA3)*PHID*E0*F3+ES03
      CALL STSTR(ES,FS)
      FS3=FS
   15 IF(AS4-0.) 16,16,17
   16 FS4=0.
      GO TO 18
   17 ES=-(DK-ALPHA4)*PHID*E0*F4+ES04
      CALL STSTR(ES,FS)
      FS4=FS
   18 IF(AS5-0.0) 19,19,20
   19 FS5=0.
      GO TO 215
   20 ES=-(DK-ALPHA5)*PHID*E0*F5+ES05
      ES5=ES
      CALL STSTR(ES,FS)
      FS5=FS
  215 TS=(AS1*FS1+AS2*FS2+AS3*FS3+AS4*FS4+AS5*FS5)
C
C     CALCULATE COMPRESSIVE FORCES IN CONCRETE
      GO TO (251,252,253),MODEL
  251 CALL CMOD1(C)
      GO TO 254
  252 CALL CMOD2(C)
      GO TO 254
  253 CALL CMOD3(C)
C
C     CHECK EQUILIBRIUM OF FORCES AND ADJUST NEUTRAL AXIS DEPTH
  254 FE=(C+TC-TS-P)
      IF(ABS(FE).LE.DEL) GO TO 26
      IF(N-1) 92,92,91
   92 DK=(DK/30.0)*(28.0+2.0*(-TC+TS+P)/C)
```



```
      GO TO 502
   91 DK=(DK/6.0)*(4.0+2.0*(-TC+TS+P)/C)
      IF(KOUNT.GT.150)GO TO 33
      KOUNT=KOUNT+1
      GO TO 28
C
C     CALCULATE MOMENT ON SECTION
C
C     MOMENT DUE TO CONCRETE COMPRESSION
   26 GO TO (261,262,263),MODEL
  261 CALL BMMOD1(BMC)
      GO TO 264
  262 CALL BMMOD2(BMC)
      GO TO 264
  263 CALL BMMOD3(BMC)
C
C     MOMENT DUE TO CONCRETE TENSION
  264 IF(ECT-ER) 29,29,30
   29 BMT=2.0*FCD*B*D**2*PHID*(-DK**3/6.+DK/2.-1./3.)
      GO TO 31
   30 GAMMA=DK+(1.0-DK)*(ER/ECT)
      BMT=2.0*FCD*B*D**2*PHID*(-DK**3/6.+GAMMA**2*DK/2.-GAMMA**3/3.)
C
C     MOMENT DUE TO STEEL FORCES
   31 BMST=AS1*FS1*ALPHA1*D+AS2*FS2*ALPHA2*D+AS3*FS3*ALPHA3*D+AS4*FS4*AL
     1PHA4*D+AS5*FS5*ALPHA5*D
C
C     MOMENT DUE TO AXIAL LOAD
      PMOM=P*(0.5*D+E)
C     SUM OF MOMENTS
      BMTOT=BMST+PMCM-BMT-BMC
      P=PO+AXVAR*BMTOT
      BMOM=BMTOT*1.E-3/12.0
      DMOM=BMTOT*100.0/(B*D**2*FCD)
      KOUNT=0
C
C     PRINT OUTPUT AND CHECK LIMITING CONCRETE STRAIN
      PHI=(PHID*E0/D)*1.E5
      ECC=(DK*PHID*E0)*1.E6
      ECT=((DK-1.0)*PHID*E0)*1.E6
      IF(N-1) 710,711,711
  710 N=1
      GO TO 502
  711 WRITE(6,123) BMCM,PHI,DMOM,PHID,P,DK,ECC,ECT,ES1,ES5
      ECC=ECC*1.E-6
      IF(N-1) 42,43,42
   43 WRITE(6,126)
      N=2
      CRCKM=BMOM
      ECC=ECC+.000001
      GO TO 28
   42 IF(N-2) 44,45,44
   45 IF(BMOM-CRCKM-2.0) 46,47,47
   46 ECC=ECC+.000001
      GO TO 28
   47 N=3
      WRITE(6,127)
```

```
      GO TO 601
   44 IF(ECC-ECU) 32,33,33
   32 ECC=ECC+.0001
      GO TO 28
   33 CONTINUE
  101 FORMAT('1 TO CALCULATE MOMENT CURVATURE CHARACTERISTICS FOR GENERA
     1L PRESTRESSED CONCRETE SECTION UNDER MONOTONIC LOAD.'//////)
C
C     FORMAT STATEMENTS
  102 FORMAT(F6.0,F6.4,2F6.1,2F6.4,I2)
  103 FORMAT(F6.5,2F7.5,3F8.0)
  104 FORMAT(5F7.6)
  105 FORMAT(5F7.4)
  106 FORMAT(5F8.5)
  107 FORMAT(5F6.5)
  108 FORMAT(5F8.6)
  109 FORMAT(F7.0,F8.6,F7.3)
  110 FORMAT(' STEEL PROPERTIES ',8X,'CONCRETE PROPERTIES',11X,'MEMBER G
     1EOMETRY'//)
  111 FORMAT(' ','ES=',F9.0,' PSI',6X,'CYLINDER STRENGTH=',F5.0,'PSI',6X
     1,'WIDTH=',F5.3,' INCHES'/)
  112 FORMAT(' ','ESUB=',F9.0,' PSI',9X,'CORE CONC.Z=',F5.1,10X,'DEPTH='
     1,F5.2,'INCHES'/)
  113 FORMAT(' ','AS1=',F6.4,' SQ.INS.',7X,'COVER CONC. Z=',F5.1,11X,'AL
     1PHA1=',F6.3/)
  114 FORMAT(' ','AS2=',F6.4,' SQ.INS.',7X,'COVER CONC. MODEL=',I1,11X,'
     1ALPHA2=',F6.3/)
  115 FORMAT(' ','AS3=',F6.4,' SQ.INS.',37X,'ALPHA3=',F6.3/)
  116 FORMAT(' ','AS4=',F6.4,' SQ.INS.',37X,'ALPHA4=',F6.3/)
  117 FORMAT(' ','AS5=',F6.4,' SQ.INS.',37X,'ALPHA5=',F6.3/)
  118 FORMAT(' ','MAX. STRAIN=',F5.4,34X,'STEEL AREA RATIO=',F6.5/)
  119 FORMAT(' ','INITIAL AXIAL LOAD=',F7.0,'LBS'/)
  120 FORMAT('1NEUTRAL AXIS BELOW SECTION'//////)
  121 FORMAT(' ','SECTION MOMENT',5X,'CURVATURE',4X,'100M/(BD**2*FCD)',2
     1X,'500*PHI*D',5X,'P',7X,'K',7X,'MAX.COMP.STRN.',2X,'MAX.TENS.STRN.
     2',1X,'TOP STSTRN',1X,'BOT.STSTRN'//)
  122 FORMAT(' ',2X,'KIP FEET',6X,'RADS./INCH*1.E-5',32X,'LBS',15X,2('MI
     1CROSTRAINS',4X)//)
  123 FORMAT(' ',F11.3,5X,F11.3,2(8X,F8.3),2X,F7.0,F7.3,2(7X,F8.0),5X,2(
     13X,F8.6))
  124 FORMAT('1NEUTRAL AXIS WITHIN SECTION'///)
  125 FORMAT(' ','CRACKING MOMENT AND CURVATURE'//)
  126 FORMAT(' ','MOMENTS AND CURVATURES IMMEDIATELY AFTER CRACKING'//)
  127 FORMAT(' ','MOMENTS AND CURVATURES FOR INCREMENTS OF ECC'//)
      END


C     ******************************************************************
C     SUBROUTINE TO CALCULATE STEEL STRESS
C     ******************************************************************
      SUBROUTINE STSTR(ES,FS)
      COMMON ESA,ESB,ESU,FSA,FSB,YMS,YMSUB,FSHYP,A
      IF(ES-0.) 40,31,31
   40 IF(ES+0.005) 32,32,33
   33 FS=ES*YMS
      GO TO 30
   32 FS=-0.005*YMS
      GO TO 30
   31 IF(ES-ESA) 33,33,21
   21 IF(ES-ESB) 22,23,23
   22 FS=FSHYP+A/ES
      GO TO 30
   23 IF(ES-ESU) 24,24,25
   24 FS=FSB+YMSUB*(ES-ESB)
      GO TO 30
   25 FS=0.
   30 CONTINUE
      RETURN
       END
C     ******************************************************************
C     SUBROUTINES FOR COVER CONCRETE MODEL 1
C     ******************************************************************
C     CONCRETE COMPRESSION FORCE
C
      SUBROUTINE CMOD1(C)
      COMMON ESA,ESB,ESU,FSA,FSB,YMS,YMSUB,FSHYP,A,ALPHA,BETA,ZETA,PSI,E
     1TA,XNU,XI,CHI,BDD,EO,ECC,E20C,E20C1,DK,FCD,Z,Z1,B,D,PHID,DCT,ABDD,
     2ESP
      IF(ECC-EO) 21,21,22
   21 ALPHA=0.
      BETA=0.
      GO TO 23
   22 IF(ECC-E20C) 24,24,25
   24 ALPHA=DK*(1.0-EO/ECC)
      BETA=0.
      GO TO 23
   25 ALPHA=DK*(1.0-EO/ECC)
      BETA=DK*(1.0-E20C/ECC)
   23 C1=DK*ALPHA**2-DK**2*ALPHA-ALPHA**3/3.0+DK**3/3.0
      C2=2.0*DK*ALPHA-ALPHA**2-DK**2
      C3=0.5*Z*BETA**2-Z*DK*BETA+Z*DK*ALPHA-0.5*Z*ALPHA**2
      C4=BETA/EO+Z*BETA-ALPHA/EO-Z*ALPHA
      C=-(FCD*B*D*(PHID**2*C1+PHID*C2)+FCD*B*D*EO*(PHID*C3+C4)-0.2*FCD*B
     1*D*BETA)
      RETURN
       END
C
C     MOMENT DUE TO CONCRETE COMPRESSION FORCE
C
      SUBROUTINE BMMOD1(BMC)
      COMMON ESA,ESB,ESU,FSA,FSB,YMS,YMSUB,FSHYP,A,ALPHA,BETA,ZETA,PSI,E
     1TA,XNU,XI,CHI,BDD,EO,ECC,E20C,E20C1,DK,FCD,Z,Z1,B,D,PHID,DCT,ABDD,
     2ESP
      C1=-DK**2*ALPHA**2/2.+DK*ALPHA**3*2./3.-ALPHA**4/4.+DK**4/12.
      C2=DK*ALPHA**2-ALPHA**3*2./3.-DK**3/3.
      C3=-Z*DK*BETA**2/2.+Z*BETA**3/3.+Z*DK*ALPHA**2/2.-Z*ALPHA**3/3.
      C4=BETA**2/(2.*EO)+Z*BETA**2/2.-ALPHA**2/(2.*EO)-Z*ALPHA**2/2.
      BMC=-(FCD*B*D**2*(PHID**2*C1+PHID*C2)+FCD*B*D**2*EO*(PHID*C3+C4)-C
     1.2*FCD*B*D**2*BETA**2/2.)
      RETURN
       END
```

```
C     ***********************************************************************
C     SUBROUTINES FOR COVER CONCRETE MODEL 2
C     ***********************************************************************
C     CONCRETE COMPRESSION FORCE
C
      SUBROUTINE CMCD2(C)
      COMMON ESA,ESB,ESU,FSA,FSB,YMS,YMSUB,FSHYP,A,ALPHA,BETA,ZETA,PSI,E
     1TA,XNU,XI,CHI,BDD,EO,ECC,E2CC,E2OC1,DK,FCC,Z,Z1,B,D,PHID,DCT,ABDD,
     2ESP
      PSI=DCT/D
      BDD=B
      IF(ECC-EO) 61,61,62
   61 ALPHA=0.
      ZETA=0.
      BETA=0.
      PSI=0.
      GO TO 90
   62 IF(ECC-ESP) 63,63,64
   63 ALPHA=DK*(1.0-EO/ECC)
      BETA=0.
      ZETA=0.
      PSI=0.
      GO TO 90
   64 IF(ECC-E2OC) 65,65,66
   65 ZETA=DK*(1.0-ESP/ECC)
      PSI=DCT/D
      IF(ZETA-PSI) 67,67,68
   67 ALPHA=DK*(1.0-EO/ECC)
      BETA=ZETA
      PSI=ZETA
      BDD=B
      GO TO 90
   68 ALPHA=DK*(1.0-EO/ECC)
      BETA=PSI
      BDD=ABDD
      GO TO 90
   66 ZETA=DK*(1.0-ESP/ECC)
      ALPHA=DK*(1.0-EO/ECC)
      PSI=DCT/D
      IF(ZETA-PSI) 69,69,70
   69 BETA=ZETA
      PSI=ZETA
      BDD=B
      GO TO 90
   70 BETA=DK*(1.0-E2OC/ECC)
      IF(BETA-PSI) 71,71,72
   71 BETA=PSI
      BDD=ABDD
      GO TO 90
   72 BDD=ABDD
   90 C1=DK*ALPHA**2-DK**2*ALPHA-ALPHA**3/3.+DK**3/3.
      C2=2.*DK*ALPHA-ALPHA**2-DK**2
      C3=Z*ZETA**2/2.-Z*DK*ZETA+Z*DK*ALPHA-Z*ALPHA**2/2.
      C4=ZETA/EO+Z*ZETA-ALPHA/EO-Z*ALPHA
      C5=Z*BETA**2/2.-Z*DK*BETA+Z*DK*ZETA-Z*ZETA**2/2.
      C6=BETA/EO+Z*BETA-ZETA/EO-Z*ZETA
      C7=PSI-BETA
```



```
      C=-(FCD*B*D*(PHID**2*C1+PHID*C2)+FCD*B*D*EO*(PHID*C3+C4)+FCC*BDD*D
     1*EO*(PHID*C5+C6)+0.2*FCD*BDD*D*C7)
      RETURN
       END
C
C     MOMENT DUE TO CONCRETE COMPRESSION FORCE
C
      SUBROUTINE BMMOD2(BMC)
      COMMON ESA,ESB,ESU,FSA,FSB,YMS,YMSUB,FSHYP,A,ALPHA,BETA,ZETA,PSI,E
     1TA,XNU,XI,CHI,BDD,EO,ECC,E2OC,E2OC1,DK,FCC,Z,Z1,B,D,PHID,DCT,ABDD,
     2ESP
      C1=-0.5*DK**2*ALPHA**2+DK*ALPHA**3*2./3.-ALPHA**4/4.+DK**4/12.
      C2=DK*ALPHA**2-ALPHA**3*2./3.-DK**3/3.
      C3=-Z*DK*ZETA**2/2.+Z*ZETA**3/3.+Z*DK*ALPHA**2/2.-Z*ALPHA**3/3.
      C4=ZETA**2/(2.*EO)+Z*ZETA**2/2.-ALPHA**2/(2.*EO)-Z*ALPHA**2/2.
      C5=-Z*DK*BETA**2/2.+Z*BETA**3/3.+Z*DK*ZETA**2/2.-Z*ZETA**3/3.
      C6=BETA**2/(2.*EO)+Z*BETA**2/2.-ZETA**2/(2.*EO)-Z*ZETA**2/2.
      C7=PSI**2/2.-BETA**2/2.
      BMC=-(FCD*B*D**2*(PHID**2*C1+PHID*C2)+FCD*B*D**2*EO*(PHID*C3+C4)+F
     1CD*BDD*D**2*EO*(PHID*C5+C6)+0.2*FCC*BDD*D**2*C7)
      RETURN
       END
C     ***********************************************************************
C     SUBROUTINES FOR COVER CONCRETE MODEL 3
C     ***********************************************************************
C     CONCRETE COMPRESSION FORCE
C
      SUBROUTINE CMCD3(C)
      COMMON ESA,ESB,ESU,FSA,FSB,YMS,YMSUB,FSHYP,A,ALPHA,BETA,ZETA,PSI,E
     1TA,XNU,XI,CHI,BDD,EO,ECC,E2OC,E2OC1,DK,FCC,Z,Z1,B,D,PHID,DCT,ABDD,
     2ESP
      PSI=DCT/D
      BDD=ABDD
      IF(ECC-EO) 61,61,62
   61 ALPHA=0.
      ETA=0.
      XNU=0.
      XI=0.
      PSI=0.
      CHI=0.
      BETA=0.
      GO TO 90
   62 ALPHA=DK*(1.0-EO/ECC)
      IF(ECC-E2OC1) 63,63,64
   63 IF(ALPHA-PSI) 65,65,66
   65 ETA=0.
      XNU=0.
      XI=0.
      PSI=0.
      CHI=0.
      BETA=0.
      GO TO 90
   66 ETA=0.
      XNU=ALPHA
      XI=PSI
      CHI=ALPHA
      BETA=PSI
```

```
      GO TO 90
   64 ETA=DK*(1.0-E20C1/ECC)
      IF(ALPHA-PSI) 67,67,68
   67 XNU=0.
      XI=0.
      PSI=0.
      CHI=0.
      BETA=0.
      GO TO 90
   68 IF(ETA-PSI) 69,69,70
   69 XNU=ALPHA
      XI=PSI
      CHI=ALPHA
      BETA=PSI
      GO TO 90
   70 BETA=DK*(1.0-E20C/ECC)
      IF(BETA-PSI) 71,71,72
   71 XNU=ALPHA
      XI=ETA
      CHI=ALPHA
      BETA=PSI
      GO TO 90
   72 XNU=ALPHA
      XI=ETA
      CHI=ALPHA
   90 C1=DK*ALPHA**2-DK**2*ALPHA-ALPHA**3/3.+DK**3/3.
      C2=2.*DK*ALPHA-ALPHA**2-DK**2
      C3=Z1*ETA**2/2.-Z1*DK*ETA+Z1*DK*ALPHA-Z1*ALPHA**2/2.
      C4=ETA/E0+Z1*ETA-ALPHA/E0-Z1*ALPHA
      C5=Z1*XI**2/2.-Z1*DK*XI+Z1*DK*XNU-Z1*XNU**2/2.
      C6=XI/E0+Z1*XI-XNU/E0-Z1*XNU
      C7=PSI-XI
      C8=Z*BETA**2/2.-Z*DK*BETA+Z*DK*CHI-Z*CHI**2/2.
      C9=BETA/E0+Z*BETA-CHI/E0-Z*CHI
      C10=PSI-BETA
      C=-(FCD*B*D*(PHID**2*C1+PHID*C2)+FCC*B*D*E0*(PHID*C3+C4)-.2*FCD*B*
     1D*ETA-FCD*BDD*D*E0*(PHID*C5+C6)-0.2*FCD*BCD*C*C7+FCD*BDC*D*E0*(PHI
     2D*C8+C9)+0.2*FCC*BCC*C*C10)
      RETURN
       END
C
C     MOMENT DUE TO CONCRETE COMPRESSION FORCE
C
      SUBROUTINE BMMOD3(BMC)
      COMMON ESA,ESB,ESU,FSA,FSB,YMS,YMSUB,FSHYP,A,ALPHA,BETA,ZETA,PSI,E
     1TA,XNU,XI,CHI,BCD,E0,ECC,E20C,E20C1,DK,FCD,Z,Z1,B,D,PHID,DCT,ABCD,
     2ESP
      C1=-DK**2*ALPHA**2/2.+DK*ALPHA**3*2./3.-ALPHA**4/4.+DK**4/12.
      C2=DK*ALPHA**2-ALPHA**3*2./3.-DK**3/3.
      C3=-Z1*DK*ETA**2/2.+Z1*ETA**3/3.+Z1*DK*ALPHA**2/2.-Z1*ALPHA**3/3.
      C4=ETA**2/(2.*E0)+Z1*ETA**2/2.-ALPHA**2/(2.*EC)-Z1*ALPHA**2/2.
      C5=-ETA**2/2.
      C6=-Z1*DK*XI**2/2.+Z1*XI**3/3.+Z1*DK*XNU**2/2.-Z1*XNU**3/3.
      C7=XI**2/(2.*E0)+Z1*XI**2/2.-XNU**2/(2.*EC)-Z1*XNU**2/2.
      C8=PSI**2/2.-XI**2/2.
      C9=-Z*DK*BETA**2/2.+Z*BETA**3/3.+Z*DK*CHI**2/2.-Z*CHI**3/3.
      C10=BETA**2/(2.*E0)+Z*BETA**2/2.-CHI**2/(2.*E0)-Z*CHI**2/2.
```



```
      C11=PSI**2/2.-BETA**2/2.
      BMC=-(FCD*B*D**2*(PHID**2*C1+PHID*C2)+FCC*B*D**2*E0*(PHID*C3+C4)+C
     1.2*FCD*B*D**2*C5-FCC*BCC*D**2*E0*(PHID*C6+C7)-C.2*FCC*BCC*D**2*C8+
     2FCD*BCC*D**2*E0*(PHID*C9+C10)+0.2*FCC*BCD*D**2*C11)
      RETURN
      END
```

```
C     ************************************************************************
C
C     MOMENT-CURVATURE RELATIONSHIPS FOR PRESTRESSED CONCRETE MEMBERS
C     UNDER CYCLIC FLEXURAL LOADING
C
C     NOVEMBER 1970
C
C     ************************************************************************
      DIMENSION ESO(12),ALPHA(12),AS(12),FW(200),FCRACK(200),EMAX(200),E
     1ZERO(200),ESMAX(12),ESUZO(12),CR(100),ELAST(200),E(200),F(200),AI(
     2 12),ESLZO(12),FS(12),ES(12),ESLAS(12),FSMAX(12),FMAX(200),EES(12)
     3,SFACT(12),SF(12),YMF(200),UF(12),YMSF(12),WLV(12),X(999),Y(999),E
     4SMIN(12),FSMIN(12)
C
C     READ CONCRETE PROPERTIES
      READ(5,101) FCD,EO,Z,ESP,MODEL,ECC1
      ER=7.5*SQRT(FCD)*EO/(2.0*FCD)
      YMC=2.*FCD/EO
      E20C=EO+.8/Z
C
C     READ STEEL PROPERTIES
      READ(5,102) ESA,ESB,ESU,FSA,FSB,FSU,SMALLP,NSP,SFA
      READ(5,123)(ESO(J),J=1,NSP)
      READ(5,123)(SF(J),J=1,NSP)
      FSHYP=(FSB*ESB-FSA*ESA)/(ESB-ESA)
      A=ESA*ESB*(FSA-FSB)/(ESB-ESA)
      YMS=FSA/ESA
      YMSUB=(FSU-FSB)/(ESU-ESB)
C
C     READ BEAM GEOMETRY AND NUMBERS OF ELEMENTS AND READINGS
      READ(5,103) B,D,ABDD,DCT,DCB,NEL,NCR,HL
      READ(5,104) (ALPHA(J),J=1,NSP)
      READ(5,104)(AS(J),J=1,NSP)
      BDD=ABDD/B
      CT=DCT/D
      CB=DCB/D
      DEL=B*D/5.
C
C     READ AXIAL LOAD VARIABLES
      READ(5,105) KOAX,PO,AXVAR
C
C     INPUT DATA LIST AND RESULTS HEADINGS
C
      WRITE(6,106)
      WRITE(6,107)
      WRITE(6,108) YMS,FCD,D,PO
      WRITE(6,109) YMSUB,Z,B,AXVAR
      WRITE(6,110) FSU,EO,ABDD
      WRITE(6,111) SMALLP,E20C,DCT
      WRITE(6,112) NSP,ESP,DCB
      WRITE(6,113) ER,NEL
      WRITE(6,114) YMC,NCR
      WRITE(6,115) MODEL
      DO 1 J=1,NSP
    1 WRITE(6,116) J,AS(J)
      WRITE(6,117)
      DO 2 J=1,NSP
```



```
    2 WRITE(6,118) J,ALPHA(J)
      WRITE(6,119)
      WRITE(6,120)
C
C     WIDTH FACTORS INITIALISATION
      DO 3 I=1,NEL
    3 FW(I)=1.
C
C     CONCRETE'COUNTERS' INITIALISATION
      DO 4 I=1,NEL
      FCRACK(I)=1.
      YMF(I)=1.
      EMAX(I)=0.
    4 EZERO(I)=0.
C
C     STEEL'COUNTERS' INITIALISATION
      DO 5 I=1,NSP
      SFACT(I)=1.
      UF(I)=1.
      ESMAX(I)=0.
      YMSF(I)=1.
      WLV(I)=0.
      ESLZO(I)=0.
    5 ESUZO(I)=0.
C
C     MEMBER TERMS INITIALISATION
      BML=0.
      PHIL=0.
      KOP=1
      PHI=0.
      KCKD=1
      BMTOT=0.
      KONA=2
      KONG=1
      KOG=1
      KOUNT=0
      KONV=1
      ENERGY=0.
      P=PO
      N=0
C
C     FACTORS FOR DEPTH TO CONFINED CORE
      EL=NEL
      TEM=EL*DCT/D
      IT=TEM
      TEM=EL*DCB/D
      IB=TEM
C
C     DETERMINATION OF STEEL RESIDENT ELEMENTS
      DO 6 M=1,NSP
      TEMP=EL*ALPHA(M)
    6 AI(M)=TEMP
C
C     READ CURVATURE REQUIREMENTS
      DO 7 I=1,NCR
    7 READ(5,122) CR(I)
C
```

```
C     COMMENCEMENT OF COMPUTATION
C
      CHANGE=.00005
      DO 801 I=1,NCR
      IF(I-1)9,10,9
   10 ECC=ECC1
      IF(CR(I)) 11,13,13
    9 IF(CR(I)-CR(I-1)) 11,8,13
   11 KODE=2
      IF(PHI-CR(I))151,151,141
  141 ECC=ECC-CHANGE
      GO TO 14
   13 KODE=1
      IF(PHI-CR(I))142,161,161
  142 ECC=ECC+CHANGE
      GO TO 14
  151 KONG=2
      ECC=ECC+CHANGE*(PHI-CR(I))/(PHI-PHIL)
      GO TO 14
  161 KONG=2
      ECC=ECC-CHANGE*(PHI-CR(I))/(PHI-PHIL)
   14 AK=-20000.
      FENA=500000.
      FENB=500000.
   69 IF(ABS(AK).LE. .01)GO TO 97
      DO 19 M=1,NSP
   18 ES(M)=-SF(M)*ECC*(AK-ALPHA(M))/AK+ESO(M)
   19 CONTINUE
      SN=EL*AK
      CC=0.
      CT=0.
      BMCC=0.
C
C     CALCULATION OF CONCRETE STRESS FOR EACH ELEMENT
      DO 20 J=1,NEL
      AB=J
      E(J)=ECC*(SN-AB+.5)/SN
      IF(E(J)-EMAX(J))21,21,22
   21 IF(E(J)-EZERO(J)) 29,29,24
   24 IF(E(J)-ELAST(J)) 25,26,26
   25 IF(EMAX(J)-E0)226,226,225
  225 F(J)=.50*YMC*YMF(J)*(E(J)-EZERO(J))
      GO TO 20
   26 IF(EMAX(J)-E0)226,226,227
  226 F(J)=YMC*(E(J)-EZERO(J))
      GO TO 20
  227 F(J)=YMC*YMF(J)*(E(J)-EZERO(J))
      GO TO 20
   22 IF(E(J)-E0) 27,27,28
   27 F(J)=FCD*(2.*E(J)/E0-(E(J)/E0)**2)
      IF(F(J)) 29,20,20
   29 IF(FCRACK(J)-.5) 30,30,31
   30 F(J)=0.
      GO TO 20
   31 IF(E(J)-EZERO(J)+ER) 30,32,32
   32 F(J)=YMC*(E(J)-EZERO(J))
      GO TO 20
```



```
   28 IF(E(J)-E20C) 33,33,34
   33 F(J)=FCD*(1.-Z*(E(J)-E0))
      GO TO 20
   34 F(J)=0.2*FCD
   20 CONTINUE
C
C     ALLOWANCE FOR AREA TAKEN BY STEEL
      DO 44 M=1,NSP
      LJ=AI(M)
      IF(F(LJ))310,311,311
  311 CC=CC-F(LJ)*AS(M)
      GO TO 44
  310 CT=CT-F(LJ)*AS(M)
   44 BMCC=BMCC-F(LJ)*AS(M)*ALPHA(M)*D
C
C     TEMPORARY SPALLING CORRECTIONS AND CALCULATION OF FORCES AND MOMENTS
C
      DO 35 K=1,NEL
      AB=K
      IF(E(K)-ESP)36,36,37
   36 F(K)=F(K)*FW(K)
      GO TO 38
   37 IF(MODEL-2) 36,40,36
   40 IF(K-IT) 41,41,42
   41 F(K)=0.
      GO TO 38
   42 IF(K-IB) 43,41,41
   43 F(K)=F(K)*BDD
   38 IF(F(K))320,321,321
  321 CC=CC+F(K)*B*D/EL
      GO TO 35
  320 CT=CT+F(K)*B*D/EL
   35 BMCC=BMCC+F(K)*B*D*D*(AB-.5)/(EL**2)
C
C     STEEL FORCES AND MOMENTS
      TS=0.
      CS=0.
      BMS=0.
      DO 45 M=1,NSP
      IF(ES(M)-ESMAX(M)) 46,46,47
   46 IF(ES(M)-ESLAS(M)) 48,48,49
   48 IF(ES(M)-ESUZO(M)) 50,50,51
   51 FS(M)=YMS*YMSF(M)*(ES(M)-ESUZO(M))
      GO TO 52
   50 IF(ES(M)-ESUZO(M)+ESA) 53,51,51
   53 IF(ES(M)-ESUZO(M)+ESB) 54,54,55
   55 FS(M)=-(FSHYP+A/(ESUZO(M)-ES(M)))
      GO TO 52
   54 FS(M)=-(FSB+YMSUB*(ESUZO(M)-ES(M)-ESB))
      GO TO 52
   49 IF(UF(M)-1.)56,951,56
  951 IF(ESMAX(M)-.009)51,51,954
  954 IF(ES(M)-ESMAX(M)+4.*WLV(M))955,955,953
  955 IF(ES(M)-ESMIN(M)-.5*WLV(M))956,952,952
  956 FS(M)=FSMIN(M)+3.*YMS*YMSF(M)*(ES(M)-ESMIN(M))
      GO TO 52
  952 FS(M)=YMS*YMSF(M)*(ES(M)-ESUZO(M)+WLV(M))
```

```
      GO TO 52
  953 FS(M)=FSMAX(M)-3.*WLV(M)*YMS*YMSF(M)+(ES(M)-ESMAX(M)+4.*WLV(M))*.7
     15*YMS*YMSF(M)
      GO TO 52
   56 IF(ESMAX(M)-(ESUZO(M)-ESLZO(M))-ES(M)) 58,58,159
  159 FS(M)=YMS*YMSF(M)*(ES(M)-ESLZO(M))
      GO TO 52
   58 FS(M)=FSB+YMSUB*(ES(M)-ESB)
      GO TO 52
   47 IF(ES(M)-ESA) 59,59,60
   59 FS(M)=YMS*ES(M)
      GO TO 52
   60 IF(ES(M)-ESB) 61,61,58
   61 FS(M)=FSHYP+A/ES(M)
      GO TO 52
   52 IF(FS(M))302,301,301
  301 TS=TS+FS(M)*SFACT(M)*AS(M)
      GO TO 303
  302 CS=CS+FS(M)*SFACT(M)*AS(M)
  303 BMS=BMS+FS(M)*SFACT(M)*AS(M)*ALPHA(M)*D
   45 CONTINUE
C
C     AXIAL LOAD MOMENT
      P=PO+AXVAR*BMTOT
      BMP=P*.5*D
C
C     EQUILIBRIUM OF FORCES
      IF(KOG-1) 64,65,64
   65 IF(ECC.LT.0.) GO TO 451
      IF(CC-CS-TS+CT-P) 66,67,68
  451 IF(CC-CS-TS+CT-P) 168,67,166
  168 AK=10.
      KOG=2
      KONA=2
      CHANGE=.0002
      GO TO 69
  166 AK=-10.
      KOG=2
      KONA=1
      CHANGE=.0002
      GO TO 69
   68 AK=10.
      KOG=2
      KONA=1
      CHANGE=.0002
      GO TO 69
   67 PHI=0.
      KOG=2
      GO TO 95
   66 AK=-10.
      KOG=2
      KONA=2
      CHANGE=.0002
      GO TO 69
   64 FE=(CC-CS-TS+CT-P)
      IF(ABS(FE).LE.DEL) GO TO 96
      IF(KONV-2)756,760,756
```



```
  760 IF(KOUNT-150)590,590,591
  591 TENSAB=(TENSA+TENSB)/2.
      IF(COMPA-COMPB)593,96,593
  593 BMCC=BMCCB+(BMCCA-BMCCB)*(TENSAB-COMPB)/(COMPA-COMPB)
      GO TO 96
  590 IF(FE)761,96,762
  762 AKA=AK
      COMPA=CC-CS
      TENSA=TS+P-CT
      BMCCA=BMCC
      GO TO 252
  761 AKB=AK
      COMPB=CC-CS
      TENSB=TS+P-CT
      BMCCB=BMCC
      GO TO 252
  756 IF(KOUNT-100)251,252,252
  252 KONV=2
      IF(AKA.EQ.0. .OR. AKB.EQ.0.)GO TO 96
      AK=AKB+(AKA-AKB)/2.
      KOUNT=KOUNT+1
      GO TO 69
  251 KOUNT=KOUNT+1
      IF(FE)752,96,753
  752 IF(ABS(FE)-FENB)754,75,75
  754 AKB=AK
      FENB=ABS(FE)
      GO TO 75
  753 IF(ABS(FE)-FENA)757,75,75
  757 AKA=AK
      FENA=ABS(FE)
   75 IF(KONA-1) 70,71,70
   71 IF(ECC-.0006)372,372,371
  371 IF(CC-CS)471,472,471
  471 AK=(AK/12.)*(10.+2.*((TS+P-CT)/(CC-CS)))
      GO TO 373
  472 AK=AK*1.1
      GO TO 373
  372 IF(CC-CS)473,474,473
  473 AK=(AK/3.)*(1.+2.*((TS+P-CT)/(CC-CS)))
      GO TO 373
  474 AK=AK*1.1
  373 IF(AK.GT.20000.) GO TO 97
      GO TO 69
   70 IF(ECC)901,8,902
  902 AK=(AK/ 6.)*( 4.+2.*((CC-CS)/(TS+P-CT)))
      GO TO 903
  901 AK=(AK/12.)*(10.+2.*((CC-CS)/(TS+P-CT)))
  903 IF(AK.LT.-20000.) GO TO 97
      GO TO 69
   96 IF(AK.EQ.0.0)GO TO 97
      PHI= ECC/(AK*D)
      IF(KONG.EQ.2)GO TO 95
      IF(KODE-2)340,341,340
  341 IF(PHI-CR(I))97,97,95
  340 IF(PHI-CR(I))95,97,97
   95 BMTOT= (BMS+BMP-BMCC)
```

```
      IF(KOAX.EQ.1) GO TO 73
      IF(KOP-1) 73,74,73
   74 KOP=2
      P=PO+AXVAR*BMTOT
      KONV=1
      KOUNT=0
      FENA=500000.
      FENB=500000.
      GO TO 75
   73 ENERGY=ENERGY+.5*(BMTOT+BML)*(PHI-PHIL)
      BML=BMTOT
      PHIL=PHI
      BMOM=BMTOT/12000.
      CURV=PHI*1.E5
      THETA=CURV*HL
      DMOM=BMTOT/(8*C**2*FCD)
      DCURV=PHI*D
      ECB=E(NEL)+.5*(E(NEL)-E(NEL-1))
      WRITE(6,121)BMOM,CURV,THETA,DMOM,DCURV,AK,ECC,ECB,CC,ES(1),ES(NSP)
     1,TS,P,ENERGY
      N=N+1
      X(N)=-CURV
      Y(N)=-BMOM
C
C     UPDATE CONCRETE 'COUNTERS'
      DO 78 K=1,NEL
      IF(E(K)-ESP)78,78,80
   80 IF(MODEL-2) 78,201,78
  201 IF(K-IT) 81,81,82
   81 FW(K)=0.
      GO TO 78
   82 IF(K-IB) 83,81,81
   83 FW(K)=BDD
   78 CONTINUE
      DO 76 K=1,NEL
      ELAST(K)=E(K)
      IF(E(K)-EMAX(K)) 76,76,77
   77 EMAX(K)=E(K)
      FMAX(K)=F(K)
      IF(E(K)-EO)135,135,136
  135 YMF(K)=1.
      GO TO 137
  136 IF(E(K)-EO-E20C)138,138,139
  138 YMF(K)=.8-(E(K)-EO)*.7/(E20C-EO)
      GO TO 137
  139 YMF(K)=.1
  137 IF(FW(K).EQ.0.)GO TO 76
      EZERO(K)=EMAX(K)-FMAX(K)/(YMC*YMF(K)*FW(K))
   76 CONTINUE
      DO 84 J=1,NEL
      IF(E(J)-EZERO(J)+ER) 85,84,84
   85 FCRACK(J)=0.
   84 CONTINUE
      IF(KCKD.EQ.2) GO TO 86
      DO 87 J=1,NEL
      IF(FCRACK(J).EQ.1.0) GO TO 86
   87 CONTINUE
```



```
      KCKD=2
      WRITE(6,124)
C
C     UPDATE STEEL 'COUNTERS'
   86 DO 188 M=1,NSP
      IF(ES(M)-ESMAX(M)) 88,88,89
   89 ESMAX(M)=ES(M)
      FSMAX(M)=FS(M)
      ESMIN(M)=ESMAX(M)
      FSMIN(M)=FSMAX(M)
      IF(ESMAX(M)-.012)921,921,922
  922 YMSF(M)=1.-(ESMAX(M)-.012)*7.7
  921 IF(ESMAX(M)-.009)988,988,923
  923 WLV(M)=ESMAX(M)*.045
  988 ESUZO(M)=ESMAX(M)-FSMAX(M)/(YMS*YMSF(M))
      IF(ES(M)-ESU)187,190,190
  190 SFACT(M)=0.
      GO TO 187
   88 IF(ES(M)-ESLAS(M))363,363,187
  363 ESMIN(M)=ES(M)
      FSMIN(M)=FS(M)
      IF(ES(M)-ESUZO(M)+ESA)361,362,362
  362 UF(M)=1.
      GO TO 187
  361 UF(M)=2.
      ESLZO(M)=ES(M)-FS(M)/YMS
  187 ESLAS(M)=ES(M)
  188 CONTINUE
   97 KOP=1
      KOG=1
      KOUNT=0
      KONV=1
      AKA=0.
      AKB=0.
      IF(KONG.EQ.2) GO TO 8
      GO TO (13,11),KODE
    8 KONG=1
  801 CONTINUE
  101 FORMAT(F5.0,F6.4,F6.1,F6.4,I3,F8.6)
  102 FORMAT(F6.5,2F7.5,3F8.0,F7.5,I2)
  103 FORMAT(5F7.3,I4,I3,F7.3)
  104 FORMAT(12F6.4)
  105 FORMAT(I2,F7.0,F7.5)
  106 FORMAT('1ANALYSIS OF PRESTRESSED CONCRETE MEMBERS SUBJECTED TO CYC
     1LIC FLEXURAL LOADING'///////////////)
  107 FORMAT(' ',7X,'STEEL PROPERTIES',18X,'CONCRETE PROPERTIES',18X,'ME
     1MBER GEOMETRY',18X,'AXIAL LOAD'//////)
  108 FORMAT(' ','YOUNGS MODULUS =',F9.0,'PSI',7X,'CYLINDER STRENGTH =',
     1F5.0,'PSI',8X,'SECTION DEPTH =',F7.3,'INCHES',9X,'INITIAL LOAD =',
     2F7.0,'LBS')
  109 FORMAT(' ','UPPER BRANCH SLOPE =',F8.0,'PSI',4X,'PARAMETER Z =',F7
     1.1,15X,'SECTION WIDTH =',F7.3,'INCHES',9X,'FACTOR  =',F7.4)
  110 FORMAT(' ','ULTIMATE STRESS =',F7.0,' PSI',7X,'STRAIN AT MAX STRES
     1S =',F6.4,7X,'BOUND WIDTH =',F7.3,' INCHES')
  111 FORMAT(' ','STEEL RATIO =',F7.5,15X,'STRAIN AT .2 MAX STRESS =',F7
     1.5,3X,'DEPTH TO TOP CORE =',F7.3,' INCHES')
  112 FORMAT(' ','NUMBER OF TENDONS =',I3,13X,'CRUSHING STRAIN =',F6.4,1
```

```
     12X,'DEPTH TO BOT CORE =',F7.3,' INCHES')
  113 FORMAT(' ',35X,'STRAIN AT CRACKING =-',F7.6,7X,'NUMBER OF ELEMENTS
     1 =',I4)
  114 FORMAT(' ',35X,'YOUNGS MODULUS =',F9.0,' PSI',6X,'NUMBER OF READIN
     1GS =',I4)
  115 FORMAT(' ','STEEL AREAS',24X,'STRESS MODEL =',I2)
  116 FORMAT(' ','AREA',I2,' =',F6.4,' SQ INS')
  117 FORMAT('0','STEEL POSITIONS')
  118 FORMAT(' ','DEPTH',I2,' =',F6.4,'D')
  119 FORMAT(    '1 MOMENT',3X,'CURVATURE',4X,'ROTATION',2X,'M/BD**2*FCD'
     1,1X,'PHI*D',6X,'K',7X,'ECC',5X,'EC(B)',4X,'CC',7X,'ES(T)',4X,'ES(B
     2)',4X,'TS',7X,'P',5X,'ENERGY'//)
  120 FORMAT(' ','KIP FEET',1X,'RAD/IN*1.E-5',2X,'RAD*1.E-5',49X,'LBS',2
     14X,'LBS',5X,'LBS',3X,'LBS IN/IN'/////)
  121 FORMAT(' ',F8.3,F10.3,F11.1,F12.6,F9.5,F10.3,F9.6,F9.6,F8.0,2F9.6,
     1F9.0,F8.0,F11.3)
  122 FORMAT(F9.7)
  123 FORMAT(12F6.5)
  124 FORMAT(' ','SECTION CRACKED OVER WHOLE DEPTH')
C
C     PLOT THEORETICAL MOMENT-CURVATURE CURVES
      CALL AINIT(1000)
      CALL AGRID(45,96,14,16,65,38,2,3)
      CALL AGRID(46,399,1,1,908,2,1,2)
      CALL AGRID(824,97,1,1,2,606,1,2)
      CALL ASCA(75,385,65,0,-550,50,13,1,2)
      CALL ASCA(825,124,0,38,-140,20,7,1,2)
      CALL ASCA(770,438,0,38,20,20,7,1,2)
      LOGICAL*1 INAME1(35)/'CURVATURE, RADIANS PER INCH/100,COC'/
      CALL ALAB(111,365,INAME1,35,1,2)
      LOGICAL*1 INAME2(16)/'MOMENT, KIP FEET'/
      CALL ALAB(780,540,INAME2,16,1,4)
      LOGICAL*1 INAME3(41)/'THEORETICAL MOMENT CURVATURE RELATIONSHIP'/
      CALL ALAB(190,675,INAME3,41,1,2)
      CALL ACRIG(825,400)
      CALL ALINE(X,Y,N,0.0,0.0,76.923,52.631,1)
      CALL ACRIG(0,0)
      CALL AEND
      END
```

```
C     ****************************************************************
C
C     INELASTIC SEISMIC ANALYSIS OF SINGLE-DEGREE-OF-FREEDOM SYSTEM
C
C     ELASTO PLASTIC ANALYSIS
C
C     MARCH 1971
C
C     ****************************************************************
      DIMENSION  T(600),A(600),X(4000),TIME(4000),V(4000),RVW(4000)
C
C     READ SYSTEM PROPERTIES
      READ(5,101) PERIOD,XLAMDA,ADT,NCARD,CMAX,CMIN
      EK=39.51/(PERIOD**2)
      IF(PERIOD-0.44)90,90,91
   90 C=CMAX
      GO TO 95
   91 IF(PERIOD-1.20)92,93,93
   92 C=CMAX-(CMAX-CMIN)*(PERIOD-0.44)/.76
      GO TO 95
   93 C=CMIN
   95 BETA=1.43*C
      VY=BETA*386.04
      XY=VY/EK
C
C     READ DIGITIZED EARTHQUAKE RECORD
      NPOINT=4*NCARD-1
      DO 81 I=1,NCARD
      READ(5,102)NC,(T(4*I+K-4),A(4*I+K-4),K=1,4),INDEX
   81 CONTINUE
C
C     INPUT DATA LIST AND RESULTS HEADINGS
      WRITE(6,103)
      WRITE(6,104)
      WRITE(6,105)
      WRITE(6,106)PERIOD,XLAMDA,C,ADT,EK,VY,XY,BETA
      WRITE(6,107)
      WRITE(6,108)
      WRITE(6,109)INDEX,NCARD,T(NPOINT)
      WRITE(6,110)
      WRITE(6,111)
C
C     INITIALISE
      TIME(1)=0.
      XDDG=A(1)
      X(1)=0.
      RVW(1)=0.
      V(1)=0.
      XDD=-XDDG*386.04
      XD=0.
      STF=EK
      K=1
      I=1
      L=2
      NYCYC=0
      JL=1
      NM=1
```



```
      DT=ADT
      TIME(1)=0.
      XZERO=0.
      XLAS=0.
      X(1)=0.
      ENERGY=0.
      DAMPF=0.
      DAMPE=0.
      GO TO 8
C
C     COMMENCEMENT OF COMPUTATION
C
C     CALCULATE GROUND ACCELERATION
    1 I=I+1
      TIME(I)=TIME(I-1)+DT
      OK=K
      OXDDG=XDDG
   10 IF(K-562) 61,61,62
   62 XDDGN=0.
      GO TO 13
   61 IF(TIME(I)-T(K+1))3,3,2
    2 K=K+1
    3 IF(T(K).EQ.T(K+1))K=K+1
      XDDGN=A(K)+(A(K+1)-A(K))*(TIME(I)-T(K))/(T(K+1)-T(K))
   13 DELGA=(XDDGN-XDDG)*386.04
      XDDG=XDDGN
C
C     APPLY EQUATIONS OF DYNAMIC EQUILIBRIUM AND NUMERICAL INTEGRATION
   35 C1=12.57143*XLAMDA*DT/PERIOD
      Q=-DELGA-C1*XDD-STF*(XD*DT+XDD*DT*DT/2.)
      P=1.+C1/2.+STF*DT*DT/6.
      DELXDD=Q/P
      DELXD=XDD*DT+DELXDD*DT/2.
      DELX=XD*DT+XDD*DT*DT/2.+DELXDD*DT*DT/6.
      OXDD=XDD
      OXD=XD
      OV=V(I)
      XDD=XDD+DELXDD
      XD=XD+DELXD
      X(I)=X(I-1)+DELX
      V(I)=V(I-1)+STF*DELX
      DT=ADT
C
C     CORRECTIONS FOR CHANGE OF STIFFNESS DURING PRESENT INCREMENT
C     AND CALCULATION OF STIFFNESS FOR NEXT INCREMENT
      IF(L.EQ.1) GO TO 8
      IF(X(I)-XLAS) 4,4,5
C     POSITIVE LOADING OR NEGATIVE UNLOADING
    5 KD=1
      IF(X(I)-XZERO-XY) 6,6,7
    6 IF(STF.EQ.0.) GO TO 12
      STF=EK
      JL=1
      GO TO 8
   12 STF=EK
      NM=2
      JL=1
```

```
      XMAX=X(I-1)
      XDD=OXDD
      XD=OXD
      GO TO 35
C     POSITIVE DISPLACEMENTS BEYOND YIELD
    7 IF(JL-2) 31,32,31
   31 IF(X(I-1).LT.(XZERO+XY)) GO TO 9
   32 STF=0.
      KK=1
      JL=1
      GO TO 8
    9 XDT=DT*(XZERO+XY-X(I-1))/(X(I)-X(I-1))
   16 STF=EK
      OTIME=TIME(I)
      OXDDGN=XDDGN
      NK=K
      TIME(I)=TIME(I-1)+XDT
      K=OK
      DT=XDT
      XDDG=OXDDG
      XDD=OXDD
      XD=OXD
      V(I)=OV
      L=1
      GO TO 10
   11 GO TO (51,52),KD
   51 XYP=X(I)
      V(I)=VY
      GO TO 53
   52 XYN=X(I)
      V(I)=-VY
   53 STF=0.
      L=2
      JL=2
      I=I+1
      TIME(I)=OTIME
      XDDGN=OXDDGN
      K=NK
      DT=ADT-XDT
      GO TO 13
C     NEGATIVE LOADING OR POSITIVE UNLOADING
    4 KD=2
      IF(X(I)-XZERO+XY) 14,14,15
   15 IF(STF.EQ.0.) GO TO 12
      STF=EK
      JL=1
      GO TO 8
C     NEGATIVE DISPLACEMENTS BEYOND YIELD
   14 IF(JL-2) 33,34,33
   33 IF(X(I-1).GT.(XZERO-XY)) GO TO 19
   34 STF=0.
      KK=2
      JL=1
      GO TO 8
   19 XDT=DT*(XZERO-XY-X(I-1))/(X(I)-X(I-1))
      GO TO 16
    8 ENERGY=ENERGY+.5*(V(I)+V(I-1))*(X(I)-X(I-1))
```



```
      RVW(I)=V(I)/386.04
      ODAMPF=DAMPF
      DAMPF=ABS(XD*12.57143*XLAMDA/PERIOD)
      DISX=ABS(X(I)-X(I-1))
      DAMPE=DAMPE+.5*(DAMPF+ODAMPF)*DISX
      WRITE(6,112)TIME(I),XDDG,XDD,XD,X(I),STF,V(I),ENERGY,DAMPE,RVW(I),
     1I
C
C     UPDATE SYSTEM COUNTERS AND COMPUTE CYCLE DUCTILITY FACTORS
      XLAS=X(I)
      OXZERO=XZERO
      IF(NM-2) 22,23,22
   23 NM=1
      GO TO (25,24),KD
   24 XZERO=X(I-1)-XY
      DUCT=(XMAX-XYP)/XY+1.0
      NYCYC=NYCYC+1
      GO TO 26
   25 XZERO=X(I-1)+XY
      DUCT=(XYN-XMAX)/XY+1.0
      NYCYC=NYCYC+1
   26 WRITE(6,113) NYCYC,KK,OXZERO,XMAX,DUCT
   22 IF(TIME(I)-35.) 20,21,21
   20 GO TO (11,1),L
   21 CONTINUE
C
C     FORMAT STATEMENTS
  101 FORMAT(2F6.4,F10.8,I4,2F4.2)
  102 FORMAT(I3,4(F8.4,F9.6),I4)
  103 FORMAT('1INELASTIC SEISMIC ANALYSIS OF SINGLE DEGREE OF FREEDOM SY
     1STEM'///)
  104 FORMAT(' ','ELASTC PLASTIC ANALYSIS'//////)
  105 FORMAT(' ','SYSTEM PROPERTIES'///)
  106 FORMAT('OPERIOD              ='F6.4'SECONDS'/
     1       'ODAMPING RATIO     ='F6.4/
     2       'OCOEFFICIENT C     ='F6.4/
     3       'OTIME INTERVAL     ='F10.8'SECONDS'/
     4       'OELASTIC STIFFNESS ='F10.5'LBF/INCH'/
     5       'OYIELD STRENGTH    ='F10.5'LBF'/
     6       'OYIELD DISPLACEMENT='F10.5'INCHES'/
     7       'OBETA              ='F7.5//////)
  107 FORMAT(' ','EARTHQUAKE RECORD'///)
  108 FORMAT(' ','EL CENTRO, MAY 18 1940, N-S'//)
  109 FORMAT('OEARTHQUAKE RECORD NO.='I4/
     1       'OFIRST'I4'CARDS'/
     2       'OFIRST'F8.4'SECONDS'//////)
  110 FORMAT('1',2X,'TIME',5X,'GROUND ACCELN',2X,'ACCELERATION',2X,'VELO
     1CITY',2X,'DISPLACEMENT',2X,'STIFFNESS',4X,'FORCE',5X,'DISSIPATED-E
     2NERGY-DAMPING',5X,'V/W'///)
  111 FORMAT(' ',1X,'SECONDS',8X,'G',9X,'INS/SEC**2',4X,'INS/SEC',4X,'IN
     1CHES',7X,'LBF/INCH',5X,'LBF',16X,'LBF*INS/LBM'///)
  112 FORMAT(' ',F10.7,2X,F12.7,F12.7,2X,F11.7,2X,F12.8,2F11.6,2X,F11.3,
     13X,F11.3,2X,F8.6,1X,I5)
  113 FORMAT('0','NC YIELD CYCLES=',I3,'KK=',I2,5X,'PREVIOUS X AT ZERO L
     1OAD=',F8.5,'INCHES',5X,'MAX X FOR CYCLE=',F9.5,'INCHES',5X,'DUCTIL
     2ITY FACTOR=',F6.2)
      END
```

```
C     ****************************************************************
C
C     INELASTIC SEISMIC ANALYSIS OF SINGLE-DEGREE-OF-FREEDOM SYSTEM
C
C     DEGRADING STIFFNESS ANALYSIS
C
C     MARCH 1971
C
C     ****************************************************************
      DIMENSION T(600),A(600),X(4000),V(4000),TIME(4000),RVW(4000)
C
C     READ SYSTEM PROPERTIES
      READ (5,101)PERIOD,XLAMDA,ADT,CMAX,CMIN
      EK=39.51/(PERIOD**2)
      IF(PERIOD-0.44)90,90,91
   90 C=CMAX
      GO TO 95
   91 IF(PERIOD-1.20)92,93,93
   92 C=CMAX-(CMAX-CMIN)*(PERIOD-0.44)/.76
      GO TO 95
   93 C=CMIN
   95 BETA=1.43*C
      VY=BETA*386.04
      XY=VY/EK
C
C     READ DIGITIZED EARTHQUAKE RECORD
      NPOINT=4*NCARD-1
      DO 81 I=1,NCARD
      READ (5,102)NC,(T(4*I+K-4),A(4*I+K-4),K=1,4),INDEX
   81 CONTINUE
C
C     INPUT DATA LIST AND RESULTS HEADINGS
      WRITE (6,103)
      WRITE (6,104)
      WRITE (6,105)
      WRITE (6,106)PERIOD,XLAMDA,C,ADT,EK,VY,XY,BETA
      WRITE (6,107)
      WRITE (6,108)
      WRITE (6,109) INDEX,NCARD,T(NPOINT)
      WRITE (6,110)
      WRITE (6,111)
C
C     INITIALISE
      TIME(1)=0.
      X(1)=0.
      V(1)=0.
      RVW(1)=0.
      XDDG=A(1)
      XDD=-XDDG*386.04
      XD=0.
      STF=EK
      K=1
      I=1
      L=2
      NYCYC=0
      JL=1
      NM=1
```



```
      DT=ADT
      XZERON=0.
      XZEROP=0.
      XCYPN=-XY
      XCYPP=XY
      ENERGY=0.
      DAMPE=0.
      DAMPF=0.
      GO TO 8
C
C     COMMENCEMENT OF COMPUTATION
C
C     CALCULATE GROUND ACCELERATION
    1 I=I+1
      TIME(I)=TIME(I-1)+DT
      OK=K
      OXDDG=XDDG
   10 IF (K-562)61,61,62
   62 XDDGN=0.
      GO TO 13
   61 IF(TIME (I)-T(K+1))3,3,2
    2 IF(TIME(I)-T(K+2))750,750,751
  750 K=K+1
      GO TO 3
  751 IF(TIME(I)-T(K+3))752,752,753
  752 K=K+2
      GO TO 3
  753 K=K+3
    3 IF (T(K).EQ.T(K+1))K=K+1
      XDDGN=A(K)+(A(K+1)-A(K))*(TIME(I)-T(K))/(T(K+1)-T(K))
   13 DELGA = (XDDGN-XDDG)*386.04
      XDDG=XDDGN
C
C     APPLY EQUATIONS OF DYNAMIC EQUILIBRIUM AND NUMERICAL INTEGRATION
   35 C1=12.57143*XLAMDA*DT/PERIOD
      Q=-DELGA-C1*XDD-STF*(XD*DT+XDD*DT*DT/2.)
      P=1.+C1/2.+STF*DT*DT/6.
      DELXDD=Q/P
      DELXD=XDD*DT+DELXDD*DT/2.
      DELX=XD*DT+XDD*DT*DT/2.+DELXDD*DT*DT/6.
      OXDD=XDD
      OXD=XD
      OV=V(I)
      XDD=XDD+DELXDD
      XD=XD+DELXD
      X(I)=X(I-1)+DELX
      V(I)=V(I-1)+STF*DELX
      DT=ADT
C
C     CORRECTIONS FOR CHANGE OF STIFFNESS DURING PRESENT INCREMENT
C     AND CALCULATION OF STIFFNESS FOR NEXT INCREMENT
      IF (L.EQ.1.OR.L.EQ.3) GO TO 8
      IF (X(I)-X(I-1))4,4,5
    5 OKD=KD
C     POSITIVE LOADING OR NEGATIVE UNLOADING
      KD=1
      IF(X(I)-XCYPP) 6,6,7
```

```
    6 IF(CKD.NE.KD) GC TC 201
      IF(X(I)-XZERON) 40,40,41
  201 IF(V(I-1)-0.) 202,203,203
  202 XZERON=X(I-1)-V(I-1)/EK
      STFP=VY/(XCYPP-XZERON)
      GO TO 12
  203 STFP=(VY-V(I-1))/(XCYPP-X(I-1))
      STF=STFP
      GO TO 204
   40 STF=EK
      GO TO 8
   41 IF(JL-2) 44,45,44
   44 IF(X(I-1).LT.XZERON) GO TO 42
   45 STF=STFP
      JL=1
      GO TO 8
   42 XDT=DT*(XZERON-X(I-1))/(X(I)-X(I-1))
      L=3
   46 STF=EK
   78 OTIME=TIME(I)
      OXDDGN=XDDGN
      NK=K
      TIME(I)=TIME(I-1)+XDT
      K=OK
      DT=XDT
      XDDG=OXDDG
      XDD=OXDD
      XD=OXD
      V(I)=OV
      GO TO 10
   43 IF(KD-1)96,97,96
   97 STF=STFP
      GO TO 98
   96 STF=STFN
   98 V(I)=0.
   47 L=2
      JL=2
      I=I+1
      TIME(I)=OTIME
      XDDGN=OXDDGN
      K=NK
      DT=ADT-XDT
      GO TO 13
   12 IF(STF.EQ.0.) NM=2
      STF=EK
      XMAX=X(I-1)
  204 XDD=OXDD
      XD=OXD
C     DISPLACEMENT BEYOND CURRENT POSITIVE YIELD POINT
      GO TO 35
    7 IF(JL-2) 31,32,31
   31 IF(X(I-1).LT.XCYPP) GO TO 9
   32 STF=0.
      KK=1
      JL=1
      GO TO 8
    9 XDT=DT*(XCYPP-X(I-1))/(X(I)-X(I-1))
```



```
   16 STF=STFP
  220 L=1
      GO TO 78
   11 STF=0.
      GO TO 47
C     NEGATIVE LOADING OR POSITIVE UNLOADING
    4 OKD=KD
      KD=2
      IF(X(I)-XCYPN) 14,14,15
   15 IF(OKD.NE.KD) GO TO 210
      IF(X(I)-XZEROP) 70,70,71
  210 IF(V(I-1)-0.)211,212,212
  212 XZEROP=X(I-1)-V(I-1)/EK
      STFN=-VY/(XCYPN-XZEROP)
      GO TO 12
  211 STFN=(-VY-V(I-1))/(XCYPN-X(I-1))
      STF=STFN
      GO TO 204
   71 STF=EK
      GO TO 8
   70 IF(JL-2) 72,73,72
   72 IF(X(I-1).GT.XZEROP) GO TO 74
   73 STF=STFN
      JL=1
      GO TO 8
   74 XDT=DT*(XZEROP-X(I-1))/(X(I)-X(I-1))
      L=3
      GO TO 46
C     DISPLACEMENT BEYOND CURRENT NEGATIVE YIELD POINT
   14 IF(JL-2) 75,76,75
   75 IF(X(I-1).GT.XCYPN) GO TO 77
   76 STF=0.
      KK=2
      JL=1
      GO TO 8
   77 XDT=DT*(XCYPN-X(I-1))/(X(I)-X(I-1))
      STF=STFN
      GO TO 220
    8 ENERGY=ENERGY+.5*(V(I)+V(I-1))*(X(I)-X(I-1))
      RVW(I)=V(I)/386.04
      ODAMPF=DAMPF
      DAMPF=ABS(XD*12.57143*XLAMDA/PERIOD)
      DISX=ABS(X(I)-X(I-1))
      DAMPE=DAMPE+.5*(DAMPF+ODAMPF)*DISX
      WRITE(6,112)TIME(I),XDDG,XDD,XD,X(I),STF,V(I),ENERGY,DAMPE,RVW(I),
     1I
C
C     UPDATE SYSTEM COUNTERS AND COMPUTE CYCLE DUCTILITY FACTORS
      IF(NM-2) 22,23,22
   23 NM=1
      GO TO (24,25),KK
   24 XZEROP=X(I-1)-XY
      OXCYPP=XCYPP
      XCYPP=X(I-1)
      DUCT=(XCYPP-OXCYPP)/XY+1.0
      NYCYC=NYCYC+1
      GO TO 26
```

```
   25 XZERON=X(I-1)+XY
      OXCYPN=XCYPN
      XCYPN=X(I-1)
      DUCT=(OXCYPN-XCYPN)/XY+1.0
   26 WRITE(6,113)NYCYC,KK,XZERON,XZEROP,XCYPN,XCYPP,DUCT
   22 IF(TIME(I)-35.)20,21,21
   20 GO TO (11,1,43),L
   21 CONTINUE
C
C     FORMAT STATEMENTS
  101 FORMAT(2F6.4,F10.8,I4,2F4.2)
  102 FORMAT(I3,4(F8.4,F9.6),I4)
  103 FORMAT('1INELASTIC SEISMIC ANALYSIS OF SINGLE DEGREE OF FREEDOM SY
     1STEM'///)
  104 FORMAT(' ','DEGRADING STIFFNESS ANALYSIS'//////)
  105 FORMAT(' ','SYSTEM PROPERTIES'///)
  106 FORMAT('0PERIOD              =',F6.4'SECONDS'/
     1       '0DAMPING RATIO      ='F6.4/
     2       '0COEFFICIENT C      ='F6.4/
     3       '0TIME INTERVAL      ='F10.8'SECONDS'/
     4       '0ELASTIC STIFFNESS ='F10.5'LBF/INCH'/
     5       '0YIELD STRENGTH     ='F10.5'LBF'/
     6       '0YIELD DESPLACEMENT='F10.5'INCHES'/
     7       '0BETA               ='F7.5//////)
  107 FORMAT(' ','EARTHQUAKE RECORD'///)
  108 FORMAT(' ','EL CENTRO, MAY 18 1940, N-S'//)
  109 FORMAT('0EARTHQUAKE RECORD NO.='I4/
     1       '0FIRST'I4'CARDS'/
     2       '0FIRST'F8.4'SECONDS'//////)
  110 FORMAT('1',2X,'TIME',5X,'GROUND ACCELN',2X,'ACCELERATION',2X,'VELC
     1ICITY',2X,'DISPLACEMENT',2X,'STIFFNESS',4X,'FORCE',4X,'DISSIPATED-E
     2NERGY-DAMPING',5X,'V/W'///)
  111 FORMAT(' ',1X,'SECONDS',8X,'G',9X,'INS/SEC**2',4X,'INS/SEC',4X,'IN
     1CHES',7X,'LBF/INCH',5X,'LBF',16X,'LBF*INS/LBM'///)
  112 FORMAT(' ',F10.7,2X,F12.7,F12.7,2X,F11.7,2X,F12.8,2F11.6,2X,F11.3,
     13X,F11.3,2X,F8.6,1X,I5)
  113 FORMAT('0',NO. YIELD CYCLES=',I3,2X,'KK=',I2,5X,'XZERON=',F9.5,'X
     1ZEROP=',F9.5,2X,'XCYPN=',F9.5,2X,'XCYPP=',F9.5,2X,'DUCTILITY FACTC
     2R=',F6.2)
      END
```



```
C     ****************************************************************
C
C     INELASTIC SEISMIC ANALYSIS OF SINGLE-DEGREE-OF-FREEDOM SYSTEM
C
C     PRESTRESSED CONCRETE MODEL ANALYSIS
C
C     APRIL 1971
C
C     ****************************************************************
      DIMENSION T(600),A(600),X(4000),TIME(4000),V(4000),RVW(4000)
C
C     READ SYSTEM PROPERTIES
      READ(5,101)PERIOD,XLAMDA,ADT,NCARD,CMAX,CMIN,GAMMA1,GAMMA2,CLF,VLI
     1,VLO
      EK=39.51/(PERIOD**2)
      IF(PERIOD-0.44)90,90,91
   90 C=CMAX
      GO TO 95
   91 IF(PERIOD-1.20)92,93,93
   92 C=CMAX-(CMAX-CMIN)*(PERIOD-0.44)/.76
      GO TO 95
   93 C=CMIN
   95 BETA=1.43*C
      VU=BETA*386.04
      XCK=VU/(CLF*EK)
      XU=XCK+(VU-VU/CLF)/(GAMMA1*EK)
      STF1=GAMMA1*EK
      STF2=GAMMA2*EK
      VCK=VU/CLF
C
C     READ DIGITISED EARTHQUAKE RECORD
      NPOINT=4*NCARD-1
      DO 99 I=1,NCARD
      READ(5,102)NC,(T(4*I+K-4),A(4*I+K-4),K=1,4),INDEX
   99 CONTINUE
C
C     INPUT DATA LIST AND RESULTS HEADINGS
      WRITE(6,103)
      WRITE(6,104)
      WRITE(6,105)
      WRITE(6,106)PERIOD,XLAMDA,C,ADT,EK,STF1,STF2,VU,VCK,XCK,XU,BETA
      WRITE(6,107)
      WRITE(6,108)
      WRITE(6,109)INDEX,NCARD,T(NPOINT)
      WRITE(6,110)
      WRITE(6,111)
C
C     INITIALISE
      TIME(1)=0.
      X(1)=0.
      RVW(1)=0.
      V(1)=0.
      XDDG=A(1)
      XDD=-XDDG*386.04
      XD=0.
      STFI=EK
      STF=EK
```

```
      DLV=VLI
      STFINO=(2.*VCK-DLV*VU)/(2.*XCK)
      STFUPP=GAMMA1*EK
      STFLOW=GAMMA1*EK
      NCK=1
      K=1
      I=1
      L=2
      JL=1
      NM=1
      NDS=0
      NINTN=2
      NINTP=2
      NICYC=0
      DT=ADT
      XIIPP=XCK
      VIIPP=VCK
      XIIPN=-XCK
      VIIPN=-VCK
      XCIPP=XIIPP
      VCIPP=VIIPP
      XCIPN=XIIPN
      VCIPN=VIIPN
      ENERGY=0.
      DAMPE=0.
      DAMPF=0.
      XMP=XU
      XMN=-XU
      XCMPP=XU
      XCMPN=-XU
      STF1P=STF1
      STF1N=STF1
      NDSP=0
      NDSN=0
      GO TO 8
C
C     COMMENCEMENT OF COMPUTATION
C
C     CALCULATE GROUND ACCELERATION
    1 I=I+1
      TIME(I)=TIME(I-1)+DT
      OK=K
      OXDDG=XDDG
   10 IF(K-562)61,61,62
   62 XDDGN=0.
      GO TO 13
   61 IF (TIME(I)-T(K+1))3,3,2
    2 IF(TIME(I)-T(K+2))750,750,751
  750 K=K+1
      GO TO 3
  751 IF(TIME(I)-T(K+3))752,752,753
  752 K=K+2
      GO TO 3
  753 K=K+3
    3 IF(T(K).EQ.T(K+1))K=K+1
      XDDGN=A(K)+(A(K+1)-A(K))*(TIME(I)-T(K))/(T(K+1)-T(K))
   13 DELGA=(XDDGN-XDDG)*386.04
```



```
      XDDG=XDDGN
C
C     APPLY EQUATIONS OF DYNAMIC EQUILIBRIUM AND NUMERICAL INTEGRATION
   35 C1=12.57143*XLAMDA*DT/PERIOD
      Q=-DELGA-C1*XDD-STF*(XD*DT+XDD*DT*DT/2.)
      P=1.+C1/2.+STF*DT*DT/6.
      DELXDD=Q/P
      DELXD=XDD*DT+DELXDD*DT/2.
      DELX=XD*DT+XDD*DT*DT/2.+DELXDD*DT*DT/6.
      OXDD=XDD
      OXD=XD
      OV=V(I)
      XDD=XDD+DELXDD
      XD=XD+DELXD
      X(I)=X(I-1)+DELX
      V(I)=V(I-1)+STF*DELX
      DT=ADT
C
C     CORRECTIONS FOR CHANGE OF STIFFNESS DURING PRESENT INCREMENT
C     AND CALCULATION OF STIFFNESS FOR NEXT INCREMENT
C
      IF(L.NE.2)GO TO 8
      IF(X(I)-X(I-1))202,203,203
  203 IF(NCK.EQ.1.AND.X(I).LT.XIIPP)GO TO 233
      NCK=2
      IF(NDSP.EQ.1.OR.X(I).GT.XCMPP)GO TO 401
      IF(NDSN-1)265,401,265
C
C     STAGE 1.   POSITIVE LOADING OR NEGATIVE UNLOADING
C     (CURRENT INELASTIC POINT=INITIAL INELASTIC POINT)
C
C     INITIAL ELASTIC CYCLES
  233 STFINT=EK
      STF=STFINT
      GO TO 8
  265 OKD=KD
      KD=1
  406 IF(X(I)-XCIPP)204,204,205
  204 IF(X(I)-XCIPN)206,206,207
C     DISPLACEMENTS LESS THAN IIPN
  206 IF(OKD.NE.KD)GO TO 221
      STF=STFLOW
      GO TO 8
  221 STFLOW=(VCIPN+ DLV*VU-V(I-1))/(XCIPN-X(I-1))
      STF=STFLOW
      XMN=X(I-1)
      NM=2
      XDD=OXDD
      XD=OXD
      GO TO 35
C     DISPLACEMENTS BETWEEN IIPN AND IIPP
  207 IF(JL-2)232,239,232
  232 IF(X(I-1).LT.XCIPN)GO TO 222
  239 JL=1
      IF(NINTN.EQ.1)GO TO 228
      IF(OKD.NE.KD)GO TO 208
      STF=STFINT
```

```
      GO TO 8
  228 IF(JL-2)234,235,234
  234 IF(X(I)-XCINTN)229,229,230
  229 STF=STFINT
      GO TO 8
  235 STF=STFINT
      JL=1
      GO TO 8
  230 XDT=DT*(XCINTN-X(I-1))/(X(I)-X(I-1))
      STF=STFINT
      L=7
  607 OTIME=TIME(I)
      OXDDGN=XDDGN
      NK=K
      TIME(I)=TIME(I-1)+XDT
      K=OK
      DT=XDT
      XDDG=OXDDG
      XDD=OXDD
      XD=OXD
      V(I)=OV
      GO TO 10
  231 STFINT=STFINO
      STF=STFINT
      NINTN=2
   65 L=2
      JL=2
      I=I+1
      TIME(I)=OTIME
      XDDGN=OXDDGN
      K=NK
      DT=ADT-XDT
      GO TO 13
  208 XCINTP=X(I-1)
      VCINTP=V(I-1)
      NINTP=1
      STFINT=(VCIPP-VCINTP)/(XCIPP-XCINTP)
      STF=STFINT
      XDD=OXDD
      XD=OXD
      GO TO 35
  222 XDT=DT*(XCIPN-X(I-1))/(X(I)-X(I-1))
      STF=STFLOW
      L=6
      GO TO 607
  223 STFINT=STFINO
      STF=STFINT
      GO TO 65
C     DISPLACEMENTS GREATER THAN IIPP
  205 IF(JL-2)240,241,240
  240 IF(X(I-1).LT.XCIPP)GO TO 215
  241 JL=1
      IF(X(I)-XMP)216,217,217
  216 STF=STFUPP
      GO TO 8
  217 IF(JL-2)237,238,237
  237 IF(STFUPP.GT.STF1P)GO TO 219
```



```
      STF=STF1P
      GO TO 8
  238 STF=STF1P
      JL=1
      GO TO 8
  219 XDT=DT*(XMP-X(I-1))/(X(I)-X(I-1))
      STF=STFUPP
      L=5
      GO TO 607
  220 STFUPP=STF1P
      STF=STFUPP
      GO TO 65
  215 XDT=DT*(XCIPP-X(I-1))/(X(I)-X(I-1))
      STF=STFINT
      L=4
      GO TO 607
  214 STFUPP=STF1P
      STF=STFUPP
      KK=1
      NINTP=2
      GO TO 65
C
C     STAGE 1.  NEGATIVE LOADING OR POSITIVE UNLOADING
C     (CURRENT INELASTIC POINT=INITIAL INELASTIC POINT)
  202 IF(NCK.EQ.1.AND.X(I).GT.XIIPN)GO TO 233
      NCK=2
      IF(NDSN.EQ.1.OR.X(I).LT.XCMPN)GO TO 501
      IF(NDSP.EQ.1)GO TO 501
  365 OKD=KD
      KD=2
  506 IF(X(I)-XCIPN)305,304,304
  304 IF(X(I)-XCIPP)307,306,306
C     DISPLACEMENTS GREATER THAN IIPP
  306 IF(OKD.NE.KD)GO TO 321
      STF=STFUPP
      GO TO 8
  321 STFUPP=(V(I-1)-(VCIPP- CLV*VU))/(X(I-1)-XCIPP)
      STF=STFUPP
      XMP=X(I-1)
      NM=2
      XDD=OXDD
      XD=CXD
      GO TO 35
C     DISPLACEMENTS BETWEEN IIPP AND IIPN
  307 IF(JL-2)344,345,344
  344 IF(X(I-1).GT.XCIPP)GO TO 322
  345 JL=1
      IF(NINTP.EQ.1)GO TO 328
      IF(OKD.NE.KD)GO TO 308
      STF=STFINT
      GO TO 8
  328 IF(JL-2)334,335,334
  334 IF(X(I)-XCINTP)330,329,329
  329 STF=STFINT
      GO TO 8
  335 STF=STFINT
      JL=1
```

```
      GO TO 8
  330 XDT=DT*(XCINTP-X(I-1))/(X(I)-X(I-1))
      STF=STFINT
      L=8
      GO TO 607
  331 STFINT=STFINO
      STF=STFINT
      NINTP=2
      GO TO 65
  308 XCINTN=X(I-1)
      VCINTN=V(I-1)
      NINTN=1
      STFINT=(VCIPN-VCINTN)/(XCIPN-XCINTN)
      STF=STFINT
      XDD=OXDD
      XD=OXD
      GO TO 35
  322 XDT=DT*(XCIPP-X(I-1))/(X(I)-X(I-1))
      STF=STFUPP
      L=9
      GO TO 607
  323 STFINT=STFINO
      STF=STFINT
      GO TO 65
C     DISPLACEMENTS LESS THAN IIPN
  305 IF(JL-2)336,337,336
  336 IF(X(I-1).GT.XCIPN)GO TO 315
  337 JL=1
      IF(X(I)-XMN)317,317,316
  316 STF=STFLOW
      GO TO 8
  317 IF(JL-2)338,339,338
  338 IF(STFLOW.GT.STF1N)GO TO 319
      STF=STF1N
      GO TO 8
  339 STF=STF1N
      JL=1
      GO TO 8
  319 XDT=DT*(XMN-X(I-1))/(X(I)-X(I-1))
      STF=STFLOW
      L=10
      GO TO 607
  320 STFLOW=STF1N
      STF=STFLOW
      GO TO 65
  315 XDT=DT*(XCIPN-X(I-1))/(X(I)-X(I-1))
      STF=STFINT
      L=1
      GO TO 607
  314 STFLOW=STF1N
      STF=STFLOW
      KK=2
      NINTN=2
      GO TO 65
C
C     STAGE 2 AND 3.  XU EXCEEDED FOR POSITIVE DISPLACEMENTS
  401 OKD=KD
```



```
      KD=1
      IF(STF.EQ.STF2.AND.OKD.NE.KD)GO TO 403
      IF(X(I).LT.XCMPP)GO TO 406
      NDSP=1
      IF(JL-2)407,408,407
  407 IF(X(I-1).LT.XCMPP)GO TO 409
  408 JL=1
      STF=STF2
      GO TO 8
  409 XDT=DT*(XCMPP-X(I-1))/(X(I)-X(I-1))
      STF=STF1P
      L=3
      GO TO 607
   43 STF=STF2
      GO TO 65
  403 IF(NDSP-1)412,405,412
  412 XCMPN=X(I-1)
      IF(XCMPN+7.*XU)432,432,431
  431 XCIPN=XCMPN*(0.24-(XCMPN/XU)*0.09)
      GO TO 433
  432 XCIPN=0.8*XCMPN
  433 VCIPN=-.50*VU
      DLV=VLD
  423 XCMPN=X(I-1)
      VCMPN=V(I-1)
      XMN=X(I-1)
      NM=2
  411 STF1N=(VCIPN-VCMPN)/(XCIPN-XCMPN)
      STFLOW=(VCIPN+DLV*VU-VCMPN)/(XCIPN-XCMPN)
      STFINO=(VCIPP-VCIPN-DLV*VU)/(XCIPP-XCIPN)
      STF=STFLOW
      XDD=OXDD
      XD=OXD
      GO TO 35
  405 IF(XCMPP-7.*XU)441,441,442
  441 XCIPP=XCMPP*(.24+(XCMPP/XU)*.09)
      GO TO 443
  442 XCIPP=0.8*XCMPP
  443 VCIPP=.50*VU
      STF1P=(VCMPP-VCIPP)/(XCMPP-XCIPP)
      GO TO 412
C
C     STAGE 2 AND 3.  XU EXCEEDED FOR NEGATIVE DISPLACEMENTS
  501 OKD=KD
      KD=2
      IF(STF.EQ.STF2.AND.OKD.NE.KD)GO TO 503
      IF(X(I).GT.XCMPN)GO TO 506
      NDSN=1
      IF(JL-2)507,508,507
  507 IF(X(I-1).GT.XCMPN)GO TO 509
  508 JL=1
      STF=STF2
      GO TO 8
  509 XDT=DT*(XCMPN-X(I-1))/(X(I)-X(I-1))
      STF=STF1N
      L=3
      GO TO 607
```

```
  503 IF(NDSN-1)512,505,512
  512 XCMPP=X(I-1)
      IF(XCMPP-7.*XU)531,531,532
  531 XCIPP=XCMPP*(.24+(XCMPP/XU)*.09)
      GO TO 533
  532 XCIPP=XCMPP*.8
  533 VCIPP=.50*VU
      DLV=VLD
      XMP=X(I-1)
      VCMPP=V(I-1)
      NM=2
  511 STFIP=(VCMPP-VCIPP)/(XCMPP-XCIPP)
      STFUPP=(VCMPP-VCIPP+DLV*VU)/(XCMPP-XCIPP)
      STFINO=(VCIPP-VCIPN-DLV*VU)/(XCIPP-XCIPN)
      STF=STFUPP
      XDD=OXDD
      XD=OXD
      GO TO 35
  505 IF(XCMPN+7.*XU)542,542,541
  541 XCIPN=XCMPN*(.24-(XCMPN/XU)*.09)
      GO TO 543
  542 XCIPN=XCMPN*.8
  543 VCIPN=-.50*VU
  523 STFIN=(VCMPN-VCIPN)/(XCMPN-XCIPN)
      GO TO 512
    8 RVW(I)=V(I)/386.04
      ENERGY=ENERGY+.5*(V(I)+V(I-1))*(X(I)-X(I-1))
      ODAMPF=DAMPF
      DAMPF=ABS(XD*12.57143*XLAMDA/PERIOD)
      DISX=ABS(X(I)-X(I-1))
      DAMPE=DAMPE+.5*(DAMPF+ODAMPF)*DISX
      WRITE(6,112)TIME(I),XDDG,XDD,XD,X(I),STF,V(I),ENERGY,DAMPE,RVW(I),
     1I
C
C     UPDATE SYSTEM COUNTERS AND COMPUTE CYCLE DUCTILITY FACTORS
      IF(NM-2)22,23,22
   23 NM=1
      GO TO (24,25),KK
   24 DUCT=XMP/XCK
      XMAX=XMP
      NICYC=NICYC+1
      GO TO 26
   25 DUCT=-XMN/XCK
      XMAX=XMN
      NICYC=NICYC+1
   26 WRITE(6,113)NICYC,KK,XMAX,XCMPN,XCMPP,DUCT
   22 IF(TIME(I)-10.)20,21,21
   20 GO TO (314,1,43,214,220,223,231,331,323,320),L
   21 CONTINUE
C
C     FORMAT STATEMENTS
  101 FORMAT(2F6.4,F10.8,I4,2F4.2,2F8.5,F7.4,2F5.3)
  102 FORMAT(I3,4(F8.4,F9.6),I4)
  103 FORMAT('1INELASTIC SEISMIC ANALYSIS OF SINGLE DEGREE OF FREEDOM
     1SYSTEM'///)
  104 FORMAT(' ','PRESTRESSED CONCRETE MODEL ANALYSIS'///////)
  105 FORMAT(' ','SYSTEM PROPERTIES'///)
```



```
  106 FORMAT('0PERIOD            ='F6.4'SECONDS'/
     1'0DAMPING RATIO     ='F6.4/
     2'0CCEFFICIENT C     ='F6.4/
     3'0TIME INTERVAL     ='F10.8'SECONDS'/
     4'0ELASTIC STIFFNESS ='F10.5'LBF/INCH'/
     5'0STIFFNESS 1       ='F10.5'LBF/INCH'/
     6'0STIFFNESS 2       ='F10.5'LBF/INCH'/
     7'0ULTIMATE STRENGTH ='F10.5'LBF/LBM'/
     8'0CRACKING STRENGTH ='F10.5'LBF/LBM'/
     9'0CRACK DISPLACEMENT='F10.5'INCHES'/
     1'0MAX M DISPLACEMENT='F10.5'INCHES'/
     2'0BETA              ='F7.5//////)
  107 FORMAT(' ','EARTHQUAKE RECORD'///)
  108 FORMAT(' ','EL CENTRO, MAY 18  1940, N-S'//)
  109 FORMAT('0EARTHQUAKE RECORD NO.='I4/
     1'0FIRST'I4'CARDS'/
     2'0FIRST'F8.4'SECONDS'//////)
  110 FORMAT('1',2X,'TIME',5X,'GROUND ACCELN',2X,'ACCELERATION'
     1 ,2X,'VELOCITY',2X,'DISPLACEMENT',2X,'STIFFNESS',4X,'FORCE',5X,'DI
     2SSIPATED-ENERGY-DAMPING',5X,'V/W'///)
  111 FORMAT(' ',1X,'SECONDS',8X,'G',9X,'INS/SEC**2',4X,'INS/SEC',4X,'IN
     1CHES',7X,'LBF/INCH',5X,'LBF',16X,'LBF*INS/LBM'///)
  112 FORMAT(' ',F10.7,2X,F12.7,F12.7,F12.7,2X,F11.7,2X,F12.8,2F11.6,2X,F11.3,
     13X,F11.3,2X,F8.6,1X,I5)
  113 FORMAT('0','NO. INELASTIC CYCLES=',I3,2X,'KK=',I2,5X,'MAX. X FOR C
     1YCLE=',F9.5,2X,'XCMPN=',F9.5,2X,'XCMPP=',F9.5,2X,'DUCTILITY FACTOR
     2=',F6.2)
C
C      PLOT DISPLACEMENT RESPONSE
       CALL AINIT(1200)
       CALL AGRID(200,200,35,7,24,40,1,1)
       CALL AGRID(200,480,35,7,24,40,1,1)
       CALL AORIG(200,480)
       CALL ALINE(TIME,X,I,0.0,0.0,4.166667,2.50,1)
       CALL AORIG(0,0)
       CALL AEND
C      PLOT FORCE DISPLACEMENT CHARACTERISTICS
       CALL AINIT(1200)
       CALL AGRID(202,149,7,7,64,43,1,1)
       CALL AGRID(650,149,7,7,64,43,1,1)
       CALL AGRID(202,450,7,7,64,43,1,1)
       CALL AGRID(650,450,7,7,64,43,1,1)
       CALL AORIG(650,450)
       CALL ALINE(X,RVW,I,0.0,0.0,1.5625,.0465116,1)
       CALL AORIG(0,0)
       CALL AEND
       END
```

APPENDIX B

MATERIALS, EQUIPMENT AND TESTING PROCEDURE FOR BEAM-COLUMN TESTS

B.1 MATERIALS

The precast elements were manufactured at the prefabricating yard of Certified Concrete Limited, Christchurch, under the close supervision of the author. The properties of the component materials are summarised in Tables B.1 and B.2. Other details were as follows:

B.1.1 Concrete

(a) Mix Properties

The concrete used in all elements was a standard mix with a design strength of 5500 psi at 28 days. A graded aggregate with $\frac{3}{4}$" maximum size was used. The aggregate was Waimakariri River gravel, which is a well-rounded greywacke stone. Rapid hardening Portland Cement was used. The mix proportions by weight were:

aggregate : cement : water = 4.57 : 1 : 0.43

The slumps obtained for the mix were $1\frac{5}{8}$" to $1\frac{7}{8}$".

(b) Control Specimens

For each element, five 6" diameter x 12" cylinders, three 6" cubes, and three 12" x 3" x 3" modulus of rupture prisms were cast in machined steel forms. The concrete was tamped according to standard ASTM C31-62T[88] compaction. The control specimens were tested immediately after the beam-column experiments, the test procedure complying with ASTM C39-64[89] and ASTM C78-64[90]. The cylinders were capped with plaster at both ends. Four of the five cylinders for each element were loaded at 2000 psi/minute to failure. The fifth cylinder was loaded in increments to determine the stress-strain characteristics of the concrete. Strains were read by demountable mechanical (Demec)

CONCRETE PROPERTIES AT TIME OF TESTING

UNIT No.		AGE days	CYLINDER STRENGTH f'_c psi	COEFF. OF VARIATION in f'_c %	CUBE STRENGTH u psi	COEFF. OF VARIATION in u %	MODULUS OF RUPTURE f'_t psi	COEFF. OF VARIATION in f'_t %
1	Beam	177	6630	5.5	8510	1.61	820	7.4
	Column	182	6570	4.8	8950	0.24	948	2.1
	Mortar	62-77	11,200	1.9	11,600	1.24	1210	8.6
2	Beam	290	6000	1.3	7870	3.48	760	11.8
	Column	266	8300	3.9	11,160	1.76	990	8.2
	Mortar	20-41	10,100	2.0	11,620	1.29	650	4.4
3	Beam	368	7640	4.4	9520	1.14	830	0.1
	Column	368	7640	4.4	9520	1.14	830	0.1
	Mortar	18-38	9130	3.2	12,130	1.32	820	2.4
4	Beam	545	7500	1.5	10,030	0.87	800	8.8
	Column	516	8080	5.6	11,550	1.12	1160	1.9
	Mortar	66-83	9560	3.6	11,760	1.30	870	0.4

Table B.2

STEEL PROPERTIES

Unit No.	Prestressing Steel									Transverse Reinforcement					
	0.276" Dia. Wire			0.200" Dia. Wire			$\frac{3}{8}$" Dia. Strand			$\frac{3}{8}$" Dia. Beam Stirrups		$\frac{3}{8}$" Dia. Column Ties		$\frac{5}{8}$" Dia. Hoops	
	Mod.of Elast. E_s $\times 10^6$ psi	0.2% Proof Stress psi	Ult. Stress f'_s psi	Mod.of Elast. E_s $\times 10^6$ psi	0.2% Proof Stress psi	Ult. Stress f'_s psi	Mod.of Elast. E_s $\times 10^6$ psi	0.2% Proof Stress psi	Ult. Stress f'_s psi	Mod.of Elast. E_s $\times 10^6$ psi	Yield Stress f_y psi	Mod.of Elast. E_s $\times 10^6$ psi	Yield Stress f_y psi	Mod.of Elast. E_s $\times 10^6$ psi	Yield Stress f_y psi
1	28.0	213,300	242,200	29.2	227,000	259,600	29.3	237,500	270,000	30.6	49,200	30.3	49,400	——	——
2	29.5	229,500	258,000	28.9	226,500	255,600	29.7	235,400	268,400	30.2	49,100	30.1	49,700	29.8	41,900
3	29.0	224,300	254,500	29.0	233,000	259,500	29.5	238,500	271,000	29.5	48,500	30.3	49,200	——	——
4	29.8	232,200	262,800	29.5	229,200	257,500	30.0	238,000	271,500	30.7	49,800	30.0	49,000	30.5	42,300

Note: (1) Ultimate steel strain, ϵ_{su}, was in the range: 0.03 to 0.04 for $\frac{3}{8}$" dia. prestressing strand

0.04 to 0.06 for 0.276" and 0.200" dia. prestressing wire

(2) For mild steel: mean ultimate stress, f'_s = 69,500 psi for $\frac{3}{8}$" dia. bars

f'_s = 65,200 psi for $\frac{5}{8}$" dia. bars

: ratio of strain at commencement of strain hardening, ϵ_{sh}, to yield strain = 10 to 16, for all bars.

: yield stress of $\frac{1}{4}$" dia. ties in anchor block, f_y = 54,000 psi

gauges from stainless steel buttons fixed to the surface of the cylinder. The Demec gauge readings were taken at four equal intervals around the circumference of the cylinders (to compensate for any eccentricity of load) on 4" gauge lengths at the mid-height of the cylinder. The cubes were uncapped, and were also loaded at 2000 psi/minute to failure. The modulus of rupture specimens were tested very slowly. The 12" x 3" x 3" prisms were simply supported over 9", point loads being applied 3" from the supports.

The results of the concrete control specimen tests in Table B.1 are the same for both beam and column only in Unit 3, as for all other units separate control specimens were made because the elements were not cast simultaneously.

B.1.2 Steel

(a) Prestressing Steel

Three sizes of prestressing tendons were used: 0.276" diameter wires, 0.200" diameter wires, and $\frac{3}{8}$" diameter strands. The prestressing wire was stress-relieved cold drawn wire with a minimum ultimate tensile stress of 100 tsi and a 0.2% proof stress of 85 tsi. The prestressing strand was stress relieved 7 wire strand, with a minimum breaking load of 21,000 lb for $\frac{3}{8}$" diameter strand. All prestressing steel complied with NZSR 32:1968[91]. It was ensured that all wire and strand was free from oil, grease or dirt, but slight rusting was allowed. Test specimens, 18" in length, were cut from surplus steel of all prestressing wires or strands after stressing. Thus the properties of every tendon in each unit could be determined. Values of ultimate tensile strength were determined from tension tests, the mean strength for each element being given in Table B.2. In addition, stress-strain curves were found for selected steel specimens using a Baty mechanical extensometer on a 2" gauge length, and an Avery 25,000 lb Universal Testing Machine Type

7109DCJ. Values of 0.2% proof stress were determined from the curves. Fig. B.1 shows the shape of the stress-strain curves for the three types of prestressing steel used. The extensometer was removed before fracture for protection and consequently the curves of Fig. B.1 are not plotted to fracture. Although the steel strain at fracture, ϵ_{su}, could not be determined accurately the approximate range of ϵ_{su} is included in Table B.2.

(b) Transverse Reinforcement

The principal transverse reinforcement used in the test specimens consisted of $\frac{3}{8}$" diameter stirrups and ties, and $\frac{5}{8}$" diameter rectangular spirals. In all cases plain bars were used, which complied with NZSS 197:1949[92]. Two 12" long specimens were taken from every length of reinforcement bar used. For each element one specimen was used to determine stress-strain characteristics. The specimen was machined to reduce the diameter over a 2" length to ensure that yield occurred within the gauge length of the Baty extensometer. The remainder of the specimens for a particular element were tested undisturbed in tension to obtain the yield and ultimate strengths, which are given in Table B.2.

B.1.3 Mortar

(a) Mix Properties

The mortar used to form the joints between the precast beam and column elements was designed to have a strength at least that of the surrounding elements. The mix comprised graded sand with 3/16" maximum size to NZSS 2129:1967[93], and rapid hardening Portland Cement.

The mix proportions by weight were:

sand : cement : water = 2 : 1 : 0.35.

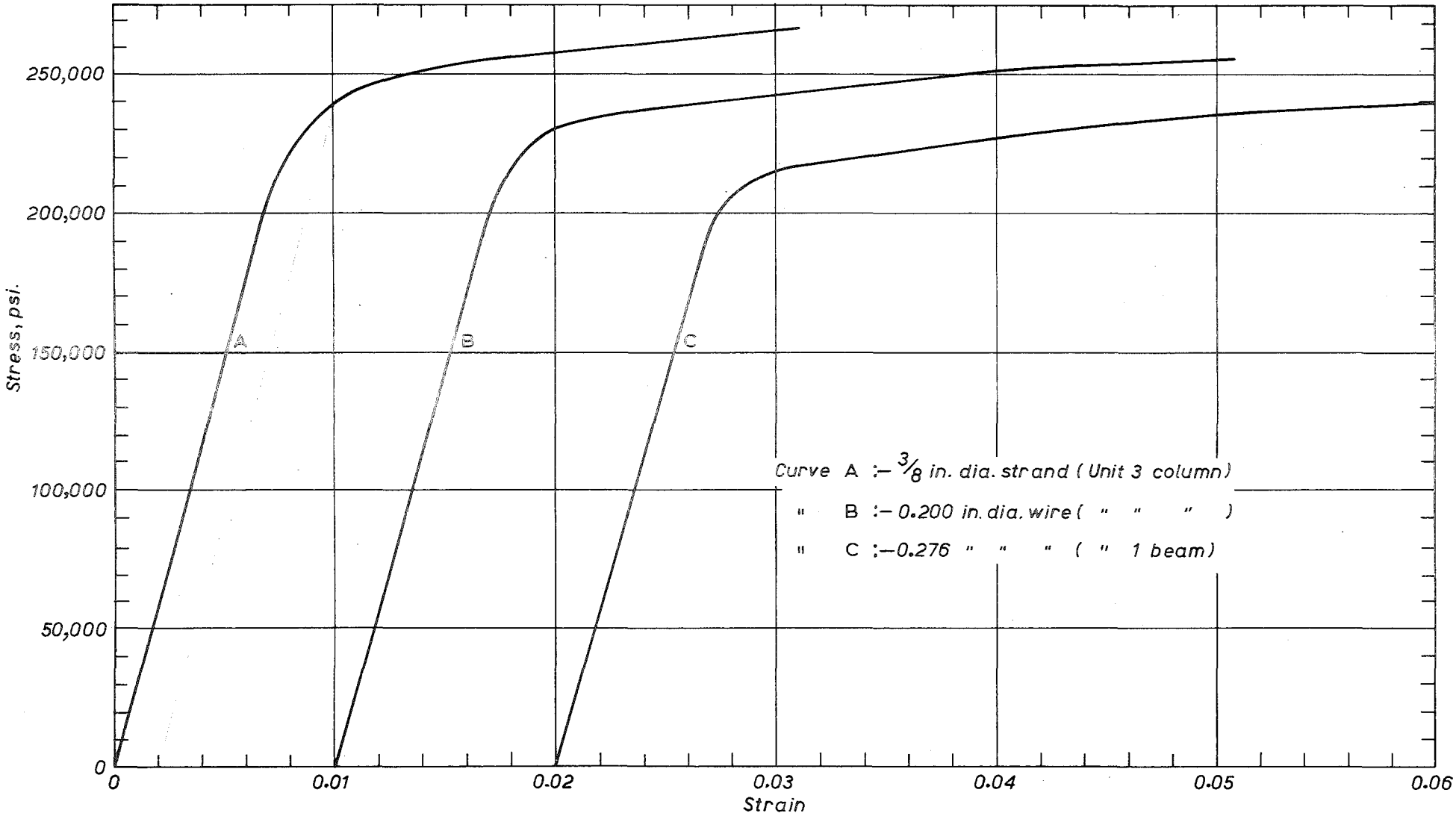

FIG. B.1 : PRESTRESSING STEEL STRESS – STRAIN CURVES

(b) Control Specimens

The mortar control specimens cast for each unit were: seven 4" diameter x 8" cylinders, three 6" cubes, and three 12" x 3" x 3" modulus of rupture prisms. Because the mortar was too dry to meaningfully apply the ASTM C31-62T[88] standard compaction, it was rammed into the moulds with wooden rammers in a similar manner to the compaction of the actual joint. Since the beam-column experiments extended over two to three weeks, and the mortar joints were formed only three weeks previously, it was felt necessary to test two cylinders before, two during and two after the experiment (plus one cylinder to determine the stress-strain characteristics). This procedure was not necessary for the beam and column control specimens because the concrete in these elements was much older than the mortar of the joints. The testing details for the mortar control specimens were the same as those already described for the beam and column control specimens.

B.1.4 Grout

After completion of stressing the post-tensioning cables were grouted. The grout proportions by weight were:

cement : water : Intraplast A Additive = 1 : 0.40 : 0.01

The cable ducts were sealed under at least 50 psi pressure.

B.2 UNIT MANUFACTURE

B.2.1 Forming Rectangular Spirals

For the columns of Units 2 and 4, where heavy transverse reinforcement was required, it was decided to use rectangular spirals rather than close ties. In these cases the transverse steel requirements (based on half the SEAOC code[51] volume of hooping) were two interlocking spirals of $\frac{5}{8}$" diameter bars at $2\frac{3}{4}$" pitch with a maximum leg length of $8\frac{1}{4}$". If closely spaced ties had been used the congestion arising from projection of the legs of the hooks into the interior of the column would have been

prohibitive.

The jig used for bending the spirals is shown in Fig. B.2. It consisted of a vertical rectangular hollow section for flexural resistance, surrounded by four 1" diameter high tensile bars to give the required radius at the corners of the spiral. The spirals were bent manually from 20 feet lengths of plain $\frac{5}{8}$" diameter bars, with welded splices between successive bars. In Fig. B.2 it may be seen where the pitch has been increased at two points to allow the beam post-tensioning cables to pass through the spiral.

B.2.2 Casting Members

(a) Preparation

The moulds for the beams of Units 1 and 2 are shown prior to casting in Fig. B.3. A concrete retarding agent was placed on the mould surfaces at regions of the elements which would form interfaces with the mortar joints. Thus after setting, the concrete in these areas could be brushed to provide a roughened surface to enhance bond.

The pretensioning forces in the $\frac{3}{8}$" dia. strands shown in the beams, and the strands and wires in the column were determined from the hydraulic jacking system, and verified by measurement of tendon extensions.

(b) Placing

Two beam elements, two column elements, and two anchor blocks were cast at a time. All units were cast horizontally, the beams on their sides and the columns on the end of the section. The concrete was compacted by immersion-type vibrators.

(c) Curing

Following concrete placement, the elements and control specimens were steam cured overnight with a maximum temperature of 175 degrees Celsius. In accordance with normal procedure at the stressing yard, four extra 4" diameter x 8" cylinders were cast and cured with the

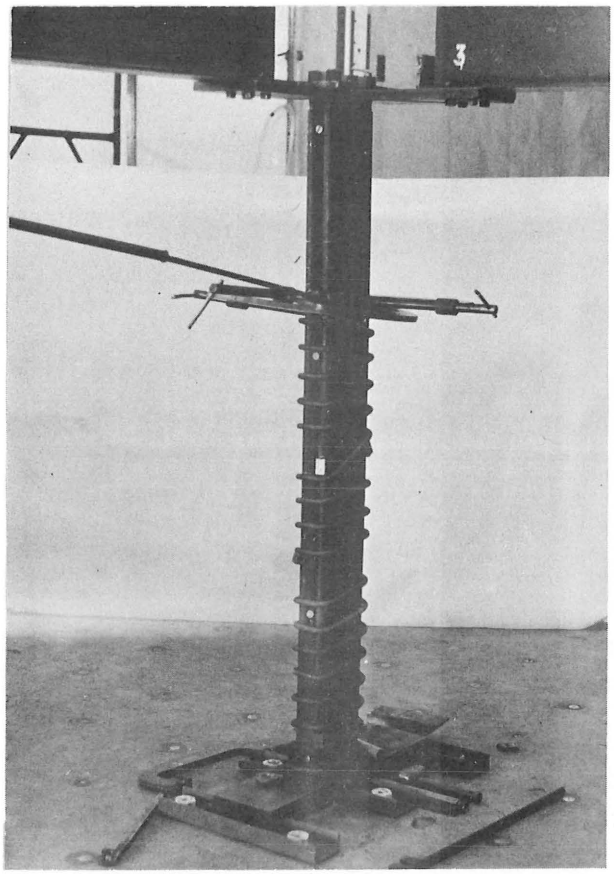

FIG. B.2 : RECTANGULAR SPIRALS RIG

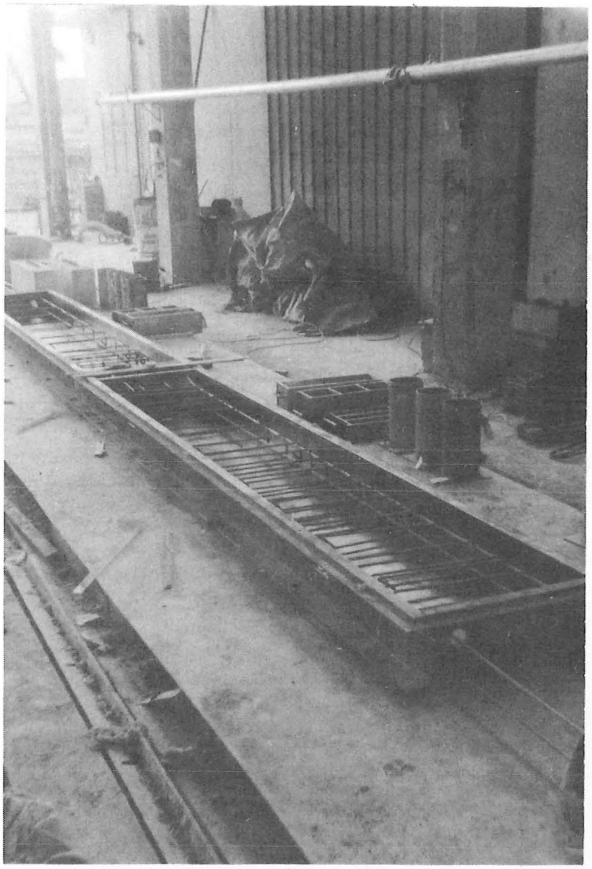

FIG. B.3 : BEAM MOULDS

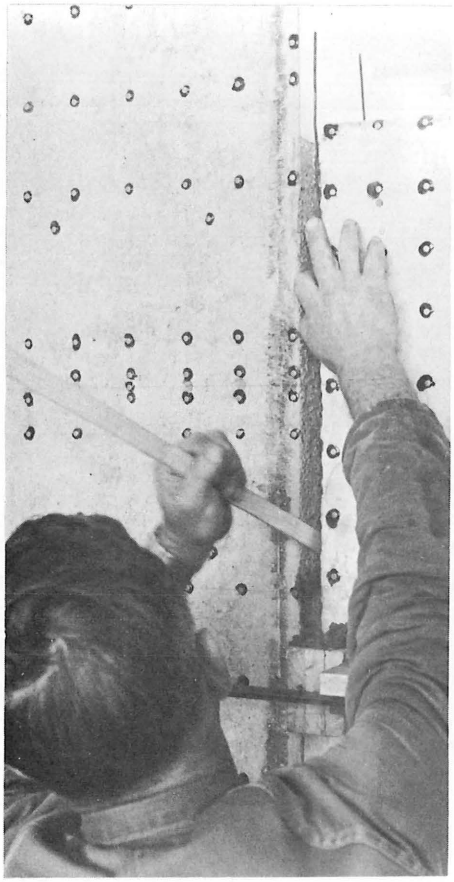

FIG. B.4 : COMPACTING MORTAR JOINT

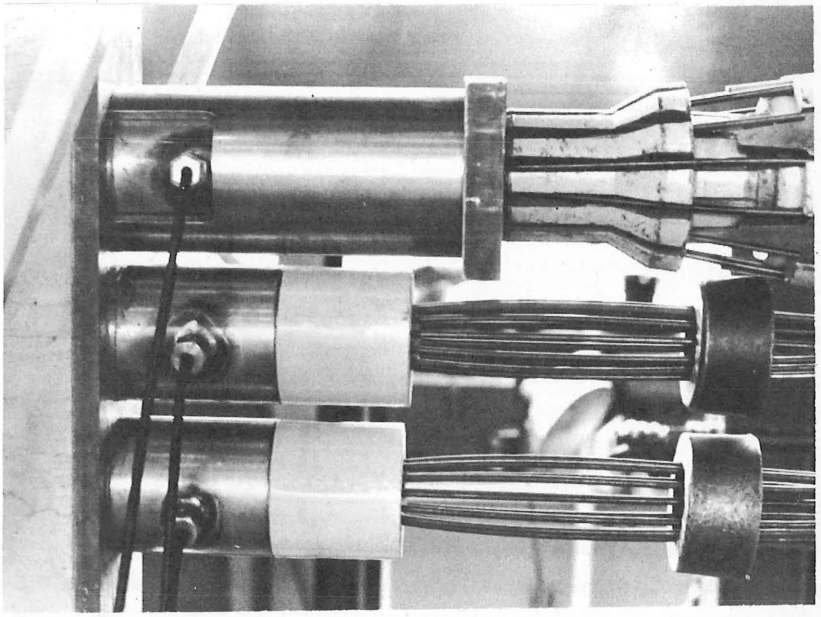

FIG. B.5 : STRESSING PROCEDURE

elements. These were used to check that the strength of the concrete was a minimum of 4,500 psi before transfer of the pretensioning force. If the concrete did not achieve the required strength after overnight steam curing, the surfaces of the elements and control specimens were kept moist until adequate strength was attained.

B.2.3 Forming Mortar Joint

The precast beam and column elements were assembled in the laboratory in preparation for forming the mortar joints.

(a) Depth of Roughening

An indication was required of the depth of roughening at the interfaces of the column, beam, and anchor block for the mortar joints in each unit. Accordingly, ten random measurements were made with vernier calipers of the depths of the interstices on each interface. The average depth for all units was approximately 1/16".

(b) Placing Mortar

The one inch thick mortar joints were "moist packed" according to NZSR 32:1968[91]. For each unit two joints were formed, one between the beam and the column and the other between the column and the anchor block. After mixing, the mortar was spread out on a mixing tray and allowed to hydrate until the mortar almost crumbled on being disturbed but on being reworked was easily remoulded by hand. The mortar was then hand rammed by wooden rammers to completely fill the joint. The side and bottom joint formwork was so placed to give the required $\frac{1}{2}$" recess. Fig. B.4 shows the ramming of the bottom mortar from the side of the joint. The formwork on that side was raised as the filling proceeded, to facilitate compaction. This was especially necessary for the joints in which a $\frac{1}{8}$" diameter wire stirrup was placed to provide internal binding for the joint. When the joint was nearly filled the upward legs of the wire stirrup shown in Fig. B.4 were bent over at the top

and covered with compacted mortar. Finally, the formwork was removed, the mortar surface tooled, and a small prestress applied to both help the bonding of the mortar to the faces of the elements and to eliminate shrinkage effects.

(c) Curing

After forming the joints, wet cloths were wrapped around to prevent loss of moisture from the mortar. The joints were kept damp until they had gained sufficient strength for the full post-tensioning force to be applied, that is until a strength exceeding twice the stress to be placed on the joint by the prestress was achieved.

(d) Effectiveness of Compaction

Although it may be preferable to include a wire stirrup in the joint to prevent loss of material under seismic load reversals, it is more difficult to achieve good compaction in this case than for an unbound joint. Even with the care taken in the laboratory, the compaction of the internally bound Unit 2 joint did not appear, after testing, to be as good as the unbound Unit 1 joint. This problem would be overcome if the joint is externally enclosed, but this may not be desirable from an architectural viewpoint.

B.2.4 Post-Tensioning Procedure

There were two special procedures required in the post-tensioning of the beams. Firstly, in Units 1 and 2 it was necessary to prestress in stages, because the configuration of two prestressing cables near the top and bottom of the section resulted in induced tensile stresses in the member on prestressing of the first cable. The following procedure was followed to minimise the opening of the mortar joint during prestressing. The bottom cable was first tensioned to half the maximum stressing load and anchored. The top cable was then fully prestressed, followed by full prestressing of the bottom cable. This procedure was

not necessary for Units 3 and 4. In these cases the central cable in the beam was fully prestressed first, and thereafter the effect of the eccentric force of the next cable stressed was not sufficient to cause tension stresses in the member.

A second problem arose from the large effect of cable slip at anchorage for the short beam lengths of the test specimens. For example, a slip of $\frac{1}{4}$" at anchorage of the cable would result in a 23% loss of prestressing force. Therefore it was necessary to compensate for this loss in order to achieve the required design stresses. Firstly, the cables were fully prestressed to the maximum allowable stress of 0.75 of the ultimate tensile strength, this being the elastic limit on the stress-strain curves for the prestressing steel. The cable forces were measured with 50-ton hollow cylindrical load cells. The loss of force on anchorage was then measured, and the required further extension of the cable to achieve design stresses was calculated. The ensuing procedure may be described with reference to Fig. B.5. A cylinder was fitted over the load cells and anchorages to bear on the beam end-plate. The wires of the cable were once more gripped in the prestressing jack and pulled back by the jack acting on the head of the cylinder. Since the anchorage and load cell moved back with the wires, brass shims of the required width could then be fitted between the load cell and the beam end-plate. A range of shims of thicknesses from 2 S.W.G. to 20 S.W.G. were prepared to cover the range of packing likely to be required. At the stage shown in Fig. B.5 the central cable had been packed first, the packing procedure has just been completed on the top cable, and the bottom cable has yet to be packed.

B.3 DESIGN STRESSES

The design stresses of the prestressing steel and concrete were chosen to repeat the final prestressing tendon forces and concrete stresses in the members of the prototype structure.

The available stresses in the prestressing steel were determined on the basis of a maximum allowable stress of $0.70f'_s$, where f'_s is the minimum specified ultimate tensile stress for the tendon. The design stresses in the tendons immediately after transfer were as follows:

0.276" dia. wire, f_s = 149,300 psi

0.200" dia. wire, f_s = 143,800 psi

$\frac{3}{8}$" dia. strand, f_s = 169,000 psi

The design compressive stresses in the concrete due to prestress immediately after transfer were as follows:

Beams: f_c = 1680 psi for Units 1 and 2

f_c = 1565 psi for Units 3 and 4

Columns: f_c = 1035 psi for all units.

B.4 THEORETICAL MAXIMUM MOMENT CAPACITIES

The theoretical maximum moment capacities were calculated by a general analysis ensuring compatibility of strains and equilibrium of forces. The compressive stress block parameters and maximum concrete strains found by Hognestad, Hanson and McHenry[68] were used to determine the stress resultant of the concrete, and the prestressing steel forces were found from actual stress-strain curves for the steel. The ultimate moments determined for nominal cylinder strengths were:

Beam section of Units 1 and 2: 174.3 kip ft., for f'_c = 6000 psi

Beam section of Units 3 and 4: 378.5 kip ft., for f'_c = 7500 psi

Column section of all Units: 105.6 kip ft., for axial load of 50 kips

120.7 kip ft., for axial load of 120 kips

(f'_c = 8000 psi in both cases)

The nominal cylinder strengths used were close to the actual cylinder strengths (see Table B.1) and the nominal column axial loads

considered were approximately the axial loads at the critical sections of Units 3 and 4. Fig. B.6 shows the interaction diagram for the columns determined from this analysis, giving the flexural strength of the column section for the range of possible axial loads.

A comparison is made in Table B.3 of the experimental maximum moments, analytically determined maximum moments from the analyses of Chapters 4 and 5, and the above theoretical moments from the stress block parameters of Hognestad, et al.

Table B.3

COMPARISON OF THEORETICAL AND EXPERIMENTAL STRENGTHS

Unit	Experimental Moment kip ft.	Analytical Moment* kip ft.	Theoretical Moment** kip ft.
Unit 1, beam	183.9	189.0	174.3
Unit 2, beam	195.2	189.5	174.3
Unit 3, upper col.	135.7	133.1	120.7
Unit 3, lower col.	115.7	114.5	105.6
Unit 4, upper col.	148.1	140.2	120.7
Unit 4, lower col.	119.2	116.4	105.6

*From analyses of Chapters 4 and 5

**From stress block parameters[68]

Clearly the analyses of Chapters 4 and 5 closely represented the experimental strengths, but the determination of maximum moment from stress block parameters gave conservative results. Comparison of the two theoretical approaches shows that the conservative results of the latter arise firstly to a small extent from the greater surface strains in the concrete at maximum moment than the limits given, but mainly because the neutral axis depth at maximum moment was smaller than that

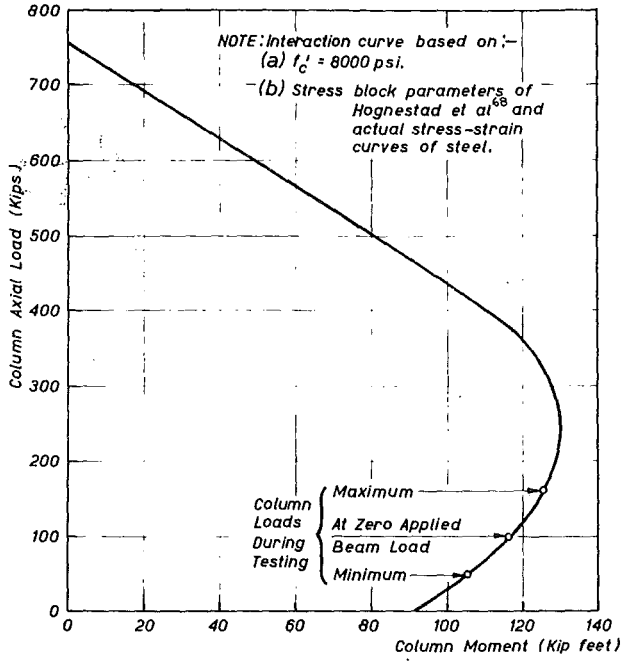

FIG. B.6 : INTERACTION DIAGRAM FOR COLUMNS

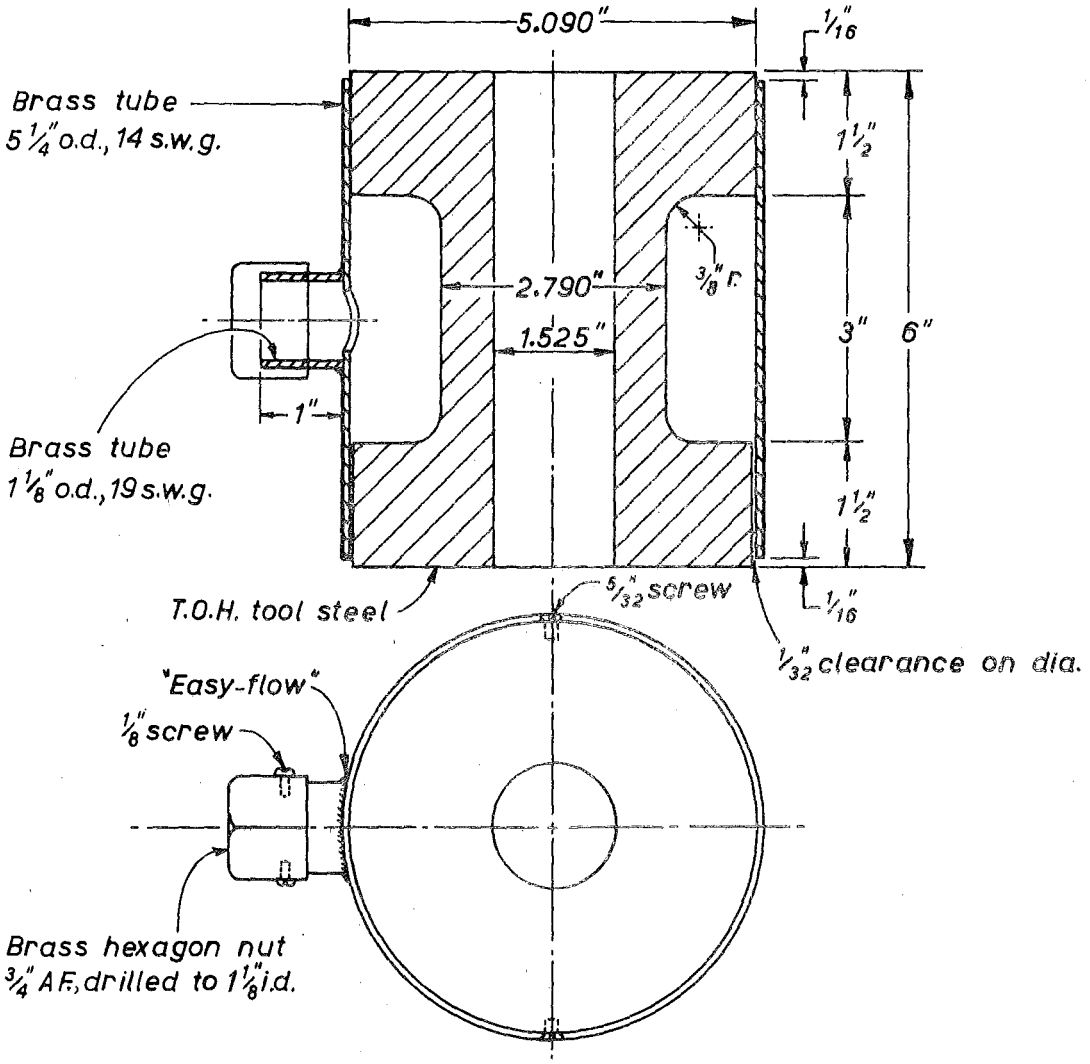

FIG. B.7 : 50-TON PRESTRESSING CABLE LOAD CELL

predicted from the concrete stress block parameters, for similar values of concrete force. Thus there was a greater lever arm and consequent greater strength in actuality. It would seem that the average concrete stress parameters are slightly conservative.

B.5 INSTRUMENTATION DEVELOPED FOR TESTING

B.5.1 Prestressing Cable Load Cells

Three 50-ton load cells were prepared to enable accurate measurement of the forces in the prestressing cables. The design and dimensions are shown in Fig. B.7. The cells were designed for a 50% overload capacity, and a maximum axial strain of 1000 microstrains to ensure stability of the strain gauges. A high yield tool steel (f_y = 38 tsi) was used.

Eight Kyowa 10 mm gauge length foil strain gauges, Type KF-10-C1-11 (temperature compensated for steel) were glued to the outside surface of the 0.633" thick hollow cylindrical tube. The gauges were placed in pairs at four equal intervals around the circumference, one of each pair being aligned axially forming an active strain gauge and the other aligned circumferentially forming a compensating strain gauge. The configuration is shown in Fig. B.8(a). The gauges were connected to form a four-arm bridge circuit.

Araldite AY 103 epoxy resin was chosen as an adhesive, because of its good insulation and shock resistant properties and its characteristic very small zero drift under cyclic loading. One disadvantage was that the araldite adhesive required heat curing in an oven to a maximum temperature of 125 degrees Celsius in order to achieve the best results. For this purpose a jig was made up, as shown in Fig. B.8(b), which could apply a spring loaded pressure to the gauges during initial heat curing. After curing and wiring the gauges, the cell was waterproofed by filling the cavity between the brass casing and the steel tube with petroleum

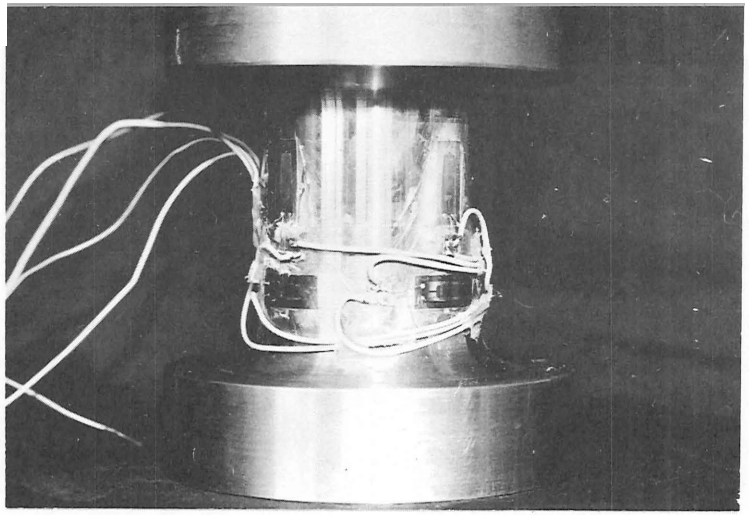

(a)

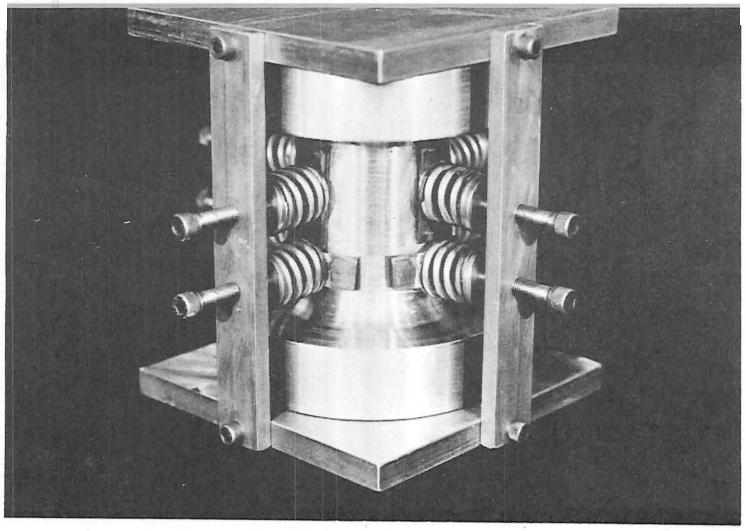

(b)

FIG. B.8 : STRAIN GAUGING 50-TON LOAD CELL

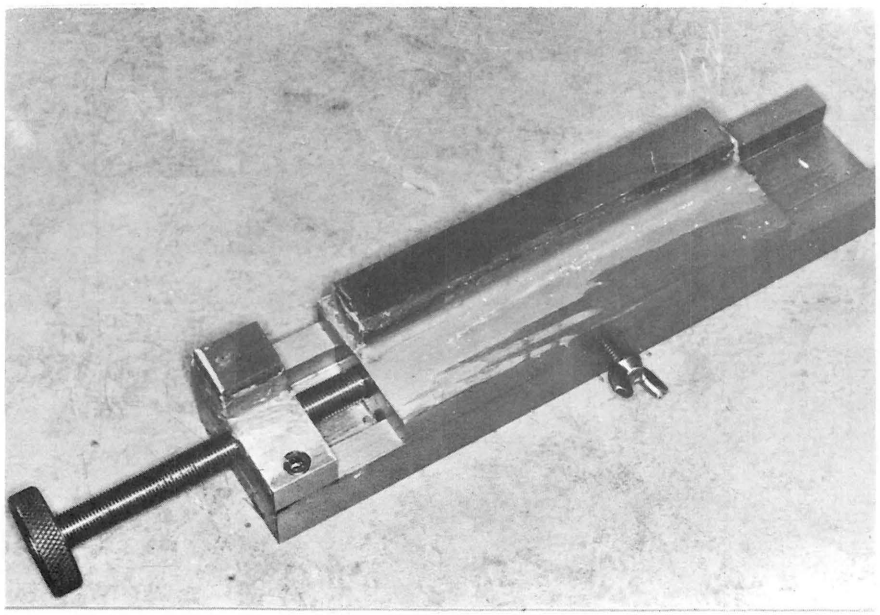

(a)

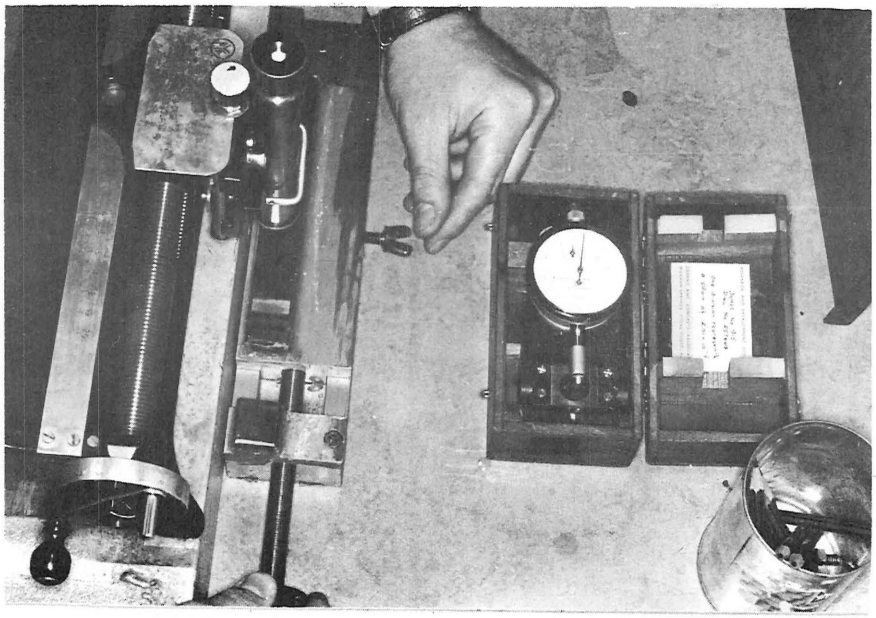

(b)

FIG. B.9 : METHOD OF CALIBRATION OF DEMEC GAUGES

based microcrystalline wax.

Prior to calibration the cells were automatically load cycled 50 times to a maximum load of 75 tons in an Avery 250,000 lb Universal Testing Machine, type 7104 DCJ. An average calibration was then taken from four load runs, using a Budd strain Bridge Model P-350. The cells were rotated by 45° each time, to eliminate any effects on the calibration of eccentricity of loading in the test machine, although such effects were found to be small. When the load cells were used on the beams, thin lead discs were placed at each face of the cell to ensure uniform bearing.

B.5.2 Measurement of Load at End of Beam

The experimental procedure for the beam-column tests required two sources of load measurement at the end of the beam; one to give an accurate reading of the load through a strain bridge, and the other to activate one axis of an X-Y plotter producing a continuous moment-rotation record. Since one load cell could not serve both these functions, and two load cells in series would have caused instability, it was necessary to strain gauge the loading bars to provide the X-Y plotter input. (The loading system at the end of the beam was arranged so that for each direction of loading two bars acted in tension). Four Kyowa KF-10-C1-11 (temperature compensated for steel) 10mm foil strain gauges were glued to each bar. Two gauges diametrically opposed and aligned axially formed the active strain gauges, and the other two gauges diametrically opposed and aligned circumferentially formed the compensating strain gauges. The gauges on the two bars were connected together to form one four-arm bridge circuit as shown in Fig. B.10. The gauges were waterproofed with micro-wax and the bars load cycled and calibrated. An 8 volt direct current input was provided to the four-arm bridge circuit by a Reid 15 volt regulated power supply, Type K2, and the output was connected to the Y axis of a Riken Denshi

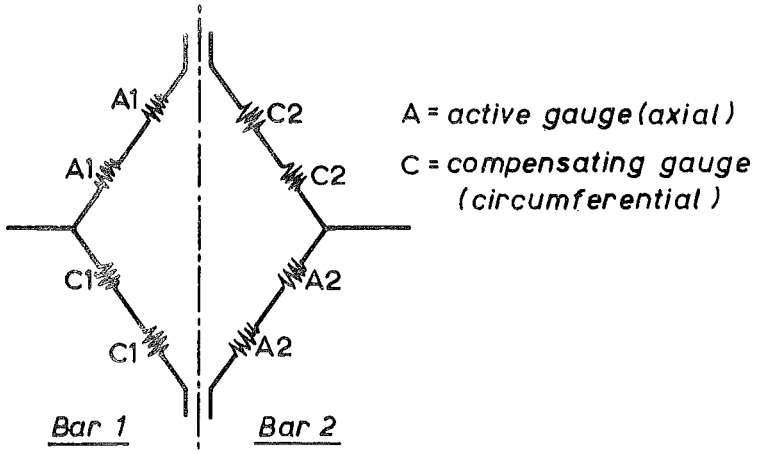

FIG.B.10 : LOADING BARS STRAIN GAUGE WIRING

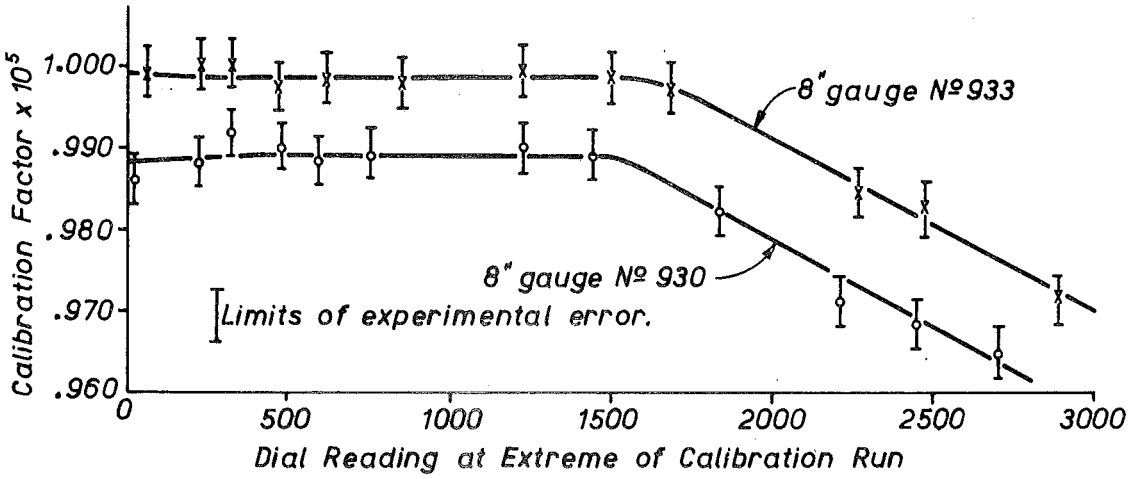

(a)

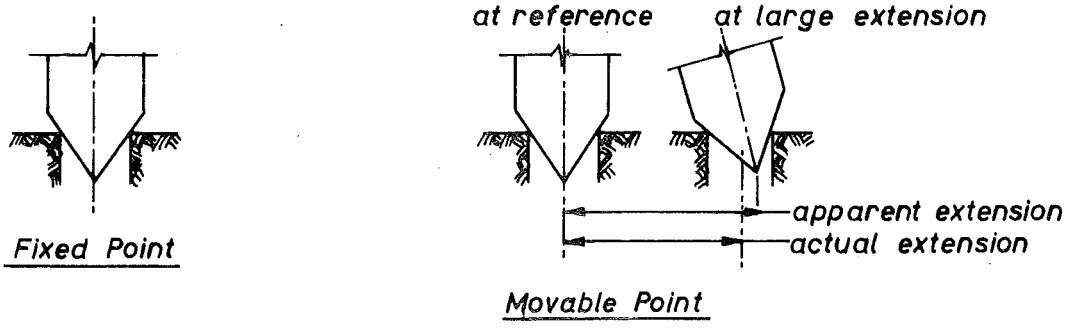

(b)

FIG. B.11 : CALIBRATION OF DEMEC GAUGES

X-Y plotter.

B.5.3 Calibration Device for Demec Gauges

During the course of testing the beam-column units, surface concrete strains were measured with demountable mechanical (Demec) gauges. It was felt to be necessary to check the gauges' calibration factors which relate differences in dial readings to strain. Although these factors were determined at the time of manufacture, considerable use of the gauges could have caused wearing of the knife edge supports and conical points resulting in a change to the original calibration.

(a) Previous Technique

A previous calibration technique which had been used at this university was tried first, and found to give insufficient accuracy. The procedure involved sticking a number of Demec points (stainless steel buttons drilled with a No. 60 hole) with sealing wax to a concrete block to give twenty 2" gauge lengths, twenty 4" gauge lengths, and ten 8" gauge lengths. The points were set at distances apart to cover the range of extensions for the gauges, and the concrete block was set up in a constant temperature room. A reading was taken with the appropriate Demec gauge at least four times for each gauge length. The dial reading of the Demec gauge at a reference gauge length was then subtracted from the mean dial reading for the gauge length considered, to give a "strain" relative to the reference. Then the absolute difference between the length of the gauge length considered and the length of the reference gauge length was found with a PYE travelling microscope. (For each gauge length the centre line of the hole in each button was calculated from location of the edges of the hole, and the gauge length was then traversed in two directions to calculate an average centre to centre distance between the buttons). Thus since the absolute difference in length between the gauge length and the reference gauge

length was known, and the difference in Demec gauge readings between the two gauge lengths had been found, a calibration factor could be determined to relate Demec gauge reading differences to strains.

However, in this approach it was difficult to determine the centre line of the holes in the buttons with sufficient accuracy. Because of wear of the Demec gauge points arising from the initial readings, the edges of the holes were burred and in some cases the holes were elongated. This resulted in relatively large errors in calculations of small length differences and it was apparent that a more accurate method was desirable.

(b) Demec Gauge Calibration Device

A device developed for calibration of Demec gauges is shown in Fig. B.9(a). It consists of a base and a sliding platform which can be moved relative to the base by means of a screw thread and knob. Fixed to the base is a case hardened block of tool steel with a No. 60 hole drilled in the top surface. Also, the sliding platform has attached to it a case hardened bar of tool steel of length $6\frac{1}{2}$", containing No. 60 holes drilled at appropriate points to give gauge lengths of 2", 4" and 8" relative to the fixed hole.

The procedure to be followed for one calibration run is as follows:

(1) With the conical points of the Demec gauge inserted in the appropriate holes, move the sliding platform relative to the fixed base with the knurled knob on the screw thread until the required initial reading on the Demec gauge is obtained. Lock the platform in position by tightening the wing nut.

(2) Take four readings between the points with the Demec gauge, and calculate the mean reading.

(3) Position a travelling microscope with its axis parallel to the axis of the calibration device. Traverse the microscope until the vertical hairline bisects a fine V inscribed on the surface of the movable bar. Read the distance. Traverse the vertical hairline away and

return until three successive readings have been taken which give an accuracy of 0.00005".

(4) Without disturbing the microscope, unlock the wing nut and screw the sliding platform to give a suitable change in length ("strain") between the fixed and sliding points, as shown in Fig. B.9(b). Lock the wing nut again.

(5) Traverse the travelling microscope until the vertical hairline once more bisects the V marked on the surface of the movable bar, and read the distance as previously. Calculate the absolute distance moved by the bar from the distance readings taken.

(6) Remove the travelling microscope and take four more readings with the Demec gauge on the points in their new relative position. Calculate the difference in the mean values of the Demec gauge readings due to the change in position of the platform.

(7) Calculate the Calibration Factor as follows:

$$\text{Calibration Factor, C.F.} = \frac{\Delta_m}{G_1 \Delta_g} \quad \begin{matrix}\text{strains per division of} \\ \text{dial gauge}\end{matrix} \qquad \ldots \text{(B.1)}$$

where G_1 = gauge length

Δ_m = absolute change in length as measured by the travelling microscope

Δ_g = change in readings of the Demec gauge.

An error analysis showed the experimental errors for this method (0.25%) to be much lower than those of the previous technique (3.5%).

For all gauges, calibration runs were carried out over the centre of the range and at the extremes corresponding to large compressive or tensile strains. For large compressive strains the calibration factors were very similar to those obtained in the middle of the range. However for large tensile strains the calibration factor decreased with increasing maximum strain. The trend is shown in Fig. B.11(a) for two 8" Demec gauges. Points are plotted between experimental limits for calibration

runs from the centre of the range. The difference only became significant at gauge readings greater than 1500 (approximately 5,000 microstrains) and then the maximum error was of the order of 2%. The reason for the difference is shown in Fig. B.11(b). When the movable point enters the hole at a large angle the apparent extension based on the centre line of the shaft at this point will be greater than the actual extension, resulting in a greater Δ_g and lower C.F. in equation (B.1).

The calibration factors obtained for the centre of the range were slightly different from those recommended by the manufacturer. The new values were used in the analysis of the beam-column experimental results.

B.6 TEST EQUIPMENT AND PROCEDURE

B.6.1 Test Frame

The test frame is shown in Figs. 3.7 and B.12. The basic A frame for application of axial load on the column was designed for a maximum vertical load of 160 kips. The reaction frame for horizontal loads from the top of the column and the beam end loading frame were both designed for nominal forces of 35 kips. However the section sizes of both the latter frames were increased considerably over those required in order to reduce frame deflections. The available deflections at the end of the beam of Units 1 and 2 were $10\frac{1}{2}$" downward and 18" upward. The available deflections were less for the deeper beams of Units 3 and 4, but were still much greater than was required. Column reactions were transferred through a steel column cap (made to a close fit, but with mortar placed between the cap and the column end to give uniform bearing) to a $2\frac{1}{4}$" diameter steel pin, greased to allow rotations, and thence to the reaction frame at the top and a floor base plate at the bottom.

Safety provisions were made in case a failure of the hydraulic

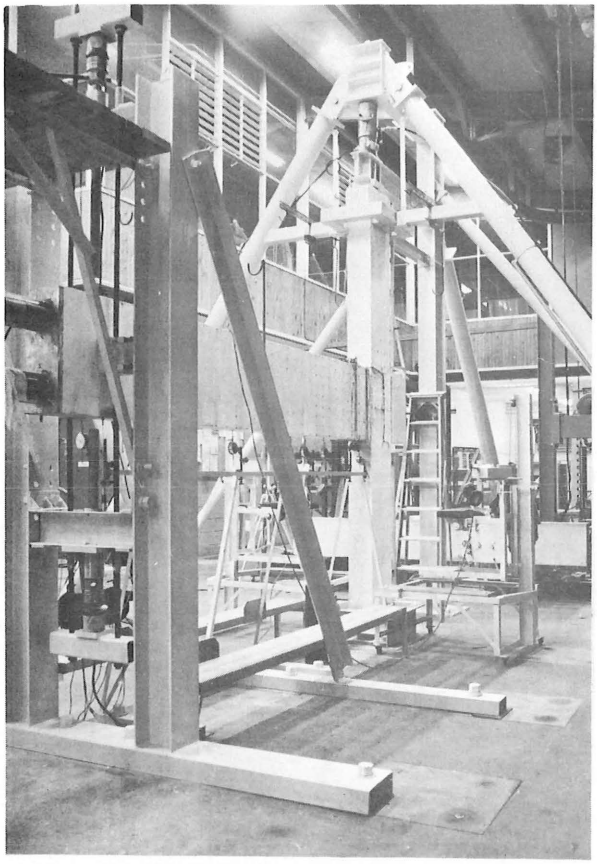

FIG. B.12 : TEST FRAME

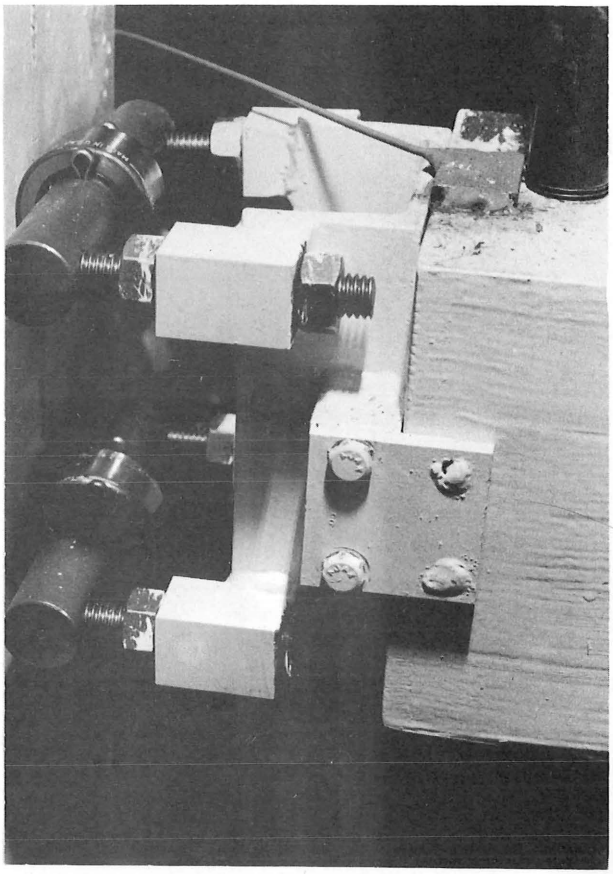

FIG. B.13 : PIVOT BLOCK

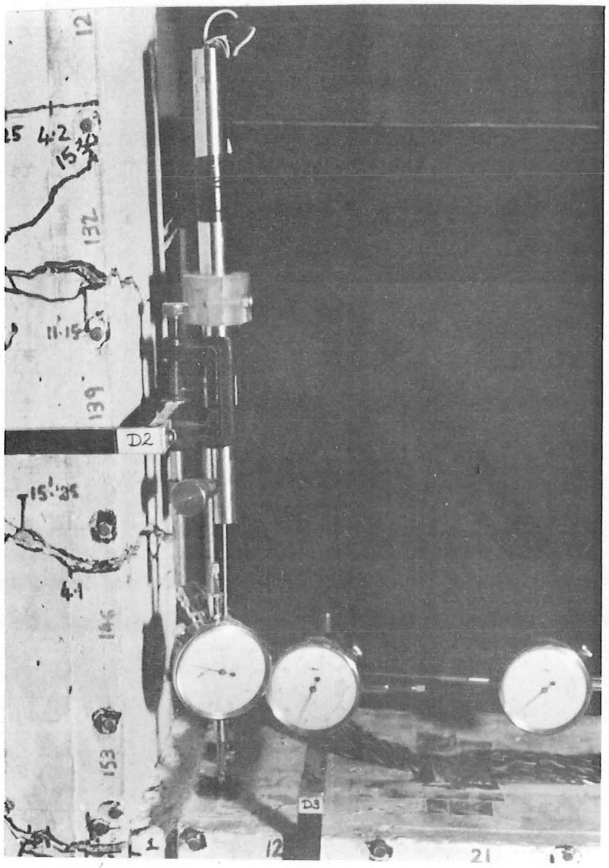

FIG. B.14 : JOINT ROTATION MEASUREMENT

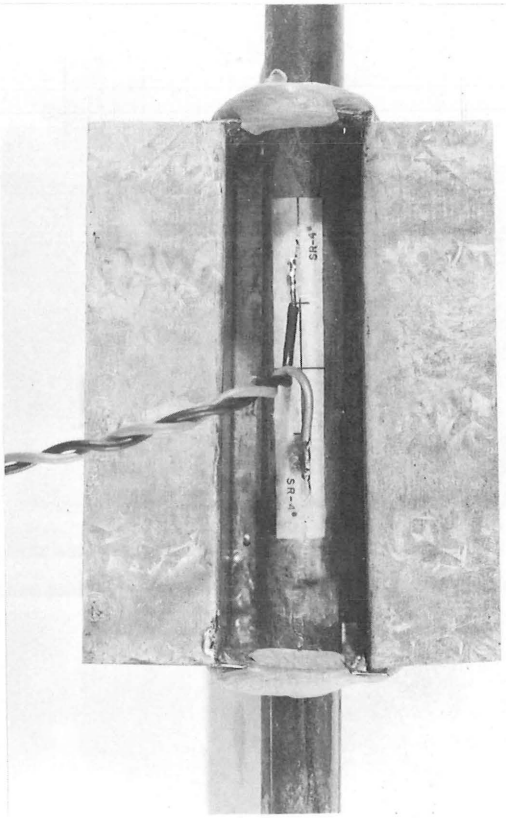

FIG. B.15 : STRAIN GAUGE

vertical loading system on the column should occur while the end of the beam was under load. A surrounding box at the base and a yoke at the top were provided to restrain the column in such an eventuality. However, these safety devices had at least 2" clearances to allow flexing of the column.

B.6.2 Load Application and Measurement

The axial load on the column was applied through a 60-ton hydraulic jack, Simplex Re-mo-trol Ram Model No. R613. The oil pressure was applied and continually regulated throughout the test by a RIEHLE test machine, Model No. F400, with a maximum capacity of 10,000 psi. A safety valve was incorporated in the hydraulic system, which could be readily closed to retain the column load should the oil pressure fall in an emergency. The column load was measured by a 50-ton Philips load cell, type PR9226/50. The load cell was calibrated on an Avery 250,000 lb Universal Testing Machine with a Budd Strain Bridge, and was found to have a repeatability of better than $\frac{1}{4}\%$.

Load was applied at the end of the beam by means of screw jacks. These were considered more suitable than hydraulic jacks as they allow the application of controlled displacements rather than constant loads, the former being much preferable for determining deformations in the plastic range. Further, for a constant deflection system such as screw jacks the creep that occurs at an increment is mainly in the magnitude of load, rather than in all the strain and deflection readings as would occur for a constant load hydraulic system.

The beam end loading system is shown in Fig. B.12. To prevent instability the load was applied through two bars acting in tension, 1" diameter high tensile steel bars being used. For example, upward beam loading was applied by the upper screw jack acting through a load cell to the cross-head, which in turn pulled the beam upward by the loading

bars. The bottom of the bars on either side of the beam were screwed into pivot blocks which were free to rotate on an axle passing through a horizontal tube cast with the beam. The pivot blocks were equipped with adjustable roller bearings to guide the end of the beam should it sway off the centre line between the upright universal column sections, at large deflections. One such pivot block is shown in Fig. B.13. The block shown is for the hidden side of the beam in Fig. B.12 (that is, the axle enters the pivot block from the right side of Fig. B.13). The screw jack not in use for a particular direction of loading was screwed back to allow sufficient clearance for beam deflection.

The two screw jacks were designed to take a maximum load of 15 tons at an extension of 24". A thrust bearing between the screw jack and the load cell took up the rotation in the jack. The load cells used were 20-ton Philips load cells, type PR9226/20. They were calibrated on an Avery 25,000 lb Universal Testing Machine, with a Budd Strain Bridge. Repeatability of calibration was again obtained to within $\frac{1}{4}$%.

B.6.3 Variation of Column Load

In the cases of Units 1 and 2, where plastic hinges formed in the beams, a variation of column load to represent the changing axial loads under seismic conditions would have had little effect on the performance of the units and was considered unnecessary. Consequently, the column jack load was maintained constant at 100 kips (0.13 of the axial load capacity of the column). This figure was obtained from the design calculations of a four storey office building, which had a gravity load due to dead load plus seismic live load of 93 kips in the first storey column. Further, the two storey prestressed concrete framed structure on which the experimental section sizes were based had a gravity load under seismic conditions of 92 kips in the ground floor column.

For Units 3 and 4 the moment capacity of the column plastic hinges was influenced by the axial loads at the critical sections. Therefore

a varying column load was applied to represent as far as possible the changing axial loads with lateral overturning moment in a framed structure. The design earthquake analysis of the four storey framed building was used as a basis. In this structure the axial load in the column varied from a minimum of 75 kips in the first floor and 94 kips in the ground floor columns for upward beam shears, to a maximum of 111 kips in the first floor column and 160 kips in the ground floor column for downward beam shears. It was not possible to represent this behaviour exactly, as in the actual building the dead load due to the first floor made a greater difference between the first and ground floor column loads than that which could be simulated in the test set up. Experimentally the difference in column loads above and below the beam was due only to the load at the end of the beam and the relatively small value of the dead load of the beam. However, these differences are not very significant and a suitable representation was chosen as follows. For upward load at the end of the beam the column jack load was varied linearly from 98 kips at zero column moment to 75 kips at the maximum column moment of 119 kip ft. The axial loads in the column below the beam simultaneously varied from 96 kips to 45 kips. For downward load at the end of the beam the column jack load was varied linearly from 98 kips at zero column moment to 127 kips at the maximum column moment of 148 kip ft. The axial load in the column below the beam simultaneously varied from 96 kips to 160 kips.

B.6.4 Crack Detection

Each unit was whitewashed prior to testing to aid detection of cracks. At each load increment cracks were observed with x 5 and x 10 magnification hand microscopes, and marked with felt-tipped pens to give better definition in the photographs of the unit. Crack widths were also measured at selected points with high magnification microscopes, capable of reading to 0.001".

B.6.5 Surface Concrete Strain Measurements

Concrete strains were measured on both sides of the unit by means of Demec gauges. The pattern of the gauge layout and all other instrumentation is shown in Figs. B.16 and B.17. In Units 1 and 2 rows of 4" gauge length, transverse to the axis of the member, were placed on the beam and column in the vicinity of the joint, and elsewhere strains were measured from 8" gauge lengths. Vertical rows of 2" gauge length were placed down the mortar joints. Sets of 8" gauge lengths were placed diagonally across the column within the joint to measure joint shear distortion, and shear displacement between the end of the beam adjacent to the column and the column itself was measured from two diagonal 8" gauge lengths across the mortar joint. The gauge layout in Units 3 and 4 was similar to that for the first two units except that rows of 2" gauge length were placed to measure the large local curvatures in the column near the joint.

The strains were measured between stainless steel buttons drilled with a No. 60 hole and fixed to the concrete with sealing wax. The gauge lengths in each column were placed sufficiently close together so that at least three readings could be taken above the neutral axis to allow the curvature to be calculated from the gradient of the compressive strain distribution. Only those gauges which were on the compressive side of the member for a particular direction of loading were read.

The strain readings taken were corrected for the effects of temperature changes during testing. The influence of temperature change on the gauge itself was measured from readings of a standard bar, and the apparent strains in the concrete due to temperature were measured from Demec points fixed to one of the test elements not in use at the time. Overall corrections of as high as 210 microstrains were measured.

For all strain readings an average was taken from corresponding gauge lengths on each side of the unit. The variation of strain from

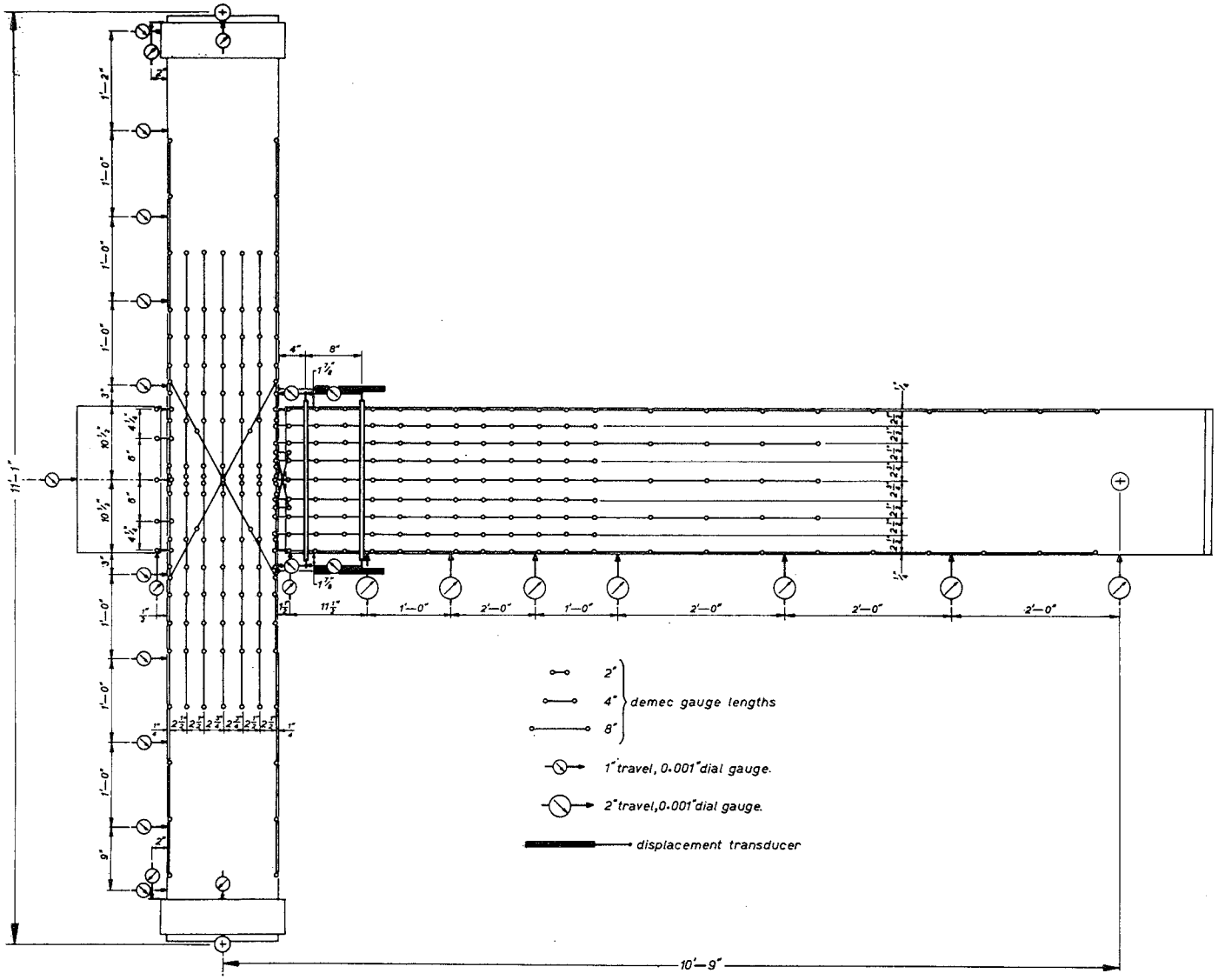

FIG. B-16 : INSTRUMENTATION OF UNITS 1 AND 2

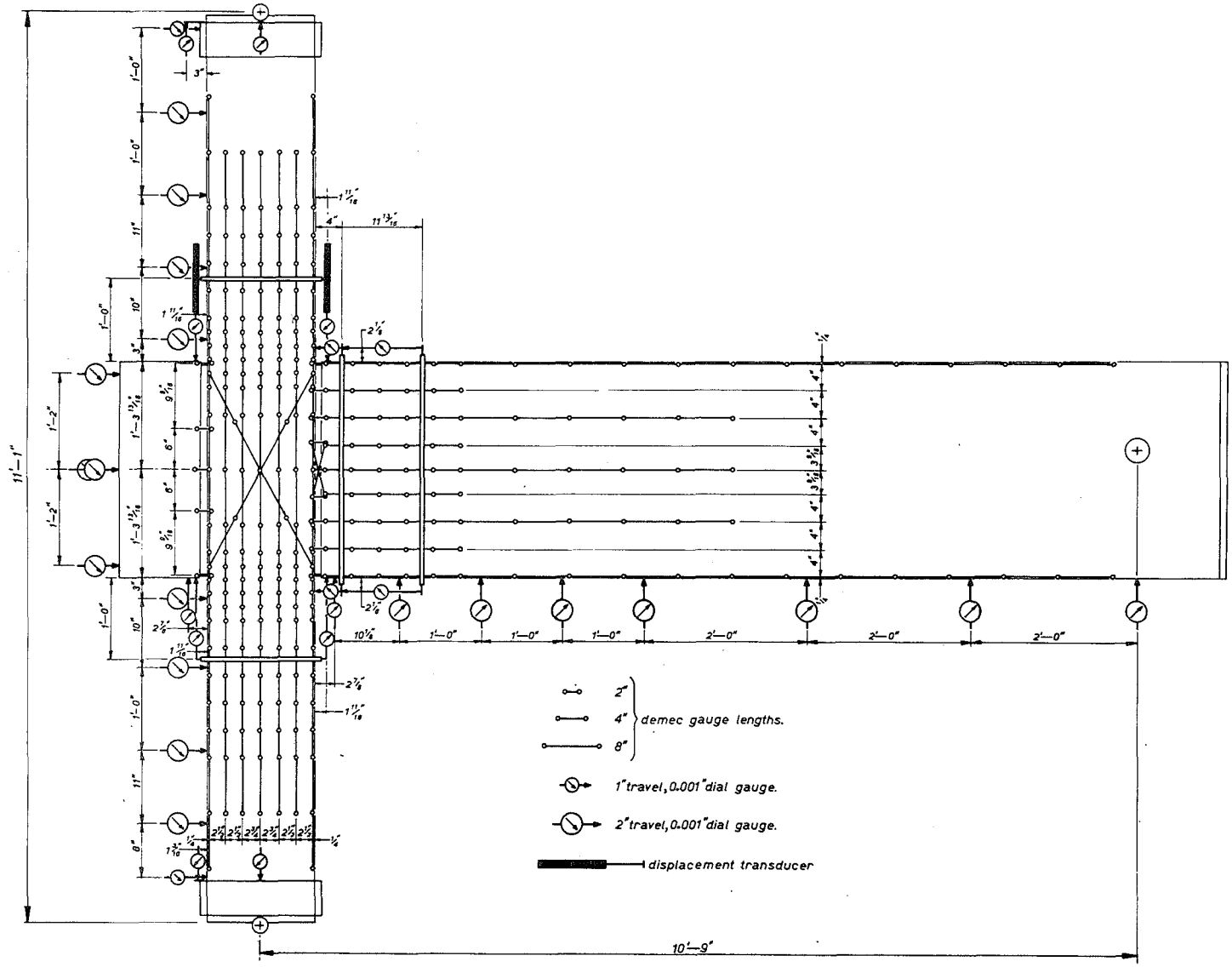

FIG. B.17 : INSTRUMENTATION OF UNITS 3 AND 4

side to side of the members was rarely greater than 10% of the strain at the compressive surface, such differences occurring mainly near the onset of crushing. For each transverse row of gauges a line of best fit was drawn through the average corrected compressive strain readings to determine the curvature.

B.6.6 Deflections

The deflected shapes of the units were measured by a number of 2"-travel and 1"-travel, 0.001" dial gauges. In Units 1 and 2 seven 2" and sixteen 1" gauges measured the deflection and in Units 3 and 4 nineteen 2" and eight 1" gauges were used. Small brass plates were glued to the concrete to provide an even bearing surface for the shafts of the gauges. The gauges for measuring beam deflection were fixed to a rigid steel stand attached to the strong-floor, and therefore the deflections measured were relative to the floor and a correction had to be made to allow for the movement of the test frame under load. This was accomplished by fixing a steel rule graduated in 0.01" to the horizontal reaction arm at the top of the column, and reading the movement at this point due to frame deflections through a theodolite. The deflection component at each dial gauge point along the beam, due to this movement at the top of the column, could then be calculated. The dial gauges were initially fixed at the centre of their travel to read cyclic deflections. Deflections rather greater than those available in this position were obtained for major load cycles by either raising or lowering the gauges as required.

The dial gauges for measuring column deflections were fixed to a rigid stand attached to the column base plate at the bottom and the test frame's reaction arm to the column at the top. Thus this dial gauge stand moved with the test frame and the deflection readings so obtained did not require correction.

A further measurement of deflection was made by deflection rules at

the beam end loading point. These were useful for measuring the very large deflections sustained at the end of the beams of Units 1 and 2. Pointers were fixed to the top surface of the pivot blocks on each side of the beam as shown in Fig. B.13. These pivot blocks remained horizontal even as the beam deflected. The deflections were read from scales graduated in 1/32" glued inside the inner flanges of the upright universal column sections of the end loading frame, and a mean value was calculated from the readings on each side. Although the end frame itself would deform slightly under load, the order of magnitude of these deformations was well within the limits of accuracy with which the scales could be read. The readings from these deflection rules had to be corrected for movements of the column reaction frame in the same manner as the dial gauges measuring the deflection of the beam.

B.6.7 Rotations

The plotting of moment-rotation curves was an important part of this study. To facilitate measurement at frequent intervals of rotations in the critical joint region, and to check curvatures calculated from Demec gauge readings, steel frameworks were placed around the members with 1"-travel 0.001" dial gauges attached at the top and the bottom. It was ensured that there would be a clearance at all times between the straps of the framework and the concrete, so that the framework would exert no confining effect on the concrete.

To measure the rotations at the beam plastic hinging in Units 1 and 2, frameworks were placed on the beam at 4" and 12" from the column face. The side straps were attached by 3/16" dia. bolts screwed into $\frac{3}{8}$" dia. horizontal rods which were cast in the beam at the top and bottom of the core. The 4" gauge length measurements were taken from the dial gauges acting right to the face of the column to ensure that all rotations in the mortar joint were included. Although there was some flexing of the

column in this region, its effect on the beam rotation measurements would be negligible. The dial gauges attached to the framework at 12" from the column measured rotations over an 8" gauge length to the first framework, excluding the mortar joint.

In Units 3 and 4 frameworks were placed around the columns as well as the beams. The beam frameworks were placed at 4" and 15-13/16" (half the overall depth of the member) from the column face. In the column of Unit 3 the frameworks were placed at 8" (half the member depth) from the top and bottom face of the beam, but this distance was increased to 12" in Unit 4 to include more of the plastic rotations. The column frameworks were attached to 3/16" dia. bolts glued into 2" deep, $\frac{3}{8}$" dia. holes drilled at the top and bottom of the core. Araldite AY103 epoxy resin was used, which has a modulus of elasticity when hardened very similar to that of concrete. The dial gauges extended to the top or bottom face of the beam or anchor block.

A continuous record of moment-rotation characteristics during testing was automatically plotted by a Riken Denshi X-Y plotter, Model F-3B. The rotation axis was activated by two Hewlett Packard displacement transducers Model 24DCDT-3000. For the first two units the transducers were placed one above and one below the beam, with the coil fixed to the framework around the beam at 12" from the column, and the core rod fixed to the face of the column. On Units 3 and 4 the transducer coils were placed on the ends of the framework around the column for the plastic hinge above the beam, and the core rods were fixed to the top faces of the beam and the anchor block. The two transducers were connected in parallel and the required 24 volt direct current input was provided by connecting two Reid 15 volt regulated power supplies, Type K2, in series. The output from the transducers to the X axis of the X-Y plotter was wired in series in such a way that extension in one and compression in the other would be additive. Shielded cables were found to be necessary to prevent interference from surrounding alternating

current sources. The combination of two transducers was calibrated with a micrometer screw device.

The visual outputs from the plotter were used to determine rotation limits for the earthquake loading sequence. However, for Units 3 and 4 under upward loading plastic rotations occurred in the column hinge below the beam, and for this direction of loading the rotation limits were calculated from the dial gauge readings on the framework around the column below the beam.

Fig. B.14 shows a displacement transducer and dial gauges attached to frameworks around the column and beam at the joint of Unit 3.

B.6.8 Steel Strains

Steel strains were measured by electrical resistance strain gauges glued to the surface of both transverse steel and prestressing tendons. The gauge locations for the transverse reinforcement are shown in Figs. 3.31 to 3.34. The beam stirrup gauges were placed in position after removing a cork block fixed between the stirrup and the mould surface on casting. However, for the column ties and hoops it was more practicable to place and waterproof the gauges prior to casting. Gauges were placed on two wires of each post-tensioning cable in such a position that when the cable was placed in the duct the gauges would be adjacent to the mortar joint. Some gauges were also placed on the column pre-tensioning strand near the joint.

In general the strain gauges used were BLH SR-4 gauges, a wire gauge of length 1", although it was necessary to use a small 2 mm gauge, Shinkoh F102B, to attach to the individual wires of the $\frac{3}{8}$" dia. strand. Gauges of these types were tested initially, and it was found that the SR-4 gauges fixed to 0.276" dia. prestressing wire behaved well up to a strain of 9,000 microstrains, and strains as high as 10,000 microstrains were recorded from the F102B gauges glued to the $\frac{3}{8}$" dia. strand. A rapid setting adhesive, Eastman 910, was used and found to be most

satisfactory. In order to find a suitable waterproofing agent a $\frac{5}{8}$" dia. bright steel rod, coated in four places with different waterproofing materials, was placed in the corrosive atmosphere of a fog room at 100% relative humidity. The materials studied were: Philips waterproofing type PR9244/05, Budd type GW-1 Waterproofing Compound, Shinkoh SN-4 synthetic rubber type moisture-proofing, and petroleum based micro-crystalline wax. The bar was removed after 22 days and the waterproofing stripped to find if rust had penetrated. There were spots of rust evident under the Philips and Budd waterproofing agents but no sign of rust beneath the Shinkoh and wax waterproofing. The four materials were also tested by coating strain gauged $\frac{3}{8}$" dia. strands and tensile testing each strand to failure. The brittle Philips waterproofing flaked off at a relatively low strain and in doing so damaged the strain gauge, but the other materials all behaved satisfactorily. It was decided to use the microcrystalline wax for waterproofing all strain gauges. This had the added advantage of providing a soft layer around the gauge to protect it during casting. The appearance of the gauge prior to applying the wax is shown in Fig. B.15. The bar was first heated to aid bond to the wax, the metal mould was then placed around the bar and the molten wax poured into the mould.

The strain gauges were wired to a switch box and strains were read by a Budd strain bridge. The strain gauges placed on the transverse reinforcement behaved satisfactorily throughout all tests. However, little useful information was obtained from the gauges fixed to the prestressing tendons as many of them appeared to be damaged during stressing operations.

B.6.9 Sequence of Operations

At the start of each test an initial set of readings was taken on the column Demec gauge lengths before application of the axial load,

with the beam supported at the end so that there was zero moment on the joint. The column was then loaded to the value of constant axial load for Units 1 and 2 and mean axial load for Units 3 and 4, the beam load checked for zero joint moment, and the full set of "zero" readings taken. This involved reading all Demec gauge lengths, dial gauges, and electrical resistance strain gauges, each series being read twice to ensure that these important initial readings were accurate. This procedure also afforded a check on the repeatability with which the Demec gauges could be read. Consideration of the two sets of zero readings for different units and different Demec gauge operators showed a standard deviation of approximately 8 microstrains in these readings in all cases.

The procedure when the full set of readings was taken at the peaks of major load cycles was as follows:

1. Adjust deflection and read initial load.
2. Read dial gauges measuring joint rotation and beam end deflection.
3(a). Read 4" Demec gauge lengths, taking temperature correction readings before and after.
(b). Simultaneously record all dial gauge readings.
4. Read load.
5(a). Read 2" Demec gauge lengths, taking temperature correction readings before and after.
(b). Simultaneously record all electrical resistance strain gauge readings.
6. Read 8" Demec gauge lengths, taking temperature correction readings before and after.
7. Read load.
8. Mark cracks.

The creep in the load was a maximum of 4% at the increment in which first concrete crushing occurred, but elsewhere creep was always less

than $1\frac{1}{2}\%$.

The number of Demec gauge and dial gauge readings was abbreviated at intermediate increments in each cycle, and in addition frequent readings were taken only of the first two items in the above sequence.

B.7 CALCULATION OF JOINT SHEAR DISTORTION

The deflection component due to shear distortion, shown in Tables 3.3 and 3.4, was calculated from 8" Demec gauge readings diagonally across the column in the joint region. The shear deformations of the column joint region for a downward load at the end of the beam are shown in Fig. B.18(a), assuming that the centre of the shear block remains on the original centre line of the column. It is apparent that the total angle of shear deformation, γ_s, may be given by:

$$\gamma_s = \frac{\gamma_{s1} + \gamma_{s2}}{2} - \gamma_{s3} \qquad \ldots (B.2)$$

The component of deflection at the end of the beam, Δ_s, is:

$$\Delta_s = L_B \gamma_s \qquad \ldots (B.3)$$

where L_B is the length from the centre of the joint to the end of the beam.

In Fig. B.18(b) the shear block has been rotated for diagrammatic purposes. Because the angles of deformation are very small, the following relationships derived from this figure apply:

From similar triangles,

$$\gamma_{s1} = \frac{\delta_1 \frac{\sqrt{l_1^2 + l_2^2}}{l_2}}{l_1} \qquad \ldots (B.4)$$

and

$$\gamma_{s2} = \frac{\delta_2 \frac{\sqrt{l_1^2 + l_2^2}}{l_2}}{l_1} \qquad \ldots (B.5)$$

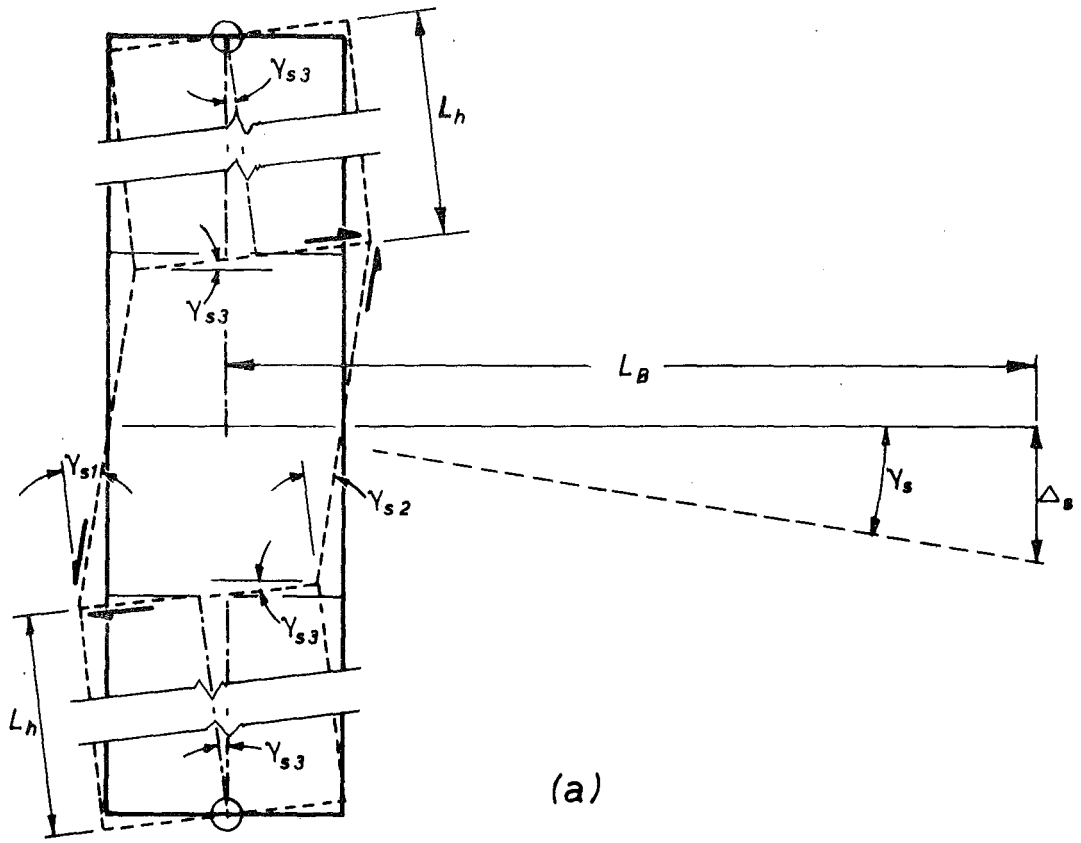

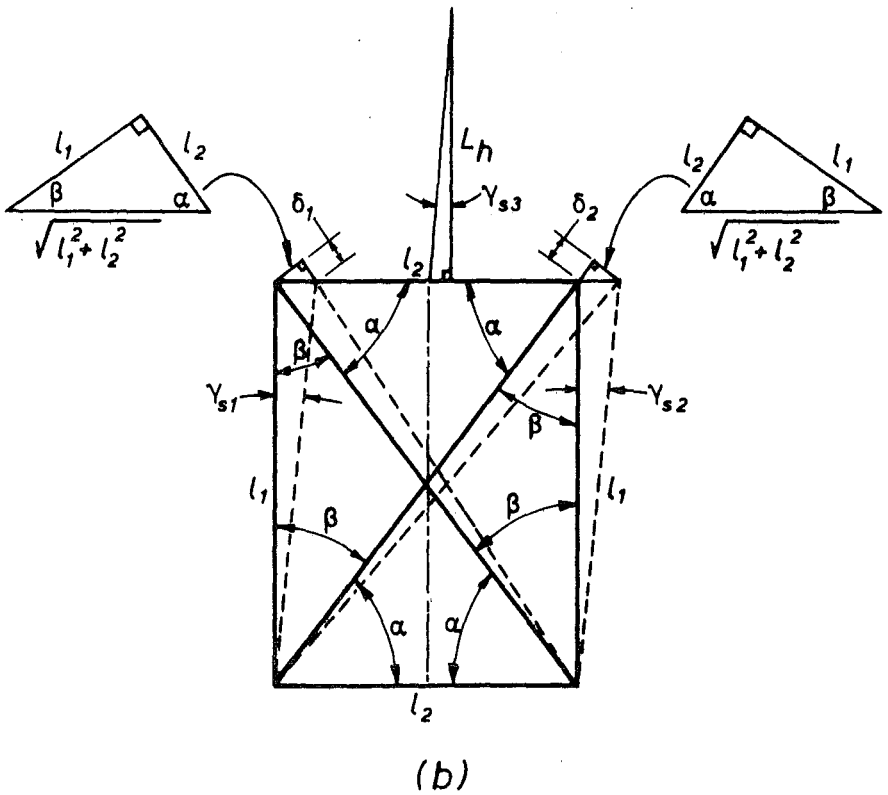

FIG. B.18 : JOINT SHEAR DISTORTION

where l_1 and l_2 are the height and breadth of the joint and δ_1 and δ_2 are the measured compression and extension of the diagonals.

Since the angle of rotation of the column sections above or below the shear block, γ_{s3}, will each be due to half the total lateral shear displacement:

$$\gamma_{s3} = \frac{1}{2}\left(\frac{\delta_1\sqrt{l_1^2 + l_2^2}}{l_2} + \frac{\delta_2\sqrt{l_1^2 + l_2^2}}{l_2} \right)/L_h \qquad \ldots (B.6)$$

where L_h is the length from the top or bottom of the shear block to the pivot points of the column.

Substituting in equations (B.2) and (B.3),

$$\Delta_s = L_B \left[\left(\frac{\delta_1 + \delta_2}{2}\right) \frac{\sqrt{l_1^2 + l_2^2}}{l_1 l_2} - \left(\frac{\delta_1 + \delta_2}{2}\right) \frac{\sqrt{l_1^2 + l_2^2}}{l_2 L_h} \right] \qquad \ldots (B.7)$$

$$\therefore \Delta_s = L_B \left(\frac{\delta_1 + \delta_2}{2}\right) \frac{\sqrt{l_1^2 + l_2^2}}{l_2} \left(\frac{1}{l_1} - \frac{1}{L_h}\right) \qquad \ldots (B.8)$$

B.8 DAMPING TESTS

An attempt was made to determine the damping characteristics of the beam-column units, by vibration testing Unit 4. An axial load was placed on the column but the beam was left free to vibrate. Two Philips velocity transducers, type PR 9265, were fixed to the unit, one at the end of the beam to measure vertical movements due to vibration of the unit, and one fixed horizontally to the top of the column to measure the amplitude of the vibration of the test frame. The output from both transducers was recorded on a Philips oscilloscript, type PT 2108. The velocity readings could be converted to displacements with the aid of the frequency. A sharp vertical blow was applied at the end of the beam

and the resulting transient vibrations measured.

Fig. B.19(a) shows the recorded vibrations at both transducers for tests before and after the beam-column experiment. Unfortunately there was a noticeable amplitude modulation effect inherent in the response. This arose because the system contained three components with different natural frequencies: the beam, the short length of column, and the test frame which had vibrations induced in it from the reaction at the top of the column. Because the vibration of the systems superimposed, a pure decay of amplitude was not obtained in either response. This precluded accurate determination of the damping ratio of the unit as the calibration of the velocity transducers was for vibrations of a simple form.

Because of the difficulty of obtaining damping measurements on the beam-column unit in the test frame, a number of damping tests were carried out on the previously tested column of Unit 2. The column was horizontally placed on rigid steel supports at each end, and the transient vibrations were measured at the centre after a sharp impact with a hammer. One such response curve is shown in Fig. B.19(b). In these cases a pure decay curve was obtained and the damping ratio could be measured accurately. An average value of 2.5% critical viscous damping was obtained. This column had been previously cracked, and thus the results support the damping ratios found in such a case by Penzien[26] for model prestressed concrete beams.

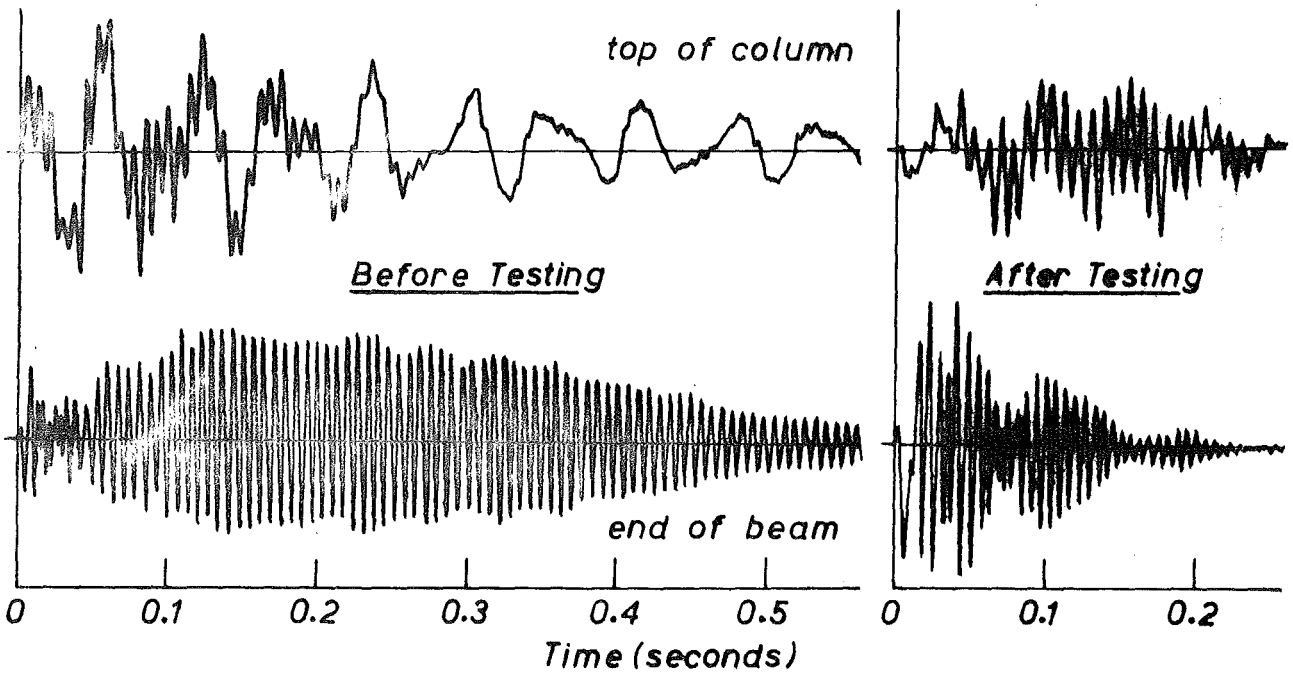

(a) Unit vibrations

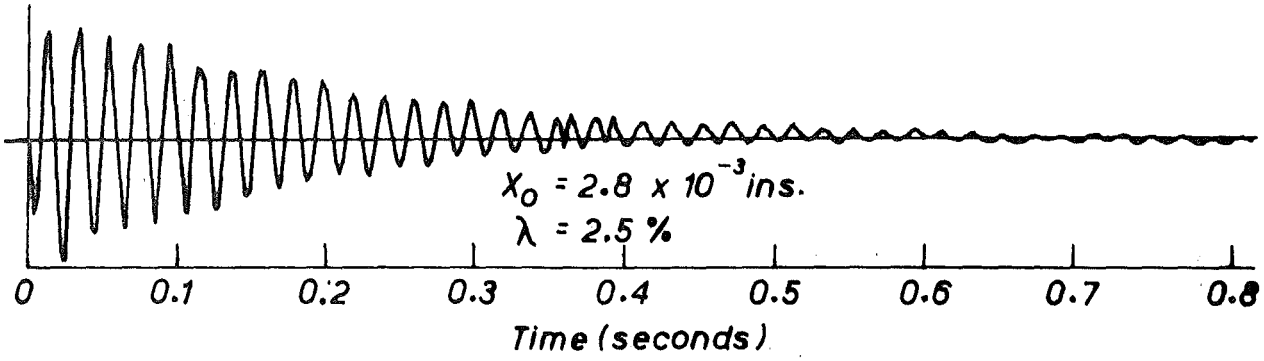

(b) Simply supported column vibrations

FIG. B.19 : DAMPING TESTS

APPENDIX C

ANALYSIS OF MOMENT-CURVATURE RELATIONSHIP FOR PRESTRESSED CONCRETE MEMBERS UNDER MONOTONIC LOAD

C.1 INTRODUCTION

The analysis of the moment-curvature relationship of a prestressed concrete section was developed in the three stages shown in Fig. 4.3, considering an eccentric prestressing force for generality. These stages represented respectively the conditions at: initial prestress alone, compression over the whole section and the neutral axis below the section, and tension over part of the section due to flexure with the neutral axis lying within the section. The negative curvature for Stage 1 was calculated directly. During Stage 2, moments and curvatures for successively decreasing values of the neutral axis depth, kD, were yielded from the solution of a quadratic equation. This was possible as the concrete strains were less than ϵ_o and the steel strains less than ϵ_{sa} in Figs. 4.1 and 4.2, and therefore quadratic and linear expressions applied for concrete and steel stresses respectively. However for the more complex stress-strain expressions applicable during Stage 3 an iterative technique had to be used. The direct solution approach was used in Stage 2 because of its greater computation speed than an iterative solution. However, the range from "decompression" to failure represents by far the largest part of the moment-curvature relationship, and therefore only the background to this stage will be presented in detail. The approach in Stage 2 is similar to that used by Sherbourne and Parameswar[57], and the algebra of the complete analysis may be found in the listing of Program 4.1 in Appendix A.

The analysis considers a fully prestressed section. Should it be desired to analyse a section including mild steel reinforcement, the required program modifications would be minor.

C.2 MOMENT-CURVATURE ANALYSIS

The analysis is based on a strain compatibility-force equilibrium approach. During Stage 3 an iterative technique is used to find the value of kD and thence the curvature, φ, and moment, M, for successive increments of the compressive concrete strain, ε_{cc}. The program time on an IBM 360/44 computer required to compute the complete moment-curvature relationship of a member, for an increment in ε_{cc} of 0.0001, is of the order of 2 minutes. The procedure at each increment during Stage 3 is as follows:

C.2.1 Strain Compatibility

The strains in the component materials are determined from the strain profile, as shown in Fig. 4.3(c).

(a) Concrete Strains

The strains in the concrete at significant points are given by:

$$\varepsilon_y = (k-y)\varphi D \quad \ldots (C.1)$$

$$\varepsilon_{c1} = (k-\alpha_1)\varphi D \quad \ldots (C.2(a))$$

$$\varepsilon_{c2} = (k-\alpha_2)\varphi D \text{ etc.} \quad \ldots (C.2(b))$$

$$\varepsilon_r = (\gamma-k)\varphi D \quad \ldots (C.3)$$

where ε_y = strain in the concrete fibre at a distance, yD, from the top

and ε_{c1} = strain in the concrete fibre at a distance, $\alpha_1 D$, from the top

ε_{c2} = strain in the concrete fibre at a distance, $\alpha_2 D$, from the top

etc.

and ε_r = strain in the concrete fibre at incipient cracking

and φ = curvature

and yD, $\alpha_1 D$, $\alpha_2 D$, kD, γD = the distances from the top fibre to: the concrete fibre, first and second prestressing tendons, neutral axis, and concrete fibre with limiting tensile strain respectively.

For analysis denote:

$$r_y = \frac{\epsilon_y}{\epsilon_o}, \quad r_{c1} = \frac{\epsilon_{c1}}{\epsilon_o}, \quad r_{c2} = \frac{\epsilon_{c2}}{\epsilon_o} \text{ etc.}, \quad r_\gamma = \frac{\epsilon_r}{\epsilon_o} \text{ and } \quad \varphi' = \frac{\varphi D}{\epsilon_o} \quad \ldots (C.4)$$

where ϵ_o is the concrete strain at maximum stress (see Fig. 4.1) and φ' is a dimensionless curvature expression.

Therefore,

$$r_y = (k-y)\varphi' \quad \ldots (C.5)$$

$$r_{c1} = (k-\alpha_1)\varphi' \quad \ldots (C.6(a))$$

$$r_{c2} = (k-\alpha_2)\varphi' \text{ etc.} \quad \ldots (C.6(b))$$

$$r_\gamma = (\gamma-k)\varphi' \quad \ldots (C.7)$$

(b) Prestressing Steel Strains

An example of the determination of strains in the prestressing tendons is shown in Fig. C.1 for the bottom tendon. In Fig. C.1(a) the strain in the steel due to prestressing force alone is called the "strain due to effective prestress", ϵ_{se}. The corresponding strain in the concrete at the level of the steel is designated ϵ_{ce}. On application of an external positive moment the state shown in Fig. C.1(b) is reached, where the concrete strain at the level of the particular tendon considered is zero. This establishes the steel strain, ϵ_s, at a datum value of zero concrete strain, as:

$$\epsilon_s = \epsilon_{se} + F\epsilon_{ce} \quad \ldots (C.8)$$

where F is the strain compatibility factor which depends on the bond, and is equal to unity if the bond is perfect.

At any stage of loading, for example Fig. C.1(c), the following holds true:

strain in the prestressing steel, ϵ_s = steel strain at the datum of zero concrete strain $\pm$ (concrete strain at the level of the steel, ϵ_c, multiplied by the strain compatibility factor, F.) Therefore the steel strains in the section are:

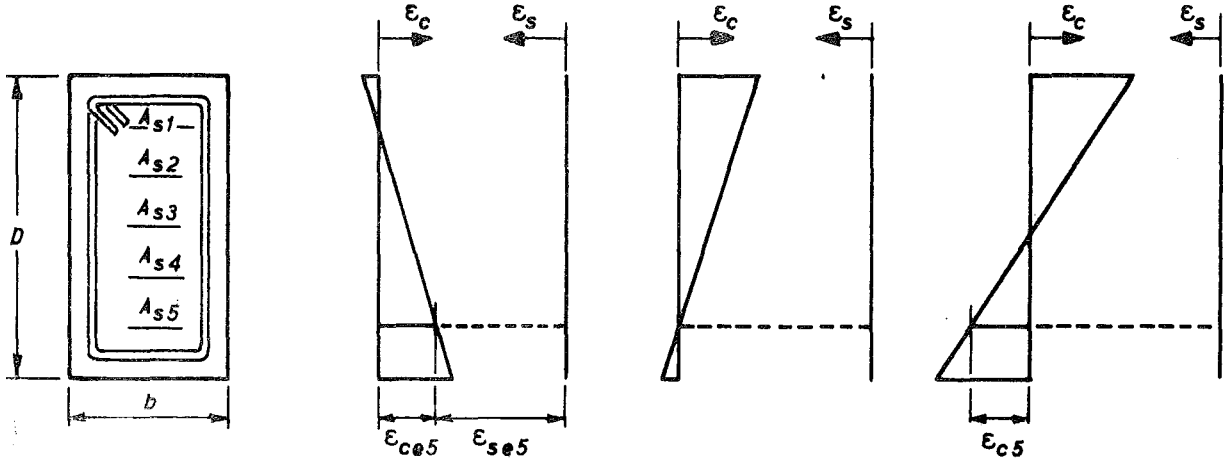

Fig. C·1 : STEEL STRAINS DURING LOADING

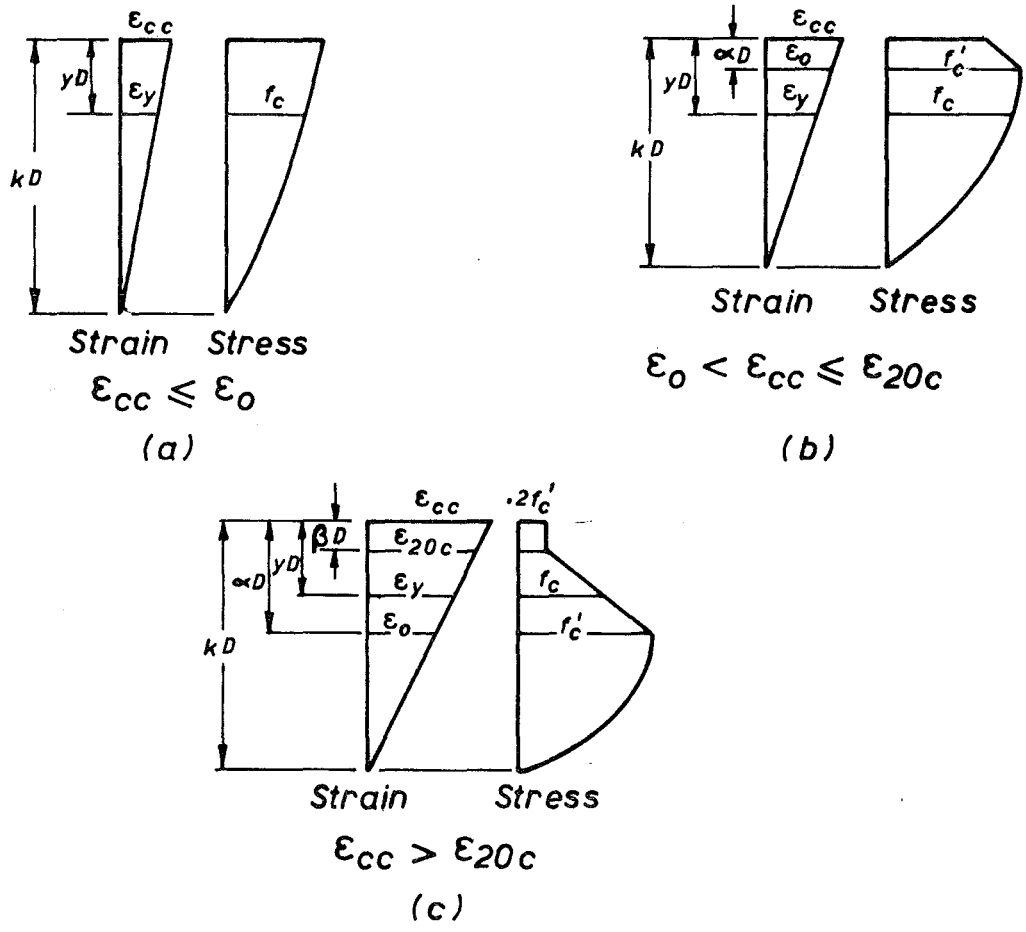

Fig. C·2 : CONCRETE STRESS BLOCKS FOR MODEL 1

$$\epsilon_{s1} = (\epsilon_{se1} + F\epsilon_{ce1}) - F\epsilon_{c1} \quad \ldots (C.9(a))$$

$$\epsilon_{s2} = (\epsilon_{se2} + F\epsilon_{ce2}) - F\epsilon_{c2} \text{ etc.} \quad \ldots (C.9(b))$$

Equation (C.9) is also applicable when the section is under axial load, as in this case an extra compressive strain will be inherent in the terms ϵ_{c1}, ϵ_{c2} etc.

Substituting for ϵ_{c1}, ϵ_{c2} etc. from equation (C.2):

$$\epsilon_{s1} = (\epsilon_{se1} + F\epsilon_{ce1}) - F(k-\alpha_1)\varphi'\epsilon_o \quad \ldots (C.10(a))$$

$$\epsilon_{s2} = (\epsilon_{se2} + F\epsilon_{ce2}) - F(k-\alpha_2)\varphi'\epsilon_o \text{ etc.} \quad \ldots (C.10(b))$$

C.2.2 Force Equilibrium

The forces due to the component materials are calculated as follows:

(a) Total Prestressing Steel Force

For a given strain profile defined by k and φ', ϵ_{s1}, ϵ_{s2} etc. are calculated, and the corresponding values of tendon stresses, f_{s1}, f_{s2} etc. are determined from the appropriate equation (4.9) to (4.11). The total prestressing steel force, T_s, is then given by:

$$T_s = A_{s1} f_{s1} + A_{s2} f_{s2} + \text{etc.} \quad \ldots (C.11)$$

(b) Tensile Force in the Concrete

The determination of tensile force in the concrete, T_c, varies according to whether or not a tension crack has occurred.

For the case where there are no cracks:

$$T_c = \int_k^1 f_c \, bD \, dy \quad \ldots (C.12)$$

Substituting for f_c from equation (4.7),

$$T_c = \int_k^1 2 \frac{f'_c}{\epsilon_o} \epsilon_y \, bD \, dy \quad \ldots (C.13)$$

From equations (C.4) and (C.5),

$$T_c = \int_k^1 2 f'_c r_y bD \, dy \qquad \ldots (C.14)$$

$$= \int_k^1 2 f'_c bD (k-y)\varphi' dy \qquad \ldots (C.15)$$

Integrating,

$$T_c = [2 f'_c bD \varphi'(-\tfrac{1}{2}k^2 + k - \tfrac{1}{2})] \qquad \ldots (C.16)$$

For the case where cracking has occurred:

$$\epsilon_{ct} > \epsilon_r$$

where ϵ_{ct} is the strain in the bottom fibre of the section, and ϵ_r is the rupture strain

Then $$\gamma = k + (1-k) \frac{\epsilon_r}{\epsilon_{ct}} \qquad \ldots (C.17)$$

and $$T_c = \int_k^\gamma f_c bD \, dy \qquad \ldots (C.18)$$

Substituting for f_c from equation (4.7) and integrating,

$$T_c = [2 f'_c bD \varphi' (-\tfrac{1}{2} k^2 + k\gamma - \tfrac{1}{2}\gamma^2)] \qquad \ldots (C.19)$$

T_c is determined from the appropriate equation (C.16) or (C.19) for given values of k and φ' .

(c) Compressive Force in the Concrete

Three models were developed for the concrete compressive stress block, the variable being the behaviour of the cover concrete at large strains. No allowance was made for reduction in concrete compression due to the area of the prestressing steel, as such areas are small and the difference was felt to be within the limits of accuracy of the analysis.

Model 1

The cover concrete follows the same stress-strain relation as the

core concrete.

From Fig. 4.3(c), the total compressive force in the concrete, C, is given by:

$$C = -\int_k^0 f_c \, bD \, dy \qquad \ldots (C.20)$$

where f_c is represented by equations (4.1) to (4.6).
For this model there were three possible stress block shapes, with increasing surface concrete strain, as shown in Fig. C.2. Substituting equations (4.1), (4.2) and (4.6) into equation (C.20), between limits of integration as set out below:

$$C = -\left\{\int_k^\alpha f'_c \, bD \left[2\frac{\epsilon_c}{\epsilon_o} - \left(\frac{\epsilon_c}{\epsilon_o}\right)^2\right] dy + \int_\alpha^\beta f'_c \, bD \left[1-Z\,(\epsilon_c - \epsilon_o)\right] dy \right.$$

$$\left. + \int_\beta^0 0.2f'_c \, bD \, dy\right\} \qquad \ldots (C.21)$$

where αD and βD are the depths to the fibres with strains of ϵ_o and ϵ_{20c} respectively.

The limits of integration, α and β, take the following values for the three representative stress blocks of Fig. C.2:

if $\epsilon_{cc} \leq \epsilon_o$ $\quad \alpha = 0, \quad \beta = 0$

$\epsilon_o < \epsilon_{cc} \leq \epsilon_{20c}$ $\quad \alpha = k\left(1 - \frac{\epsilon_o}{\epsilon_{cc}}\right), \quad \beta = 0$

$\epsilon_{cc} > \epsilon_{20c}$ $\quad \alpha = k\left(1 - \frac{\epsilon_o}{\epsilon_{cc}}\right), \quad \beta = k\left(1 - \frac{\epsilon_{20c}}{\epsilon_{cc}}\right)$

For integration ϵ_c takes the value ϵ_y, and from substitution for $\frac{\epsilon_y}{\epsilon_o}$ from equation (C.4),

$$C = -\left\{\int_k^\alpha f'_c \, bD \, (2r_y - r_y^2)dy + \int_\alpha^\beta f'_c \, bD \, \epsilon_o \left[\frac{1}{\epsilon_o} - Z(r_y - 1)\right]dy \right.$$

$$\left. + \int_\beta^0 0.2f'_c \, bD \, dy\right\} \qquad \ldots (C.22)$$

Substitute for r_y from equation (C.5),

$$C = -\left\{\int_k^{\alpha} f'_c\ bD\ [2(k-y)\varphi' - (k-y)^2\varphi'^2]dy + \int_{\alpha}^{\beta} f'_c\ bD\ \epsilon_o\left\{\frac{1}{\epsilon_o} - Z[(k-y)\varphi' - 1]\right\}dy\right.$$

$$\left. + \int_{\beta}^{0} 0.2f'_c\ bD\ dy\right\} \qquad \ldots (C.23)$$

The resulting algebraic expression with variables k and φ' is included in the program listing in Appendix A.

Model 2

The cover concrete follows the same stress-strain relation as the core concrete up to a spalling strain, ϵ_{sp}, of 0.004. Any cover concrete at a strain greater than 0.004 is considered to have spalled.

For this model there are seven possible stress block shapes, depending on the maximum surface concrete strain, ϵ_{cc}, and the degree of confinement as represented by the slope, Z, of the "falling" branch of the concrete stress-strain curve. It is assumed that the spalling strain, ϵ_{sp}, will not exceed ϵ_{20c} (i.e. $Z \lesssim 400$). All cases are shown in Fig. C.3.

The compressive force is calculated from substitution of equations (4.1), (4.2) and (4.6) into equation (C.20), and integration between the limits below:

$$C = -\left\{\int_k^{\alpha} f'_c\ bD\ \left[2\frac{\epsilon_c}{\epsilon_o} - \left(\frac{\epsilon_c}{\epsilon_o}\right)^2\right]dy + \int_{\alpha}^{\zeta} f'_c\ bD\ [1 - Z(\epsilon_c - \epsilon_o)]dy\right.$$

$$\left. + \int_{\zeta}^{\beta} f'_c\ b''D\ [1 - Z(\epsilon_c - \epsilon_o)]dy + \int_{\beta}^{\psi} 0.2f'_c b''Ddy\right\} \qquad \ldots (C.24)$$

where αD and βD are as defined previously,

and ζD is the depth to the fibre with a strain of 0.004

and ψD takes the value of the constant, hD, depth to the top of the stirrup

and b'' is the width to the outsides of the stirrup.

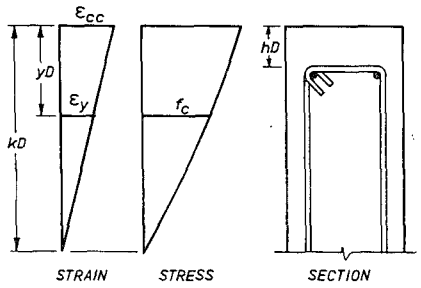

(a) $\varepsilon_{cc} \leq \varepsilon_o$

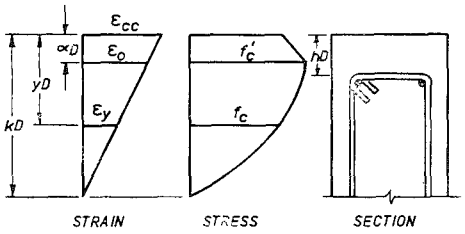

(b) $\varepsilon_o < \varepsilon_{cc} \leq \varepsilon_{sp}$

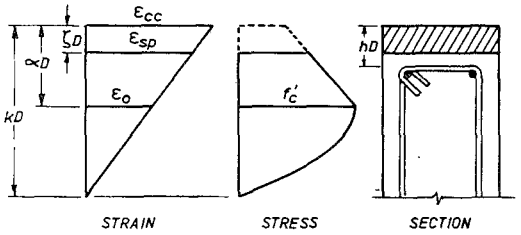

$\zeta < h$

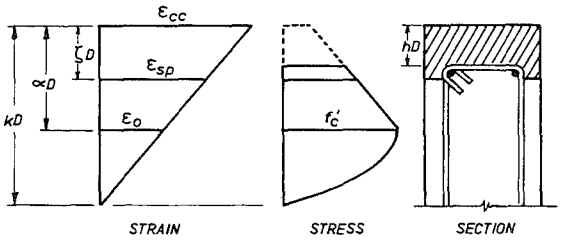

$\zeta > h$

(c) $0.004 < \varepsilon_{cc} \leq \varepsilon_{20c}$

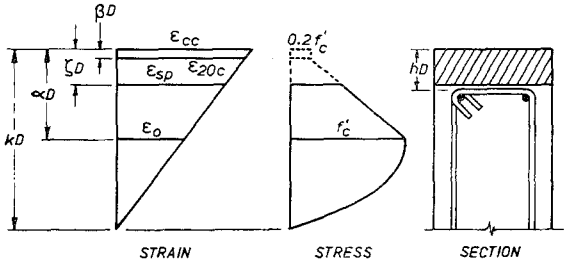

$\zeta < h$

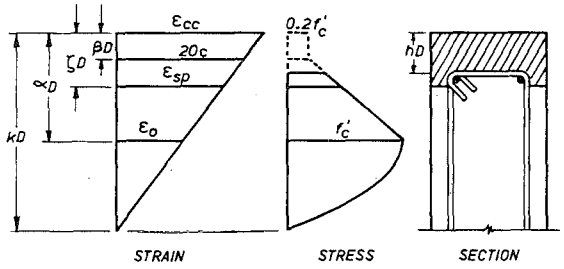

$\beta < h < \zeta$

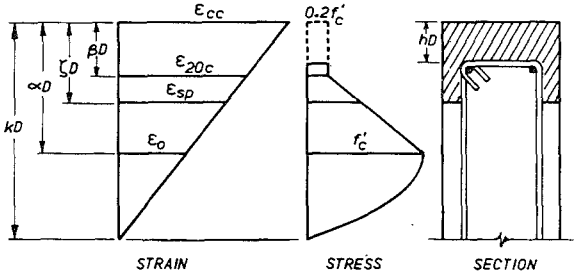

$\beta > h$

(d) $\varepsilon_{20c} < \varepsilon_{cc}$

Fig. C·3 : CONCRETE STRESS BLOCKS FOR MODEL 2

In order to satisfy all stress blocks of Fig. C.3 the limits of integration take the following values:

Region (a) $\quad \epsilon_{cc} \leq \epsilon_o$

$\alpha = 0, \quad \zeta = 0, \quad \beta = 0, \quad \psi = 0$

Region (b) $\quad \epsilon_o < \epsilon_{cc} \leq \epsilon_{sp}$

$\alpha = k(1 - \frac{\epsilon_o}{\epsilon_{cc}}), \quad \zeta = 0, \quad \beta = 0, \quad \psi = 0$

Region (c) $\quad \epsilon_{sp} < \epsilon_{cc} \leq \epsilon_{20c}$

if $\zeta < h$: $\alpha = k(1 - \frac{\epsilon_o}{\epsilon_{cc}}), \quad \zeta = k(1 - \frac{\epsilon_{sp}}{\epsilon_{cc}}), \quad \beta = \psi = \zeta$

if $\zeta > h$: $\alpha = k(1 - \frac{\epsilon_o}{\epsilon_{cc}}), \quad \zeta = k(1 - \frac{\epsilon_{sp}}{\epsilon_{cc}}), \quad \beta = \psi = h$

Regiond (d) $\quad \epsilon_{20c} < \epsilon_{cc}$

if $\zeta < h$: $\alpha = k(1 - \frac{\epsilon_o}{\epsilon_{cc}}), \quad \zeta = k(1 - \frac{\epsilon_{sp}}{\epsilon_{cc}}), \quad \beta = \psi = \zeta$

if $\beta < h < \zeta$: $\alpha = k(1 - \frac{\epsilon_o}{\epsilon_{cc}}), \quad \zeta = k(1 - \frac{\epsilon_{sp}}{\epsilon_{cc}}), \quad \beta = \psi = h$

if $\beta > h$: $\alpha = k(1 - \frac{\epsilon_o}{\epsilon_{cc}}), \quad \zeta = k(1 - \frac{\epsilon_{sp}}{\epsilon_{cc}}), \quad \beta = k(1 - \frac{\epsilon_{20c}}{\epsilon_{cc}}), \quad \psi = h$

From substitution of equations (C.4) and (C.5) into equation (C.24) and integrating the resulting expression, the algebraic expressions in the listing of Program 4.1 are derived.

Model 3

The cover concrete may follow a different stress-strain relation from the core concrete subsequent to a strain of ϵ_o.

This model allows for the different degrees of confinement between the cover and core concretes. Assumptions implicit in the model are discussed in more detail in Section 4.2.3. There are seven possible stress block shapes as shown in Fig. C.4.

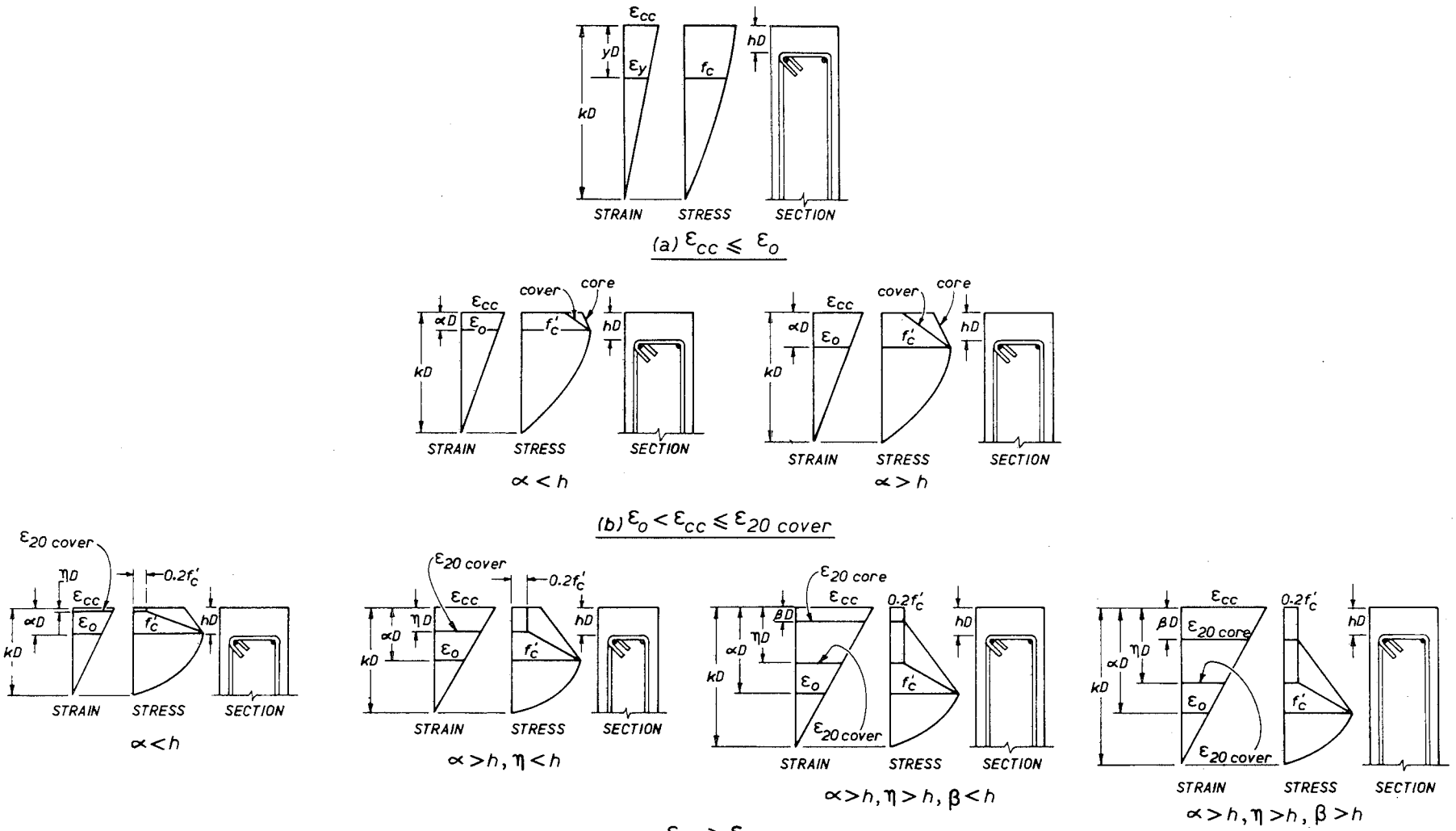

Fig. C·4 : CONCRETE STRESS BLOCKS FOR MODEL 3

From equations (C.20), (4.1), (4.2) and (4.6),

$$C = -\left\{\int_k^{\alpha} f'_c\, bD\left(2\frac{\epsilon_c}{\epsilon_o} - \left(\frac{\epsilon_c}{\epsilon_o}\right)^2\right)dy + \int_{\alpha}^{\eta} f'_c\, bD[1-Z_{cover}(\epsilon_c-\epsilon_o)]dy + \int_{\eta}^{o} 0.2f'_c bDdy\right.$$

$$-\int_{\nu}^{\xi} f'_c b''D[1-Z_{cover}(\epsilon_c-\epsilon_o)]dy - \int_{\xi}^{\psi} 0.2f'_c b''Ddy + \int_{\chi}^{\beta} f'_c b''D[1-Z_{core}(\epsilon_c-\epsilon_o)]dy$$

$$\left.+\int_{\beta}^{\psi} 0.2f'_c b''Ddy\right\} \qquad \ldots (C.26)$$

where βD and ηD are the depths to fibres with strains of ϵ_{20c} for the core and cover concretes respectively ($\epsilon_{20\ core}$ and $\epsilon_{20\ cover}$).

The limits of integration are as follows:

Region (a) $\quad \epsilon_{cc} \leq \epsilon_o$

$\alpha = 0, \quad \eta = 0, \quad \nu = 0, \quad \xi = 0, \quad \psi = 0, \quad \chi = 0, \quad \beta = 0$

Region (b) $\quad \epsilon_o < \epsilon_{cc} \leq \epsilon_{20\ cover}$

if $\alpha < h$: $\quad \alpha = k\left(1 - \frac{\epsilon_o}{\epsilon_{cc}}\right), \quad \eta = 0, \quad \nu = 0, \quad \xi = 0, \quad \psi = 0, \quad \chi = 0, \quad \beta = 0$

if $\alpha > h$: $\quad \alpha = k\left(1 - \frac{\epsilon_o}{\epsilon_{cc}}\right), \quad \eta = 0, \quad \nu = \alpha, \quad \xi = h, \quad \chi = \alpha, \quad \beta = h, \quad \psi = h$

Region (c) $\quad \epsilon_{cc} > \epsilon_{20\ cover}$

if $\alpha < h$: $\quad \alpha = k\left(1 - \frac{\epsilon_o}{\epsilon_{cc}}\right), \quad \eta = k\left(1 - \frac{\epsilon_{20\ cover}}{\epsilon_{cc}}\right), \quad \nu = 0, \quad \xi = 0,$

$\psi = 0, \quad \chi = 0, \quad \beta = 0$

if $\alpha < h, \quad \eta > h$: $\quad \alpha = k\left(1 - \frac{\epsilon_o}{\epsilon_{cc}}\right), \quad \eta = k\left(1 - \frac{\epsilon_{20\ cover}}{\epsilon_{cc}}\right), \quad \nu = \alpha,$

$\xi = h, \quad \psi = h, \quad \chi = \alpha, \quad \beta = h$

if $\alpha > h, \ \eta > h, \ \beta < h$: $\quad \alpha = k\left(1 - \frac{\epsilon_o}{\epsilon_{cc}}\right), \quad \eta = k\left(1 - \frac{\epsilon_{20\ cover}}{\epsilon_{cc}}\right), \quad \nu = \alpha,$

$\xi = \eta, \quad \psi = h, \quad \chi = \alpha, \quad \beta = h$

f $\alpha > h$, $\eta > h$, $\beta > h$: $\alpha = k(1 - \frac{\epsilon_o}{\epsilon_{cc}})$, $\eta = k(1 - \frac{\epsilon_{20\ cover}}{\epsilon_{cc}})$, $\nu = \alpha$,

$$\xi = \eta,\ \psi = h,\ \chi = \alpha,\ \beta = (1 - \frac{\epsilon_{20\ core}}{\epsilon_{cc}})$$

The algebraic expressions resulting from firstly substitution of quations (C.4) and (C.5) into equation (C.26) and then integration are hown in the program listing.

(d) Equilibrium and Iteration

For each value of neutral axis depth assumed for a given surface oncrete strain, the equilibrium of forces is tested as follows:

$$C = T_s + T_c + P \qquad \ldots (C.27)$$

here C, T_s, T_c and P are the forces due to concrete compression, teel tension (and compression at large curvatures in a concentrically restressed member), concrete tension, and axial load.

Should equilibrium not be satisfied to within $bD/5$ lbs, a further rial value of neutral axis depth is taken. A rapid close on the rrect value is obtained by use of the following expression, which is milar to that proposed by L.L. Jones[78]:

$$kD = \frac{kD}{6.0}\left[4.0 + 2.0\,\frac{(T_s + T_c + P)}{C}\right] \qquad \ldots (C.28)$$

2.3 Calculation of Curvature and Moment

Once force equilibrium has been satisfied for a particular surface ncrete strain, curvature and moment may be calculated directly. The rvature is given by:

$$\varphi = \epsilon_{cc}/kD \qquad \ldots (C.29)$$

The moment is calculated from the sum of the moments due to the mponent forces within the section:

(a) Moment Due to Prestressing Steel

Moments due to the individual tendon forces are taken about the top of the section. Thus the total moment due to the steel, M_S, becomes:

$$M_S = A_{s1}\, f_{s1}\, \alpha_1 D + A_{s2}\, f_{s2}\, \alpha_2 D + \text{etc.} \qquad \ldots (C.30)$$

(b) Moment Due to Tensile Concrete Force

The appropriate expression for moment due to the tensile force in the concrete, M_T, depends on whether or not the section has cracked.

If the section has not cracked, the moment from equation (C.15) becomes:

$$M_T = \int_k^1 2f'_c\, bD^2(k-y)y\, \varphi' dy \qquad \ldots (C.31)$$

Integrating,

$$M_T = 2f'_c bD^2\varphi'\left(-\frac{k^3}{6} + \frac{k}{2} - \frac{1}{3}\right) \qquad \ldots (C.32)$$

Similarly where cracking has occurred, equation (C.18) leads to:

$$M_T = \int_k^\gamma 2f'_c\, bD^2\, (k-y)y\, \varphi'\, dy \qquad \ldots (C.33)$$

where γ is given by equation (C.17)

Integrating,

$$M_T = 2f'_c bD^2\varphi'\left(-\frac{k^3}{6} + \frac{\gamma^2 k}{2} - \frac{\gamma^3}{3}\right) \qquad \ldots (C.34)$$

(c) Moment Due to Compressive Concrete Force

The value of moment due to the compressive force in the concrete, M_C, depends on which model has been used to represent the cover concrete.

Model 1

From equation (C.23),

$$M_C = -\left\{\int_k^\alpha f'_c bD^2[2(k-y)\varphi' - (k-y)^2\varphi'^2]ydy + \int_\alpha^\beta f'_c bD^2\varepsilon_o\left\{\frac{1}{\varepsilon_o} - Z[(k-y)\varphi' - 1]\right\}ydy + \int_\beta^0 0.2f'_c bD^2 ydy\right\} \qquad \ldots (C.35)$$

where the limits of integration take the values for Model 1 in Section C.2.2.

Model 2

From equation (C.24),

$$M_C = -\left\{\int_k^{\alpha} f'_c bD^2[2(k-y)\varphi' - (k-y)^2\varphi'^2]ydy + \int_{\alpha}^{\zeta} f'_c bD^2\epsilon_o\{\frac{1}{\epsilon_o} - Z[(k-y)\varphi' - 1]\}ydy\right.$$

$$\left. + \int_{\zeta}^{\beta} f'_c b''D^2\epsilon_o\{\frac{1}{\epsilon_o} - Z[(k-y)\varphi' - 1]\}ydy + \int_{\beta}^{\psi} 0.2f'_c b''D^2ydy\right\} \quad \ldots (C.36)$$

where the limits of integration take the values for Model 2 in Section C.2.2.

Model 3

From equation (C.26),

$$M_C = -\left\{\int_k^{\alpha} f'_c bD^2[2(k-y)\varphi' - (k-y)^2\varphi'^2]ydy\right.$$

$$+ \int_{\alpha}^{\eta} f'_c bD^2\epsilon_o\{\frac{1}{\epsilon_o} - Z_{cover}[(k-y)\varphi' - 1]\}ydy + \int_{\eta}^{o} 0.2f'_c bD^2ydy$$

$$- \int_{\nu}^{\xi} f'_c b''D^2\epsilon_o\{\frac{1}{\epsilon_o} - Z_{cover}[(k-y)\varphi' - 1]\}ydy - \int_{\xi}^{\psi} 0.2f'_c b''D^2ydy$$

$$\left. + \int_{\chi}^{\beta} f'_c b''D^2\epsilon_o\{\frac{1}{\epsilon_o} - Z_{core}[(k-y)\varphi' - 1]\}ydy + \int_{\beta}^{\psi} 0.2f'_c b''D^2ydy\right\} \quad \ldots (C.37)$$

where the limits of integration take the values for Model 3 in Section C.2.2.

(d) Moment Due to Axial Load

The moment, M_p, due to axial load, taken about the top surface of the section, is as follows:

$$M_p = P(0.5D + e) \quad \ldots (C.38)$$

where e is the eccentricity, and is zero for a concentric axial load.

(e) Sum of Moments

The resultant moment, M, on the section is found by summation:

$$M = M_S + M_T + M_P - M_C \qquad \ldots (C.39)$$

where M_S, M_T, M_P and M_C are the moments due to steel force, concrete tension, axial load, and concrete compression respectively.

APPENDIX D

REPEATED LOAD TESTS ON PRESTRESSING WIRE

D.1 TEST SPECIMENS

Three 0.276" dia. high tensile wires were tested. All three were samples of cables used in the beams of Units 1 and 2. The ultimate tensile strength, f'_s, of two of the wires was 244,000 psi, but the third was of a higher strength batch, f'_s = 268,000 psi.

D.2 TEST EQUIPMENT

Loads were applied by an Avery 25,000 lb Universal testing machine Type 7109 DCJ. Strains were measured over a 2 inch gauge length by an Instron G-51-14 strain gauge extensometer. The extensometer was calibrated to a Budd Strain Bridge using a micrometer screw device. It was found to have zero hysteresis error to within the limits of accuracy of the micrometer.

D.3 LOADING SEQUENCE

Cycles of unloading and reloading were made at successively higher values of steel strain, and finally the specimens were loaded to failure. The measured stress-strain curves for one of the prestressing steel specimens is shown in Fig. 5.3.